Université de Toulouse

THÈSE

En vue de l'obtention du

DOCTORAT DE L'UNIVERSITÉ DE TOULOUSE

Délivré par :
Université Toulouse III Paul Sabatier (UT3 Paul Sabatier)

Discipline ou spécialité :
Chimie

Présentée et soutenue par :
KOZINETS Ekaterina
le : jeudi 5 décembre 2013

Titre :

Complexes diène du rhodium et de l'iridium portant des ligands diphénylphosphinoferrocényl thioéther : synthèse, activation et hydrogénation catalytique.

Ecole doctorale :
Sciences de la Matière (SDM)
Unité de recherche :
Laboratoire de Chimie de Coordination-LCC-CNRS-UPR 8241
Directeur(s) de Thèse :
BELKOVA Natalia
MANOURY Eric
Rapporteurs :
BRUNEAU Christian
TRIFONOV Alexander

Membre(s) du jury :

CHAUVIN Remi	Examinateur
SHUBINA Elena	Examinateur
POLI Rinaldo	Invité

Université Toulouse III Paul Sabatier (UT3 Paul Sabatier)

Kozinets Ekaterina

Diene complexes rhodium and iridium with diphenylphosphino ferrocenyl thioether ligands: synthesis, activation, catalytic hydrodenation

Chimie Organométallique et de Coordination

THESE

Supervisors of thesis:
Eric MANOURY
Natalia BELKOVA

Toulouse 2013

Acknowledgements

Résumé de thèse

Sujet: Diene complexes de rhodium et d'iridium avec diphenylphosphino ferrocényl thioéther ligands: synthèse, l'activation, l'hydrogénation catalytique

De nouveaux complexes dienes du rhodium portant des ligands diphénylphosphinoferrocénylthioéther [Rh(P,SR)(diene)]X (diène = cyclooctadiène (COD), norbornadiène (NBD); X = Cl^-, BF_4^-) ont été synthétisés et entièrement caractérisés. La structure moléculaire des complexes cationiques [Rh(P,SR)(diène)]$^+BF_4^-$ révèle une géométrie plan carré légèrement distordue. Pour les complexes chlorure [Rh(P,SR)(diène)Cl], l'utilisation des spectroscopies RMN et IR complétées par une étude théorique par DFT a permis de proposer une géométrie plan carré avec le diène, le chlorure et le phosphore coordonnés au métal, la fonction thioéther restant en dehors de la sphère de coordination.

Les complexes de rhodium [Rh(P,SR)(diène)]X catalysent l'hydrogénation des cétones et sont donc de bons modèles fonctionnels pour l'étude de l'hydrogénation asymétrique des cétones par les complexes d'iridium [Ir(P,SBu^t)(COD)Cl]. Pour les composés [Rh(P,SBu^t)(diène)]X, les vitesses de réaction et les énantiosélectivités évoluent dans le sens COD-Cl > COD-BF_4 > NBD-BF_4 > NBD-Cl. Pour les complexes portant des ligands diéniques NBD, les vitesses de réaction et les énantiosélectivités évoluent dans le sens Bu^t >> Et > Ph > Bz.

En utilisant la RMN du parahydrogène, nous avons établi que l'activation du précatalyseur était obtenue par réaction des complexes [Rh(P,SBu^t)(diène)]X avec le dihydrogène en deux étapes via l'obtention d'un composé intermédiaire [Rh(P,SR)(alcène-alkyl)] ([Rh(P,SR)(1-κ-4,5-η-C_8H_{13})] pour les complexes COD) suivie de la formation d'un complexe solvaté [Rh(P,SR)$(Solv)_2]^+$ (Solv = MeOH, MeCN, acétone). L'hydrogénation des ligands NBD est plus rapide que celle des ligands COD. Le complexe [Rh(P,SBu^t)$(MeOH)_2]^+$ provoque un échange H/D très rapide entre H_2 et le solvant deutéré via une espèce dihydrure [Rh(P,SBu^t)$(MeOH)_2H_2]^+$ accessible énergiquement d'après des calculs DFT. L'addition de ligand L (py or MeCN) à une solution de [Rh(P,SBu^t)(diène)]X en présence de H_2 à basse température a résulté en la formation d'espèces dihydrures diastéréoisomères [Rh(P,SBu^t)$L_2H_2]^+$ dont la structure a été établie sur la base des résultats RMN.

Mots clés: l'hydrogenation, complexes de rhodium et d'iridium, mécanisme d'activation.

Summary

Subject : Diene complexes rhodium and iridium with diphenylphosphino ferrocenyl thioether ligands: synthesis, activation, catalytic hydrodenation.

New diene rhodium complexes with diphenylphosphinoferrocenylthioether ligands [Rh(P,SR)(diene)]X (diene = COD, NBD; X = Cl^-, BF_4^-) were synthesized and fully characterized. The molecular structure of the cationic complexes $[Rh(P,SR)(diene)]^+BF_4^-$ shows a slightly distorted square planar geometry. For the chloride complexes, [Rh(P,SR)(diene)Cl], a combination of NMR and IR spectroscopy and DFT calculations points to a four coordinate square planar geometry with the diene ligand, the chlorine and the phosphorus atoms in the coordination sphere and with a dangling thioether function. It was found that rhodium complexes [Rh(P,SR)(diene)]X are good structural and functional models to study the ketone asymmetric hydrogenation mechanism catalyzed by the iridium complexes [Ir(P,SBu^t)(COD)Cl]. For the [Rh(P,SBu^t)(diene)]X derivatives the rate of hydrogenation and the enantioselectivity change in the order COD-Cl > COD-BF_4 > NBD-BF_4 > NBD-Cl. For the complexes with the NBD ligand the activity/enantioselectivity change in the order But >> Et > Ph > Bz. By use of parahydrogen NMR spectrometry, it was established that the catalyst activation involves the reaction of the rhodium complexes [Rh(P,SBu^t)(diene)]X with dihydrogen, which occurs in two steps through the generation of an intermediate [Rh(P,SR)(alkene-alkyl)]([Rh(P,SR)(1-κ-4,5-η-C_8H_{13})] for the COD complexes) followed by the formation of a solvated complex $[Rh(P,SR)(Solv)_2]^+$ (Solv = MeOH, MeCN, acetone). Hydrogenation of the NBD ligand proceeds faster than that of the COD ligand. The rhodium complex $[Rh(P,SBu^t)(MeOH)_2]^+$ promotes a very rapid H/D exchange between H_2 and the deuterated solvent via a dihydride species $[Rh(P,SBu^t)(MeOH)_2H_2]^+$, which is accessible according to the DFT calculations. Addition of L (py or MeCN) to the solution of [Rh(P,SBu^t)(diene)]X in the presence of H_2 at low temperature results in the formation of a diastereomeric dihydride species [Rh(P,SBu^t)L_2H_2]+, the structure of which was established on the basis of the NMR spectroscopic data.

Keywords: hydrogenation, rhodium and iridium complexes, activation mechanism.

ABBREVIATIONS

II.1-R	[Rh(P,SR)(NBD)Cl]
II.2-R	[Rh(P,SR)(NBD)]BF_4
II.3-R	[Rh(P,SR)(COD)Cl]
II.4-R	[Rh(P,SR)(COD)]BF_4
A	Absorbsion
Bu^t	*tert*-butyl
Bz	Benzyl
COD	Cyclooctadiene
COE	Cyclooctene
COSY	Correlation spectroscopy
Cp	Cyclopentadienyl
DFT	Density functional theory
Et	Ethyl
δ	Chemical shift
HMBC	Heteronuclear Multiple Bond Correlation
HMQC	Heteronuclear Multiple Quantum Correlation
IR	Infrared spectroscopy
J	Coupling constant
k	Rate constant
MeCN	Acetonitrile
MeOH	Methanol
NBD	Norbornadiene
NMR	Nuclear magnetic resonance
NOE	Nuclear Overhauser Effect
OPSY	Only *Para*hydrogen SpectroscopY
ORTEP	Oak Ridge Thermal Ellipsoid Plot Program
Ph	Phenyl
PHIP	*Para*hydrogen induced polarization
Pr^iOH	Isopropyl alcohol
P,SR	CpFe[η^5-1,2-$C_5H_3(CH_2SR)(PPh_2)$]
Py	Pyridine
THF	Tetrahydrofurane
UV	Ultraviolet

List of tables

List of figures

Talbe of contents

Introduction

Complexes of Rh^I and Ir^I are commonly employed as catalysts in a variety of hydrogenation processes. The most popular examples include the so-called "Wilkinson's catalyst", $[Rh(PPh_3)_3Cl]$ [1], and $[Ir(L)_2(COD)]^+$ (L = PPh_3, $PMePh_2$, py), the latter of which displays high activities even with relatively hindered C-C double bonds [2]. Complexes of type $[M(diene)Cl]_2$ or $[M(diene)_2]^+$ [M = Rh or Ir, diene = 1,5-cyclooctodiene (COD), norbornadiene (NBD)], and particularly those of iridium, have also proven suitable as precatalysts for the ionic hydrogenation of polar substrates such as ketones and imines in the presence of appropriate ligands, mostly diphosphines [3-9]. A notable example of this is provided by Ir^I-catalyzed imine hydrogenation as used in the multi-ton scale industrial production of the herbicide metolachor [10, 11].

A new family of chiral ferrocenyl P,S ligands of general formula $CpFe[\eta^5\text{-}1,2\text{-}C_5H_3(CH_2SR)(PPh_2)]$, henceforth abbreviated as (P,SR), has been developed in our laboratories within the last few years. These ligands are characterized by having only the planar chirality of the 1,2 substitution at one of the two cyclopentadienyl rings, as opposed to many other ferrocene-based chiral ligand which combine this with a central chirality in another part of the ligand such as, amongst many, TRAP [12-16], Josiphos-type diphosphines, including industrially important xyliphos [10,11], taniaphos [17-19], walphos [20] or phosphine-oxazolines [21-24] (see Scheme 0.1).

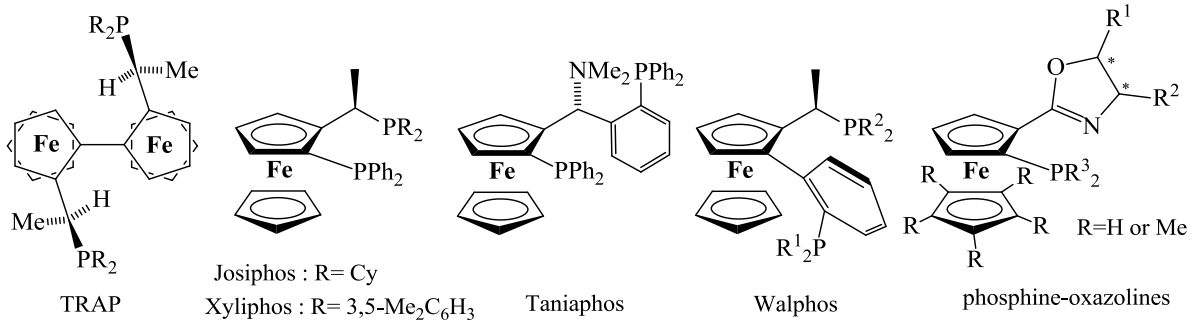

Scheme 0.1 Important chiral ferrocene ligands bearing planar and central chirality.

The coordination chemistry of our chiral ferrocenyl (P,SR) ligands has been extensively studied with various metals. One particularly striking feature is worth being pointed out. Because of its stereochemically active lone pair, the sulfur atom becomes a center of chirality upon coordination and therefore two diastereoisomer could in principle be obtained for each metal complex containing these ligands. However, without exception, the coordination is totally diastereoselective, meaning that the central chirality on sulfur generated by coordination is fully controlled (see Scheme 0.2) [25-28. The observed diastereoisomer is in each case the one where the sulfur lone pair points towards the metal-

containing side of the substituted Cp ring (*endo*) and the sulfur R substituent points away from the iron atom (*exo*), whereas the other diastereoisomer where these two positions are exchanged is never observed.

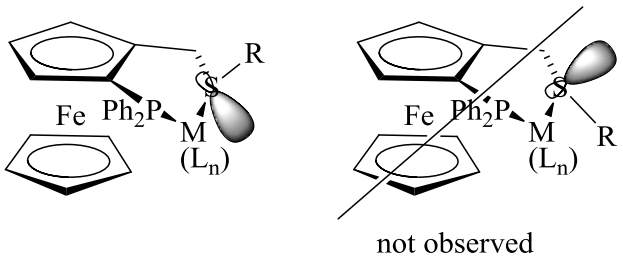

Scheme 0.2 Diastereoselective coordination of the phosphine thioether ligands

These ligands have been applied to several asymmetric catalytic reactions, such as the asymmetric allylic substitution [29, 30] and the asymmetric methoxycarbonylation [31]. In particular, it was found that iridium complexes containing these ligands, [IrCl(COD)(P,SR)], are excellent precatalysts for the hydrogenation of acetophenones, yielding high activities and enantioselectivies [25, 32]. With a catalyst charge of only 0.2 mol %, full conversions could be obtained after 8 h at 10°C with enantiomeric excesses up to >99%. This study constituted the first report of iridium complexes with P,S ligands of any kind in such reactions. Therefore, several mechanistic issues had to be addressed. It was demonstrated that dihydrogen as well as a strong base are necessary for catalytic activity. It was also shown that non-enolizables ketones can be hydrogenated under these conditions proving that the ketones themselves and not the enol tautomers are the actual substrates. It was also demonstrated that the COD ligand in the precatalysts was hydrogenated and expelled as cyclooctene during the catalytic reactions. However, besides this useful information, the detailed mechanism of the precatalyst activation and the nature of the active catalyst remained essentially unclear.

In order to further clarify the mechanistic details of this hydrogenation reaction, our two research groups have embarked in a theoretical (with the collaboration of Pr Agusti Lledos in Barcelona, study still in progress) and experimental mechanistic project. This Ph.D. work is part of this effort. It was decided to synthesize and investigate rhodium analogues of the iridium precatalysts of the ketone hydrogenation reaction as functional models, for mechanistic investigations, especially on the activation part. This choice was suggested by literature reports, which will be highlighted in Chapter I, that solvated rhodium complexes obtained by hydrogenation of the diene ligand from precursors of type $[Rh(diene)(LL)]^+$ or $[Rh(diene)_2]^+$/LL or $[RhCl(diene)]_2$/LL (LL = bidentate ligand, typically a biphosphine) are under certain conditions isolable or at least stable in solution, whereas the corresponding iridium species do not seem to be sufficiently stable. In addition, these new chiral

complexes are of interest by themselves as potential catalysts for asymmetric hydrogenation but also for other asymmetric catalytic reactions.

We will therefore start this thesis with a bibliographical overview of the syntheses of iridium and rhodium complexes bearing a diene ligand and of their reactivity under dihydrogen pressure in Chapter 1. The new results obtained in this thesis will subsequently be presented in Chapter 2, which is organized in three separate sections. In the first section, the synthesis and characterization of new Rh complexes with (P,SR) ligands will be reported. The second section reports catalytic applications of these complexes in a few reactions. It will be shown that although less active than the related Ir systems in ketone hydrogenation, these Rh complexes are not only structural but also functional models of the previously investigated Ir analogues. Finally, the third section will present spectroscopic investigations of the precatalyst activation step carried out partly with the help of *para*hydrogen NMR spectroscopy and partly with UV-visible spectroscopy in an attempt to obtain additional information on the chemical nature of the catalytically active complex.

I Literature review

I.1 [M(L,L')(diene)]X complexes: synthesis, characterization, structure

There are three possible molecular geometries for rhodium and iridium complexes [M(L,L')(diene)X], were L,L' is a bidentate ligand (Scheme I.1), for which over 1000 examples are reported in the literature. In this chapter we will focus on rhodium and iridium complexes which were synthesized in the past 10 years.

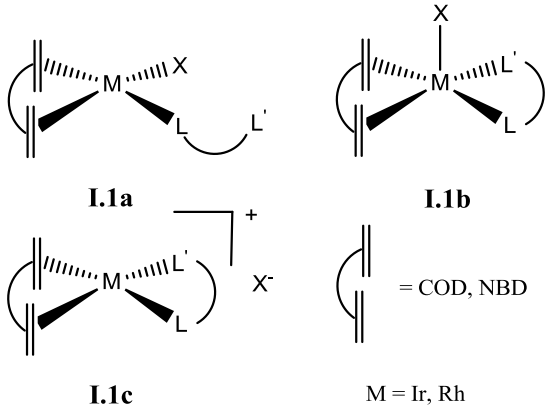

Scheme I.1 Possible molecular geometries for [M(L,L')(diene)]X complexes (M = Rh, Ir).

According to the literature data the most common geometry for rhodium as well as for iridium complexes is **I.1c** when X^- is a non-coordinating anion (mostly PF_6^-, BF_4^-, $CF_3SO_3^-$ and ClO_4^-). When X is a coordinating halide anion, the 5-coordinate geometry of type **I.1b** is more common for Ir^I complexes, while for Rh^I complexes the geometry of type **I.1a** occurs more often. Complexes of type [M(L,L')(diene)X] with a halide anion are generally prepared by addition of the L,L-ligand to the $[M(diene)Cl]_2$ precursor. The cationic complexes, on the other hand, are usually prepared from the halide complexes by addition of a non-coordinating anion salt, the reaction being often helped by the addition of Ag^+ or Tl^+ which displace the reaction by forming corresponding insoluble silver or thallium halides.

I.1.1 NHC ligands

Complexes with N-heteocyclic carbenes (NHCs) as ligands have been widely recognized and extensively reviewed recently [33, 34]. The coordination of an NHC to the metal center usually requires the activation of a ligand precursor, which is normally an azolium salt. Transmetalation from an Ag^I-NHC complex has become the most widely used route to obtain NHC-metal complexes. Thus a two-step transmetalation process was used to prepare cyclooctadiene rhodium complexes with

imidazolium ligands (Scheme I.2) [35]. The first step involves deprotonation of the imidazolium salt in dihlorometane solution at room temperature with silver oxide to form the silver carbene species; the addtition of $[Rh(COD)Cl]_2$ precursor to the product of this reaction and stirring reaction mixture at reflux leads to the rhodium complex. Depending on the linker length, two different kinds of compounds **I.5-n-Bu** and **I.8-n-Bu** were predominantly formed (**I-5** for n = 3 and 4; **I-5** for n = 1 and 2). When the transmetalation reaction was carried out in one pot (without purification of the intermediate product), however, the chelate complex **I.5-2-Bu** was observed instead of the bis-Rh(I) species **I.8-2-Bu.** The square planar structure of **I.5-2-Bu** and **I.5-3-Bu** was confermed by X-ray diffraction analysis. When the transmetalation was carried out at 25 °C, the products were bis-Rh(I) species for all values of n = 1, 2, 3, 4 (**I.8-n-Bu**). Attempts to convert the isolated bis-Rh(I) complexes into the chelated mononuclear **I.5-n-Bu** complexes were unsuccessful. When the bis-imidazolium bromides were used as ligand precursor, KPF_6 was added to the reaction mixture to obtain the PF_6^- salts **I.5-n-R, I.6-n-R** or **I.7-n-R**.

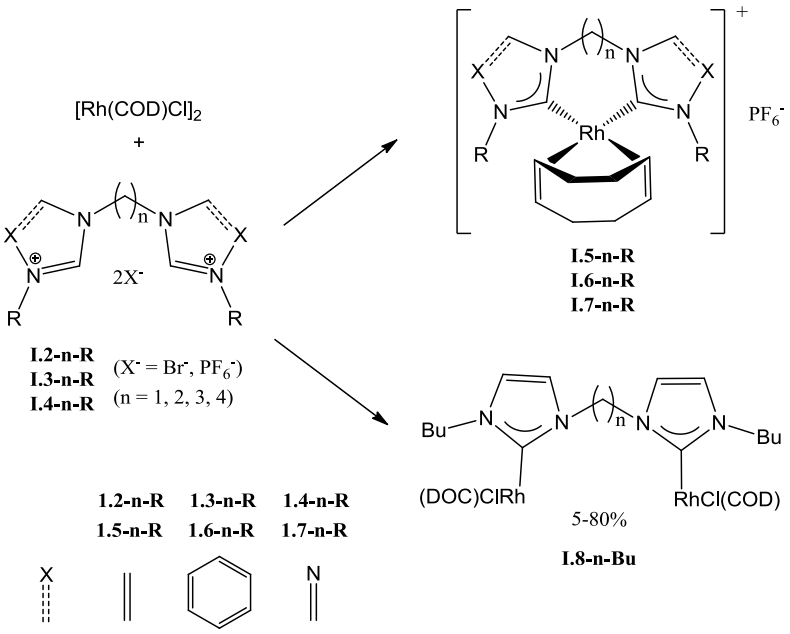

Scheme I.2

Cationic rhodium complexes of type **I.5-n-R** (n = 2, R = Me, Pr^i, Cy, Ph, Mes) and **I.7-n-R** (n = 1, R = Pr^i; n = 2, R = Me, Pr^i, 4-Pr^iPh, Ph; n = 3, R = Pr^i, Ph) were synthesized by addition of the imidazolium or triazolium salt to an ethanol solution containing NaH and $[Rh(COD)Cl]_2$ and stirring at 40-50°C. Cationic rhodium complexes type of **I.6-n-R** (n = 2, 3; R = Me, Pr^i, Ph) were obtained by the addition of $[Rh(COD)(OEt)]_2$ in THF to a solution of NaOEt and benzimidazolium salt in methanol at room temperature (Scheme I.2). They were obtained in high yields (80-98%) and the formation of dinuclear rhodium species was not observed [36]. Complex **I.5-3-Me** was obtained by deprotonation

of the imidazolium salt precursor with KOBu^t and stirring the reaction mixture with $[Rh(COD)Cl]_2$ in THF at room temperature [37].

The reaction of **I.9** with $[M(COD)Cl]_2$ (M = Rh, Ir) in the presence of NEt_3 yielded two different types of ligand coordination depending on the metal used (Scheme I.3) [38]. For rhodium, the reaction gives the monometalated complex **I.10b**, where the ligand adopts a monodentate coordination mode, while for iridium the bidentate coordination occurs to produce **I.11**. The monodentate iridium compound **I.10a** was obtained only as a 70:30 mixture with **I.11** already after 10 min of reaction.

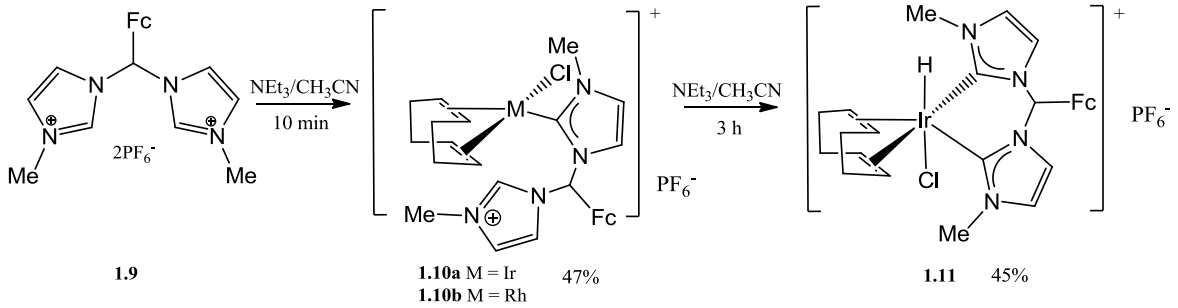

Scheme I.3

The cationic iridium complex **I.13** with a bidentate Y-shaped tris-NHC ligand was obtained with 83% yield according to Scheme I.4 [39].

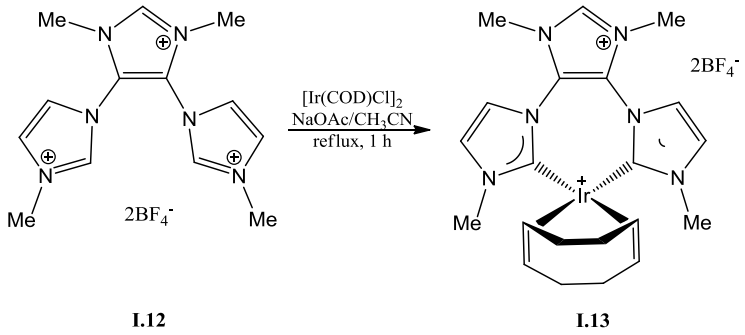

Scheme I.4

A series of rhodium and iridium complexes of quinoline-tethered NHCs have been synthesized via silver transmetalation (Scheme I.5) in 94-97% yields [40]. Deprotonation of imidazolium ions using Bu^{t}OK in the presence of $[Rh(COD)Cl]_2$ afforded a mixture of chelated and monodentate complexes, while only the chelated complexes where obtained for the iridium analogues.

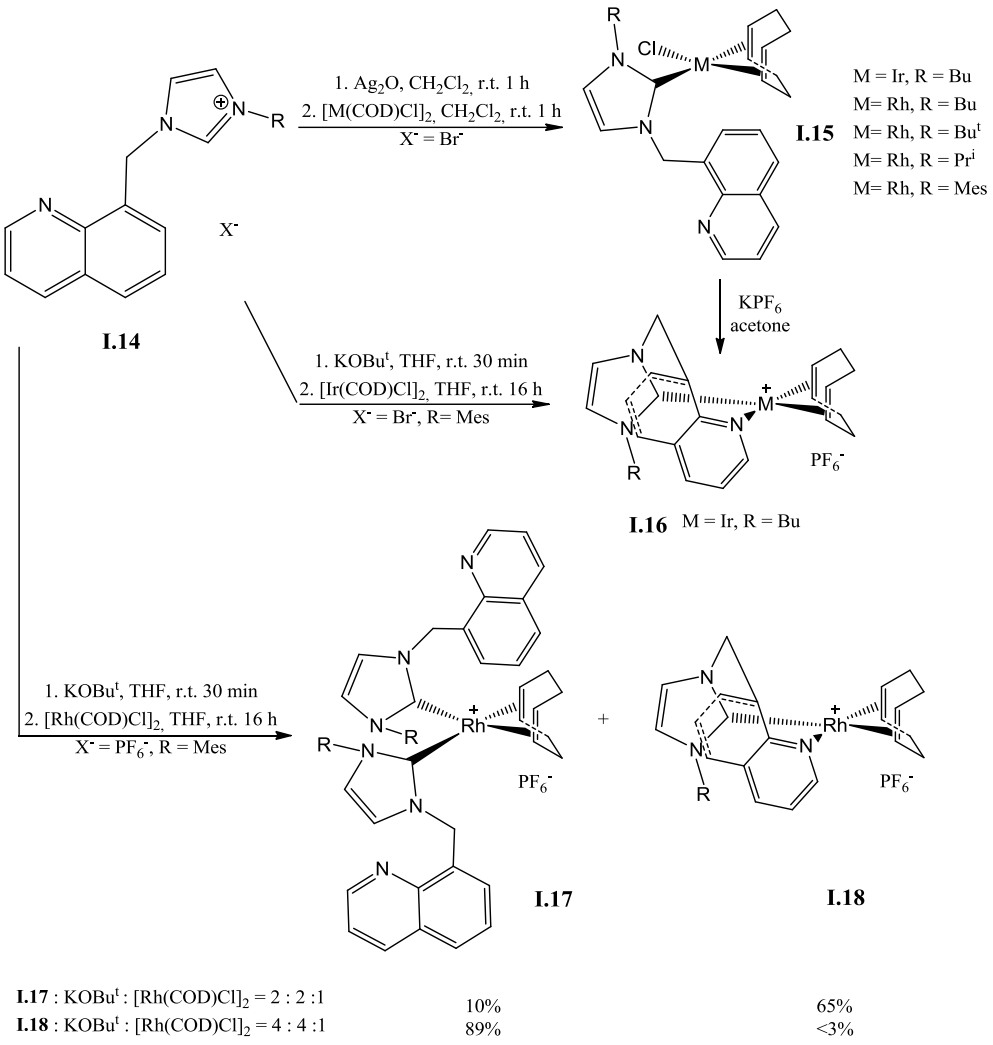

Scheme I.5

Reaction of $[Rh(COD)Cl]_2$ with $KOBu^t$ and subsequent treatment with 1-benzyl-3-(5,7-dimethyl-1,8-naphthyrid-2-yl)imidazol-2-ylidene **I.19** gives complex **I.20** (Scheme I.6) with monodentate coordination of the ligand in a good yield (81%), the structure was confirmed by X-ray analysis [41].

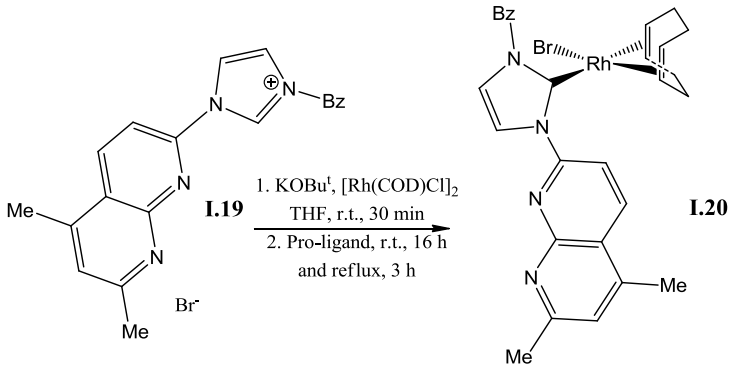

Scheme I.6

Rhodium complexes **I.22-R** were synthesized by in situ deprotonation of the bis(imidazolium) salts **I.21-R** with 2 equiv. of KOAc and reaction with $[Rh(COD)Cl]_2$ (Scheme I.7) [42, 43]. Using only 1 equiv. of KOAc led to the almost exclusive formation of the unsymmetrical intermediate **I.23**.

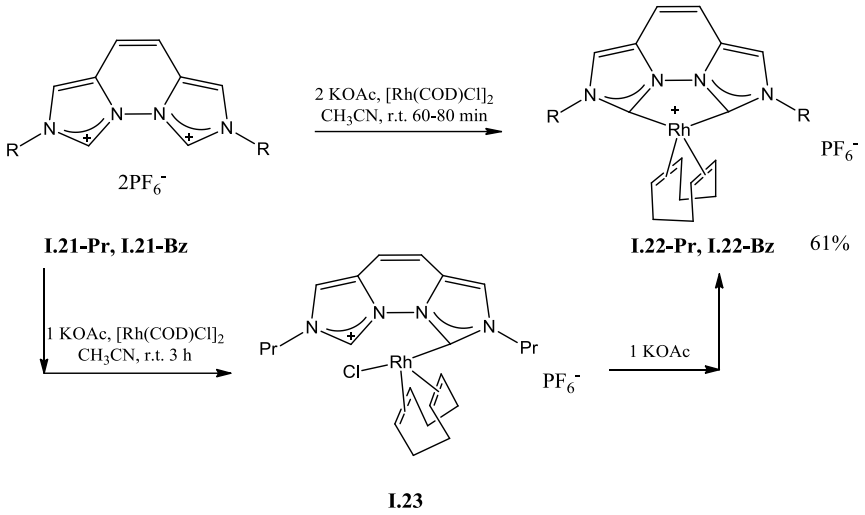

Scheme I.7

Silver transmetalation was used for the synthesis of cyclooctadiene rhodium complexes with imidazolium-phenoxyimine precursor (Scheme I.8) [44]. The structure of the chloride complex was confirmed by X-ray diffraction analysis.

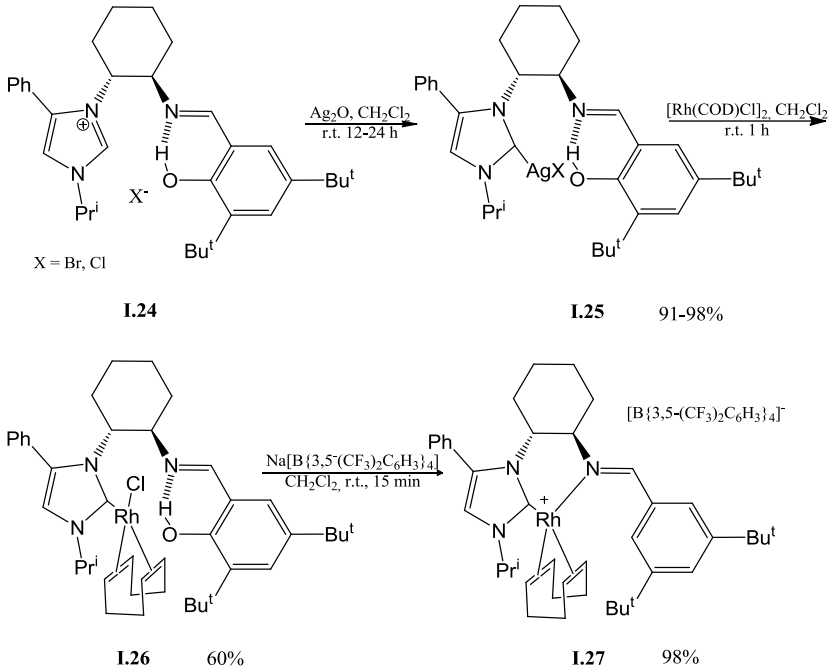

Scheme I.8

The cyclooctadiene rhodium and iridium cationic complexes with imidazolium-linked cyclophane ligand were prepared accorging to Scheme I.9 [45]. The norbornadiene rhodium complex was obtained similarly by reaction of $[Rh(NBD)Cl]_2$ with *ortho*-cyclophane bromide. The cyclooctadiene rhodium complex was also obtained as its bromide salt in 60% yield from *ortho*-cyclophane bromide, $[Rh(COD)Cl]_2$ and NaOAc at 98 °C. The single crystal X-ray studies are consistent in all cases with the formulation of the complexes as ionic compounds with a non-interacting counterion.

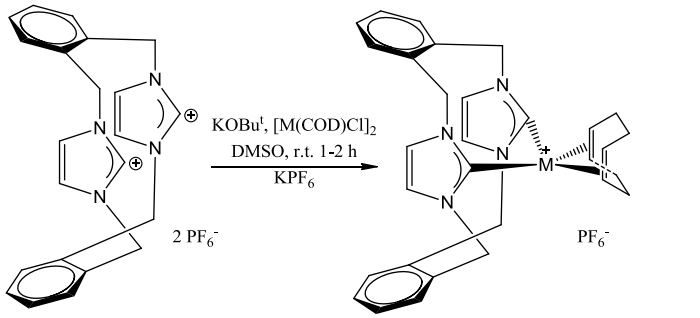

I.28 **I.29**

Scheme I.9

The cationic rhodium complexes **I.35-1-Me** [46], **I.33-1-Me**, **I.32-1-Me**, **I.34-1-Me** [47], **I.35-1-diPh**, **I.35-1-Pr^i** [48], **I.32-1-Bz** [49], **I.35-1-*o*-MeBz**, **I.34-1-CHMePh**, **I.32-1-Pr^i** [50], **I.34-1-diPh** and **I.33-0-Me** [51] supported by chiral NHC ligands based on the *trans*-9,10-dihydro-9,10-ethanoanthracene-11,12-di(1-alkyl)azolidine-2-ylidene backbone were synthesized according to Scheme I.10 in 4-92% yield.

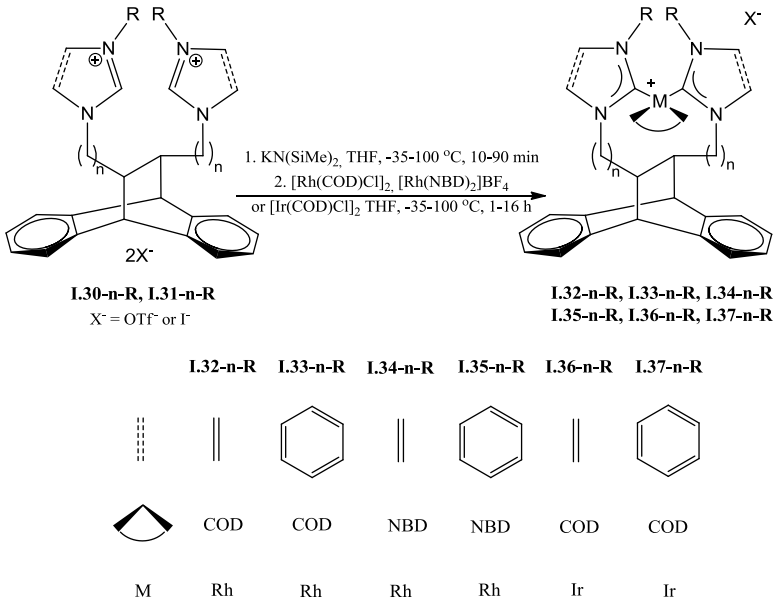

I.30-n-R, I.31-n-R
X$^-$ = OTf$^-$ or I$^-$

I.32-n-R, I.33-n-R, I.34-n-R
I.35-n-R, I.36-n-R, I.37-n-R

	I.32-n-R	I.33-n-R	I.34-n-R	I.35-n-R	I.36-n-R	I.37-n-R
	COD	COD	NBD	NBD	COD	COD
M	Rh	Rh	Rh	Rh	Ir	Ir

Scheme I.10

The iridium complex **I.36-1-Bz** [49] was obtained in 48% yield following the same procedure. The iridium complexes **I.37-1-diPh** and **I.37-1-Pr^i** [50], on the other hand, were synthesized from [Ir(acac)(COD)] using Cs_2CO_3 instead of $KN(SiMe)_2$, in yields of 89-99%.

The rhodium [52] and iridium [53] pyridinyl NHC complexes **I.39-R** – **I.42-R** were synthesized from the silver complexes by a transmetalation reaction according to Scheme I.11.

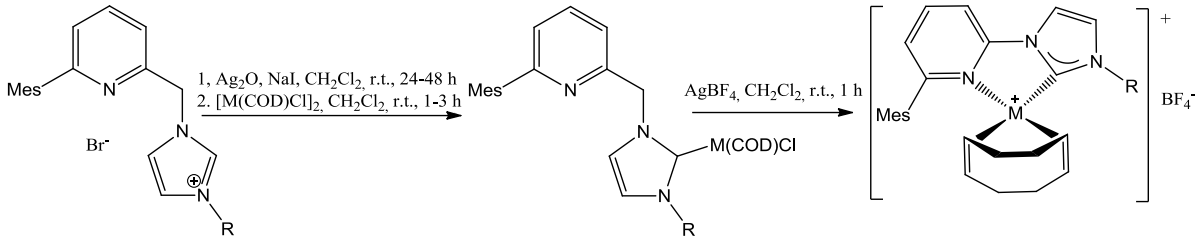

I.38-R

I.39-R (M = Ir, R = Mes, Me)
I.40-R (M = Rh, R = Mes)

73-99%

I.41-R (M = Ir, R = Mes, Me)
I.42-R (M = Rh, R = Mes)

86-96%

Scheme I.11

The iridium complexes containing a NHC-thiazole (**I.43** [54]) or a variety of NHC-oxazoline (**I.44-R^1,R^2** [55]) ligands were obtained from the corresponding azolium salts by stirring the ligand, $[Ir(COD)Cl]_2$, and LiOBu^t (NaOBu^t) in THF at r.t. for 3 h (for **I.43**, refluxing for 1 h to generate the free carbene and then stirring at r.t. overnight). Ion exchange from I^- to $BAr^F{}_4^-$ for **I.43** was accomplished by addition of H_2O followed by $NaBAr^F{}_4$.

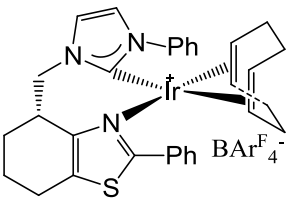

I.43 30%

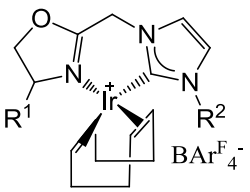

I.44-R^1, R^2 44-83%

R^1 = Bu^t, R^2 = Me
R^1 = Pr^i, R^2 = Me
R^1 = Bu^t, R^2 = Pr^i
R^1 = Bu^t, R^2 = Bu^t
R^1 = Bu^t, R^2 = neopentyl
R^1 = Bu^t, R^2 = isobutyl
R^1 = Bu^t, R^2 = 2,4,6-Me$_3$C$_6$H$_2$

R^1 = 1-Ad, R^2 = Me
R^1 = 1-Ad, R^2 = Pr^i
R^1 = 1-Ad, R^2 = 2,4,6-Me$_3$C$_6$H$_2$
R^1 = 1-Ad, R^2 = neopentyl
R^1 = 1-Ad, R^2 = Bu^t

R^1 = 2,6-Me$_2$C$_6$H$_3$, R^2 = Me
R^1 = 2,6-Me$_2$C$_6$H$_3$, R^2 = Pr^i
R^1 = 2,6-Me$_2$C$_6$H$_3$, R^2 = 2,4,6-Me$_3$C$_6$H$_2$
R^1 = 2,6-Me$_2$C$_6$H$_3$, R^2 = neopentyl
R^1 = 2,6-Me$_2$C$_6$H$_3$, R^2 = Bu^t

Chloride (**I.46**) and cationic (**I.47**) iridium complexes with 1,2,4-triazole ligands were synthesized according to the Scheme I.12 respectively in 84% and 64% yield from **I.45** [56]. The **I.46** complex was obtained as a mixture of two atropoisomers in a 1/1.6 ratio because of restricted rotation along the Ir-carbenic carbon axis.

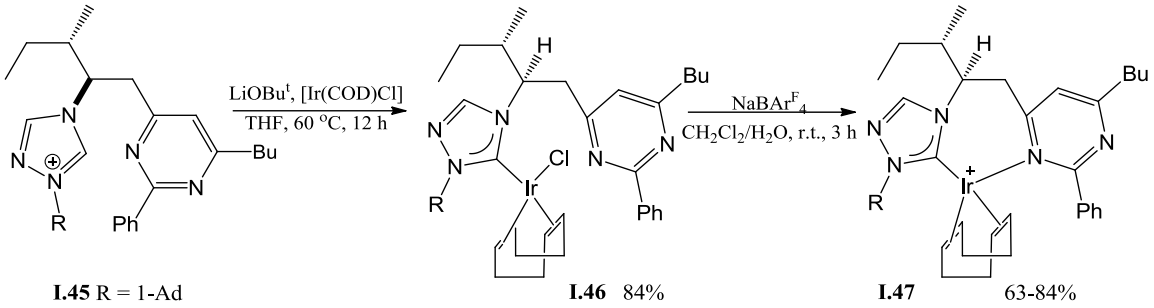

Scheme I.12

Iridium complexes with phosphino-NHC (**I.48**) and phosphinooxy-NHC (**I.49**) ligands were obtained in 69-75% yield by deprotonation of the corresponding imidazolium salts with $NaOBu^t$ in the presence of $[Ir(COD)Cl]_2$ in THF at ambient temperature and characterized by standard 2D-NMR techniques [57].

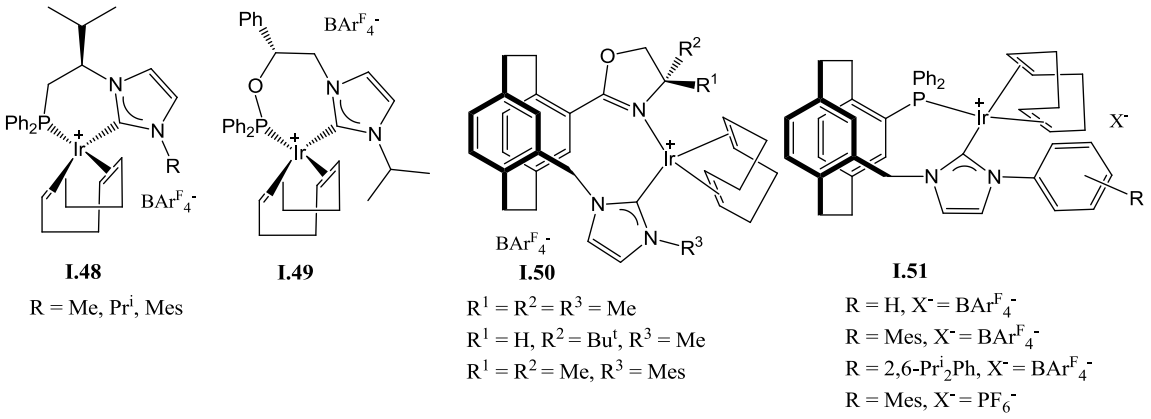

Iridium complexes **I.50** [58] and **I.51** [59] were obtained in 48-91% yield according to the same reaction at 60°C. Ion exchange was accomplished by addition of H_2O and CH_2Cl_2 followed by $NaBAr^F_4$ or KPF_6.

The iridium complex **I.53** with an amine functionalized NHC ligand was synthesized by transmetalation from the Ni(II) complex **I.52** and $[Ir(COD)Cl]_2$ (Scheme I.13) [60]. Complex **I.54** was obtained from complex **I.53** by simple anion exchange with $NaBAr^F_4$. Addition of HCl to **I.53** afforded the iridium(III) hydride complex **I.55** as a mixture of two isomers. The phosphine-amine iridium complex **I.57** was synthesized by transmetalation using the silver complex. Structure of complexes **I.53**, **I.55** and **I.57** was confirmed by X-ray analysis.

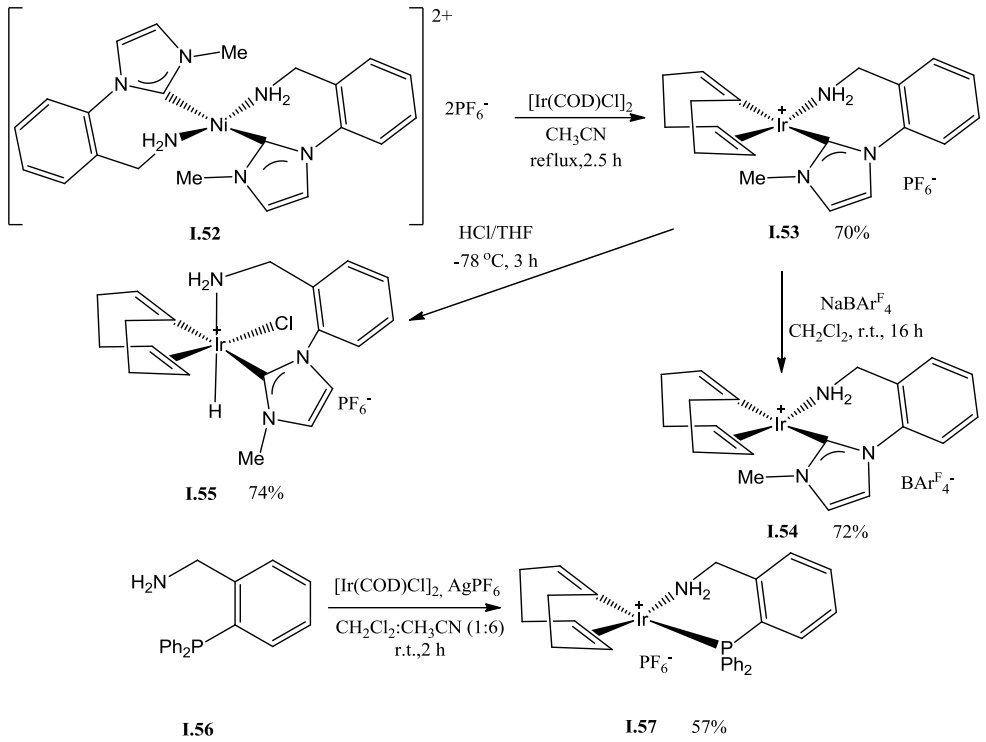

Scheme I.13

A series of neutral and cationic rhodium and iridium complexes based on hemilabile O-donor- and N-donor-functionalized NHC ligands have been synthesized [61]. The hemilabile fragment is coordinated to the iridium center in cationic complexes **I.65**, **I.66** but remains uncoordinated in complexes **I.58-I.64**. The structure of **I.59** (M = Ir) has been determined by X-ray diffraction. The rhodium and iridium complexes **I.58-I.61** containing methoxy-functionalized NHC ligands were synthesized in 64-90% yields by stirring of $[M(COD)(\mu\text{-OMe})]_2$ and corresponding imidazolium bromide (iodide in case of **I.60**) in the THF (or acetone) solution at room temperature. The synthesis of the iridium complexes **I.62** containing dimethylamino-functionalized NHC ligands was carried out in two steps: reaction of imidazolium salt with $[Ir(COD)(\mu\text{-OMe})]_2$ followed by addition of NaH then H_2O (yield 69-72%). Reaction of the bromo complexes **I.58** and **I.59** with $AgBF_4$ in acetone in the presence of 1 equiv. of CH_3CN resulted in formation of the cationic complexes **I.63** and **I.64** in 61-85% yields. The synthesis of the cationic complexes **I.65** and **I.66** was carried out in two steps using a transmetalation reaction. In the first step Ag_2O and imidazolium bromide were refluxed in CH_2Cl_2 for 90 min to obtain the NHC-silver complex. In the second step the solvated salt $[Ir(COD)(OCMe_2)_2]BF_4$, prepared in situ from $AgBF_4$ and $[Ir(COD)Cl]_2$, was added to the solution of the NHC-silver complex and the reaction mixture was stirred for 3 h at room temperature to give the products in 60-77% yields.

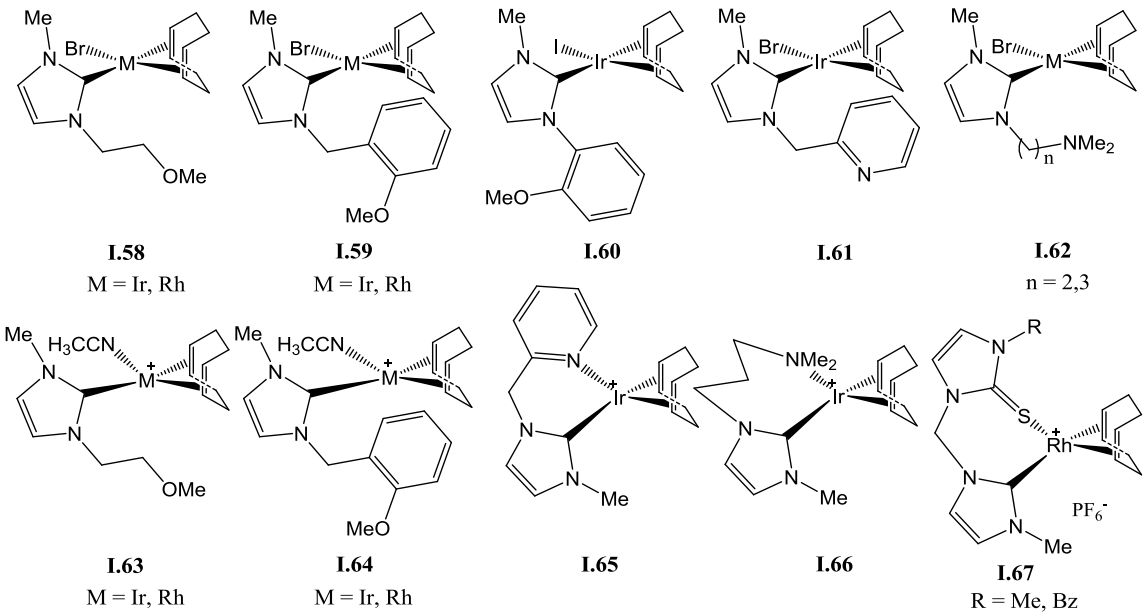

Rhodium complexes **I.67** with NHC-thione ligands were obtained by reaction of the corresponding imodazolium salts with $[Rh(COD)Cl]_2$ in CH_2Cl_2 at room temperature in the presence of NEt_3 [62].

Neutral and cationic rhodium complexes with NHC-oxazoline ligand were synthesised according to the Scheme I.14 [63, 64, 65]. The structure of the complexes was determined by X-ray analysis. It was found that the neutral rhodium complexes have a five coordinated square pyramidal (for the NBD complexes) or trigonal bipyramidal (for the COD complexes) geometry.

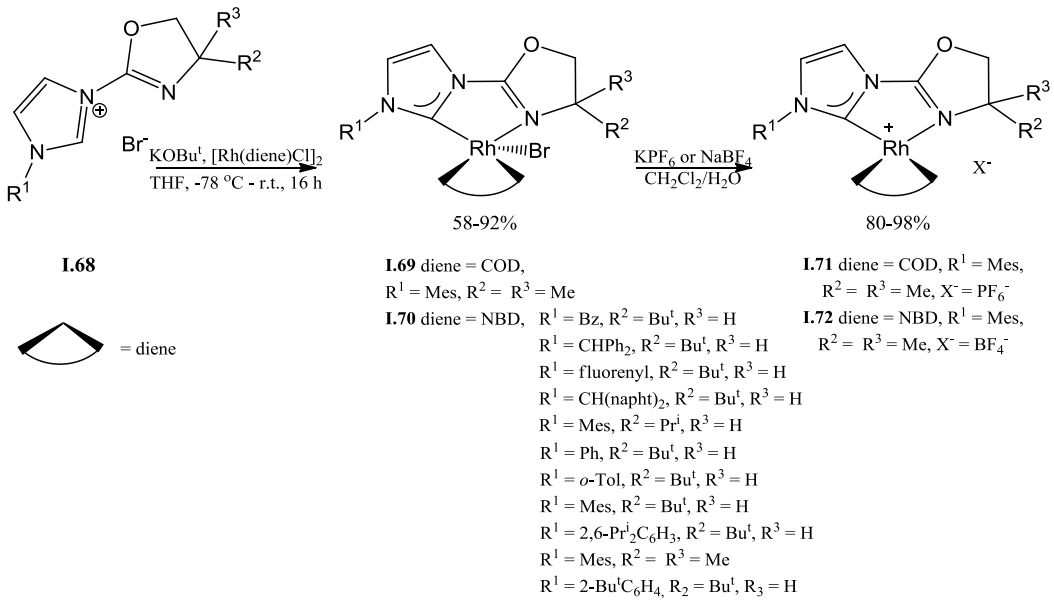

Scheme I.14

I.1.2 Diphosphine ligands

The dicationic rhodium complexes **I.73** and **I.74** were found to have a five coordination geometry [66, 67]. They were synthesized in 72% yields by stirring of $[Rh(COD)Cl]_2$ and the corresponding imidazoliophosphine salts in dichloromethane solution at room temperature. The structure of the complexes was established on the basis of NMR and HRMS data and by derivatization to CO adduct.

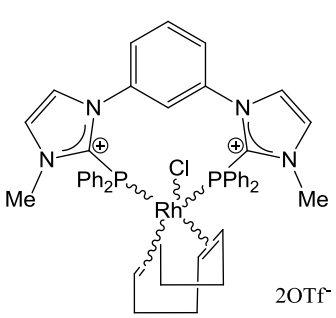

I.73

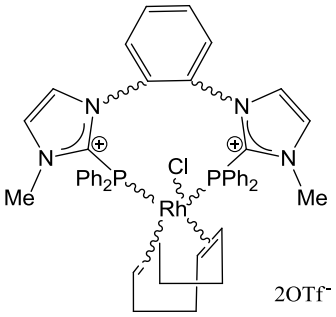

I.74

P,P ligands such as phosphines with alkyl or aryl groups were the first effective ligands used for catalytic asymmetric hydrogenation reactions [68, 69]. Nowadays complexes with a great variety of P-O and P-N bond containing ligands have been demonstrated to have the ability to catalyze a number of organic processes. Recently new rhodium complexes of type $[Rh(P,P)(COD)]SbF_6$ (P,P = (*R*)-3H-BenzP*, (*R*)-3H-QuinoxP*) were obtained in 86-90% yields by addition of 1 equiv. of $[Rh(COD)_2]SbF_6$ to a dichloromethane solution of the corresponding P,P ligand **I.75** or **I.76** [70]. Rhodium complexes $[Rh(P,P)(COD)]BF_4$ with bidentate phosphine/phosphinite ligands **I.77** and **I.78** [71] and bis(diamidophosphite) ligands **I.79** - **I.85** [72] were prepared according to the same procedure in 44-90% yield from $[Rh(COD)_2]BF_4$. The synthesis of other rhodium and iridium complexes, containing different P,P ligands is detailed in a recent review [73].

The rhodium complexes $[Rh(P,P)(COD)]BF_4$ with the aminophosphane/phosphinite ligands **I.86-R** were obtained in 52-92% yields by addition of 1 equiv of $[Rh(COD)_2]BF_4$ to a dichloromethane solution of the corresponding P,P ligand and stirring the reaction mixture for at room temperature [74].

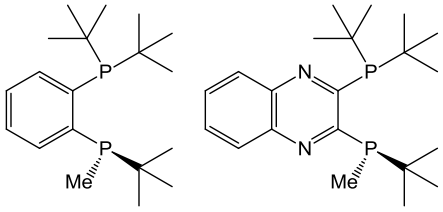

I.75
(*R*)-3H-BenzP*

I.76
(*R*)-3H-QuinoxP*

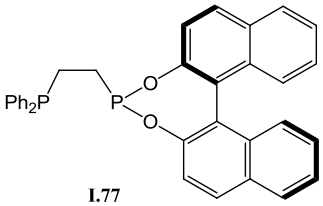

I.77

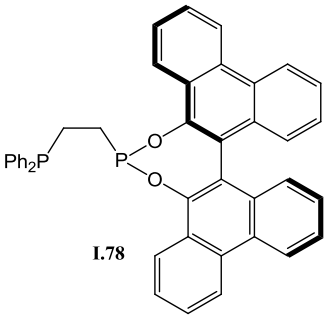

I.78

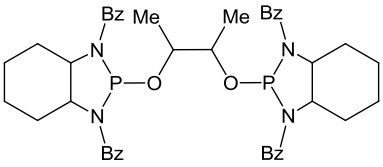

I.79

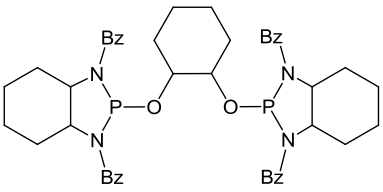

I.80

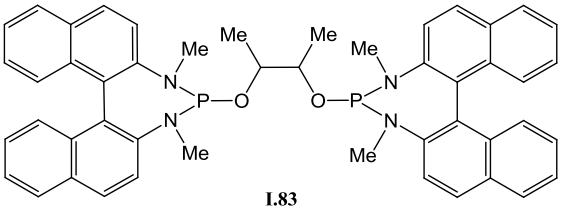

I.83

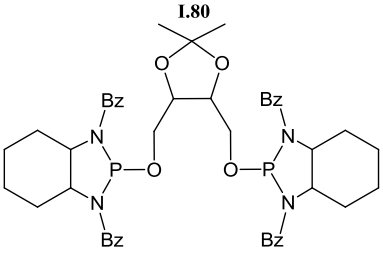

I.81

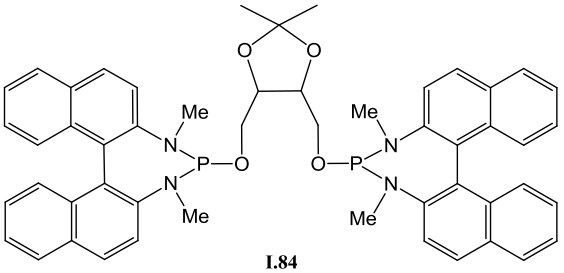

I.84

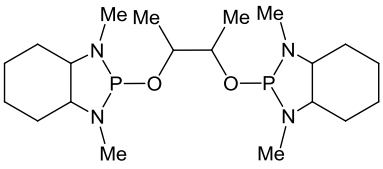

I.82

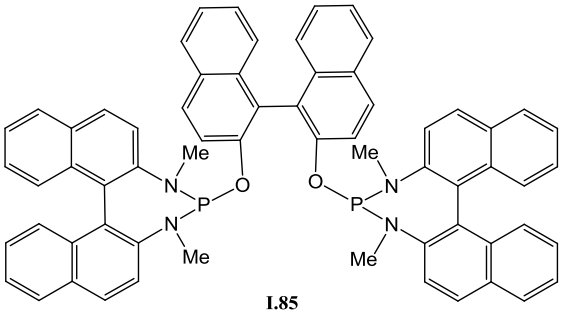

I.85

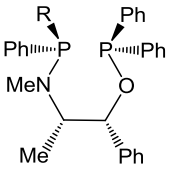

I.86-R

R =

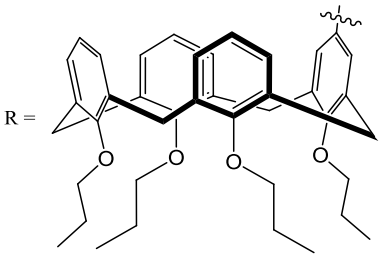

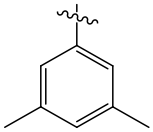

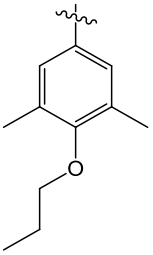

I.1.3 P,N ligands

Rhodium and iridium complexes supported by P,N bidentate ligands have attracted considerable attention. Neutral and charge separated rhodium compounds [Rh(P,N)(diene)X] **I.88** and **I.89** with indene-supported P,N ligand **I.85** were syntesized according to the Scheme I.15 [75].

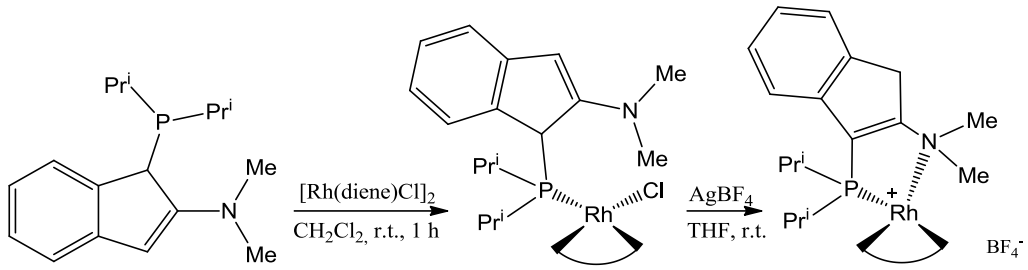

I.87 **I.88** 86-96% **I.89** 87-94%

Scheme I.15

A similar procedure was used for the synthesis of neutral and cationic rhodium complexes [Rh(P,N)(COD)X] **I.91-R** and **I.92-R** with the 7-phospha-3-methyl-1,3,5-triazabicyclo[3.3.1]nonane P,N ligand precursor **I.90-R** (Scheme I.16) [76]. All complexes were fully characterized by NMR and X-ray analysis. All compounds feature a square planar geometry. Complex **I.91-Me** shows a weak interaction between the rhodium center and the *N*-methyl group: the Rh···N distance (3.045 Å) is 0.755 Å shorter than sum of van der Waals radii for Rh and N (3.800 Å).

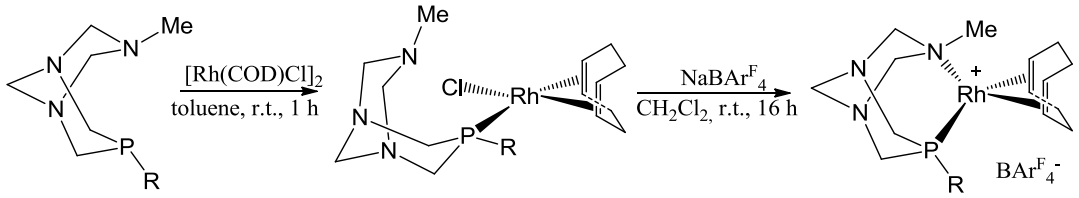

I.90-R
R = Me, Ph

I.91-R
90-93%

I.92-R
73-78%

Scheme I.16

The reaction of $[M(diene)Cl]_2$ (M = Ir, Rh) with 2-pyridyl- and 2-imidazolylphosphines in dichloromethane at room temperature resulted in the formation of the four coordinate, square planar complexes **I.93**-**I.96** in 84-99% yields [77]. In case of the rhodium complex **I.93** with R = Pr^i, R^1 = CF_3 and R^2 = H the use of crude ligand was not sufficient because of the formation of 20-30% of the bromo derivative **I.97**, rationalized by the formation of LiBr during the ligand synthesis and further coordination of Br^- to the metal. The identity of this compound was established by X-ray analysis of a single crystal composed of a solid solution of the chloride and bromide compounds. The reaction of **I.93** (R = Pr^i; R^1 = R^2 = H) with $AgBF_4$ in chloroform at 50°C resulted in the cationic complex **I.99**. The iodide complex **I.98** was obtained in 63% yield by stiring the same chloride complex **I.93** with $AgBF_4$ in dichloromethane at room temperature followed by addition of NaI.

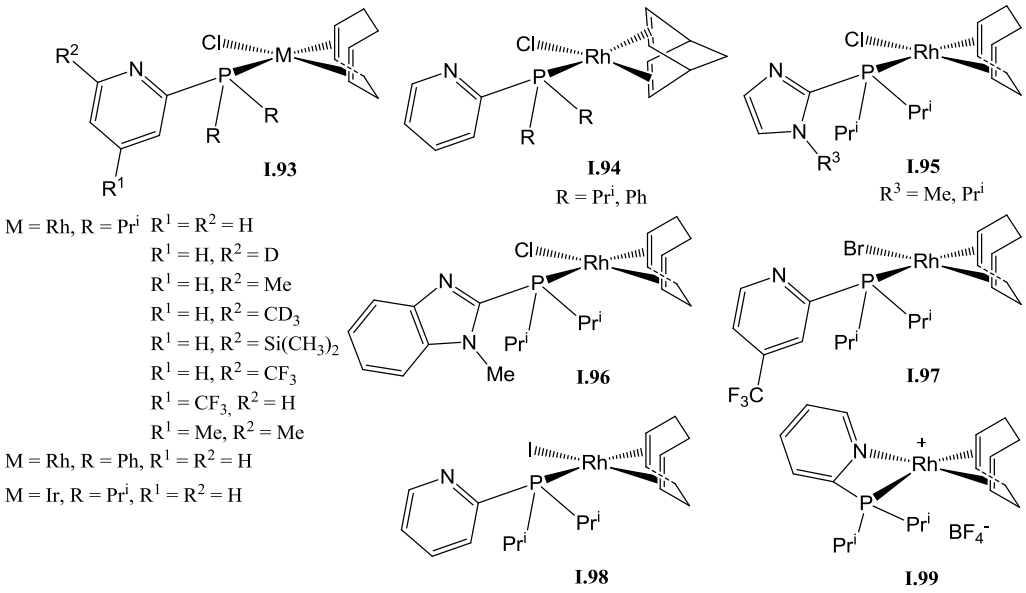

The cationic iridium complexes **I.102** and **I.103** containing the diphenylphosphinite ligands **I.100** and **I.101** were obtained according to the Scheme I.17 and isolated as the $BAr^F_4^-$ salts in 80-97% yields [78].

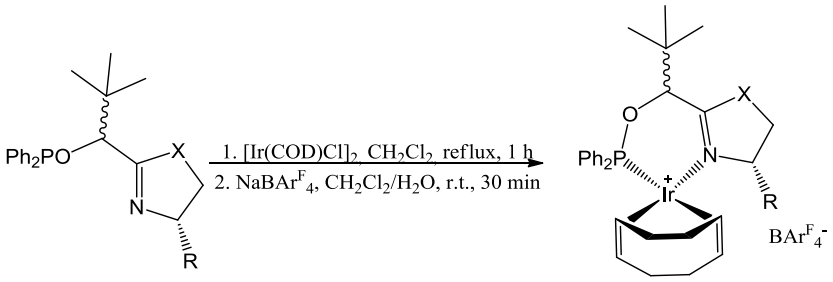

I.100 X = O, R = Pr^i or Bu^t
I.101 X = S, R = Pr^i

I.102 X = O, R = Pr^i or Bu^t
I.103 X = S, R = Pr^i

Scheme I.17

The cationic rhodium complexes **I.105** were synthesized as the BF_4^- salts in 71-83% yields by addition of $[Rh(NBD)_2]BF_4$ to the corresponding phosphine-amine **I.104** (Scheme I.18) [79]. A rhodium complex [Rh(P,N)(COD)]OTf **I.105** ($R^1 = R^2 = H$) was obtained in 63% yield by protonation of phosphine-amido rhodium complex **I.106** with trifluoromethanesulfonic acid.

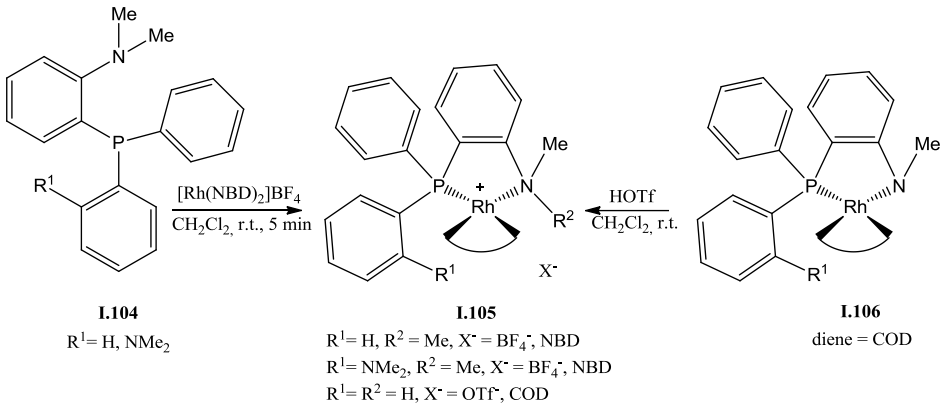

Scheme I.18

Complexation of the phosphino-oxazoline ligands **I.107** to $[Ir(COD)Cl]_2$ followed by anion exchange with $NaBAr^F_4$ in a two-phase dichloromethane/water system led to the cationic iridium complexes **I.108** in 83–98% yields (Scheme I.19) [80].

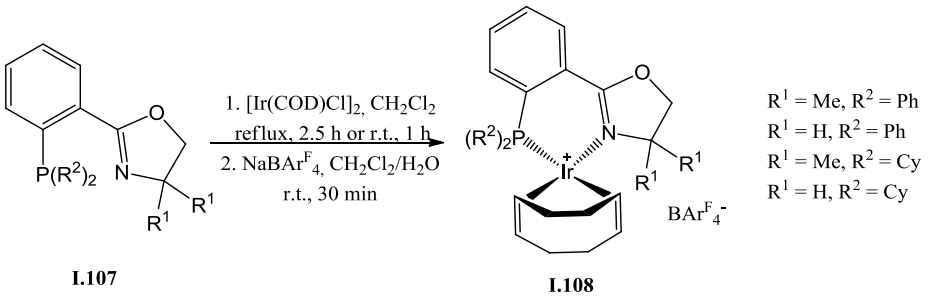

Scheme I.19

The cationic P,N-ferrocenyl iridium complexes **I.109** were obtained in 88-90% yields by reaction of the corresponding ligands **I.110** with $[Ir(COD)Cl]_2$ in dichloromethane followed by the addition of $NaBAr^F_4$ in water (Scheme I.20) [81].

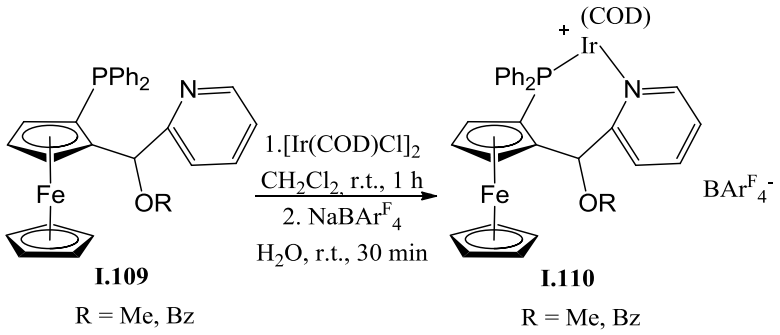

Scheme I.20

The cationic iridium phosphino-imine complex **1.112** was synthesized using aniline as the amine source in a condensation reaction with a phosphine aldehyde, which is generated in situ by deprotonation of the phosphonium dimer **I.111** with base (Scheme I.21) [82]. The addition of NH_4PF_6 yielded the product as the PF_6^- salt in 82% yield. If $NaPF_6$ or KPF_6 were used instead, a mixture of cationic imine and the neutral enamino complexes were observed. Changing the amine from aniline to hydroxylamine and using either the Rh or the Ir precursor resulted in the formation of the phosphino-oxime complexes **I.113**. These complexes were formed as PF_6^- salts, where the rhodium complex was isolated in 70% yield, and the iridium complex in 97% yield.

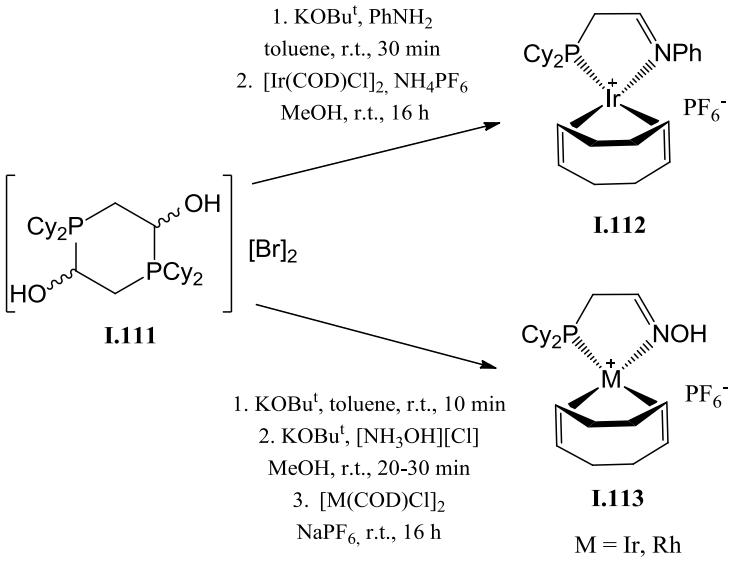

Scheme I.21

I.1.4 P,O ligands

The reaction of 2-(*ortho*-phosphinophenyl)-functionalised 1,3-dioxolanes or dioxanes **I.114-n-R** with $[M(diene)Cl]_2$ (M = Ir, Rh, diene = COD, NBD) resulted in the formation of the corresponding [M(P,O)(diene)Cl] complexes **I.115-n-R**, **I.116** and **I.117** with monodentate coordination of the ligand (Scheme I.22) [83, 84]. The coordination geometry at the Rh center in **I.115-n-R** was established by X-ray analysis as distorted square planar. The presence of a Rh-Cl bond was confirmed by FTIR spectra where the absorption of the Rh-Cl-stretching vibrations are located around 283 cm^{-1} [83]. The cationic rhodium complexes **I.118-R** of type $[Rh(P,O)(COD)]^+$ could be isolated as PF_6^- salts by reacting the complexes **I.115-0-R** with $TlPF_6$, while this reaction was not suitable for obtaining the corresponding dioxane derivatives. However, the $[Rh(P,O)(COD)]BF_4$ salts **I.119-R** could be prepared by direct reaction of the ligands **I.115-1-R** with $[Rh(COD)_2]BF_4$. Compound **I.120** was obtained by reaction of the chloride complex **I.116** with $AgClO_4$ [84].

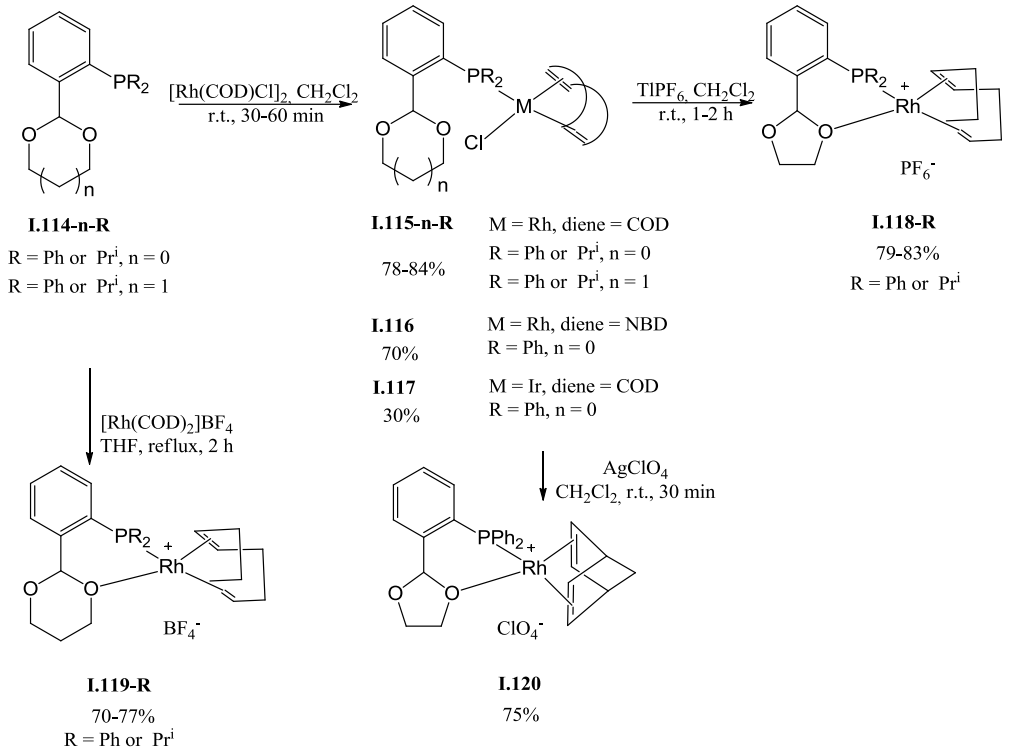

Scheme I.22

The cationic rhodium complexes **I.122** containing the iminophosphorane ligands **I.121** were synthesized in 87-90% yields by addition of $[Rh(COD)_2]BF_4$ to the corresponding ligand precursor (Scheme I.23) [85].

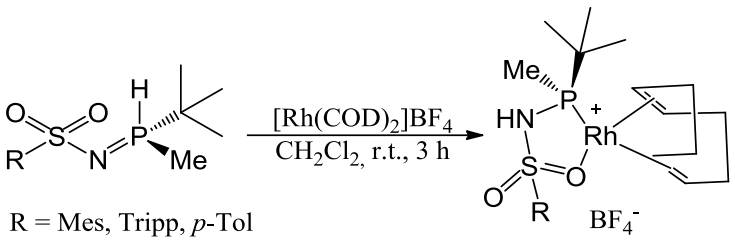

I.121 **I.122**

Scheme I.23

I.1.5 P,S ligands

The neutral P,S-ferrocenyl iridium complexes **I.124-R** were obtained in 86-89% yields by reaction of the corresponding ligand precursors **I.123-R** with $[Ir(COD)Cl]_2$ in dichloromethane in a 2:1 ratio at room temperature (Scheme I.24) [25, 32].

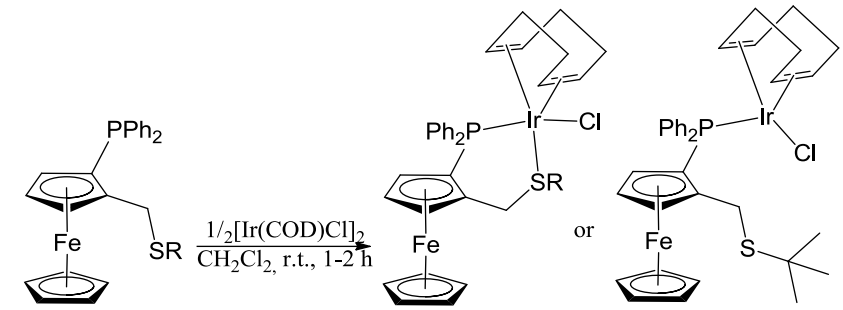

I.123-R

R = Me, Bu^t, Ph, Bz

I.124-R

R = Me, Ph, Bz

Scheme I.24

The four compounds show similar spectroscopic properties in solution, but have different structures in the solid state. Whereas **I.124-Et**, **I.124-Ph** and **I.124-Bz** proved to be five coordinate, their **I.124-Bu^t** analogue is only four coordinate (κ^1:P) with a dangling thioether group. The geometry of **I.124-Bu^t** corresponds quite closely to an ideal square planar with Ir···Cl distance 2.3625(8) Å. The coordination geometry of **I.124-Et**, **I.124-Ph** and **I.124-Bz**, on the other hand, may be best viewed as intermediate between a distorted trigonal-bipyramid and distorted square-pyramid. The Ir···Cl distances in **I.124-Et** and **I.124-Ph** are longer relative to four coordinate complex **I.124-Bu^t** (Ir-Cl distances: 2.3625(8) for **I.124-Bu^t**, 2.5739(19) for **I.124-Et** and 2.5576(12) Å for **I.124-Ph**). For metal/ligand ratios higher than one, the compounds **I.125-R** (R = Et, Bu^t, Ph) were obtained, resulting from the chloride abstraction by the excess iridium metal on complex **I.124-R**. The structure of **I.145-Ph** was confirmed by single-crystal X-ray diffraction. For **I.124-Bu^t** an additional slow equilibration with a third product **I.126**, which contains a bridging P,S-ligand spanning two Ir centers, was observed (Scheme I.25).

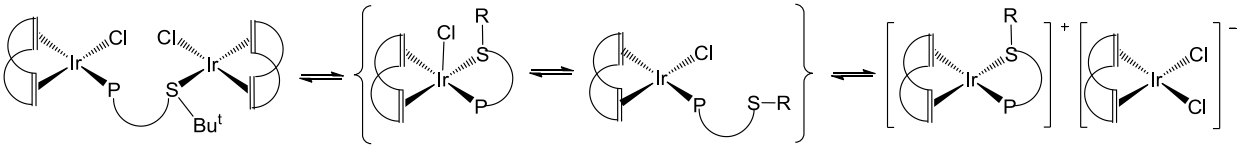

I.126

I.124-R

R=Et, Bu^t, Ph

I.125-R

R=Et, Bu^t, Ph

Scheme I.25

I.1.6 Other miscellaneous P,Z ligands

A series of cationic square-planar rhodium complexes of type $[Rh(R_2P(CH_2)_nZ)(COD)]^+$ **I.127-I.130**, which contained a diverse range of functionalized hemilabile ligands of type $R_2P(CH_2)_nZ$ (n = 1-3; Z = OMe, OEt, NMe_2, SMe), where synthesized, isolated as BF_4^- salts, and spectroscopically characterized [86, 87, 88].

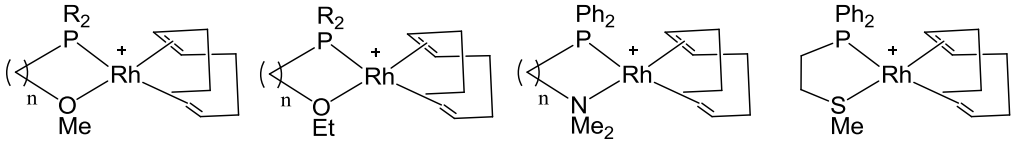

BF_4^- BF_4^- BF_4^- BF_4^-

I.127-n-R **I.128-n-R** **I.129-n-Ph** **I.130**

n = 2, R = Ph
n = 2, R = 4-MeC_6H_4
n = 2, R = 2-MeC_6H_4
n = 3, R = Ph

n = 2, R = Ph
n = 2, R = 4-MeC_6H_4
n = 2, R = 4-$CF_3C_6H_4$
n = 3, R = Ph
n = 3, R = 4-MeC_6H_4
n = 3, R = 4-$CF_3C_6H_4$

n = 2, 3

The preparation of these cationic complexes **I.127-I.130** was accomplished by using several synthetic strategies (Scheme I.26). The reaction of the P,Z ligands with 0.5 equiv. of $[Rh(COD)Cl]_2$ in acetone or THF gave neutral intermediate complexes [Rh(P,Z)(COD)Cl] that were reacted with $AgBF_4$ to afford the target complexes after elimination of AgCl. According to this method complexes **I.127-2-Ph**, **I.127-3-Ph**, **I.128-2-Ph**, **I.128-3-Ph**, **I.128-3-4-$CF_3C_6H_4$**, **I.129-2-Ph** and **I.130** were prepared in 43-88% yields. Alternatively, the compounds could be prepared by addition of 1 equiv. of the P,Z ligand to the solvated complex $[RhS_2(COD)]^+$ (S = acetone or THF) that was formed in situ by the reaction of $[Rh(COD)Cl]_2$ with 2 equiv. of $AgBF_4$. All complexes shown were prepared according to this method in 46-87% yields. In some cases, the complexes were also obtained from $[Rh(COD)_2]BF_4$. This method was used for the preparation of complexes such as **I.127-2-Ph**, **I.128-3-Ph**, **I.128-2-Ph**, **I.128-2-4-MeC_6H_4**, **I.128-2-4-$CF_3C_6H_4$**, **I.128-3-Ph** and **I.128-3-4-$CF_3C_6H_4$** in 40-65% yields. Finally, complexes **I.127-2-Ph**, **I.128-2-4-MeC_6H_4** and **I.128-3-4-MeC_6H_4** were also prepared in 46-70% yields by the reaction of the methoxy-bridged complex $[Rh(COD)(OMe)]_2$ with the appropriate phosphonium salt of the functionalized phosphine.

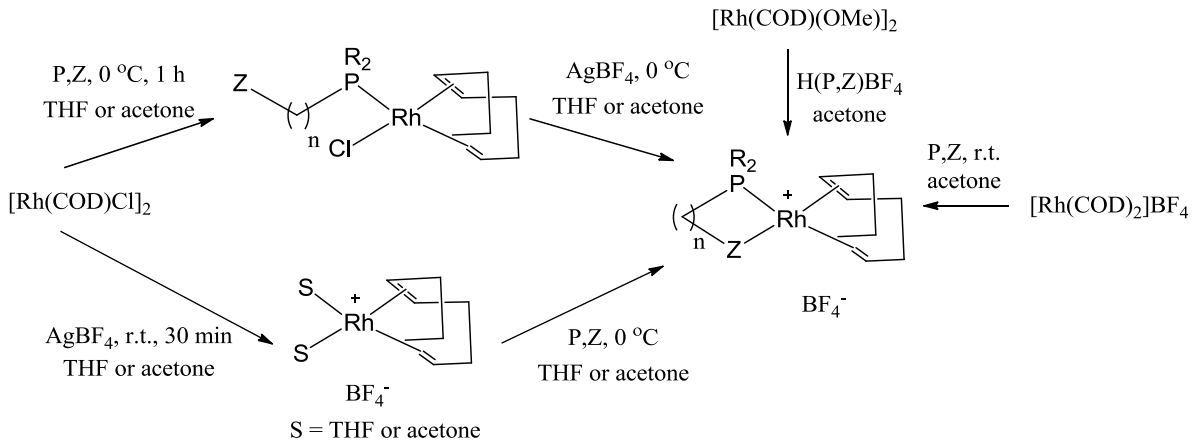

Scheme I.26

Using the first two methods, new rhodium complexes related to **I.138-3-Ph** with NBD and TFB (tetrafluorobenzobarrelene) ligands in place of COD were synthesized in 55-61% yields [87]. The crystal structure of **I.136-2-Ph**, **I.136-2-4-MeC$_6$H$_4$**, **I.138-3-Ph**, **I.137-3-Ph** and **I.137-2-3-MeC$_6$H$_4$** have been determined by X-ray analysis. All complexes show a square planar geometry with bidentate coordination of the ligand. However, the P,O ligand in complex **I.137-2-3-MeC$_6$H$_4$** was linked to the rhodium atom in a monodentate (κ^1-P) manner, with the fourth coordination position occupied by an acetone molecule (which was used as a solvent). The NMR spectrum in solution showed the absence of the corresponding resonances for coordinated acetone and the presence of resonances that were typical of chelated phosphine ligand.

I.1.7 N,N and N,O ligands

Several rhodium and iridium complexes with bidentate N,N ligands were synthesized. Thus cationic rhodium and iridium complexes containing pyrazolyl-triazolyl ligands as N-donors **I.132** were prepared according to Scheme I.27 in 64-93% yields [89]. The structure of the complexes was determined by X-ray analysis. The rhodium complex **I.133** containing the (*R*)-1,1'-binaphthyl-2,2'-diamine ligand was obtained in quantitative yield by addition of $AgBF_4$ to the dichloromethane solution of the ligand and $[Rh(COD\text{-}Ph)Cl]_2$ [90].

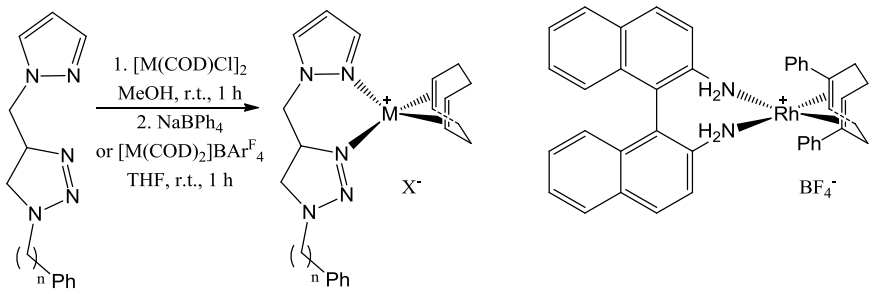

I.131 **I.132** **I.133**

M = Rh, Ir; n = 1, 0; X^- = BPh_4^-
M = Rh, Ir; n = 1; X^- = $BAr^F{}_4^-$

Scheme I.27

Stirring of a variety of β-amino alcohols and $[Rh(COD)Cl]_2$ in toluene solution at room temperature resulted in the formation of the rhodium complexes **I.134-I.138** with the ligand monodentate κ^1:N coordination in 85-96% yields [91]. The structure of a few of these complexes was proven by X-ray analysis. It was found that the individual complexes are packed in the crystal through intermolecular O-H···Cl and N-H···Cl hydrogen bonds from the dangling hydroxyl group and the ligated amino groups to the chlorido ligands of neighboring molecules. Complexes **I.134-I.138** were converted into the corresponding triflate salts **I.139-I.143** that feature a chelating κ^2:N,O coordination

of the aminoalcohol ligands in 88-98% yields by addition of TlO_3SCF_3. In solid state structures of **I.139-I.143**, the cationic complexes and their counterions are linked by hydrogen-bonding of the coordinated amino and hydroxyl donors to the triflate anion acceptors. Attempts to obtain cationic rhodium complexes by reaction with soluble silver salts such as $AgBF_4$ or AgO_3SCF_3 resulted in the deposition of elemental silver rather than precipitation of silver chloride with concominant decomposition of the compounds.

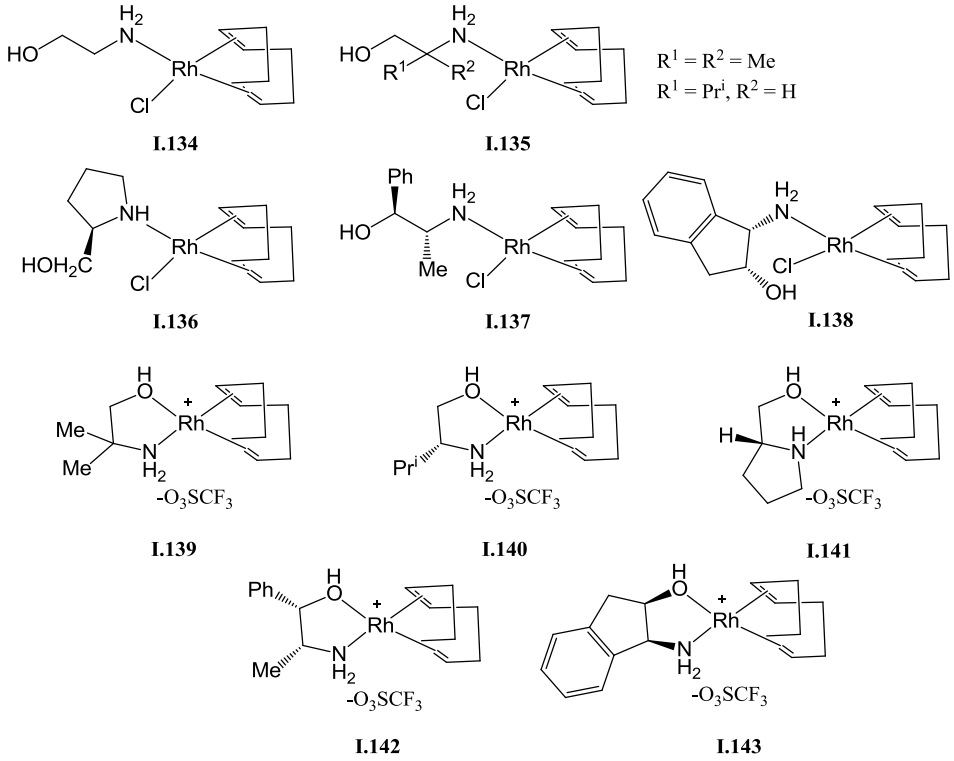

I.2 Activation of [M(L,L')(diene)X] complexes

I.2.1 Activation of rhodium complexes

Since the development by Noyori and coworkers of efficient catalytic systems for the asymmetric hydrogenation of non-functionalized ketones [68, 69, 92], much effort has been devoted to the asymmetric hydrogenation of polar substrates [93], ketones [94] but also imines [95-98] or heteroarenes [99], because of their great scientific and practical importance. Mechanistic studies of the Rh-catalyzed asymmetric hydrogenation began shortly after the discovery of the efficient diphosphine–Rh catalysts.

I.2.1.1 Formation of solvated complexes

Studies of the stoichiometric hydrogenation of [Rh(L,L')(diene)X] or $[Rh(L,L')(diene)]^+$ complexes began with the works of R. R. Schrock [100, 101, 102]. Addition of H_2 to the solution of

$[RhL_2(NBD)]^+$ (**I.144**, L = PPh_3, $PPhMe_2$, PPh_2Me, $AsPh_3$, PMe_3, $AsPhMe_2$, PPh_2Cy (Cy = C_6H_{11}); Solv = acetone, ethanol or acetonitrile) leads to the formation of dihydride complexes $[RhH_2L_2(Solv)_2]^+$ (**I.145**) or $[RhH_2L_2(Solv^1)(Solv^2)]^+$ (in a mixed solvent) and to the hydrogenation of NBD to norbornane [103] (Scheme I.28). The hydrogenation of $[Rh(dppe)(NBD)]^+$ (**I.146**, dppe = 1,2-bis(diphenylphosphino)ethane) was studied by J. Halpern *et al.* [104]. In methanol solution **I.146** was found to react with H_2 yielding norbornane and a cationic Rh(I) complex $[Rh(dppe)]^+$ (**I.147**). This result is in marked contrast to that reported in [100, 101, 102] for $[Rh(PPh_3)_2(NBD)]^+$, for which the reaction with H_2 under same conditions yields the Rh(III)-dihydride complex **I.145** (Scheme I.28) Complexes **I.145** (Solv = CH_3CN, EtOH, acetone) were isolated and characterized by IR and ^1H NMR in CH_2Cl_2 [103].

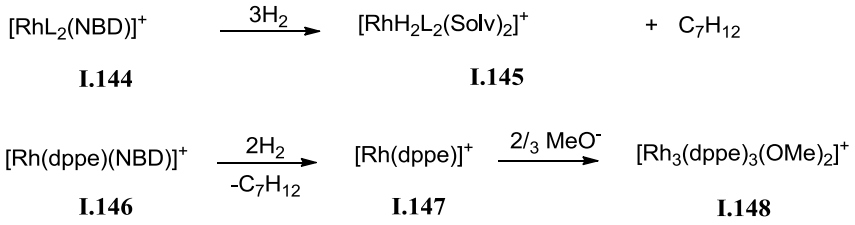

Scheme I.28

Complex **I.147** was isolated as the BF_4^- salt and shown by single-crystal X-ray diffraction to have a methanol-free structure corresponding to discrete binuclear $[Rh_2(dppe)_2]^{2+}$ ions in which each Rh atom is bonded to two P atoms of a diphos ligand and, through symmetrical π-arene coordination, to a phenyl ring of the diphos ligand of the second Rh atom [104]. In methanol solution, $[Rh_2(dppe)_2][BF_4]_2$ apparently dissociates into mononuclear $[Rh(dppe)]^+$ ions, which are probably saturated by solvent coordination. When a base (OMe^- or a sterically hindered amine such as triethylamine) was added to a methanol solution of $[Rh(dppe)]^+$ a new species $[Rh_3(dppe)_3(OMe)_2]^+$ (**I.148**) was observed, the structure of which was established by single crystal X-ray diffraction.

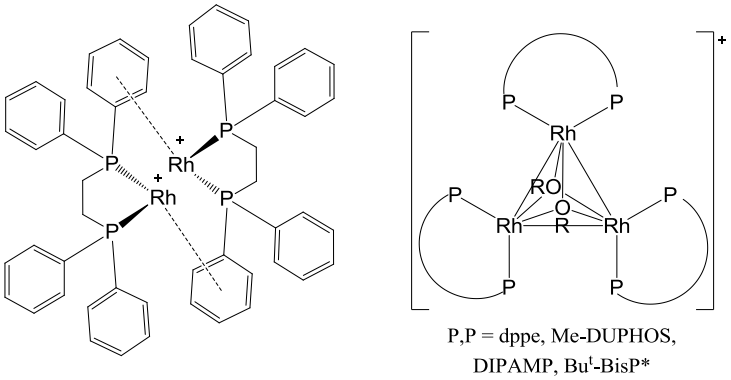

I.147

P,P = dppe, Me-DUPHOS, DIPAMP, Bu^t-BisP*
R = Me, H
I.148-R

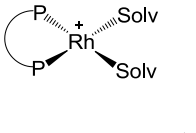

$[Rh(P,P)(Solv)_2]^+$

I.149

Since that time Rh solvated complexes $[Rh(P,P)(Solv)_2]^+$ **I.149** with different diphosphine ligands containing two formally vacant coordination sites were obtained and reliably characterized both in solution and in the solid state. P,P ligands used in the studies of rhodium complexes activation are presented on Fig I.1.

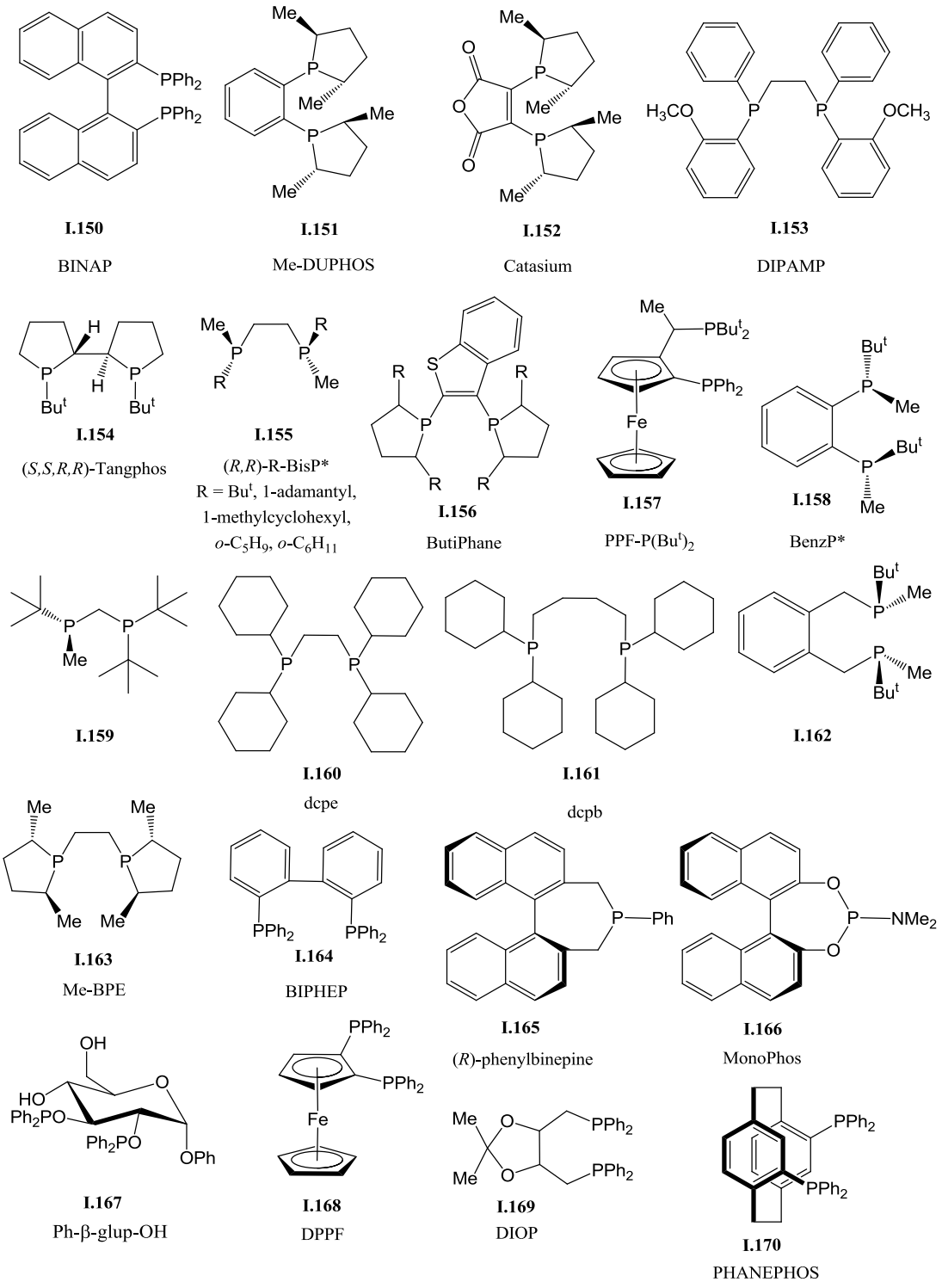

Fig. I.1. P,P ligands used in the studies of rhodium complexes activation

Thus hydrogenation of $[Rh(BINAP)(diene)]^+$ (BINAP = 1,1'-binaphthalene-2,2'-diylbis(phenylphosphine), **I.150**; diene = COD or NBD) in methanol resulted in the solvated complex **I.149** (P,P = BINAP, Solv = MeOH) [105, 106]. A single crystal of this complex suitable for X-ray analysis was obtained as the BF_4^- salt, as well as single crystals of salts of other solvated complexes such as $[Rh((R)\text{-BINAP})(acetone)_2]BF_4$ and $[Rh((S)\text{-BINAP})(THF)_2]BF_4$ [107]. In other coordinating solvents such as EtOH, Pr^iOH and propylene carbonate the hydrogenation of $[Rh(BINAP)(NBD)]^+$ also led to the corresponding solvated complexes. However, their formation was established only in solution.

A single crystal suitable for X-ray analysis was also obtained for the solvated complex $[Rh(dpephos)(acetone)_2]^+$ (**I.171**) as a salt with the carborane ion $CB_{11}H_6Cl_6^-$, which was generated by hydrogenation of $[Rh(dpephos)(NBD)]CB_{11}H_6Cl_6$ in acetone [108]. However, complex **I.172**, in which the sulfur donor is expected to bind more strongly with the Rh center, does not react with H_2. The hydrogenation of complex **I.173** also resulted in the formation of a solvated complex [108].

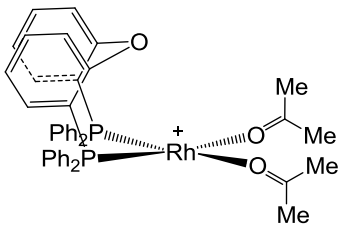

I.171

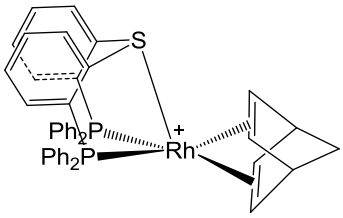

I.172

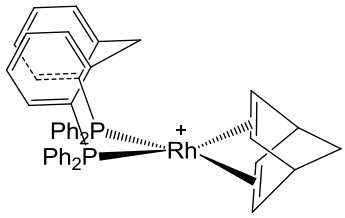

I.173

The formation of solvated complexes usually results in an induction time, which is manifested in the catalytic asymmetric hydrogenation of prochiral olefins by a distinct activity increase during the hydrogenation as a result of the simultaneous hydrogenation of the prochiral substrate and of the diene in the precatalyst. As long as the diene ligand is coordinated to the metal, a certain amount of the catalyst is unavailable for the intended asymmetric hydrogenation because the diene complex is catalytically inactive or much less active than the solvated complex. This feature was proven by an in situ NMR spectroscopy study of the asymmetric hydrogenation of (*Z*)-methyl-*N*-benzoylaminocinnamate in CD_3OD with a precatalyst containing the diphosphine ligand 1,2-bis(2,5-dimethylphospholano)benzene (Et-DUPHOS, **I.151**), $[Rh(Et\text{-}DUPHOS)(COD)]^+$ [109]. The new signals showing up on increasing conversion from substrate to product are not due to the major catalyst-substrate complex and there are more species besides the expected solvated complex $[Rh(Et\text{-}DUPHOS)(CD_3OD)_2]^+$ [109]. The nature of these species will be addressed later.

The rate of hydrogenation of the rhodium complexes depends on the phosphine ligand, diene and also the anion in some cases. The hydrogenation of COD and NBD for complexes of type

[Rh(L,L')(diene)]$^+$ in the presence of BF_4^- as counterion was quantified for the ligands BINAP, Me-DUPHOS, Catasium (**I.152**) [105], DIPAMP (**I.153**, 1,2-bis[(2-dimethoxyphenyl)(phenyl-phosphino)]ethane) [110], (*S*,*S*,*R*,*R*)-Tanghos (**I.154**), (*R*,*R*)-Bu^t-BisP* (**I.155**) [111] and (*R*,*R*)-R-ButiPhane (**I.156**) (R = Me, Et, Pr^i) [112] in methanol, ethanol, isopropanol, THF, TFE and propylene carbonate. To compare several precatalysts in terms of the expected induction period and the time needed for quantitative elimination of the diene, pseudo rate constants $k'_{2\text{diene}}$ for the diene hydrogenation were determined according to Scheme I.29 (see Table I.1). The degree of conversion determined from pseudo rate constants as a function of prehydrogenation time was tested and verified by means of ^{31}P NMR spectroscopy. It was found that the NBD complexes are always hydrogenated much faster (> 2 orders of magnitude) than the corresponding COD complexes under the same conditions in all solvents.

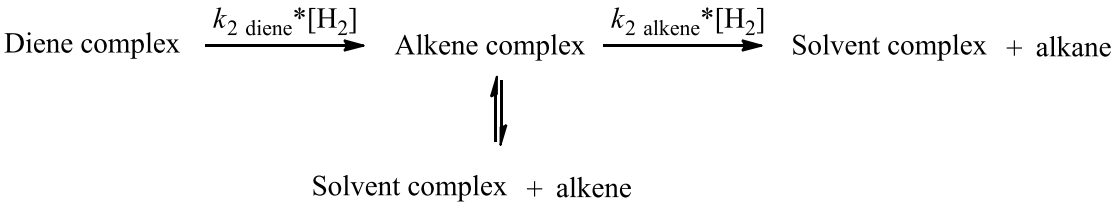

Scheme I.29 Reaction sequence for the hydrogenation of diene complexes to the corresponding solvated complexes and the alkanes.

Table I.1 Pseudo rate constants k'$_{2\ \text{diene}}$ (min^{-1}) of catalytic diene hydrogenations for several ligands and solvents.

Ligand	Diene	Solvent					
		MeOH	THF	Propylene carbonate	EtOH	Pr^{i}OH	TFE
Me-DUPHOS	COD	0.115	0.16	0.14			
	NBD	35.2	39.0	18.0			
BINAP	COD	0.23	0.28	0.14			
	NBD	26.8	20.5	16.6			
Catasium	COD	0.05	ca. 0.15	0.085			
	NBD	24.9	11.8	9.4			
DIPAMP	COD	0.0028					
	NBD	ca. 9	5.0	4.8	13.2	5.9	3.9
Tanghos	COD	0.375					
	NBD	194.4					
Bu^t-BisP*	COD	0.21					
	NBD	89.9					
Me-ButiPhane	COD	0.119					
Et-ButiPhane	COD	0.031					
Pr^i-ButiPhane	COD	0.009					

For very slow olefin hydrogenations such as those of complexes $[Rh(L,L')(COD)]^+$ with ligands Me-DUPHOS, Et-DUPHOS and dppe, the UV/Vis spectroscopic monitoring of the stoichiometric hydrogenation proved to be an appropriate method to determine the desired pseudo rate constants (k'_{2diene} = 0.1177, 0.028 and 0.0033 min^{-1} respectively) [105]. The rate constants for complexes with DIPAMP **I.153**, Tanghos **I.154**, Bu^t-BisP* **I.155** and R-ButiPhane **I.156** ligands determined by UV/Vis spectroscopic monitoring were similar to those obtained independently from a fit of the catalytic hydrogenation kinetics [110, 111, 112]. The transformation of the [Rh(BINAP)(COD)]X precatalyst, where X = BF_4^-, OTf^- or BAr^{F-}, into active species is not influenced by the chosen counterion [106], as could be expected since these are "non-coordinating" anions.

The cationic rhodium solvated complex **I.149** (P,P = PPF-P(Bu^t)$_2$ = {(*R*)-(-)-1-[(*S*)-2-(diphenylphosphino)ferrocenyl]ethylbis(*tret*-butyl)phosphine}, **I.157**; Solv = THF) was obtained by hydrogenation of [Rh(PPF-P(Bu^t)$_2$)(NBD)]BF_4 in THF under 1 bar of hydrogen pressure at ambient temperature in 2 min. This complex proved to be a suitable catalyst for the asymmetric ring opening reaction of benzo-7-oxabicyclo-[2.2.1]heptadiene [113].

Hydrogenation of the precatalyst [Rh(*R*,*R*)-BenzP*)(NBD)]SbF_6 (BenzP* = 1,2-bis(*tert*-butylmethylphosphino)benzene, **I.158**) with 1 atm of H_2 at ambient temperature smoothly gave the corresponding solvated complex **I.149** in 10 min [114]. Complex **I.149** with P,P = (*R*)-(*tert*-butylmethylphosphino)(di-*tert*-butylphosphino)methane (**I.159**) and Solv = CD_3OD was obtained according to the same procedure in 1.5 h from the methanol solution of [Rh(**I.159**)(COD)]BF_4 [115] and characterized spectroscopically in solution. Complexes **I.149** with P,P = 1,2-bis(dicyclohexyl-phosphino)ethane, (dcpe, **I.160**) or 1,2-bis(dicyclohexyl-phosphino)butane (dcpb, **I.161**) and Solv = MeOH were also prepared by hydrogenation of the corresponding cationic rhodium-diene complexes $[Rh(P,P)(diene)]^+$ (diene = COD, NBD) in methanol [116].

I.2.1.2 Solvated dihydride complexes and further speciation

It was found that complexes **I.149** react with dihydrogen at low temperatures with formation of the corresponding dihydride rhodium complexes $[Rh(P,P)(Solv)_2H_2]^+$ (**I.174**, Scheme I.30). Two isomers **I.174a** and **I.174b** as shown in the Scheme I.30 are expected when the P,P ligand is non-symmetric. The first observed complex of this type was $[Rh(Bu^t\text{-BisP*})(CD_3OD)_2H_2]^+$ which was obtained by hydrogenation of **I.149** (P,P = Bu^t-BisP*, Solv = CD_3OD) at -90°C [117]. The reaction is reversible and stereoselective, the two isomers **I.174a** and **I.174b** being formed in a 10:1 ratio. It was observed that the dihydrides can interchange their positions intramolecularly without ligand dissociation. The hydrogenation of the same complex using HD gave a mixture of four compounds, namely two diastereomeric pairs of isotopomers.

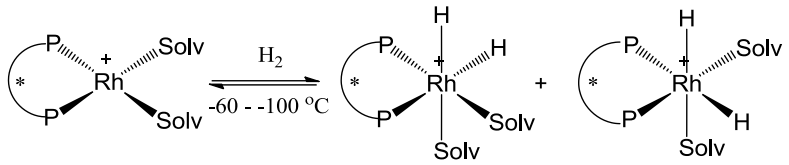

I.149 **I.174a** **I.174b**

Scheme I.30

The hydrogenation of related $[Rh(R\text{-}BisP^*)(CD_3OD)_2]^+$ complexes with R = 1-adamantyl, 1-methylcyclohexyl, *o*-C_5H_9 and *o*-C_6H_{11} (**I.155**) is equally equilibrated and yielded similar dihydride complexes **I.174** in equilibrium with the starting Rh^I solvated complex [118]. The diastereomeric ratio in the dihydride products varies from 10:1 to 20:1 depending on the ligand and did not change when the temperature was varied from -100 to -50°C.

Unlike all the previously described examples, the hydrogenation of complex $[Rh(P,P)(NBD)]^+$ with P,P = (S,S)-α,α'-Bis(*tert*-butylphosphino)-*o*-xylene (**I.162**) with 2 atm of dihydrogen for 10 min at -70°C gave the solvated dihydride complexes $[Rh(\mathbf{I.162})(CD_3OD)_2H_2]^+$ of types **I.174a** and **I.174b** quantitativelyin a 1 : 0.07 ratio [119]. The dihydrides were stable as long as the temperature was kept below -20°C, but when heated to 20°C further transformation of the solvated dihydride complexes took place, yielding a bridging binuclear complex **I.175**.

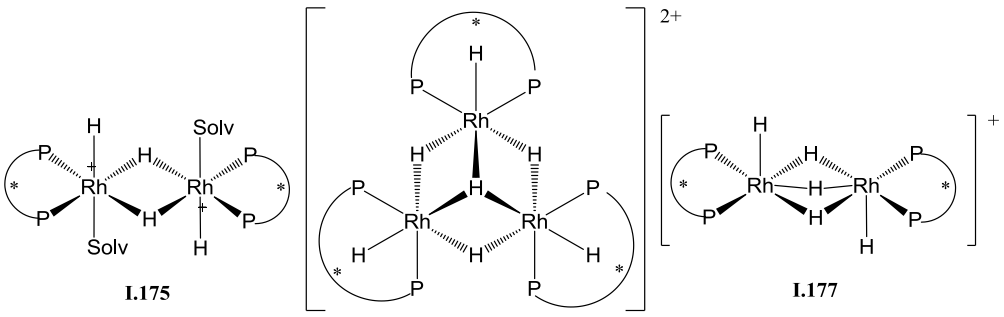

I.175

P,P = **I.161**
Solv = MeOD

I.176

P,P = Tangphos, Me-DUPHOS, Bu^t-BisP*, Me-BPE, dcpe, dcpb

I.177

P,P = dcpe, dcpb, Me-BPE

The solvated-dihydride complexes $[Rh(Tangphos)(MeOH)_2H_2]^+$ (Tangphos = **I.154**) and $[Rh(Me\text{-}BPE)(MeOH)_2H_2]^+$ (Me-BPE = **I.163**) of type **I.174** were observed at -80°C with a $[Rh(Tangphos)(MeOH)_2H_2]^+$:$[Rh(Tangphos)(MeOH)_2]^+$ ratio of 4 : 96. For this phosphine ligand the solvated-dihydride complexes could be detected only when the diene of the precatalyst was hydrogenated at -20°C and the solution inside the NMR tube was instantaneously cooled to -80°C [116].

The stoichiometric hydrogenation of $[Rh(P,P)(diene)]^+$ complexes (P,P = Me-DUPHOS, (*S,S,R,R*)-Tanghos, (*R,R*)-Bu^t-BisP*) in MeOH at 25°C leads to the formation of not only the solvated complexes but also of the trinuclear rhodium hydride complexes **I.176**, which precipitates from the solution when it stands for some time (hours) under a hydrogen atmosphere [111]. Complexes **I.176** were fully characterized by NMR, ESI-MS and IR spectroscopy. The X-ray structure features three rhodium centers bridged by one μ_3-hydride, three edge bridging μ_2-hydrides and one terminal hydride on each rhodium atom. The unit cell contains two BF_4^- anions defining the Rh_3 species **I.176** as a dication which therefore contains Rh(III). Dissolution of the isolated crystals in MeOH under an argon atmosphere leads to the solvated complexes **I.149**, thus indicating that the formation of these species is reversible. When $[Rh(Bu^t\text{-BisP*})(NBD)]^+$ was hydrogenated at -20°C and the solution was cooled down to -90°C immediately afterwards, only the solvated-dihydride complexes **I.174** were observed. However, when NBD was hydrogenated at 25°C and the solution was slowly cooled down, both the solvated dihydrides **I.174** and the trinuclear rhodium complex **I.176** could be detected at the same time.

When the solvated complex **I.149** (P,P = Tangphos; S = MeOH) was generated at room temperature and slowly cooled to -90°C under a hydrogen atmosphere, the trinuclear rhodium-hydride complexes **I.176** could be detected. When, however, the solutions of $[Rh(DCPE)(COD)]^+$ or $[Rh(DCPB)(COD)]^+$ were hydrogenated for 4-6 h at room temperature, the cationic dinuclear Rh(III)-hydride complexes **I.177** were formed, the structure of which was determined by single crystal X-ray analysis [116].

Under certain conditions, the solvated complex **I.149** (P,P = Me-BPE), the solvate-hydride **I.174** and the trinuclear rhodium-hydride complex **I.176** (Solv = MeOH) can coexist in solution [116]. Additionally, the dinuclear rhodium-hydride complex **I.177** could be also detected when either slightly changing the temperature during the hydrogenation of the diene (from -20°C to room temperature) or during the low-temperature NMR measurement (from -90 to -75°C). At the constant temperature of -75°C the concentration of the solvated-dihydride complex **I.174** decreased with time, along with concomitant increase of those of the trinuclear and dinuclear rhodium-hydride complexes **I.176** and **I.177**. Because both the trinuclear rhodium-hydride **I.176** and the solvated complex **I.149** are stable at room temperature, it follows that the solvated-dihydride **I.174** and the dinuclear rhodium hydride complex **I.177** must be intermediates in the formation of the trinuclear complexes. From the experimental findings, a reversible reaction sequence for the formation of the trinuclear rhodium hydride complexes **I.176** was deduced (Scheme I.31). The process is reversible and no other species were detected for these electron-rich ligands (Me-BPE, dcpe, dcpb). For the system with P,P = dcpe

(**I.160**) and Solv = MeOH, the equilibrium composition of the **I.149**- **I.176** mixture at room temperature in methanol was 60 : 40 [116].

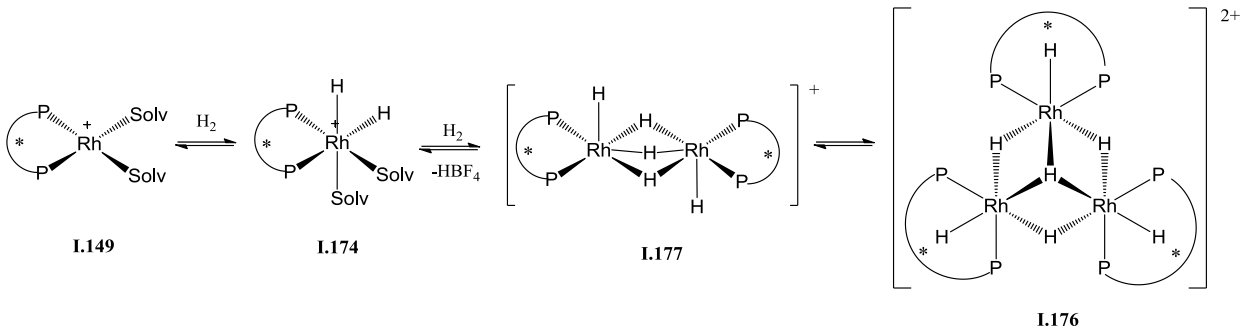

I.149 **I.174** **I.177** **I.176**

Scheme I.31

The vibrational frequencies of the terminal-, μ_2-, and μ_3-X (X = H, D) in the trinuclear rhodium complexes **I.176** were calculated and experimentally determined by Raman and IR spectroscopy for P,P = Tangphos, Bu^t-BisP* and Me-BPE [120]. The IR spectrum displays a week band at about 2060 cm^{-1} for the Rh-H$_{terminal}$ vibrations. To show that this band corresponds to the terminal Rh-H band, two similar complexes were synthesized and investigated: the deuterated analogue {[Rh(Tangphos)D]$_3$(μ_2-D)$_3$(μ_3-D)}(BF$_4$)$_2$ and a trinuclear complex bearing no hydride at all, [Rh$_3$(Tangphos)$_3$(μ_3-Cl)$_2$]BF$_4$ (**I.178**). The trinuclear deuteride complex was obtained by the same method used for the synthesis of **I.176**, except that D$_2$ was used instead of H$_2$ and MeOD instead of MeOH. The trinuclear chlorido complex **I.178** (P,P = Tangphos) was synthesized by addition of methanol solution of NaCl to **I.149**. The IR/Raman spectra of these hydride-free complexes do not show the band at 2060 cm^{-1}. For the deuterated analogue {[Rh(Tangphos)D]$_3$(μ_2-D)$_3$(μ_3-D)}(BF$_4$)$_2$ a new band appears in the IR spectrum at 1460 cm^{-1} and more clearly in the Raman spectrum at 1474 cm^{-1}, which was assigned to terminal Rh-D vibrations (ν_{RhH}/ν_{RhD} = 1.4). The vibration of the μ_2-hydrogen atoms was assigned unequivocally to a band observed at about 1500 cm^{-1} in the Raman spectrum. In the corresponding IR spectrum the μ_2 Rh-H was assigned only tentatively. In the deuterated complex, the μ_2-Rh-D vibrations were found at 1068 cm^{-1} (Raman) and 1025 cm^{-1} (IR), displaying a correct isotope ratio ν_{RhH}/ν_{RhD} = 1.40-1.46. Because of the overlapping with other vibrations of the backbone, the μ_3-hydride vibration was only tentatively assigned to the a band observed at 1120 cm^{-1} (Raman) and 1110 cm^{-1} (IR) and shifted to 805 cm^{-1} (Raman)/788 cm^{-1} (IR) in the deuterated species. A strong Raman deformation mode of the Rh$_3$H$_7$ core was found at 738 cm^{-1} which was shifted to 527 cm^{-1} in the spectra of the D species.

As mentioned above the addition of a NaCl or NaBr to the cationic solvated complexes **I.149** leads to the formation of the trinuclear μ_3-halide bridged complexes [Rh$_3$(P,P)$_3$(μ_3-Y)$_2$]BF$_4$ (**I.178**). The complexes with P,P = Me-DUPHOS, DIPAMP, Bu^t-BisP* or Tangphos and Y = Cl were characterized by NMR and X-ray analysis (in case of P,P = Tangphos single crystals were not

obtained) [121]. Such complexes were formed together with neutral halide-bridged dinuclear ones of type $[Rh_2(P,P)_2(\mu_2\text{-}Y)]_2$ (**I.179**). Depending on the steric bulk of the diphosphine, on the bridging halide anion and on the solubility, the dinuclear species was formed selectively, as for instance when P,P = BINAP or Et-DUPHOS and Y = Cl. Compound $[Rh_2(Et\text{-}DUPHOS)_2(\mu_2\text{-}Cl)]_2$ was crystallographically characterized. The trinuclear μ_3-halide bridged complex **I.178** (P,P = (*R*)-BINAP, Y = Cl), however, was obtained and crystallized as the triflate salt when the experiment was repeated in a MeOH-CH_2Cl_2 mixture [121].

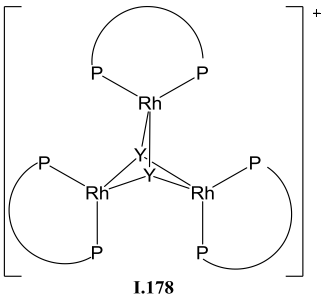

I.178

Y = Cl; P,P = Me-DUPHOS, DIPAMP, BINAP, Bu^t-BisP*, Tangphos
Y = Br; P,P = Me-DUPHOS

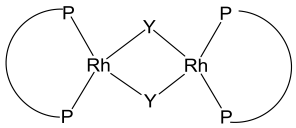

I.179

Y = Cl; P,P = Me-DUPHOS, DIPAMP, BINAP, Et-DUPHOS, Bu^t-BisP*, Tangphos
Y = Br; P,P = Me-DUPHOS, DIPAMP

The synthesis of bromo-bridged multinuclear complexes was investigated with Me-DUPHOS and DIPAMP ligands. In case of Me-DUPHOS single crystals of both the neutral dinuclear and the cationic trinuclear complexes were isolated. In case of DIPAMP only the neutral dinuclear **I.179** was formed, as proven by NMR spectroscopy. It was found that the formation of the trinuclear species **I.178** takes place through a reversible consecutive reaction from the neutral dinuclear complex **I.179** as the intermediate (Scheme I.32).

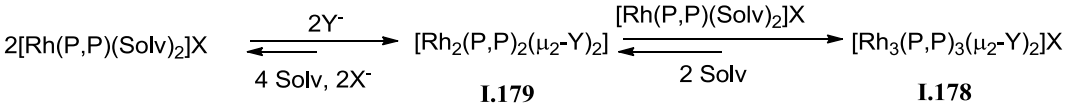

Scheme I.32

By addition of NEt_3 to **I.149** several trinuclear complexes were synthesized in yields of isolated product up to 90% [121, 122]. The addition of 2 equiv of NEt_3 to a methanol solution of **I.149** (P,P = Me-DUPHOS, DIPAMP, Bu^t-BisP*) led to the formation of the trinuclear μ_3-methoxy derivatives $[Rh_3(P,P)_3(\mu_3\text{-}OMe)_2]BF_4$ (**I.148-R** with R = Me). When a mixture of NEt_3/H_2O was added instead of pure NEt_3, mixed methoxy-hydroxy derivatives $[Rh_3(DPPE)_3(\mu_3\text{-}OH)_x(\mu_3\text{-}OMe)_{2-x}]BF_4$ could be isolated (x ~ 0,5). The pure hydroxy derivatives **I.148-R** (P,P = Me-DUPHOS, DIPAMP; R = H) were obtained by addition of aqueous NEt_3 to the solution of corresponding rhodium complexes **I.149** in

THF or acetone. Single crystals suitable for X-ray analysis were obtained for all complexes. It was quantified that basic additives such as NEt_3 can negatively influence the catalytic activity of the rhodium complexes for the hydrogenation of olefins owing to the fast formation of inactive trinuclear complexes. Exploratory analysis showed that appropriate prochiral olefins can be basic enough to initiate the formation of trinuclear complexes without other basic additives. By means of acidic additives the formation of trinuclear complexes can be thwarted or the decomposition of trinuclear complexes can be accelerated and the catalyst can therefore be maintained in the active form.

In low polarity solvents such as dichloromethane and dichloroethane, but also in triflouroethanol, the hydrogenation of the cationic precursor $[Rh(BINAP)(NBD)]BF_4$ resulted in the formation of a μ-(η^6-aryl) dimer $[Rh(BINAP)]_2(BF_4)_2$ in which the dinuclear dication is analogous to complex $[Rh_2(dppe)_2]^{2+}$ shown above (**I.147**). This product was characterized both in the solid state (X-ray analysis) and in solution (NMR) [107]. Hydrogenation of $[Rh(DIPAMP)(diene)]BF_4$ (diene = COD, NBD; DIPAMP = 1,2-bis[(2-dimethoxyphenyl)(phenylphosphino)]ethane) in methanol led not only to the formation of the expected solvated complex **I.149** but also to the arene-bridged dimeric species $[Rh(DIPAMP)]_2(BF_4)_2$ **I.180**. The dimer was characterized by X-ray analysis and by an extensive NMR solution study [110]. From a highly concentrated solution of **I.149** (P,P = (*S*,*S*)-DIPAMP, Solv = MeOH, BF_4^- salt) a crystal of the phehyl-phenyl-bridged $[Rh((S,S)\text{-DIPAMP})]_2(BF_4)_2$ (**I.180a**) could be isolated. Low temperature dissolution of these crystals in CD_2Cl_2 led to equilibrium between the two dimeric species **I.180a** and **I.180b**, the second one corresponding to a phenyl-*o*-anisyl-briged complex. It was proven that the equilibration can also occur via the solvated complex **I.149** in MeOD-*d*$_4$ (see Scheme I.33).

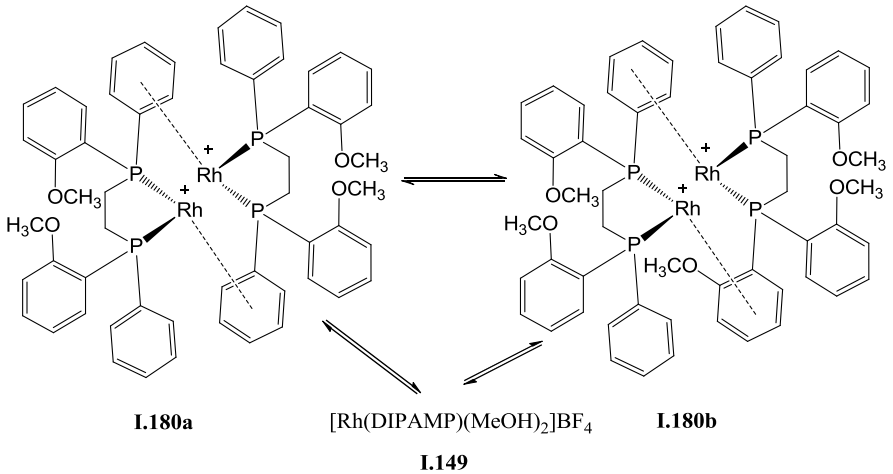

Scheme I.33

Equilibration between **I.180a** and **I.180b** is fast at ambient temperature (already in 1 min after the dissolution of **I.180a** in CD_2Cl_2 the UV/vis spectrum is constant). The exchange is however slow

enough to yield separate resonances in the ^{31}P NMR spectrum for **1.180a** and **I.180b**, in equilibrium with **I.149**, in CD_3OD [110]. For the determination of concentrations of the solvate complex **I.149** and the dimers **1.180** ^{1}H NMR data (signals of the methoxy groups of the ligand) were used.

Other systems containing dimeric Rh-phosphine species have been observed in solution [123]. The reaction of racemic $[Rh(BIPHEP)(NBD)]^+$ (BIPHEP = bis(phosphanyl) biphenyl, **I.164**) in non polar solvents for 30 min at room temperature under hydrogen (1 atm) gave a dimeric product $[Rh(BIPHEP)]_2^{2+}$ of type **I.147**, which consists of a mixture of homo- and hetero-chiral diastereomers in a 40:60 ratio, but the hetero-chiral complex isomerized slowly to the homo-chiral one at room temperature over 48 h. When solvated complexes **I.149** (P,P = R-BisP* with R = *o*-C_5H_9 and *o*-C_6H_{11}; Solv = CD_3OD) were hydrogenated the dihydrides $[Rh(R\text{-}BisP^*)(CD_3OD)_2H_2]^+$ (**I.174**) were formed in the mixture with $[Rh(R\text{-}BisP^*)]_2^{2+}$ complex of type **I.147** [118].

Similar to these results, treatment of the CD_2Cl_2 solution of $[Rh(\mathbf{I.165})_2(NBD)]^+$ complex, where **I.165** is the monodentate ligand (*R)*-phenylbinepine, with 1 atm H_2 at ambient temperature yielded after 10 minutes a dimer of type **I.147** in equilibrium with the solvated complex **I.149** [124]. In this species, the monophosphine ligand plays the role of a bidentate bridging ligand and coordinates second Rh center through one of its naphthyl groups. Reaction with H_2 of the same $[Rh((R)\text{-phenylbinepine})_2(NBD)]^+$ complex in a CD_2Cl_2/CD_3OD or CD_2Cl_2/THF-d_8 mixture resulted in the formation of solvated dihydrides **I.174a** and **I.174b**, with Solv = CD_3OD and THF respectively.

Hydrogenation of $[Rh(MonoPhos)_2)(NBD)]^+$ **(**MonoPhos = 3,5-dioxa-4-phosphacyclo-hepta[2,1-a:3,4-a']dinaphthalen-4-yl)dimethylamine, **I.166**) in CH_2Cl_2 at 1 bar total pressure also gave rise to the formation of a bimetallic complex $[Rh(MonoPhos)_2]_2^{2+}$ of type **I.147**; no solvated complexes were detected by NMR spectroscopy in this case [125].

Hydrogenations are usually carried out in simple alcohols, but aromatic solvents, water, or alcohol/aromatic solvent mixtures can also be used. It has been reported that aromatic solvents such as benzene can inhibit asymmetric hydrogenation. For example, the hydrogenation of ethyl-α-benzoyloxycrotonate with the very active $[Rh(Et\text{-}DUPHOS)(COD)]^+$ complex does not work in benzene, whereas high selectivity and activity are observed in other solvents [126]. When the benzene solution of the catalyst precursor $[Rh(Et\text{-}DuPHOS)(COD)]^+$ was hydrogenated in the absence of substrate for 1 h at 60 psi of hydrogen the formation of inactive $[Rh(Et\text{-}DUPHOS)(benzene)]^+$ complex (**I.181**), which was characterized by means of ^{31}P NMR spectroscopy, was observed (Scheme I.34) [126].

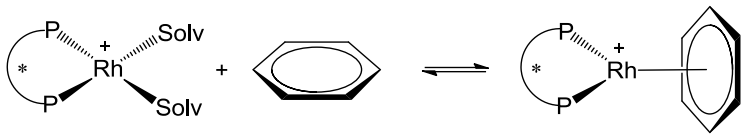

I.149 **I.181**

Scheme I.34 Equilibrium between solvated complex, unbound arene and rhodium-η^6-arene complex.

The addition of benzene or toluene to a solution of the solvated complex **I.149** (P,P = (*R*,*R*)-Et-DUPHOS or (*S*,*S*)-Me-DUPHOS, Solv = MeOH) in methanol led quantitatively to the corresponding arene complexes of type **I.181**. The formation of these complexes was confirmed by means ^{31}P and ^{103}Rh NMR spectroscopy and by X-ray diffraction on single crystals of the BF_4^- salts [127]. Formation of other arene complexes such as $[Rh((DIPAMP)(benzene)]^+$, $[Rh((DIPAMP)(p\text{-xylene})]^+$ and $[Rh((Ph\text{-}\beta\text{-glup-OH})(toluene)]^+$ (Ph-β-glup-OH = phenyl-2,3-bis(*O*-diphenylphospahyl-β-$_D$-gluco-pyranoside, **I.167**) from the corresponding methanol complexes was also confirmed by means of ^{31}P or ^{103}Rh NMR spectroscopy. Kinetic investigations that quantitatively describe the inhibiting influence of the η^6-arene Rh complexes on the catalytic activity were also reported in the same contribution.

The stability constants (Scheme I.34) of several rhodium-arene-diphosphane complexes with a range of diphosphanes [e.g. DUPHOS, DIPAMP, Tanghos, DPPF (1,1'-bis(diphenyl-phosphino)ferrocene, **I.168**), DIOP (4,5-bis(diphenylphosphinomethyl)-2,2-dimethyl-1,3-dioxolane, **I.169**)] and a range of aromatic compounds (e.g., benzene, toluene, aniline, 2,6-dimethylaniline, N-methylaniline) at various temperatures (278-318 K) have been measured [128]. These constants were determined by the classic titration method with monitoring by UV/Vis spectroscopy or by following the equilibration reaction with a UV/Vis diode array in combination with a stopped-flow apparatus. The solid state structures of seven rhodium-η^6-arene complexes $[Rh((Me\text{-}DUPHOS)(aniline)]BF_4$, $[Rh((Me\text{-}DUPHOS)(benzene)]BF_4$, $[Rh((Tangphos)(benzene)]BF_4$, $[Rh((DPPE)(benzene)]BF_4$, $[Rh((DPPE)(toluene)]BF_4$, $[Rh((Et\text{-}DUPHOS)(1,3,5\text{-trimethylbenzene})]BF_4$ and $[Rh((DIOP)(toluene)]BF_4$ were obtained.

It was found that higher-substituted arenes always lead to higher stability constant, which could be explained when considering the inductive effect of a methyl group and/or the mesomeric effect of an amino group on the electron density of the aromatic ring. Calculated stability constants (K'_A, L/mol) for $[Rh((Me\text{-}DUPHOS)(arene)]BF_4$ complexes increase from 105 (for benzene) through 23540 (for aniline) to 33522 (for *N*-methylaniline). For one ligand class, it appears that the equilibrium constant depends mostly on the type of arene, whereas the rate of equilibration is more sensitive to the nature of the diphosphane ligand.

Despite their lower stability compared to analogous diphosphine complexes bearing five-membered chiral chelate rings, the arene rhodium complexes **I.181** with BINAP, which forms seven-

membered rings, were prepared by adding excess of arene to a solution of **I.149** (P,P = BINAP, Solv = MeOH) in methanol, isolated and characterized by X-ray diffraction [129].

It has been shown that **I.149** (P,P = DPPF, Solv = MeOH) reacts with aniline and its derivatives to give stable η^6-arene complexes. The X-ray structures of three such complexes [Rh((DPPF)(η^6-2,6-dimethylaniline)]BF_4, [Rh((DPPF)(η^6-*N*-methylaniline)]BF_4 and [Rh((DPPF)(η^6-aniline)]BF_4 have been reported [130].

The formation of [Rh((*R*,*R*)-R-ButiPhane)(η^6-benzene)]$^+$ complexes were highlited by using the UV/Vis spectroscopic titration method. It was found that the hydrogenation rate of the diene to generate the active catalytic species and the stability of the benzene complexes are negatively affected by the steric bulk of the chiral ligand [112].

I.2.1.3 Catalyst-substrate complexes

Addition of a substrate to the solvated complexes resulted in formation of catalyst-substrate complex. All substrates used in the studies of rhodium complexes activation are presented on Fig I.2.

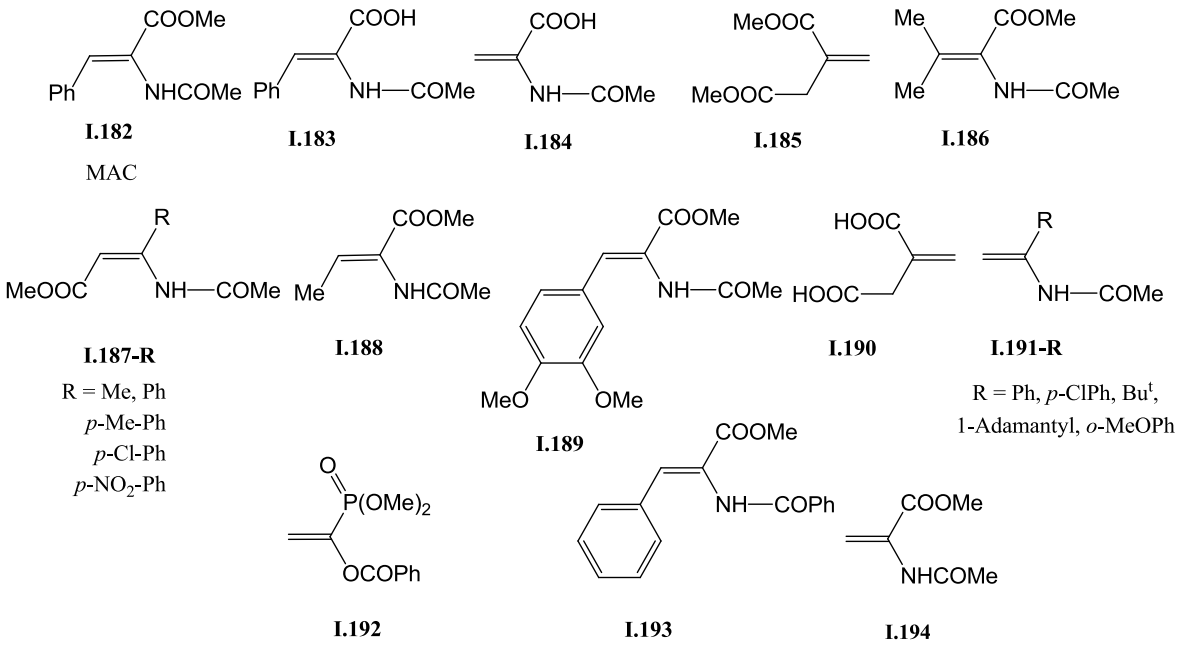

Fig. I.2. Substrates used in the studies of rhodium complexes activation

Thus, the addition of a 2-fold excess of MAC (MAC = (*Z*)-α-acetylaminocinnamate, **I.182**) to the solvated complex **I.149** (P,P = Bu^t-BisP*, Tangphos, Me-BPE, dcpe and dcpb, Solv = MeOH) resulted in the formation of the catalyst-substrate complex **I.195** (Scheme I.35) [116, 117]. All these complexes present the typical bidentate coordination of the substrate to rhodium through the double bond and the amide oxygen atom. However whereas only one catalyst-substrate complex is formed with achiral ligands (dcpe, dcpb), two possible diastereomers are formed with the chiral C_2-

symmetrical ligands. At room temperature only one average signal in ^{31}P NMR spectrum was observed, whereas at lower temperature (-60 to -95 °C) two separate signals for a major and a minor diastereomer could be detected, showing that the two species are rapidly exchanging. The molecular structure of the only one isolated complex [Rh(Tangphos)(MAC)]BF_4 **I.195a** corresponds to that of the diastereomer which is detected in solution according to the NOESY-NMR spectrum [116].

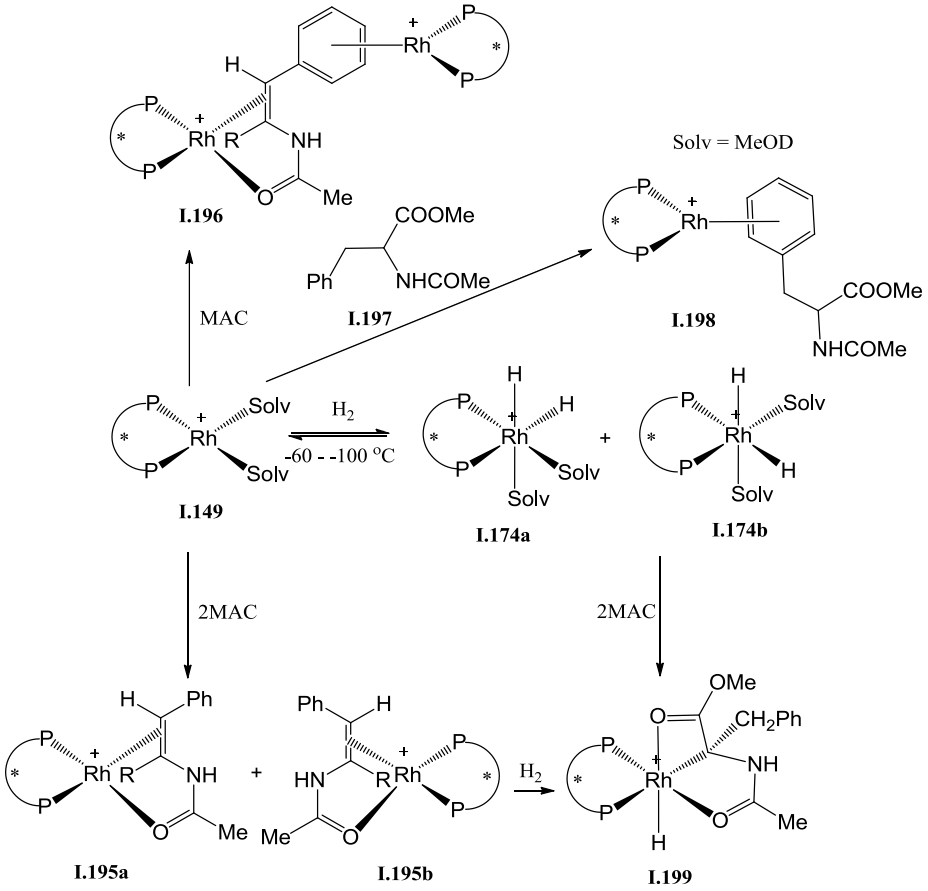

Scheme I.35

When less than 2 equiv MAC was added to **I.149** (P,P = Bu^t-BisP*, Solv = MeOH) the formation of two diastereomers of binuclear complex **I.196** in 10:1 ratio was observed simultaneously to the formation of the catalyst-substrate complex **I.195** [98]. The solvated complex **I.149** is also capable of reversibly coordinating a molecule of the hydrogenation product **I.197** with formation of the catalyst-product complex **I.198** in which the product is η^6-coordinated to rhodium by the phenyl ring. Binding of the product **I.197** is weaker than binding of the substrate **I.182**. Addition of 2-fold excess of **I.182** to a solution of the dihydride **I.174** (P,P = Bu^t-BisP*, Solv = MeOH) in equilibrium with **I.149** at -100°C under hydrogen resulted in immediate disappearance of the NMR signals of **I.174** and appearance of a new hydride species **I.199**. At -50°C the signals of **I.199** disappeared and signals of the hydrogenation product **I.197**, of **I.149**, and of the catalyst-product complex **I.198** appeared

simultaneously. The absolute configuration of the monohydride complex **I.199** corresponds to that of the (*R*)-hydrogenation product (99% *ee*). When the solution of **I.195a/I.195b** was hydrogenated with 2 atm of H_2 at -80°C for 2 h the monohydride **I.199** was formed in high concentration besides the solvated complex **I.149** and the dihydrides **I.174a/I.174b** in equilibrium with residual **I.195**. When the same experiment was carried out in the presence of a 2-fold execess of **I.182**, an NMR spectrum containing only the signals of **I.195** and **I.199** was obtained.

Addition of **I.182** to the rhodium dihydrides **I.174 (**P,P = R-BisP* with R = 1-adamantyl or 1-methylcyclohexyl, Solv = CD_3OD) also resulted in the formation of complexes **I.195a/I.195b** [118]. Catalyst-substrate complexes $[Rh(Bu^t\text{-BisP*})(substrate)]^+$ with other substrates such as (*Z*)-α-acetylaminocinnamatic acid **I.183**, (*Z*)-α-acetylaminoacrylic acid **I.184**, dimethyl itaconate **I.185**, methyl *β*,*β*-dimethyl-(*Z*)-α-acetylaminocinnamate **I.186** were also obtained [99].

The two diastereomers of the catalyst-substrate complex **I.195** can interconvert both intramoleculary and intermoleculary via complete dissociation to the solvate complex **I.149** and the corresponding substrate. The ratio of diastereomers at low temperature varies from 10 : 1 in $[Rh(R\text{-BisP*})(MAC)]^+$ and 12 : 1 in $[Rh(Bu^t\text{-BisP*})(\mathbf{I.185})]^+$ to 3 : 1 in $[Rh(Bu^t\text{-BisP*})(\mathbf{I.183})]^+$, and 1 : 1 in $[Rh(Bu^t\text{-BisP*})(\mathbf{I.184})]^+$. No other compounds were found in the NMR spectra of $[Rh(R\text{-BisP*})(MAC)]^+$ and $[Rh(Bu^t\text{-BisP*})(\mathbf{I.184})]^+$ in CD_3OD, whereas $[Rh(Bu^t\text{-BisP*})(\mathbf{I.185})]^+$ equilibrates with a considerable amount of the solvated complex **I.149**. In case of substrate **I.183** the equilibrium mixture contained only 25% of $[Rh(Bu^t\text{-BisP*})(\mathbf{I.183})]^+$ at -95°C. The four substrates **I.182**, **I.183**, **I.184** and **I.185** gave enantioselectivities of over 98% in the hydrogenation catalysed by the solvate complex **I.149** (P,P = Bu^t-BisP*, Solv = CD_3OD), while **I.186** gave a poor enantioselectivity. It was found that the binding of this substrate was very weak: when a 2-fold excess of **I.186** was added to a solution of **I.149**, the $[Rh(Bu^t\text{-BisP*})(\mathbf{I.186})]^+$: $[Rh(Bu^t\text{-BisP*})(CD_3OD)_2]^+$ ratio was only 1:10.

The monohydride intermediates $[RhH(R\text{-BisP*})(MAC)]^+$ (R = 1-adamantyl or 1-methylcyclohexyl) and $[RhH(Bu^t\text{-BisP*})(\mathbf{I.186})]^+$ (**I.199**) were also generated by the reaction of the solvated dihydride complexes **I.174** (P,P = R-BisP*, Solv = CD_3OD) with the corresponding substrate at -100°C, or by hydrogenation of the corresponding catalyst-substrate complexes **I.195** at -80°C [118]. The reactions of **I.174** with the substrate proceeded more cleanly, but the alternative methodology afforded higher concentrations of the monohydrides **I.199** if longer reaction time were applied.

The hydrogenation of **I.195a/195b** (P,P = (*R*,*R*)-BenzP*), obtained from the corresponding **I.149** and 2 equiv of **I.182**, for 30 min at 2-3 atm H_2 at -90°C did not result in the formation of any hydrogenation product. However, when the temperature was raised to -50 °C, hydrogenation was completed after 30 min, and no intermediates were detected [114].

The diastereomeric catalyst-substrate complexes [Rh(**I.159**)(MAC)]$^+$ of type **I.195** were obtained in a 5 : 1 ratio by mixing the corresponding solvated complex with MAC at -100°C [115]. It was found that they are in rapid equilibrium with partially dissociated complex **I.200** (P,P = **I.159**; only one diastereomer was observed in ^{31}P NMR spectrum).

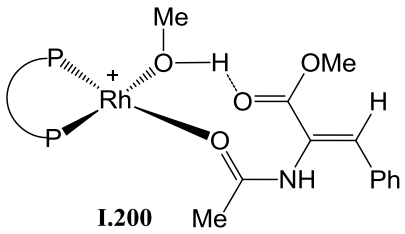

I.200

The reaction of the trinuclear rhodium-hydride complex **I.176** (P,P = dcpe **I.160**) with MAC under an argon atmosphere led to the respective catalysts-substrate complex **I.195** [116]. Single crystals of the catalyst-substrate complex of type **I.195a** (P,P = (*R*,*R*)-DIPAMP) as the BF_4^- salt were grown from a solution of [**I.153**]$(BF_4)_2$ and MAC in Pr^{i}OH [110].

Addition of MAC (2 equiv) to the solution of [Rh((*R*)-phenylbinepine)$_2$]$_2^+$ complex of type **I.147** in CD_2Cl_2 also leads also to the catalyst-substrate complex **I.195** (P,P = ((*R*)-phenylbinepine)$_2$) [124]. At ambient temperature two diastereomers **I.195a** and **I.195b** are observed in a 4:1 ratio interconverting with the corresponding solvated complex **I.149** and with each other. At -90°C the signals of each diastereomer are split into two sets due to the presence of conformers caused by hindered rotation around the Rh-P bonds.

For this phosphine ligand (P,P = (*R*)-phenylbinepine) and Solv = MeOH or THF the hydrogenation of **I.195** at -90°C (1 atm H_2, 40 min) and the reaction of **I.174** with MAC at low temperatures (-50 to -30°C, 20 – 60 min) always led to the product of MAC hydrogenation with 99% *ee* [124]. The characterized intermediates of this process are the monohydride **I.199**, the 2:1 catalyst-substrate complex **I.196** and the final catalyst-product complex **I.198**.

The addition of MAC to the dimeric Rh species [Rh(MonoPhos)$_2$]$_2^{2+}$ of type **I.147** also led to the formation of two diastereomeric catalyst-substrate adducts **I.195** (major and minor) which were detected and characterized by ESI-MS and NMR spectroscopy at different temperatures [125]. The minor adduct turned out to be kinetically more labile as it could be detected in the NMR spectrum only at low temperature. Addition of H_2 to **I.195** led to the formation of the hydrogenated product **I.197** with the expected *ee* value (93%) and configuration (*S*). **I.197** remains bound to the metal in a new Rh-product adduct **I.198** from which it can be displaced upon addition of fresh MAC. It was concluded that the major adduct is less reactive towards the activation of H_2 and that the Rh/phosphoramidite

system follows a mechanism that was defined as “anti-lock-and-key”, or alternatively termed “major/minor”.

The addition of MAC (**I.182**) and of methyl (*Z*)-3-*N*-acetylamino-3-(R)-acrylate (**I.187-R**, R = Me, Ph) to the solvated complex **I.149** (P,P = (*R*,*R*)-R-ButiPhane, Solv = MeOH) led to the formation of the corresponding catalyst-substrate complexes [93]. The hydrogenation of **I.187-Me** is a first order reaction in substrate concentration (low stability of the catalyst-substrate complex, the equilibrium is shifted toward the solvated complex). In contrast, when the substrate is MAC or **I.187-Ph**, the rate law has a zero order dependence on substrate (high stability of the catalyst-substrate complex). The four stereoisomeric catalyst-substrate complexes that are expected for system [Rh((*R*,*R*)-Pr^{i}-ButiPhane)(**I.187-Ph**)]$^{+}$ were detected by means of ^{31}P NMR spectroscopy at room temperature while the corresponding solvent complex was not observed. Crystals suitable for X-ray analysis were obtained for one of four possible stereoisomers as the BF_4^- salt.

Dimethyl itaconate (**I.185**) forms two diastereoisomeric catalyst-substrate complexes **I.195** with **I.149** (P,P = DIPAMP, Solv = MeOH), which are significantly less stable than the corresponding Rh-DIPAMP complexes with α-dehydroamino acid derivative (*Z*)-methyl acetamidocinnamate **I.188** (the stability constant is $6{\cdot}09.10^{1}$ versus $6.89{\cdot}10^{4}$ L/mol). An X-ray analysis of the isolated substrate complex as the BF_4^- salt shows the coordination of the olefinic double bond and β-carbonyl oxygen. The crystallographically characterized complex was identified as a major intermediate via solid state NMR spectroscopy, whereas hydrogenation of this complex leads to the minor enantiomer [131].

The hydrogenation of **I.187-Ph** with **I.149** (P,P = Et-DUPHOS) in MeOH or Pr^{i}OH at 25°C and 1 bar of hydrogen pressure was studied and the BF_4^- salt of the catalyst-substrate complex [Rh((Et-DUPHOS)(**I.187-Ph**)]$^{+}$ of type **I.195** was isolated and characterized by X-ray diffraction. Chelate binding of the prochiral olefin occurs – as in α-substituted analogues – through the double bond and the carbonyl oxygen [132]. The assignment of the isolated catalyst-substrate complex as either the major or the minor complex was not obvious, since the ratio of the complexes at room temperature in both solvents was approximately 1:1. The hydrogenation of **I.187-R** (R = Ph, *p*-Me-Ph, *p*-Cl-Ph, *p*-NO_2-Ph) catalyzed by **I.149** (P,P = DIPAMP) in MeOH at 25°C and 1 bar of hydrogen pressure was also studied and four [Rh(DIPAMP)(**I.187-R**)]BF_4 salts were isolated and characterized by X-ray diffraction. One common peculiarity of these compounds is that the OMe group of DIPAMP interacts with the rhodium center as a hemilabile ligand. For all these cationic complexes the major/minor ratio was 10:1 at room temperature in MeOH. Three single crystals were identified as the major substrate complexes by low-temperature ^{31}P NMR spectroscopy. It was found that in case of β-aminoacrylates the catalyst-substrate complex led to the major product of the asymmetric hydrogenation. The main cause for this lies in the slight difference in reactivities of the diastereomeric substrate complexes. The classical major/minor concept is based on the fact that the minor substrate complex is much more

reactive than the major substrate complex, but this extreme difference in reactivity was not evident in the substrate complexes with β-aminoacrylates.

The X-ray structure of the catalyst-substrate complex of type **I.195** (P,P = DIPAMP) with the DOPA derivative (*Z*)-2-benzoylamino-3-(3,4-dimethoxyphenyl)-methyl-propionate (**I.189**) has also been reported [133]. At room temperature the ratio of the [Rh(DIPAMP)(**I.189**)]$^+$ diastereoisomers equals 78:22. By freezing out the interconversion between major and minor substrate complexes, it was shown that the X-ray structure undoubtedly corresponds to the major complex [134]. It was proven that this system acts according to the major-minor concept.

The hydrogenation of dimethyl itaconate (**I.185**) catalyzed by **I.149** (P,P = Ph-β-glup-OH (**I.167**), Solv = MeOH) (ratio **I.185**/**I.147** is 50:1) is a pseudo-first-order reaction in methanol. This means that during the asymmetric hydrogenation, the equilibrium solvated complex/prochiral olefin-substrate complex is shifted toward the former. The addition of toluene to this system (molar ratios of methanol/toluene = 1320:1 and toluene/Rh = 14:1) led to a 25% decrease of the activity, which was attributed to the formation of inactive η^6-arene derivatives [127].

The hydrogenation of **I.187-Me** catalyzed by **I.149** (P,P = DIPAMP, Solv = MeOH, 1%) is a pseudo-zero-order reaction in methanol: the equilibrium is shifted toward the substrate complex and the rate does not depend on the concentration of the substrate. The addition of *p*-xylene to this system in molar methanol/*p*-xylene ratios from 1323:1 or 650:1 leads to diminished activity without change of enantioselectivity and the hydrogenation is no longer a pseudo-zero-order reaction. The proportion of blocking arene complex increases with increasing substrate conversion, and thus the activity decreases continuously.

It was proven that the trinuclear rhodium complex **I.176** is not sufficient for a complete hydrogenation of MAC: only after 25 days the rhodium complex **I.176** is no longer present in solution, being completely converted to the catalyst-substrate complex **I.195** and the η^6-arene complex with hydrogenated product H_2-MAC, **I.198**; the hydrogenation product was 90.1% enantiopure [111]. The *in situ* formation of the halide-bridged multinuclear complexes **I.178** in the catalytic reactions leads to an activity decrease or even to a total inactivity [121], as shown in the case of the asymmetric hydrogenation of MAC (**I.182**) and dimethyl itaconate (**I.185**).

During the asymmetric hydrogenation of itaconic acid (**I.190**) catalyzed by **I.149** (P,P = DIPAMP, Me-DUPHOS; Solv = MeOH) a deactivation with increasing substrate concentration was observed [135]. Itaconic acid formed two complexes (major and minor) with both catalysts, which display significantly smaller P,P coupling constants in the ^{31}P NMR in comparison to complexes with the dimethyl ester analogue. The X-ray structure of the complex isolated with the DIPAMP ligand, **I.201**, revealed a neutral Rh(III)-alkyl complex with a tridentate binding of the substrate via both carboxylate groups and an Rh-C bond to the quaternary carbon atom originating from the double bond.

Complex **I.201** is not hydrogenated under normal pressure and is thus the cause of the observed deactivation (Scheme I.36). The X-ray structure of the neutral complex [Rh((DIPAMP)(α-methyl itaconate)] (**I.202**), obtained from a solution of **I.149** (P,P = DIPAMP, Solv = MeOH) and α-methyl itaconate, further supports this pathway.

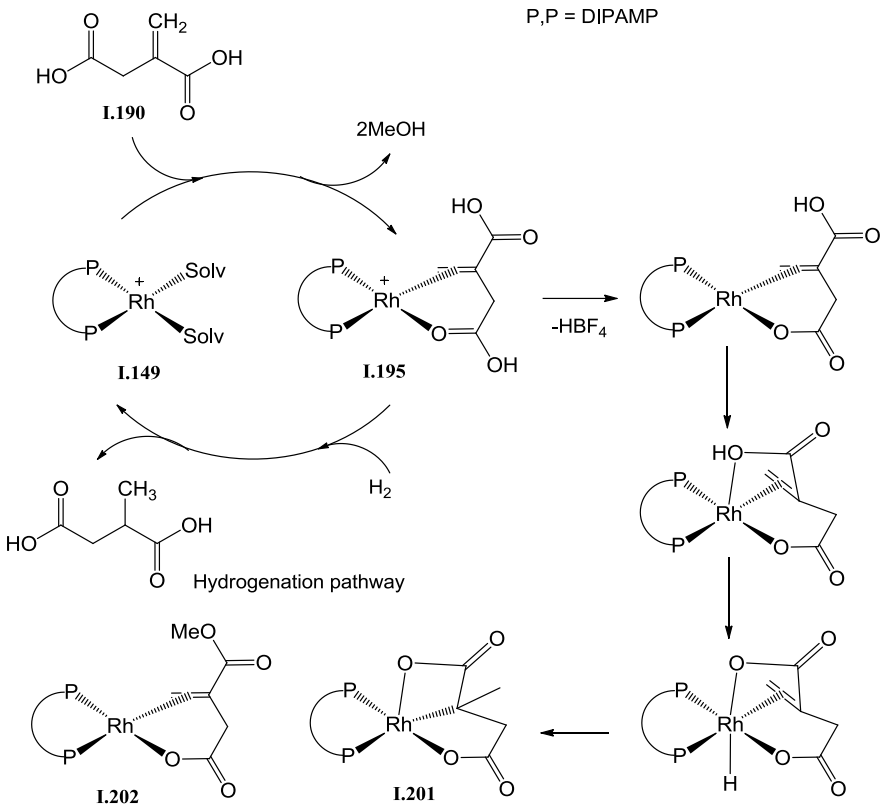

Scheme I.36

The catalyst-substrate complex **I.204** was formed by the reaction of the COD rhodium complex **I.203** containing a chiral P,S-ligand with (*Z*)-methyl acetamidocinnamate (**I.188**) under 1 atm of hydrogen pressure in THF at room temperature (Scheme I.37) [136]. Only one of four possible diastereomers was observed in solution as confirmed by ^{1}H and ^{31}P NMR spectroscopy. The X-ray crystallographic analysis of a crystals of **I.204** revealed the structure of the preferred isomer. Upon further hydrogenation, complex **I.204** led to the observed major enantioner of the product. In this case the major intermediate determines the selectivity of the reaction in terms of the lock-and-key principle rather than the major-minor concept.

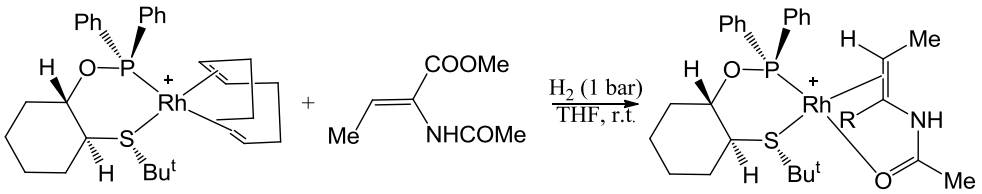

I.203 **I.188** **I.204**

Scheme I.37

Addition of a 2-fold excess of the enamides **I.191-R** (R = Ph or *p*-ClPh) to the solvated complex **I.149** (P,P = Bu^t-BisP*, Solv = CD_3OD) at -20°C resulted in the immediate formation of two diastereomers of the catalyst-substrate complex of type **I.195** in a ratio changing from 1 : 4 at -90°C to 2 : 1 at 0°C for R = Ph and from 13 : 1 at -90°C to 3 : 1 at 0°C for R = *p*-ClPh [137]. In both cases, no detectable amounts of the solvated complex **I.149** could be observed in the spectra in the -90 to +30°C temperature range. The conformation of major and minor isomers were elucidated from the NMR data. The rate of intermolecular interconversion for the two [Rh(Bu^t-BisP*)(**I.191-R**)]$^+$ diastereomers is significantly faster than for the catalyst-substrate complexes of dehydroamino acids. Either the addition of **I.191-Ph** to the solution of the dihydride complex **I.174** at -100°C or the hydrogenation of the catalyst-substrate complex [Rh(Bu^t-BisP*)(phenylenamide)]$^+$ at -100°C produced the catalyst-product complex of type **I.198** directly. The same result was obtained when catalyst-substrate complex [Rh(Bu^t-BisP*)(*p*-chlorophenylenamide)]$^+$ was hydrogenated at -100°C. Addition of a 2-fold excess of the enamide **I.191-Bu^t** or **I.191-Adamantyl** to **I.149** (P,P = Bu^t-BisP*, Solv = CD_3OD) resulted in formation of the corresponding catalyst-substrate complexes [Rh(Bu^t-BisP*)(**I.191-R**)]$^+$ (R = Bu^t, Adamantyl) of type **I.195**, which differ significantly in structure and stability from those examined above with R = Ph and *p*-ClPh. A significant amount of the solvated complex **I.149** remains present at equilibrium with either product even at -90°C. In both cases only one isomer of the corresponding catalyst-substrate complex was observed in the temperature range from -90 to +30°C.

Hydrogenation of the the equilibrium mixture of the solvated complex **I.149**, the free enamide **I.191-Bu^t** (or **I.191-Adamantyl)** and the catalyst-substrate complex [Rh(Bu^t-BisP*)(**I.191-R**)]$^+$ (R = Bu^t or 1-adamantyl) at -100°C for 7 min led to observation of the monohydride intermediates **I.205a** and **I.205b**. In both cases two isomers were observed in a 10 : 1 ratio. Complexes **I.205a** and **I.205b** are revatively stable below -85°C; at higher temperatures they decompose rapidly, affording the solvated complex **I.149** and the hydrogenation products.

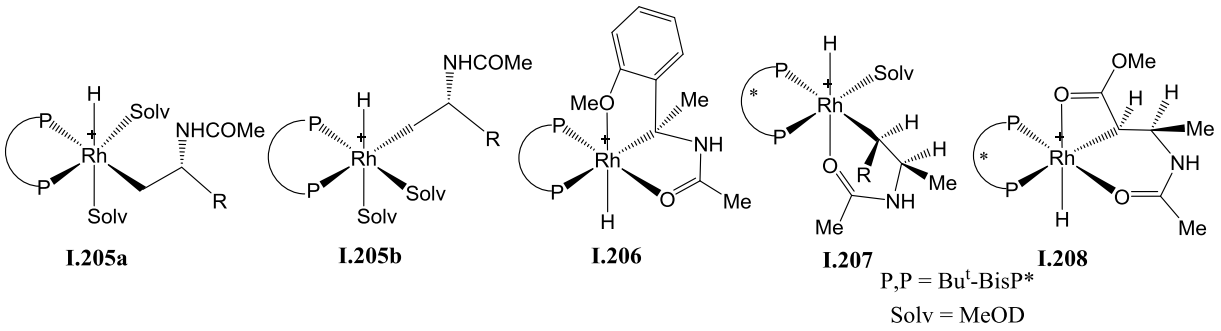

In case of the enamide **I.191-*o*-MeOPh** the complex of type **I.195** obtained by addition of a 2-fold excess of substrate to **I.149** (P,P = Bu^t-BisP*, Solv = MeOH) exists in solution as a mixture of two interconverting diastereomers: the ratio changes from 15 : 1 at -90°C to 6 : 1 at 0°C. Hydrogenation of this equilibrium mixture at -100 °C resulted in the detection of two isomers (**I.205a** and **I.206**) of the monohydride intermediate in a 44 : 100 ratio.

Addition of a 2-fold excess of (*E*)-3-*N*-acetylamino-3-methyl-acrylate (**I.187-Me**) to an equilibrium mixture of **I.149**, **I.174**, and H_2 at -100°C (P,P = Bu^t-BisP*, Solv = MeOH) resulted in the immediate and quantitative conversion of **I.174** to the monohydride intermediates **I.207** (R = COOMe) and **I.208** (two diastereomers) in a 0.7 : 1 ratio [138]. When the temperature was raised to -10°C, **I.207** rearranged to the **I.208**. At higher temperatures all hydride complexes decomposed producing the hydrogenation product and regenerating **I.149**. When an equimolar mixture of **I.187-Me** and **I.174** was hydrogenated for 10 min at -80°C, complete conversion of the substrate to the monohydride complexes **I.207** and **I.208** was achieved.

Complexation of dimethyl-1-benzoyloxyethenephosphonate (**I.192**, 2-fold excess) to **I.149** (P,P = Bu^t-BisP*, Solv = MeOH) to yield the catalyst-substrate complex [Rh(Bu^t-BisP*)(**I.192**)]$^+$ of type **I.195** was fast and quantitative in the -100 to +60°C temperature range. Reaction of the same substrate **I.192** (2-fold excess) with the dihydride complex **I.174** (P,P = Bu^t-BisP*, Solv = MeOH) at -100 °C led to the monohydride intermediates **I.209a,b** in a 100 : 5 ratio. Raising the temperature to -30°C resulted in the disappearance of **I.209a,b** in favor of **I.210a,b** with a 100 : 5 ratio. These transformations are probably stereospecific and are proposed to occur via the monodentate intermediates **I.211a,b**. The hydrogenation of the catalyst-substrate complex [Rh(Bu^t-BisP*)(**I.192**)]$^+$ with 2 atm of H_2 carried out for 10 min at -30°C, on the other hand, gave **I.210** with a **I.210a** : **I.210b** ratio of 5 : 1 [139].

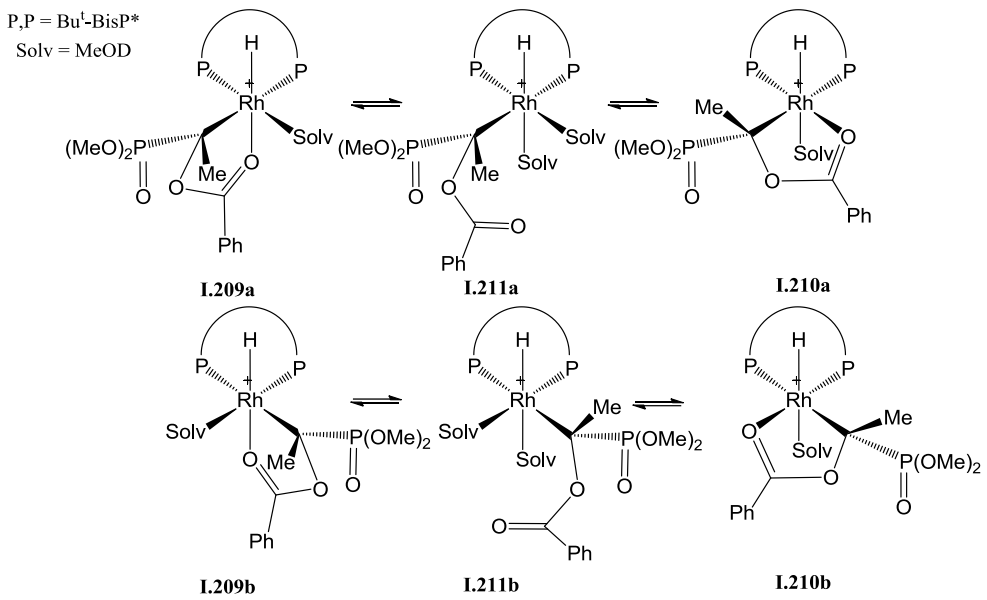

When an equivalent amount of (*Z*)-methyl-*N*-benzoylaminocinnamate (**I.193**) was added to the solution of the dihydride **I.174** (P,P = **I.162**, Solv = CD_3OD), the slow formation of a mixture of monohydride intermediates **I.212a-d** at -80 °C was observed, whereas the reaction is immediate at -40 °C. Independent of the reaction temperature, the isomer ratio is 1 : 0.29 : 0.12 : 0.05, and the isomers **I.212b** and **I.212d** inconvert reversibly [100]. All observed complexes **I.212a-d** are stable below 0°C. At higher temperatures they decompose, producing the hydrogenation product and regenerating **I.149**. When a 2-fold excess of the substrate **I.193** was used in a similar experiment, the clean formation of the solvated complex **I.149** (P,P = **I.162**, Solv = CD_3OD) and the catalyst-substrate complex [Rh(**I.162**)(**I.193**)]$^+$ of type **I.195** were observed. Only one isomer of **I.195** was detected in the temperature range from -100 to +20°C. The solvated complex exhibited a dynamic behavior that was attributed to a conformational equilibrium.

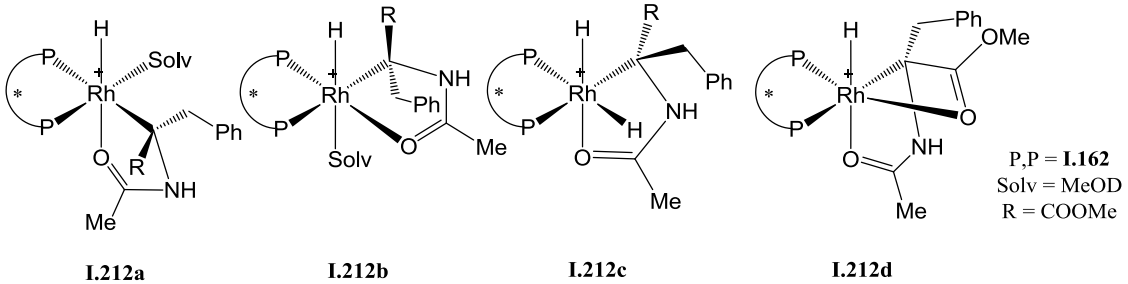

The low temperature reaction of **I.174** (P,P = **I.162**, Solv = CD_3OD) with **1.192** started at -70°C, producing initially a great number of hydride signals in the ^1H NMR spectrum. Upon raising the temperature to 20°C only two hydrides of type **I.207** and **I.208** were observed.

Para-hydrogen was used for the NMR identification of transient intermediates such as the agostic hydride species **I.213** when MAC (**I.182**) or methyl (*Z*)-α-acetylaminoacrylate (**I.194**) was added to the methanol solution of $[Rh(P,P)(diene)]^+$ (P,P = PHANEPHOS (**I.170**); diene = COD, NBD) at -10 to -30°C [140].

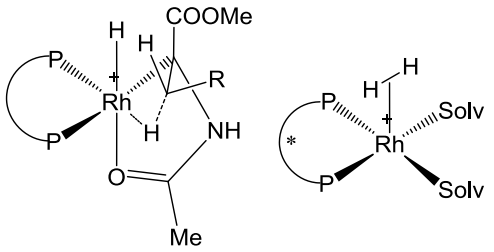

I.213-R **I.214**

R = H, Ph
P,P = PHANEPHOS

When the hydrogenation of the substrates was completed, two diastereomers **I.174** could be observed in ratio 2 : 1 [141]. This species was also evidenced when the catalyst precursor $[Rh(PHANEPHOS)(diene)]^+$ was hydrogenated in the absence of substrate at -40°C. When the substrate MAC was subsequently added to this solution held at -80°C, rapid formation of the agostic dihydride **I.213-Ph** was observed.

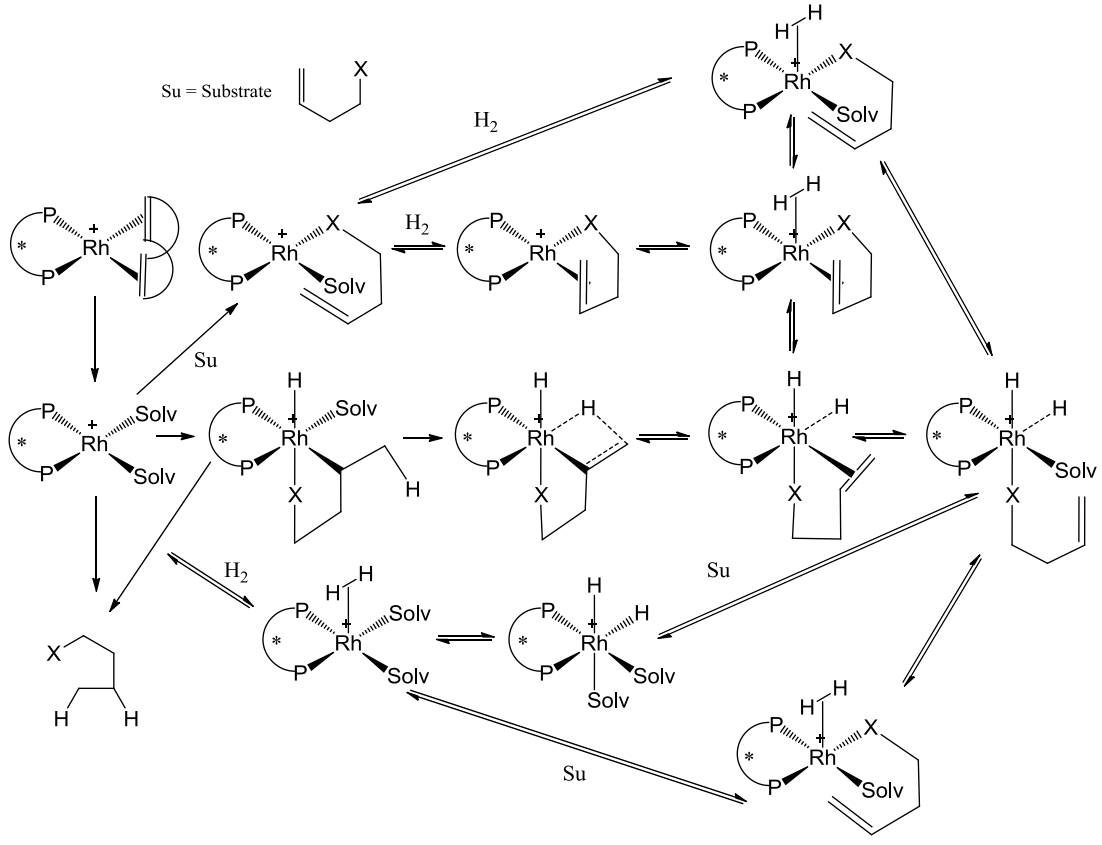

Scheme I.38

It was possible to detect another intermediate, the molecular dihydrogen complex **I.214**, when substrate **I.193** ^{13}C-labeled α to the P was used in the low-temperature reaction with complex **I.174** (P,P = Bu^t-BisP* **I.155**, Solv = CD_3OD). The position and the coupling pattern of the α-carbon atom, the high-field shift of one of the phosphorus atoms, as well as fast conversion to the monohydride **I.209** at -95°C gave reason to assume the structure **I.214**, but the signal of the coordinated dihydrogen ligand was not found in the ^{1}H NMR spectrum. On the basis of all the obtained data on reaction intermediates the following mechanism of asymmetric hydrogenation was proposed (Scheme I.38) [142].

The stereoselection mechanism in asymmetric hydrogenation catalyzed by rhodium complexes was discussed on the basis of the structure of dihydrides, catalyst-substrate complexes and other intermadiates [143].

The reactivity of arene-stabilized diene rhodium complexes with H_2 was also studied [144]. Addition of 90 psi of H_2 at room temperature to the solution of the cationic rhodium complex $[Rh(PCy_2biPh)(diene)]^+$ **I.215 (**diene = NBD, PCy_2biPh = 2-(dicyclohexylphosphino)biphenyl) in C_6D_5Cl or CD_2Cl_2 yields the Rh(III) dihydride complex $[Rh(PCy_2biPh)H_2]^+$ (**I.216**) after 4 days (Scheme I.39). Reaction in the more coordinating solvent acetone-d_6 did not yield **I.216**. Instead, acetone displaced the η^2-bound arene moiety and coordinated to the metal center to form a square-planar Rh(I) NBD complex with the phosphine and acetone ligands occupying the remaining two sites. Addition of 90 psi of H_2 at room temperature to the solution of $[Rh(PCy_2biPh)(COD)]^+$ in CD_2Cl_2 generated a η^6-arene stabilized Rh(I) alkene complex $[Rh(PCy_2biPh)(COE)]^+$ (**I.217**). A small amount of dihydride complex **I.216** was observed upon heating complex **I.217** to 60°C in the presence of H_2 after 1 day, whereas complete decomposition was observed after 3 days at this temperature. X-ray quality crystals of complex **I.217** were obtained in the presence of the $BAr^F{}_4^-$ counterion (Ar^F = 3,5-$C_6H_3(CF_3)_2$); the complex adopts a two-legged piano-stool geometry in which the phosphorus donor atom and the alkene are the legs. Compound **I.217** can also be prepared independently by the reaction of $[Rh(COE)_2Cl]_2$ with 2 equiv of PCy_2biPh and $NaBAr^F{}_4$ in CH_2Cl_2 at room temperature. Reaction of the iridium complex $[Ir(PCy_2biPh)(COD)]^+$ in CH_2Cl_2 with H_2 at room temperature and normal pressure for 15 min resulted in the formation of the dihydride complex **I.216** (M = Ir) [145], the solid state structure of which was determined by X-ray crystallography as the $BAr^F{}_4^-$ salt. It exhibits a three-legged piano-stool geometry in which the arene moiety of the phosphine biphenyl group is coordinated in an η^6 fashion to Ir. A similar geometry was also proposed for the cationic rhodium dihydride analogue on the basis of NMR spectroscopy.

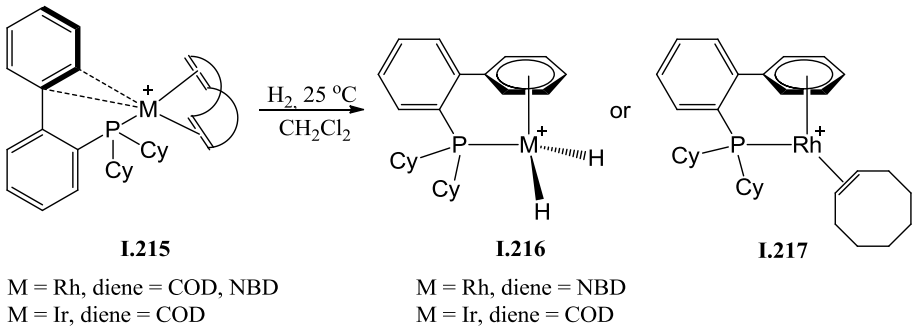

I.215 **I.216** **I.217**

M = Rh, diene = COD, NBD
M = Ir, diene = COD

M = Rh, diene = NBD
M = Ir, diene = COD

Scheme I.39

I.2.2 Activation of iridium complexes

The reaction of the iridium complex **I.110** (see Scheme I.20) containing a chiral phosphinooxazoline ligand (PHOX, **I.109**) with dihydrogen was studied by NMR spectroscopy [146, 147]. After dihydrogen was bubbled through a solution of **I.110** in THF in NMR tube at -40°C for 5 min a single dihydride complex $[Ir(PHOX)(COD)H_2]^+$ **I.218** was formed (Scheme I.40). No spectral changes for this compound were observed upon slow warming from -40 to 0°C within 45 min, suggesting that the kinetically preferred H_2 addition product is also thermodynamically favored. The highly selective formation of only one of four possible diastereomers results from the steric effects of PHOX combined with a strong electronic influence of the coordinating N and P atoms, favoring the addition of a hydride *trans* to the Ir-N bond. When the solution containing complex **I.218** was warmed to 0°C under dihydrogen and kept at that temperature for 30 min, the gradual conversion of **I.218** to two new hydride complexes **I.219** was observed with concomitant formation of cyclooctane.

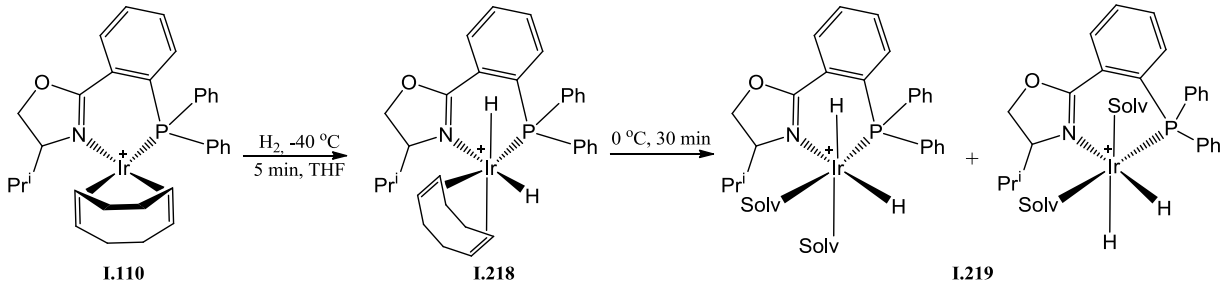

I.110 **I.218** **I.219**

Scheme I.40

It was also established that H_2 oxidatively adds to neutral phosphineamido complexes such as **I.220** and also to the corresponding protonated cationic amino complexes (e.g. **I.220H**$^+$ in Scheme I.41), to yield dihydrido Ir(III) derivatives (**I.221** and **I.221H**$^+$, respectively) [148].

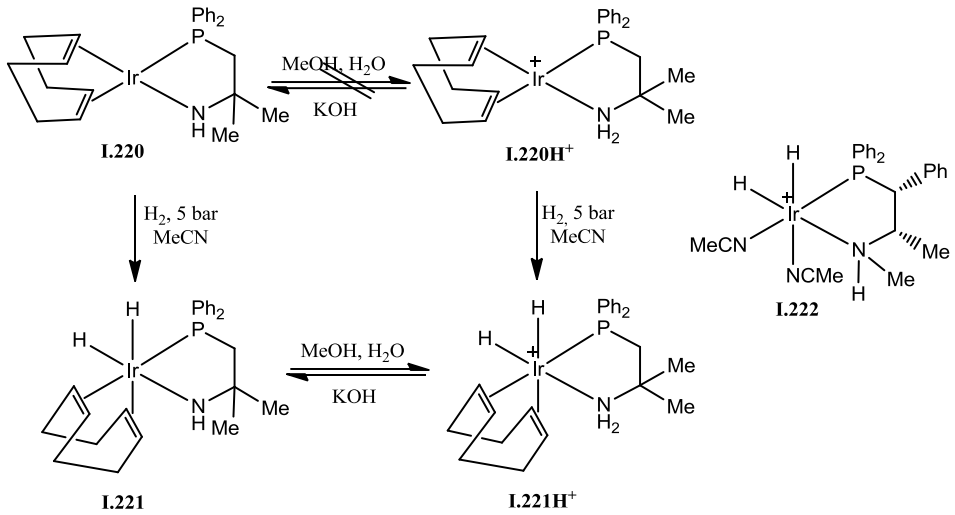

Scheme I.41

Whereas the Ir(I) complexes do no undergo rapid acid/base equilibration, the Ir(III) complexes do, this being attributed to the better availability of the N lone pair in the electronically saturated Ir(III) species. These Ir(III) products are capable to undergo H/D exchange between the coordinated NH proton(deuteron) and H_2. At longer reaction times, however, the COD ligand is removed by hydrogenation, yielding solvated Ir(III) hydrides **I.222**.

These complexes were found to be effective catalyst in asymmetric ketone hydrogenation. On the basis of the above observations a mechanism was proposed for the hydrogenation catalytic cycle (Scheme I.42) which involves ketone coordination (**B** to **C**) and insertion into an Ir(III)–H bond (**C** to **D**) of a neutral Ir(III) amido species in which the positions formerly occupied by the COD ligand are saturated by solvent molecules. However, the reactivation by H_2 would not occur by H_2 addition to the neutral alkoxide intermediate but rather to a cationic species obtained after protonolysis of the Ir-alkoxide function (**D** to **E**), liberating the hydrogenated product [148].

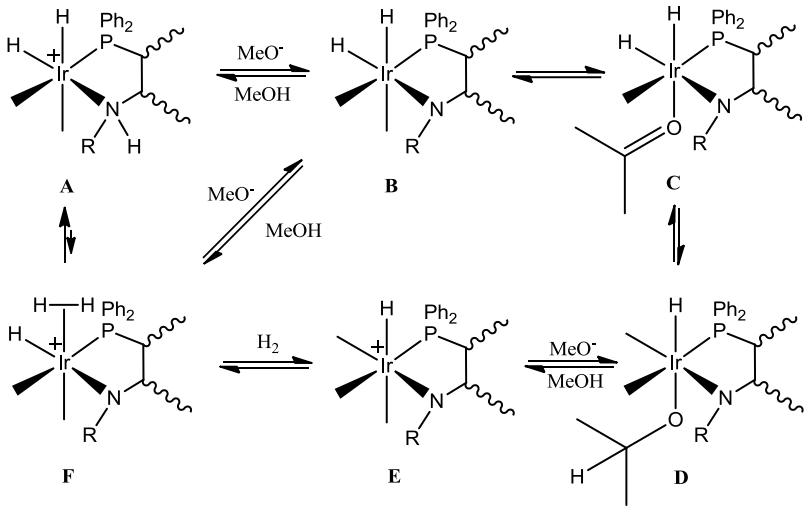

Scheme I.42

The cationic iridium complexes $[Ir(DIOSRS)(COD)]^+$ (**I.223**, R = Et, Pr) with dithioether ligands reacted with H_2 in CD_2Cl_2 at -70 °C and normal pressure for 20 min to form two corresponding dihydride species $[Ir(DIOSRS)(COD)H_2]^+$ (**I.224**) (Scheme I.43) [149]. The major and minor isomers were formed in a 5 : 3 ratio by the attack of H_2 through the seven-membered ring face.

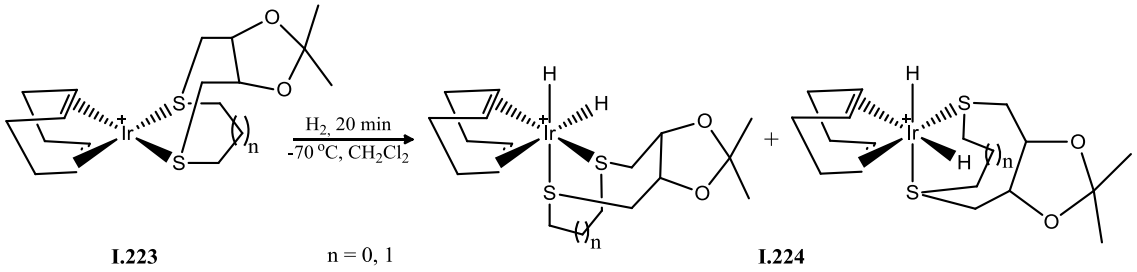

Scheme I.43

The addition of H_2 to a solution of the cationic diene iridium complex $[Ir(NHC)(PPh_3)(COD)]^+$ (**I.225**) containing a monodentate NHC ligand, which was found to be an effective catalyst for the hydrogenation of quinolines, in toluene in the presence of PPh_3 and of the noncoordinating base DBU (1,8-diazabicyclo[5,4,0]undec-7-ene) resulted in the formation of the neutral meridional trihydride complex **I.226** (Scheme I.44) [150]. Addition of 1 equiv of the strong acid $[H(Et_2O)_2]BArF_4$ to complex **I.226** afforded the single species **I.227**, wich was identified by NMR spectroscopy.

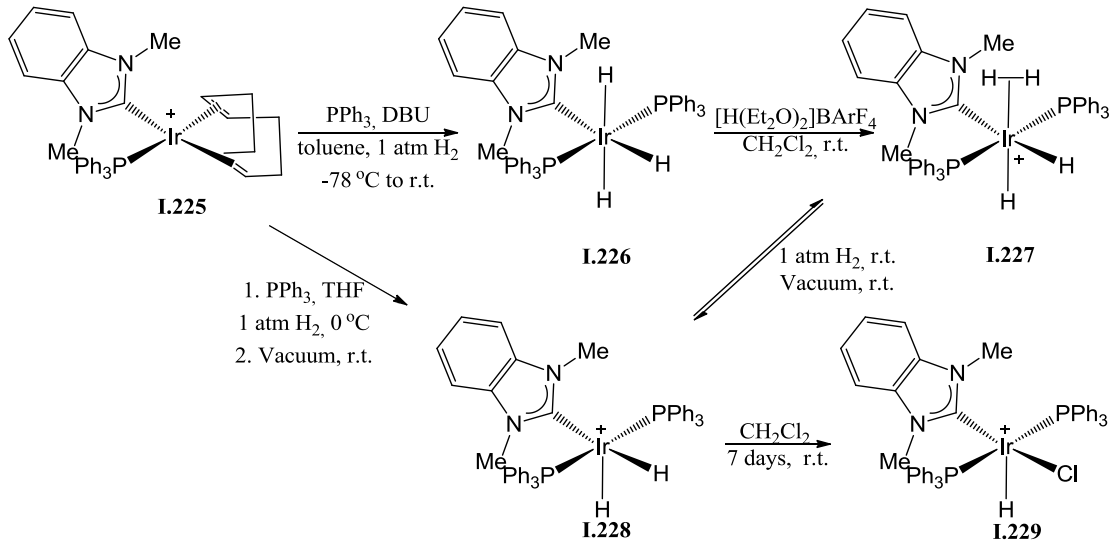

Scheme I.44

A different iridium hydride **I.228** was isolated from the reaction of the precatalyst **I.225**, PPh_3, and dihydrogen in THF, in the absence of base. The structure of **I.228** was confirmed by X-ray

crystallography on a crystal of the PF_6^- salt. Treatment of **I.228** with H_2 forms complex **I.227**, whereas standing in CD_2Cl_2 over several day at room temperature led to complex $[Ir(NHC)(PPh_3)_2HCl]^+$ (**I.229**). This is a possible mode of catalyst deactivation in catalytic reactions run in CD_2Cl_2. The X-ray analysis on a crystal of the PF_6^- salt shows that the monohydride complex **I.229** is square pyramidal with the H ligand in the apical position.

Finally, previous work in our own laboratory has shown that the addition of H_2 to the [Ir(P,SR)(CO)Cl] complexes **I.230** with the P,SR ligand **I.123-R** (R = Ph, Bu^t) could in principle lead to a variety of stereoisomers [26]. The results, obtained under kinetically and thermodynamically controlled conditions, lead to the global Scheme I.45. The diaserioisomeric products **I.231a** and **I.231b** result from the H_2 oxidative addition across the S-Ir-CO axis, whereas product **I.232a** (only one diastereomer was observed) originates from the slower addition over the P-Ir-Cl axis. Products **I.233a** and **I.233b** result from the kinetic products **I.231a,b** by an intramolecular isomerisation process.

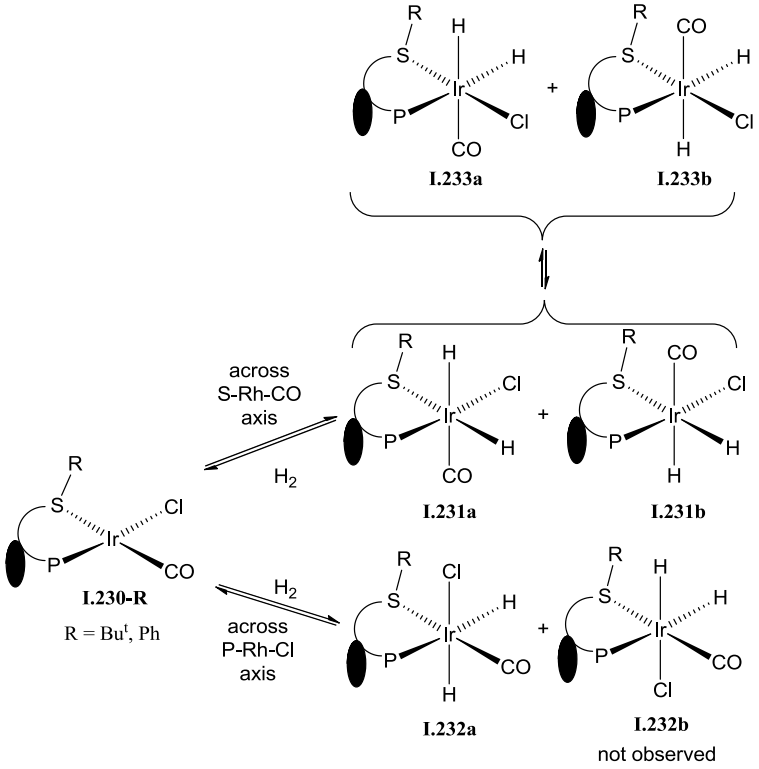

Scheme I.45

As conclusive remarks to this literature survey, we point out that, despite that diene complexes of rhodium and iridium are well known pre-catalysts in the hydrogenation of various substrates, all the reported literature studies have addressed this type of catalytic system (mostly for Rh and very little for Ir) under the conditions in which they catalyze the hydrogenation of functionalized alkenes. On the basis of these studies it was presumed that in coordinating solvents such as methanol the active form of the catalyst would consist of some type of solvated species. At that, solvated Ir species appear less

stable and therefore less amenable to spectroscopic and mechanistic investigations than those of Rh. Addition of a prochiral substrate (olefin bearing –COO- or –CONH- functional groups, able to coordinate to the metal) to the solution of a solvated complex led, as expected, to the formation of two diastereomeric catalyst–substrate complexes in the case of chiral C_2-symmetric diphosphine ligands. Relatively good stability of these complexes allowed their spectroscopic characterisation. The dihydrido Rh complexes with diphosphines, which could be another catalitically impotant species, were found rather elusive and difficult to detect.

II Results and discussion

II.1 Synthesis and coordination chemistry of [Rh(P,SR)(diene)X] complexes (P,S = CpFe[η^5-1,2-$C_5H_3(CH_2SR)(PPh_2)$], diene = COD, NBD, X = Cl^-, BF_4^-)

As pointed out in the Introduction, it was recently found that the iridium complexes [Ir(P,SR)(COD)Cl] are excellent precatalysts for the hydrogenation of acetophenone, yielding high activities and enantioselectivies [25, 32]. These promising results prompted us to study the catalytic properties of the corresponding rhodium complexes. In this first section, we will describe the synthesis and characterization of rhodium compounds having the same ligands and stoichiometry of the previously investigated Ir complexes. However, whereas only Ir systems containing COD as diene had been the subject of previous investigations, rhodium analogues with either COD or NBD were synthesized, because of the knowledge pointed out in Chapter 1 that the NBD complexes are generally activated more rapidly than the COD complexes. Before using these compounds for the catalytic studies, it was necessary to understand their structure and behavior in solution in order to verify whether the Rh compounds are good structural models of the Ir precatalysts.

II.1.1 Synthesis

The addition of the (P,SR) ligand **I.123** (1 equiv per Rh atom) to a dichloromethane solution of $[Rh(NBD)Cl]_2$ or $[Rh(COD)Cl]_2$ yielded the corresponding adducts [Rh(P,SR)(NBD)Cl], **II.1-R**, and [Rh(P,SR)(COD)Cl], **II.3-R**, see Scheme II.1. For the NBD reagent, the complete series with R = Bu^t, Ph, Bz and Et was obtained as pure derivatives as shown by the NMR and HRMS analyses. Concerning the COD series, although all compounds could be obtained in solution as shown by the spectroscopic analyses, only the Bu^t derivative **II.3-Bu^t** could be isolated as a pure product. Starting from **II.1-Bu^t**, addition of $NaBF_4$ in dichloromethane led to the precipitation of NaCl and formation of [Rh(P,SBu^t)(NBD)]BF_4, **II.2-Bu^t**, in sufficient purity. The complete series of the BF_4 salts containing the COD ligand, [Rh(P,SR)(COD)]BF_4, **II.4-R**, on the other hand, was more conveniently obtained by addition of (P,SR) to a solution of compound $[Rh(COD)_2]BF_4$. All these were isolated in a pure state.

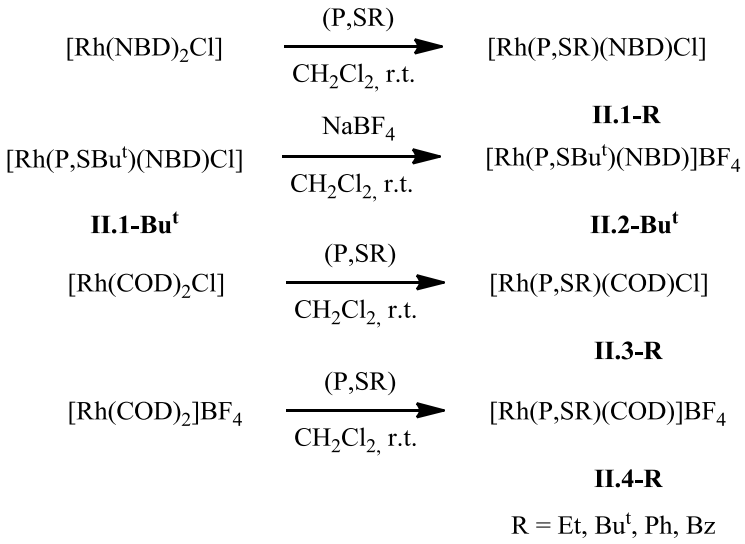

Scheme II.1

II.1.2 Characterization of the [Rh(P,SR)(diene)]$^+$ salts II.2-R and II.4-R

The characterization of the salts **II.2-R** and **II.4-R** was straightforward. Their NMR spectra in $CDCl_3$ show the ^1H, ^{13}C and ^{31}P chemical shifts and coupling patterns expected for the square planar coordination around the Rh^I center. In particular, Rh coupling is visible for selected ^{13}C resonances of the diene ligand and for the phosphine ^{31}P resonance (the latter is collected in Table II.1 for all compounds).

Table II.1 ^{31}P NMR data for the Rh complexes in $CDCl_3$ (δ in ppm with the $^2J_{PRh}$ in Hz in parentheses).

R	**II.1-R**	**II.2-R**	**II.3-R**	**II.4-R**
But	23.6 (159)	26.1 (158)	21.0 (148)	23.8 (143)
Ph	23.8 (154)		28.0 (166)	22.1 (144)
Bz	20.3 (147)		31.1 (170)	21.8 (144)
Et	21.3 (148)		22.8 (144)	22.9 (144)

The molecular geometry of compounds **II.2-But**, **II.4-Ph** and **II.4-Bz** was confirmed by single crystal X-ray diffraction. Whereas compound **II.2-But** contains only the cation and the anion in the crystal, compounds **II.4-Ph** and **II.4-Bz** crystallize with one molecule of dichloromethane per ion pair. Views of the three cations are shown in Fig. II.1 and relevant bond distances and angles for the three compounds are compared in Table II.2.

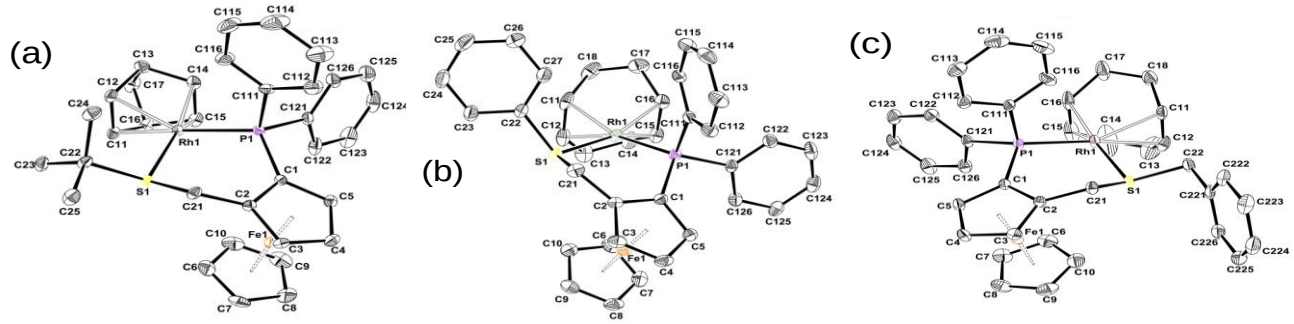

Fig. II.1. Molecular views of the cationic complexes in compounds **II.2-Bu^t** (a), **II.4-Ph** (b) and **II.4-Bz** (c) with the atom-labelling scheme. Displacement ellipsoids are drawn at the 30% probability level. The BF_4^- counterion and H atoms have been omitted for clarity.

The geometry is typical of $[Rh(L,L')(diene)]^+$ complexes where L,L' is a chelating ligand, of which over 1000 examples are reported in the literature. The two midpoints of the donating ene functions and the P and S donor atoms define an approximate square planar configuration, which is quite typical of d^8 Rh^I. As a matter of fact, the geometry is nearly ideal for **II.4-Ph**, with trans angles quite close to 180° (P–Rh–X1 and S–Rh–X2 = 178.6(3) and 174.69(6)°, respectively; X = midpoints of the C=C bonds, see Table II.2), whereas it is more distorted for **II.4-Bz**. A close inspection of the structure of **II.4-Bz** shows that this distortion is related to a twist of the COD ligand, which is caused by a van der Waals repulsion between one of the COD CH=CH donating groups (C11–C12) and the CH_2 group of the benzyl substituent on sulfur (C22). A similar van der Waals repulsion, namely a 2.16 Å contact between the H atoms on one of the Bu^t methyl groups (C23) and on atom C12 of the NBD ligand, explains the even larger distortion observed in **II.2-Bu^t** (P–Rh–X1 and S–Rh–X2 = 163.54(4) and 166.20(4)°, respectively; see Table II.2). As expected, the X1–Rh–X2 angle is much smaller for the NBD ligand with a value of 69.943(11)°, similar to the angle observed in related compound. Another peculiar geometrical feature is that the sulfur substituent is placed anti relative to the CpFe moiety of the ferrocene group for the three complexes. Upon coordination, the sulfur atom becomes chiral and therefore two different diastereoisomers could be obtained in principle, with the sulfur substituent either *syn* or *anti* to the CpFe moiety. Similarly to all previously reported complexes containing ligands of this family, without exception [25], a single compound is obtained in solution and the sulfur substituent is placed on the side opposite (*anti*) to the FeCp group with respect to the S–C–C–C–P chelate. Consequently, the observed diastereomer has the configuration (S_{fc}, S_S) or (R_{fc}, R_S) for **II.2-Bu^t** and for **II.4-Ph** and (R_{fc}, S_S) or (S_{fc}, R_S) for **II.4-Bz**. The two Cp rings are roughly eclipsed with the largest twist angle, τ, 7.5(4)° for **II.4-Bz**.

Table II.2 Selected experimental (from X-ray diffraction) and computed (by DFT/B3LYP optimizations) bond lengths (Å) and angles (°) in compounds **II.2-R** and **II.4-R**.

	II.2-Bu^t		**II.2-Ph**	**II.4-Bu^t**	**II.4-Ph**		**II.4-Bz**
	X-ray	**DFT**	**DFT**	**DFT**	**X-ray**	**DFT**	**X-ray**
Distances[a]							
Rh-P	2.2587(13)	2.331	2.343	2.354	2.2858(15)	2.354	2.2796(10)
Rh-S	2.3641(13)	2.452	2.402	2.508	2.3378(11)	2.421	2.3194(10)
Rh-X1	2.1231(3)	2.165	2.145	2.179	2.119(2)	2.184	2.1198(3)
Rh-X2	2.0066(4)	2.032	2.047	2.062	2.040(5)	2.069	2.0199(3)
Rh-C11	2.229(5)	2.263	2.260	2.302	2.227(4)	2.310	2.210(4)
Rh-C12	2.229(5)	2.283	2.248	2.270	2.227(4)	2.271	2.240(4)
Rh-C15	2.118(5)	2.159	2.169	2.173	2.169(4)	2.182	2.127(5)
Rh-C16	2.127(5)	2.141	2.159	2.183	2.142(4)	2.188	2.142(5)
C11-C12	1.358(8)	1.409	1.404	1.408	1.368(8)	1.404	1.352(8)
C15-C16	1.384(8)	1.383	1.385	1.384	1.391(7)	1.385	1.380(11)
Angles[a]							
P-Rh-S	92.64(5)	92.2	92.6	90.3	92.30(3)	90.9	93.24(4)
P-Rh-X1	163.54(4)	165.6	168.8	175.8	178.6(3)	177.2	168.29(3)
P-Rh-X2	93.84(13)	97.6	99.6	92.5	93.01(6)	93.5	91.59(3)
S-Rh-X1	103.01(3)	102.0	98.5	93.1	88.83(12)	91.0	90.95(3)
S-Rh-X2	166.20(4)	163.5	166.1	171.6	174.69(6)	172.6	168.21(3)
X1-Rh-X2	69.943(11)	69.2	69.6	84.4	85.87(17)	84.9	86.423(13)

[a]X1 and X2 are the midpoints of the coordinating C=C functions, C11-C12 and C14-C15 (for the NBD complexes) or C15-C16 (for the COD complexes), respectively.

A few other $[Rh(P,S)(diene)]^{n+}$ complexes of d^8 Rh^I have been previously described, some being cationic with a phosphine–thioether [151-155] or phosphine–phosphine sulfide [156, 157] ligand, others being neutral with a phosphine–thiolato ligand [156, 158, 159], but the Rh–S distance does not appear to be too sensitive to this modification. The Rh–P and Rh–S distances found for **II.4-Ph** and **II.4-Bz** (see Table II.2) compare quite well with the average in the above mentioned examples (Rh–P: 2,29(3) Å and Rh–S: 2,36(3) Å). Whereas the Rh–P distances are quite similar for the three compounds, the Rh–S distance is significantly shorter in **II.4-Bz**, suggesting a better binding ability of the benzyl derivative, and longer in **II.2-Bu^t**, probably reflecting the greater steric bulk of the sulphur substituent which is also responsible for the greater geometry distortion (vide supra). There are no reasons to doubt that the solution structures of the other **II.4-R** compounds are identical to the solid state structure found for **II.4-Ph** and **II.4-Bz**.

DFT/B3LYP geometry optimizations were carried out by Dr. Oleg Filippov in the INEOS group for the cations of **II.2-Bu^t** and **II.4-R** with R = Bu^t and Ph. The results are also reported in Table II.2. For compounds **II.2-Bu^t** and **II.4-Ph**, the optimized geometry reproduced quite well the experimentally observed one, except for a slight overestimation of the Rh–P, Rh–S and Rh–C distances (by 0.08 Å on average for Rh–S and Rh–P, 0.04 Å for Rh–C). Whereas the calculated Rh–P

distance is essentially the same in all four compounds, the Rh–S distance increases from Ph to the more bulky Bu^t substituent, in agreement with the experimental evidence. Views of all optimized geometries are provided in Fig. II.2.

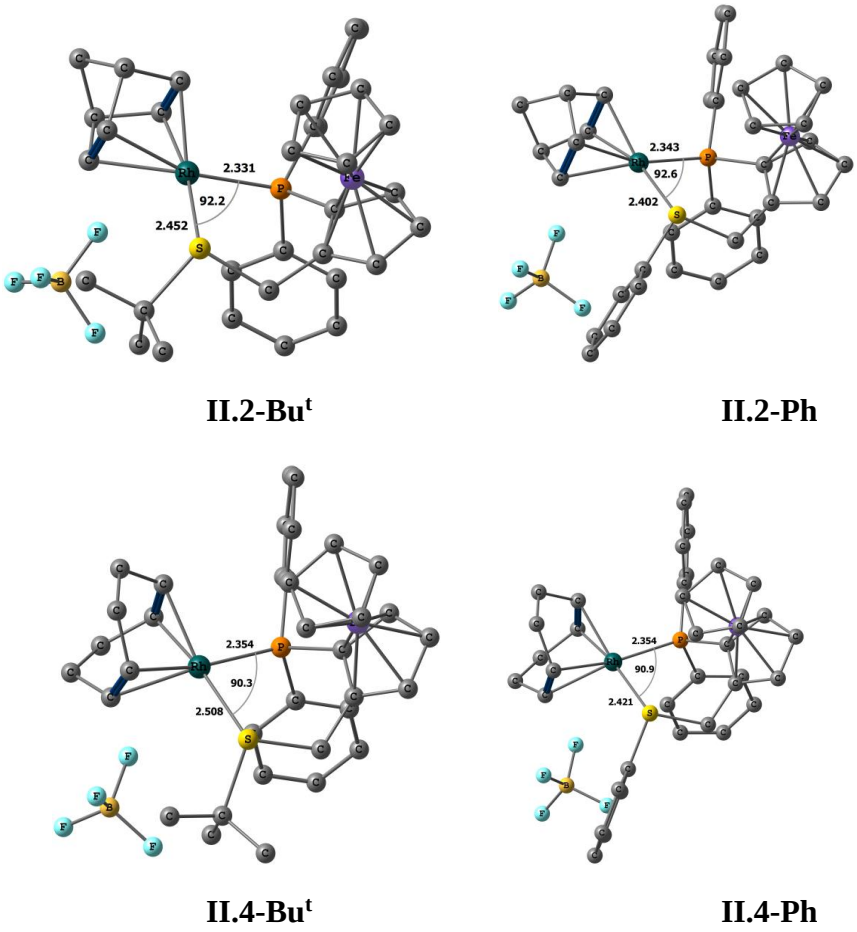

II.2-Bu^t **II.2-Ph**

II.4-Bu^t **II.4-Ph**

Fig. II.2 DFT(B3LYP) optimized geometry of **II.2-R** and **II.4-R** (R = Ph, Bu^t). Hydrogen atoms are omitted for clarity.

II.1.3 Characterization of the chloride complexes II.1-R and II.3-R

The solution and solid state structures of the neutral chlorido complexes cannot be assigned as easily as those of BF_4^- salts because of the presence of five potentially coordinating ligands. We were unfortunately unable to obtain single crystals for any of these compounds, preventing us from determining the solid state structure. It is also relevant to point out that the structure adopted by the related iridium complexes (**I.124-R**) depends on the nature of the thioether substituent [25]. For R = Bu^t, the molecule has a square planar geometry with a (COD)ClP coordination environment and a dangling thioether function (i.e. structure **I.1a** in Scheme I.1), whereas the compounds with R = Et, Ph and Bz prefer a pentacoordinated square pyramidal geometry with a loosely bonded axial Cl ligand (structure **I.1b**). These structural motifs seem to be maintained in solution, according to the observed

differences in the NMR properties, notably the ^{31}P resonance. The Rh complexes **II.1-R** and **II.3-R** could conceivably adopt structure **I.1a** or **I.1b**, but a third possibility (**I.1c**) with a chelating (P,S) ligand and an outer sphere chloride ion, related to those observed for **II.2-Bu^t**, **II.4-Ph** and **II.4-Bz** by simple replacement of the BF_4^- ion with Cl^-, can also be imagined.

Since no suitable single crystals for a diffraction analysis could be obtained for any of the compounds **II.1-R** and **II.3-R**, their structure was addressed by a combination of spectroscopic techniques (IR, NMR) and DFT calculations.

As shown in Table II.1, the ^{31}P chemical shift and Rh coupling for compounds **II.1-R** and **II.3-R** do not greatly differ from those of the BF_4^- salts **II.2-R** and **II.4-R**. This is an expected occurrence if the chloride complexes adopted structure **I.1c**. It should be remarked that the ^{31}P chemical shift in the [Ir(P,SR)(COD)Cl] (**I.124-R**) and $[Ir(P,SR)(COD)]^+$ compounds was found diagnostic for discriminating structures of type **I.1a** (δ −4.2 for R = Ph and −3.1 for R = Et) from **I.1b** (δ 15.7 for R = Bu^t) and **I.1c** (δ 11.0 for R = Ph and 14.5 for R = Bu^t). Therefore, the similarity between the resonances of the chloride complexes **II.1-R** and **II.3-R** with those of the BF_4^- salts **II.2-R** and **II.4-R** that are known to adopt structure **I.1c** is consistent with a structure of type **I.1c** for the chloride complexes. This argument, however, can in no way be considered conclusive because the metal nature may have a different effect on the chemical shift of the different structural types.

Another useful comparison comes from the detailed analysis of the ^1H spectra. Most protons (i.e. diene, PPh_2) are not expected to greatly respond to the structural type. The $FcCH_2S$ protons, on the other hand, may be sensitive to the thioether coordination, namely discriminate between **I.1a** and **I.1b**/**I.1c**. The two protons of this group, whether the S atom is coordinated or not, are diastereotopic and therefore always give rise to an AB pattern. This feature was also observed for the free ligands and for the sulfur-protected version of the free ligand, (**II.5-R**), the ^1H and ^{13}C resonances of which are collected in Table II.3 together with those of the isolated compounds **II.1-R** - **II.4-R**.

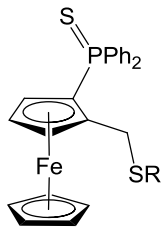

II.5-R

R = Me, Bu^t, Ph, Bz

It can be noted that the two doublets of the AB pattern in the ^1H NMR are very close to each other in the (P,SR) and (S=P,SR) molecules ($\Delta\delta < 0.4$ ppm). This difference is systematically much greater for the cationic complexes in the BF_4^- salts where the S atom is coordinated to the Rh centre

(0.83 ppm in **II.4-Bz** and >1 ppm for all other examples). It can be argued that the enantioselective sulfur coordination makes a further magnetic discrimination of the two CH_2 protons, thereby increasing their chemical shift difference. Considering now the chlorido derivatives, we note that three of them exhibit a small chemical shift difference (0.13 for **II.1-Bz**, 0.31 for **II.1-Et**, ca. 0.3 for **II.3-Bu^t**), whereas the Δδ values are much greater for the other two compounds (1.22 for **II.1-Bu^t**, 1.09 for **II.1-Ph**) and comparable to those of the cationic complexes. These results would tend to suggest that the thioether function is not coordinated to the Rh center in complexes **II.1-Bz**, **II.1-Et** and **II.3-Bu^t** (e.g. structure **I.1a**), whereas coordination might occur for the other two derivatives. Analysis of the FcCH_2S ^{13}C chemical shift does not bring any additional clarification, since this resonance appears to be very little sensitive to the chemical environment as shown in Table II.3.

Table II.3 Selected ^{1}H (Δδ in parentheses) and ^{13}C NMR (in italics) data for the Fc*C*H_2S group in complexes **II.1-R - II.4-R** (δ in ppm).

R	**II.1-R**	**II.2-R**	**II.3-R**	**II.4-R**	(**I.123-R**)[a]	(**II.5-R**)[b]
Bu^t	5.06; 3.84 (1.22) *28.8*	3.96; 2.81 (1.15) *29.1*	ca. 4.2; 3.91 (ca. 0.3) *28.6*	ca. 4.0; 2.69 (ca. 1.3) *29.2*	3.80; 3.63 (0.17) *27.4*	3.99; 3.96 (0.04) *26.7*
Ph	5.3; 4.2 (1.09) *34.1*			4.17; 3.04 (1.15) *37.9*	4.17; 4.09 (0.08) *34.2*	4.42; 4.35 (0.07) *33.3*
Bz	4.13; 4.00 (0.13) *31.3*			3.50; 2.67 (0.83) *31.5*	3.72; 3.65 (0.07) *31.1*	4.14; 3.77 (0.37) *30.5*
Et	4.37; 4.06 (0.31) *30.8*			ca. 4.0; 2.70 (ca. 1.3) *30.3*	3.74; 3.74 (0.00) *30.9*	4.09; 3.87 (0.22) *30.3*

[a]Free ligand, data from ref. [29]. [b]Ligand protected at phosphorus atom (**II.5-R**), data from ref. [29].

Since the NMR analysis does not allow an unambiguous assignment of the chemical structure for the chlorido derivatives, additional studies were carried out by solid state IR spectroscopy, although limited to the P,SBu^t derivatives. Spectra in the lower fingerprint region (600–250 cm^{-1}) were measured in the solid state for **II.1-Bu^t**, **II.2-Bu^t**, **II.3-Bu^t**, **II.4-Bu^t** and also for [Ir(P,SBu^t)(COD)Cl] (**I.124-Bu^t**), for which the solid state structure was unambiguously shown by X-ray diffraction to be of type **I.1a**, and the results are reported in Fig. II.3. The M–Cl stretching region shows various bands, the most intense one having a higher frequency for the iridium compound **I.124-Bu^t** (295 cm^{-1}) than for the rhodium compounds **II.1-Bu^t** and **II.3-Bu^t** (271 and 288 cm^{-1}, respectively). The assignment of these bands to the Ir–Cl and Rh–Cl stretching vibrations, respectively, was confirmed by the calculations (vide infra). On going to the tetrafluoroborate salts **II.2-Bu^t** and **II.4-Bu^t**, the major band disappears in agreement with the removal of the Cl^- ligand from the metal coordination sphere. These observations are in favor of a coordination geometry of type **I.1a** or **I.1b** (Scheme I.1).

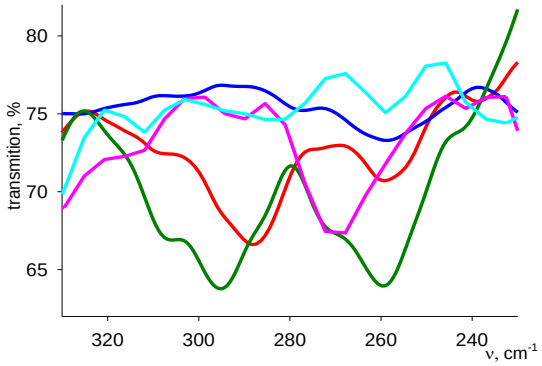

Fig. II.3 Solid state IR spectra (lower fingerprint region) of **II.3-Bu^t** (red line), **II.4-Bu^t** (blue line), **II.1-Bu^t** (pink line), **II.2-Bu^t** (cyan line) and **I.124-Bu^t** (green line).

Geometry optimizations for all three types of structures were carried out by Dr. Filippov at the same computational level as for the cationic complexes described above. The calculations were carried out for complexes **II.1-R** and **II.3-R** for R = Bu^t and Ph in order to evaluate the effect of the R substituent and the diene ligand. The geometry of the iridium analogue **I.124-Bu^t** was also optimized and was found to agree quite well with that obtained experimentally in the solid state. The most significant metric parameters for all optimized structures are summarized in Table II.4.

Table II.4 Selected bond lengths (Å) and angles (°) in the DFT optimized geometries of **II.1-Ph**, **II.1-Bu^t**, **II.3-Ph**, **II.3-Bu^t**, and **I.124-Bu^t**.

	II.1-Ph		**II.1-Bu^t**		**II.3-Ph**		**II.3-Bu^t**	**I.124-Bu^t**	
								DFT	X-ray[a]
ΔE, kcal mol^{-1}	0	3.1	0	8.2	0	3.8			
Distances									
M-P	2.407	2.394	2.400	2.344	2.447	2.413	2.418	2.403	2.3312(9)
M-Cl	2.390	2.459	2.382	2.572	2.405	2.428	2.406	2.420	2.3625(8)
M-X1[b]	2.098	2.068	2.101	2.198	2.109	2.117	2.120	2.105	2.0859(6)
M-X2[b]	2.014	2.018	2.016	1.969	2..034	2.021	2.029	2.017	1.9988(5)
M···S	5.918	2.824	5.903	2.702	6.269	3.674	5.556	5.533	-
Cl···H[c]	2.451	2.586	2.497	3.491	2.534	2.509	2.759	2.818	
C=C (1)	1.390	1.401	1.389	1.379	1.392	1.390	1.390	1.402	1.392(4)
C=C (2)	1.413	1.418	1.413	1.445	1.412	1.415	1.412	1.428	1.418(4)
Angles									
P-M-X1	168.3	158.9	169.7	163.8	177.1	175.7	175.5	176.0	177.594(17)
P-M-X2	99.3	102.9	100.7	95.0	95.5	97.1	95.8	95.5	93.369(19)
P-M-Cl	97.3	88.6	95.3	96.9	90.8	88.0	90.6	91.2	92.49(2)
Cl-M-X1	92.5	92.7	93.1	94.7	87.3	88.2	87.9	87.7	87.904(18)
Cl-M-X2	163.1	159.0	163.5	134.8	171.8	169.7	169.9	170.0	172.601(17)
X1-M-X2	70.6	70.5	70.6	68.8	86.1	86.4	86.2	86.1	86.434(11)

[a] Data from ref. [25]. [b]X is the center of the C=C bond (X1 for the C=C bond cis to the Cl ligand and X2 for the C=C bond cis to the P ligand) . [c]Distance to the hydrogen of CH_2SR bridge.

All attempts to optimize the geometry of $[Rh(P,SR)(diene)]^+$ with Cl^- as a counteranion (e.g. a geometry of type **I.1c** in Scheme I.1) led to the dissociation of the thioether arm to allow formation of the rhodium–chloride bond (i.e. an optimized geometry of type **I.1a** in Scheme I.1). The geometry of the only local energy minimum obtained for **II.3-Bu^t** is quite similar to that of the iridium analogue, with the sulfur atom far away from the Rh center (5.556 Å). Similar optimized geometries are also adopted by the other complexes (**II.1-Ph**, **II.1-Bu^t**, **II.3-Ph**). Replacement of the S atom in the coordination sphere of **II.2-R** or **II.4-R** by the Cl atom in **II.1-R** or **II.3-R** systematically lengthens the M–P bond by ca. 0.05 Å (cf. Table II.3 and Table II.4).

A second, higher energy minimum was also found for complexes **II.1-Ph**, **II.1-Bu^t** and **II.3-Ph**. In these structures, the sulfur donor function has rearranged to place itself along the z direction perpendicularly to the square plane defined by the other four ligands, loosely interacting with the metal center, defining a pseudo pentacoordinated square-pyramidal geometry like that of **I.1b** in Scheme II.3, except that the axial coordination position of the square pyramid is occupied by the sulfur atom instead of the Cl atom (type **I.1b′**). All optimized geometries are shown in Fig. II.4. The Rh–S distance is too long to be considered an interaction for compound **II.3-Ph** (3.674 Å), whereas it signals a genuine 5-coordinate geometry for **II.1-Ph** (2.824 Å) and **II.1-Bu^t** (2.702 Å), when considering that the axial interaction for 5-coordinate square pyramidal d^8 complexes is lengthened by the d_z^2 electron pair. The shorter Rh–S separation for the Bu^t derivative may be related to the greater donating power of the SBu^t donor function. On the other hand, this geometry is more destabilized relative to the square planar global minimum for **II.1-Bu^t** (by 8.2 kcal mol^{-1}) than for **II.1-Ph** (3.1 kcal mol^{-1}). The greater steric bulk of the Bu^t group may be responsible for this difference. All attempts to optimize a type **I.1b** geometry led to one of the above mentioned minima. Therefore, the geometry optimizations are in favor of a structure of type **I.1a** for compounds **II.1-R** and **II.3-R**, irrespective of the nature of the R substituent (at least for Ph and Bu^t).

(a) II.1-Bu^t

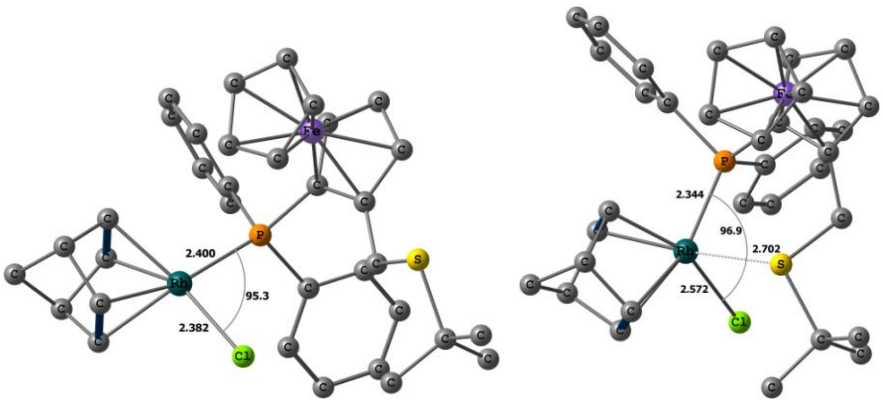

Type I.1b (0.0 kcal/mol) **Type I.1b′ (8.2 kcal/mol)**

(b) II.1-Ph

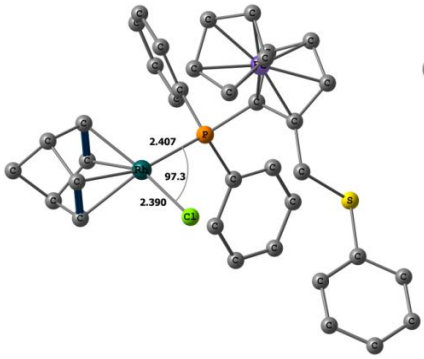

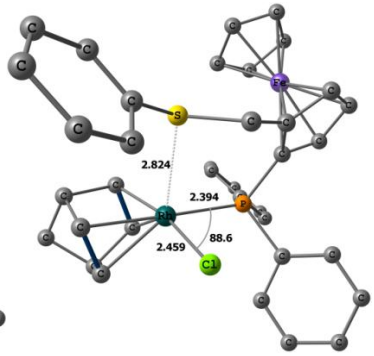

Type I.1b (0.0 kcal/mol) **Type I.1b′ (3.1 kcal/mol)**

(c) II.3-Ph

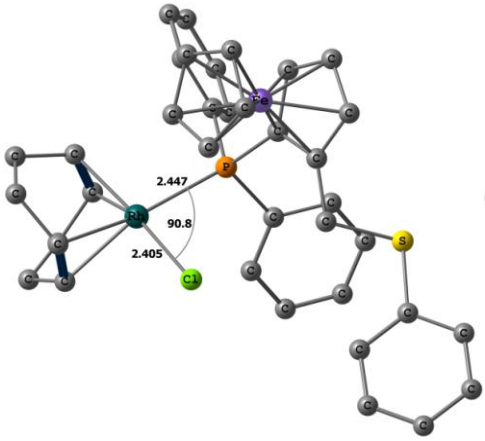

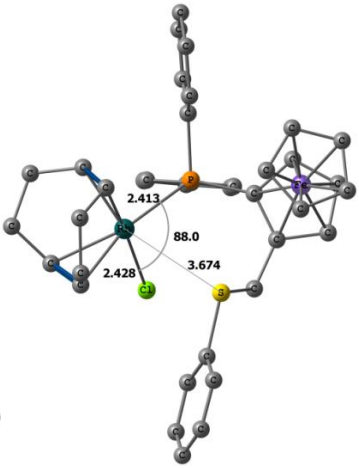

Type I.1b (0.0 kcal/mol) **Type I.1b′ (3.8 kcal/mol)**

(d) II.3-Bu^t **(e) I.124-Bu^t**

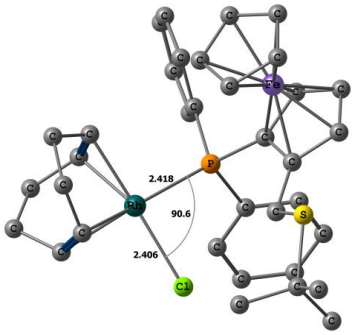

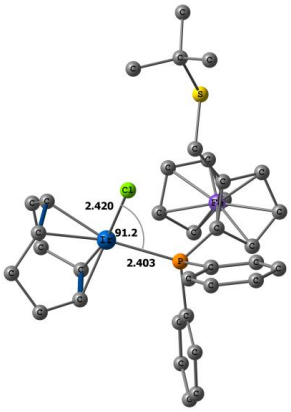

Fig. II.4 DFT(B3LYP) optimized geometries of **II.1-R**, **II.3-R** (R = Ph, Bu^t) and **I.124-Bu^t**. Hydrogen atoms are omitted for clarity.

It is now of interest to analyze the calculated IR spectra of the observed minima and compare them with the experimental ones reported in Fig. II.3. According to the calculations the M–Cl stretching vibration is coupled with M-(diene) stretches in all rhodium complexes and contributes mostly to two intense bands, which exhibit a greater frequency difference in the COD series. The analysis is rather simple for the COD compound **II.3-Bu^t** and for the iridium analogue, since only a minimum of type **I.1a** was optimized. The computed spectra for these two compounds, as well as for the salt **II.4-Bu^t**, are shown in Fig. II.5. These spectra match rather closely those observed experimentally, confirming the type **1.1a** structure. The calculated maximum absorption for the strongest M–Cl stretching band is at 279 cm^{-1} for the Ir complex and at 277 cm^{-1} for the Rh complex **II.3-Bu^t**, whereas the spectrum of **II.4-Bu^t** does not show any strong band in this region. The adoption of a structure of type **I.1a** by compound **II.3-Bu^t** is also in line with the suggestion of the ^{1}H NMR spectrum (AB pattern of the CH_2SBu^t moiety, vide supra).

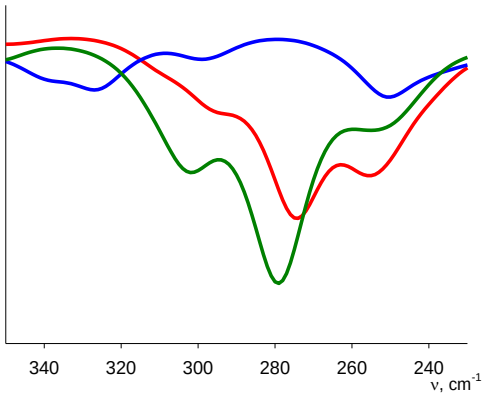

Fig. II.5 Calculated IR spectra (lower fingerprint region) of **II.3-Bu^t** (red line), **II.4-Bu^t** (blue line) and **I.124-Bu^t** (green line).

The calculated spectra for the type **I.1a** and type **I.1b′** minima of compounds **II.1-Bu^t** and **II.1-Ph** are shown in Fig. II.6. It can be seen that the Rh–Cl stretching band for the type **I.1a** minima is very similar to that of compound **II.3-Bu^t** (286 and 273 cm^{-1} for the strongest absorption). On the other hand, the Rh–Cl vibration is shifted to much lower frequencies in the type **I.1b′** minima of **II.1-Ph** (247 cm^{-1}), and especially of **II.1-Bu^t** (208 cm^{-1}).

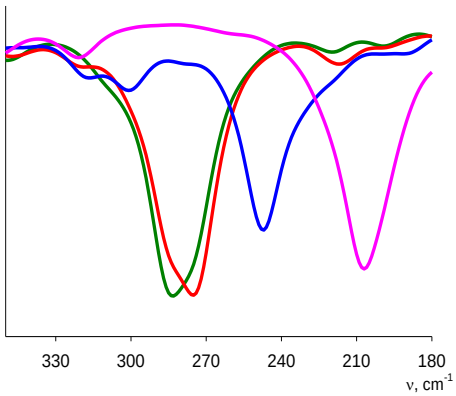

Fig. II.6 Calculated IR spectra (lower fingerprint region) of **II.1-Bu^t** type **I.1a** (green line), **II.1-Ph** type **I.1a** (red line), **II.1-Bu^t** type **I.1b′** (pink line) and **II.1-Ph** type **I.1b′** (blue line).

This effect can obviously be attributed to the coordination of the sulfur atom, which provides additional electron density to the metal center and labilizes the Rh–Cl bond, an effect which is stronger for the Bu^t derivative where the Rh–S distance is shorter. In agreement with this argument, the Rh–Cl distance is shorter for the type **I.1a** minima of compounds **II.1-Bu^t** and **II.1-Ph** (2.382 and 2.390 Å, respectively) and longer for the type **I.1b′** geometries of **II.1-Ph** (2.459 Å) and particularly **II.1-Bu^t** (2.572 Å). The difference between the calculated Rh–Cl frequencies for the type **I.1a** and **I.1b′** minima ($\Delta\nu$) is 78 cm^{-1} for **II.1-Bu^t** and 26 cm^{-1} for **II.1-Ph**. On the other hand, the experimental Rh–Cl stretching frequency in **II.1-Bu^t** is only 17 cm^{-1} lower than that of compound **II.3-Bu^t**. Therefore, we conclude that the structure adopted by compound **II.1-Bu^t** is most likely of type **I.1a** in the solid state, like that of compound **II.3-Bu^t**. However, the large chemical shift difference for the CH_2SBu^t AB resonances in the ^{1}H NMR spectrum suggests that a structure of type **I.1b′** might be more favorable in solution for this compound. If this is the case, the difference is certainly a consequence of the lower steric encumbrance of the norbornadiene ligand relative to cyclooctadiene.

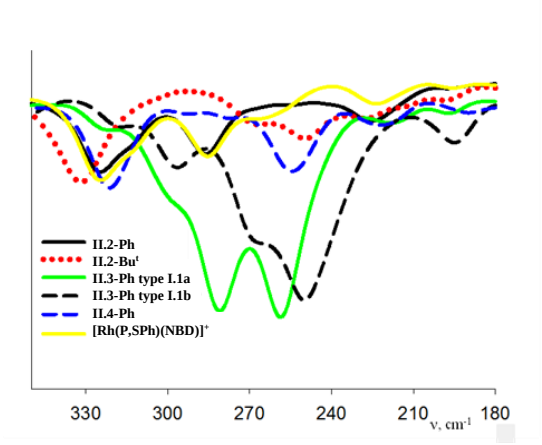

Fig. II.7 Calculated IR spectra (lower fingerprint region) for complexes **II.1-R** (R = Ph, Bu^t), **II.3-Ph**, **II.4-Ph** and [Rh(P,SPh)(NBD)]$^+$.

The calculated spectra of compounds **II.1-Ph** and **II.3-Ph** (Fig. II.7) exhibit similar features, with the major bands in the 260–280 cm^{-1} range for the type **I.1a** structures and in the 240–270 cm^{-1} range for the type **I.1b′** structures.

Thus, rhodium complexes associating chiral ferrocenyl phosphine–thioethers and diene (COD or NBD) ligands have been synthesized and fully characterized. For the chloride complexes, for which X-ray structural analyses could not be carried out, the combination of NMR and IR spectroscopy and DFT calculations indicates that they adopt a square planar geometry with a dangling thioether function. A second, pentacoordinated structure with a square pyramidal geometry and the thioether function placed in the axial position is however easily accessible. The cationic complexes, on the other hand adopt a standard square planar bis-chelated structure.

II.1.4 Conclusive remarks

Rhodium compounds having the same formula of the previously investigated [Ir(P,SR)(COD)Cl] (R = Bu^t, Et, Ph, Bz) have been prepared and characterized. Analogous chloride complexes with NBD in place of COD have also been prepared and characterized, as well as charge separated complexes $[Rh(P,SR)(diene)]^+BF_4^-$ (diene = COD, NBD). The BF_4^- salts do not present any structural ambiguity contrary to the chloride complexes in view of the strong coordinating power of the Cl^- anion. Because of the lower tendency of Rh^I to expand its coordination sphere relative to Ir^I, these complexes always adopt a four coordinate geometry in the solid state with a coordinated Cl atom and a dangling thioether function, similar to the structure previously determined for the [Ir(P,SBu^t)(COD)Cl] complex. In solution, however, the presence of a weak interaction between the thioether function and the Rh^I center is not to be excluded on the basis of the ^1H NMR evidence. Therefore, the rhodium complexes can be considered at least in part as good structural models of the [Ir(P,SR)(COD)Cl] complexes used as ketone hydrogenation pre-catalysts.

II.2 Catalytic activity of the [M(P,SR)(diene)X] complexes (M = Rh, Ir) in the asymmetric hydrogenation of unsaturated substrates and in the isomerisation of allylic alcohols

This second section presents catalytic studies of different reactions in the presence of the new Rh complexes described in part II.1. The main purpose of these catalytic studies was to see whether the Rh complexes are not only good structural models but also good functional models of the Ir analogues in the hydrogenation of ketones, in order to proceed later to a more detailed study of the activation process (part II.3). Therefore, the section will begin with the exploration of the catalytic activity in ketone hydrogenation. However, preliminary catalytic investigations of these complexes in other reactions have also been carried out and the corresponding results will also be presented.

II.2.1 Asymmetric hydrogenation of ketones

Acetophenone (**II.6**) hydrogenation (Scheme II.2) was chosen as a standard reaction to investigate the influence of the diene and X ligands on the catalytic performance of rhodium complexes. The rhodium complexes with the Bu^t substituent on the sulfur atom were initially used. To compare the catalytic activity of rhodium and iridium complexes under the same conditions the activity of iridium chloride complex with (P,SBu^t)-, COD- ligands was also investigated. The reactions were carried out under the conditions (hydrogen pressure, temperature, ratio of reagents; see footnote to Table II.5) that were optimized in previous studies [71, 72] for the iridium complexes. The results of the investigations are summarized in Table II.5 and Fig. II.8.

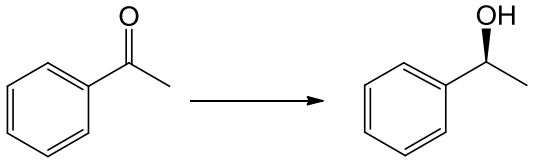

II.6 **II.7**

Scheme II.2 Reagents: [M(P,SR)(diene)X], H_2, Pr^iOH, MeONa.

Table II.5 Representative results of the asymmetric hydrogenation of acetophenone in the presence of complexes (*R*)-[M(P,SBu^t)(diene)X].[a]

Entry	Catalyst	*t*, h	Conversion, %	*ee*, %[b]
1	**I.124-Bu^t**	2	99	60
2	**II.3-Bu^t**	2	16	54
3	**II.1-Bu^t**	2	13	44
4	**II.4-Bu^t**	2	22	32
5	**II.2-Bu^t**	2	24	31
6	**I.124-Bu^t**	5	>99	63
7	**II.3-Bu^t**	5	57	48
8	**II.1-Bu^t**	5	22	42
9	**II.4-Bu^t**	5	45	32
10	**II.2-Bu^t**	5	37	36
11	**I.124-Bu^t**	16	>99	58
12	**II.3-Bu^t**	16	90	33
13	**II.1-Bu^t**	16	54	30
14	**II.4-Bu^t**	16	77	35
15	**II.2-Bu^t**	16	51	33

[a]Reaction conditions: catalyst ($6.4\cdot10^{-3}$ mmol), NaOMe ($3.2\cdot10^{-2}$ mmol), acetophenone (3.2 mmol), T = 25 °C and P_{H2} = 30 bar. Solvent = Pr^iOH (2 mL). The conversion and *ee* were determined by GC. [b]The *ee* is reported with respect to the *R*- configuration.

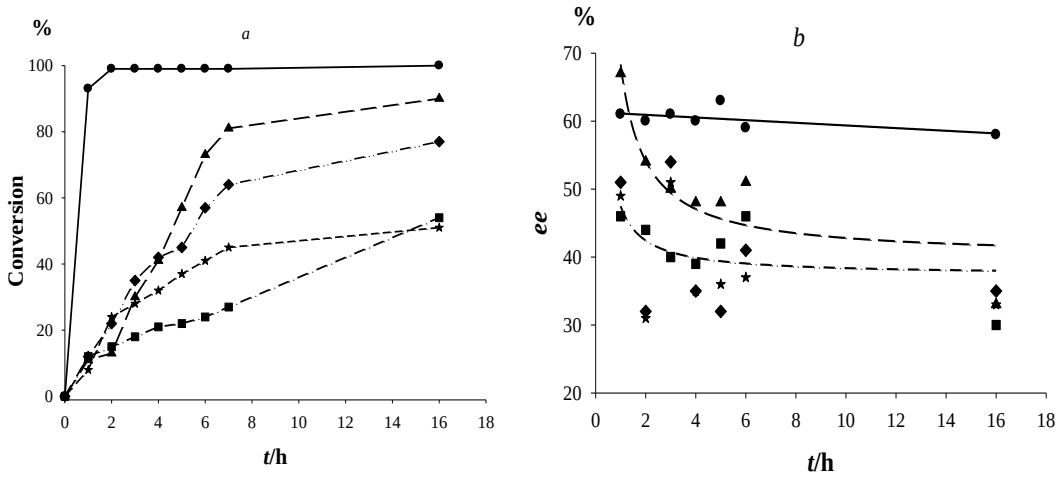

Fig. II.8. Dependence of the acetophenone conversion (*a*) and *ee* of the (*R*)-1-phenylethanol product **II.7** (*b*) on reaction time for several complexes with (*R*)-(P,SBu^t) ligand: **I.124-Bu^t** (●); **II.3-Bu^t** (▲); **II.1-Bu^t** (■); **II.4-Bu^t** (♦) and **II.2-Bu^t** (⋆).

Under these conditions the iridium complex **I.124-Bu^t** has higher activity and enantioselectivity, giving a quantitative conversion of acetophenone after 2 h (see Table II.5, Entry *1*). The initial activity (measured from the conversion after 1 hour) of all four rhodium precatalysts is nearly the same and much lower than that of **I.124-Bu^t** (see Fig. II.8). It is interesting to note that the activity of the COD complexes is higher than that of the NBD complexes, as particularly noticeable after 5 – 7 h of reaction. In case of the COD derivatives, the complex with the Cl^- anion is more active than that with the BF_4^- anion (*cf*. entries *2*/*4*, *7*/*9*, and *12*/*14* in Table II.5), while for the NBD derivatives, the dependence is opposite (*cf*. entries *3*/*5*, *8*/*10*, and *13*/*15*). Full conversion of the substrate was achieved within 72 h for all rhodium catalysts.

It was established that the precatalysts of type $[M(L,L')(diene)]^+$ (L,L' = diphosphine ligand) can be activated by H_2 [107, 124]. When alcohol (ROH) was used as a solvent the reaction gives complexes of type $[M(L,L')(ROH)_2]^+$ and the products of partial or total diene hydrogenation [105, 109]. Assuming a similar reaction mechanism for complexes **II.1-II.4**, each pair of precatalysts with different diene and the same anion is expected to give the same catalytically active spesies $[M(L,L')(ROH)_2]^+$. Indeed, the absence of an induction period and the same initial (after 1 h) activity for all rhodium complexes indicate a high activation rate and the formation of catalytically active species having the same structure. The investigation of the precatalyst [M(L,L')(diene)X] structure revealed that Cl^- ion is located in the metal coordination sphere, successfully competing with sulfur atom of the P,SR-ligand for binding to the rhodium atom in the solid state. This structure should be preserved in slightly polar noncoordinating solvents like $CDCl_3$. This phenomenon (competitive coordination of Cl^- instead of S) can also occur in case of the catalytically active form of the complex, but the solvent used (Pr^iOH) should stabilize ionic complexes better than neutral chloride complexes.

Therefore, we can propose that the catalysts are $[M(L,L')(ROH)_2]^+X^-$ complexes. The similarity in the initial rates for the 4 rhodium complexes (after 1h) suggests a low effect of the counter anion at this stage. However, the decays of these initial rates are strongly dependent on the nature of the anion and even more surprinsigly on the diene ligand originally present in the precatalyst. This phenomenon may be related to ligand redistibution processes leading to dimers, trimers,…with bridging P,SR-ligands as already observed for iridium analogues [25]. This slow ligand redistribution may be favored by the presence of hydride ligands on rhodium during the catalytic hydrogenation and affected further by the nature of X^-.

For the iridium complex the enantiomeric excess (*ee*) remains essentially constant during the course of the reaction, which demonstrates that the product does not racemize under the reaction conditions since the conversion is complete already after 2h. In case of the rhodium complexes, on the other hand, we observe a significant *ee* decrease with the conversion (see Fig. II.8*b*). A control experiment run in the presence of **II.3-Bu^t** shows that 1-phenylethanol does not racemise under the catalytic conditions ($6.4\cdot10^{-3}$ mmol of catalyst, $3.2\cdot10^{-2}$ mmol of NaOMe and 3.2 mmol of 1-phenylethanol in 2 mL of Pr^{i}OH, T = 25 °C and P_{H2} = 30 bar). However, we wondered whether the substrate itself could be involved in a racemization reaction by transfer hydrogenation. For these reasons, (4'-methoxy)acetophenone (1-10 mol%) was added to (*R*)-1-phenylethanol in the presence of **II.1-Bu^t**, **II.2-Bu^t** or **II.3-Bu^t**. After 2 h under catalytic conditions, the *ee* of (*R*)-1-phenylethanol dropped from 100% to 93-98% depending on the catalyst. This result clearly shows a slow racemization process in the presence of a ketone, probably because of its ability to act as an alternative hydrogen source in transfer hydrogenation. However, the observed drift of the enantioselectivity could be also caused by a change of catalytically active form during the course of the reaction, because of ligand redistribution as proposed above and also because of the coordination of the reaction product 1-phenylethanol to the metal atom. Indeed, this phenomenon has recently been proposed for a phebox–ruthenium catalyst in order to rationalize the evolution of the *ee* with conversion for the enantioselective hydrogenation of (4'-methoxy)acetophenone [160]. It was further shown that the use a bulky chiral alcohol, (*S*)-1-(9-anthracenyl)ethanol, as an additive (2–10 mol%) in this process significantly improved the enantioselectivity (up to 93% *ee*) for the 1-(4'-methoxy)phenylethanol product compared to the 56% *ee* that was obtained by the reaction without the alcohol [143].

The influence of the R substituent on the sulfur atom of the phosphinoferrocenyl-thioether ligand on the catalytic activity of the rhodium complexes was then investigated for the NBD-Cl series of complexes (**II.1**). The complex with R = Bu^t is much more active and stereoselective than those with the Et, Ph and Bz substituents (Table II.6, Fig. II.9).

Table II.6. Results of the asymmetric hydrogenation of acetophenone in the presence of complexes **(*S*)-II.1-R** depending on the reaction time and substituent on the S atom.[a]

Entry	Catalyst	*t*, h	Conversion, %	*ee* , %[b]
16	**II.1-Et**	1	9	27
17	**II.1-Ph**	1	13	32
18	**II.1-Bz**	1	12	12
19	**II.1-Et**	2	13	25
20	**II.1-Ph**	2	18	26
21	**II.1-Bz**	2	13	14
22	**II.1-Et**	5	28	22
23	**II.1-Ph**	5	25	23
24	**II.1-Bz**	5	26	9
25	**II.1-Et**	16	33	21
26	**II.1-Ph**	16	28	22
27	**II.1-Bz**	16	30	9

[a]Reaction conditions: catalyst ($6.4\cdot10^{-3}$ mmol), NaOMe ($3.2\cdot10^{-2}$ mmol), acetophenone (3.2 mmol), T = 25 °C and P_{H2} = 30 bar. Solvent = Pr^{i}OH (2 mL). The conversion and *ee* were determined by GC. [b]The *ee* is reported with respect to the *S*-configuration.

For the last three complexes the conversion did not increase after 5 h of reaction, indicating low stability of the catalytically active species. The influence of the sulfur R substituent on the catalytic activity of the iridium analogues was investigated earlier for the complexes containing the COD ligand. All the iridium complexes have essentially the same activity (conversion 92 – 99% after 2 h of reaction), but the enantioselectivity depends on the R substituent changing from 77 to 43% in the series Bz > Et> Bu^{t} > Ph [32].

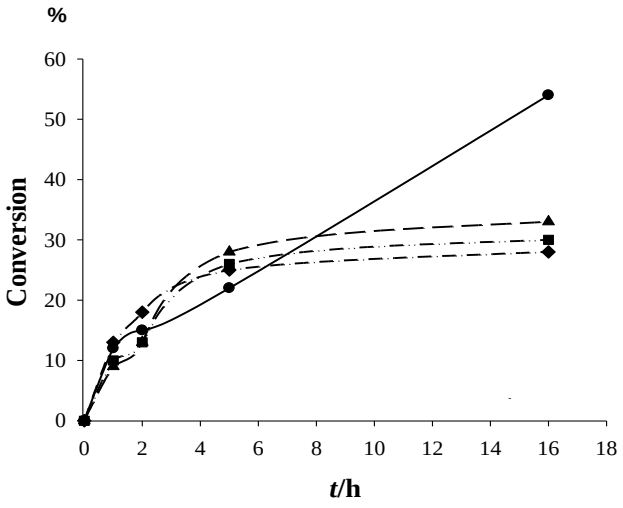

Fig. II.9. Time dependence of the acetophenone conversion for complexes **(*R*)-II.1-Bu^{t}** (●); **(*S*)-II.1-Et** (▲); **(*S*)-II.1-Ph** (■); **(*S*)-II.1-Bz** (♦).

In order to increase the rate of hydrogenation we increased the amount of the rhodium precatalysts (Table II.7). These experiments were run with all precatalysts containing the Bu^t substituent (**II.1-4**) and for the full series of substituents for system **II.1**. The use of 1% rhodium complexes *vs.* substrate allowed us to obtain high conversions already after 2 h and to increase the *ee* up to 41-51% in case of the Bu^t derivatives (Table II.7, entry *1-4*, *8-19*), but the *ee* remained low for the complexes with R = Et, Ph and Bz substituents (see Table II.7, entry *5-7*, *20-22*). These data further confirm the trend of activity / enantioselectivity in the order Bu^t >> Et > Ph > Bz for the NBD complexes **II.1**. For the four (P,SBu^t)-complexes the dependence of the acetophenone conversion on the amount of precatalyst is nonlinear (Fig. II.10), suggesting the presence of concentration dependent equilibria between different species with different catalytic activity. Therefore, the catalytic mechanism is more complex than previous literature suggestions [105, 124].

Table II.7. Results of the asymmetric hydrogenation of acetophenone as a function of the catalyst/substrate ratio.[a]

Entry	Catalyst	Initial **II.6**, mmol	Amount of catalyst, % mol	Conversion, %	*ee*, %
1	**(*R*)-II.3-Bu^t**	3.2	0.2	16	54[e]
2	**(*R*)-II.1-Bu^t**	3.2	0.2	13	44[e]
3	**(*R*)-II.4-Bu^t**	3.2	0.2	22	32[e]
4	**(*R*)-II.2-Bu^t**	3.2	0.2	24	31[e]
5	**(*S*)-II.1-Et**	3.2	0.2	13	25[c]
6	**(*S*)-II.1-Ph**	3.2	0.2	18	26[c]
7	**(*S*)-II.1-Bz**	3.2	0.2	13	14[c]
8	**(*R*)-II.3-Bu^t**	2.1	0.3	74	54[e]
9	**(*R*)-II.1-Bu^t**	2.1	0.3	27	44[e]
10	**(*R*)-II.4-Bu^t**	2.1	0.3	51	49[e]
11	**(*R*)-II.2-Bu^t**	2.1	0.3	27	42[e]
12	**(*R*)-II.3-Bu^t**	1.3	0.5	88	49[e]
13	**(*R*)-II.1-Bu^t**	1.3	0.5	54	46[e]
14	**(*R*)-II.4-Bu^t**	1.3	0.5	68	42[e]
15	**(*R*)-II.2-Bu^t**	1.3	0.5	57	51[e]
16	**(*R*)-II.3-Bu^t**	0.6	1	99	44[e]
17	**(*R*)-II.1-Bu^t**	0.6	1	92	51[e]
18	**(*R*)-II.4-Bu^t**	0.6	1	97	41[e]
19	**(*R*)-II.2-Bu^t**	0.6	1	93	50[e]
20	**(*S*)-II.1-Et**	0.6	1	51	31[c]
21	**(*S*)-II.1-Ph**	0.6	1	39	27[c]
22	**(*S*)-II.1-Bz**	0.6	1	40	19[c]

[a]Reaction conditions: catalyst ($6.4\cdot10^{-3}$ mmol), NaOMe ($3.2\cdot10^{-2}$ mmol), acetophenone (3.2 mmol), T = 25 °C and P_{H2} = 30 bar; solvent = Pr^iOH (2 mL), reaction time 2 h. The conversion and *ee* were determined by GC. [b]The *ee* is reported with respect to the *R*- configuration. [c]The *ee* is reported with respect to the *S*- configuration.

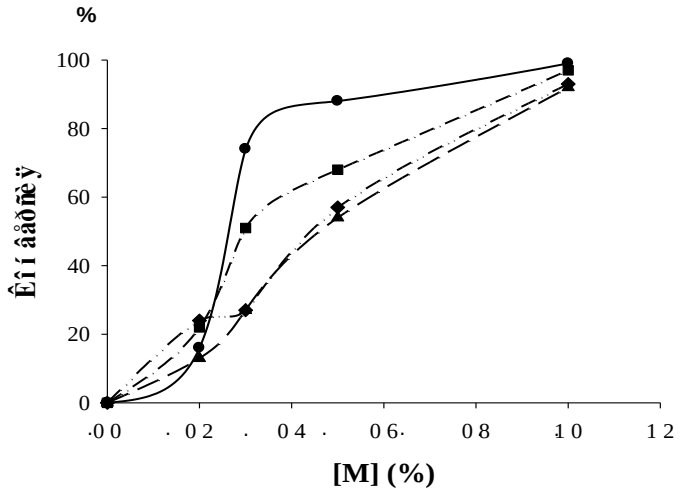

Fig. II.10. Dependence of the acetophenone conversion on [M] after 2 h of reaction for complexes **II.3-Bu^t** (●); **II.1-Bu^t** (▲); **II.4-Bu^t** (■) and **II.2-Bu^t** (♦).

The rhodium complexes were also tested in the hydrogenation of 4-fluoroacetophenone (**II.8**) and *tert*-butyl phenyl ketone (**II.9**) (Scheme II.3). In the case of **II.8**, the catalytic activity for all complexes is similar to that observed in the hydrogenation of acetophenone (Table II.8), the trends as a function diene and anion are the same and a similar erosion of enantioselectivity with conversion was observed, whatever the precatalysts used (Table II.8, entries *2-5*, *7-10*, *12-15*). For the hydrogenation of the more hindered **II.9** all the complexes (including the iridium system) showed lower catalytic activity as expected and also a lower enantioselectivity (Table II.8, entries *16-20*). Interestingly the activity of the NBD rhodium complexes in this reaction is higher than that of COD-derivatives, in contrast to the hydrogenation of acetophenone and 4-fluoroacetophenone.

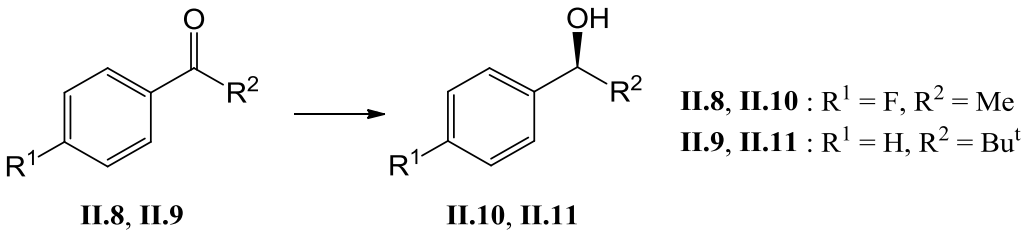

Scheme II.3 Reagents: [M(P,SR)(diene)X], H_2, Pr^{i}OH, MeONa.

Table II.8. Results of the asymmetric hydrogenation of 4-fluoroacetophenone (**II.8**) and *tert*-butyl phenyl ketone (**II.9**) as a function of the reaction time.[a]

Entry	Catalyst	Ketone		*t*, h	Conversion, %	*ee*, %[b]
		R^1	R^2			
1	**(*R*)-I.124-Bu^t**	F	Me	2	94	58
2	**(*R*)-II.3-Bu^t**	F	Me	2	16	60
3	**(*R*)-II.1-Bu^t**	F	Me	2	15	43
4	**(*R*)-II.4-Bu^t**	F	Me	2	15	51
5	**(*R*)-II.2-Bu^t**	F	Me	2	16	52
6	**(*R*)-I.124-Bu^t**	F	Me	5	99	58
7	**(*R*)-II.3-Bu^t**	F	Me	5	26	54
8	**(*R*)-II.1-Bu^t**	F	Me	5	25	40
9	**(*R*)-II.4-Bu^t**	F	Me	5	26	53
10	**(*R*)-II.2-Bu^t**	F	Me	5	27	47
11	**(*R*)-I.124-Bu^t**	F	Me	16	100	57
12	**(*R*)-II.3-Bu^t**	F	Me	16	86	29
13	**(*R*)-II.1-Bu^t**	F	Me	16	41	36
14	**(*R*)-II.4-Bu^t**	F	Me	16	67	42
15	**(*R*)-II.2-Bu^t**	F	Me	16	64	33
16	**(*R*)-I.124-Bu^t**	H	Bu^t	16	49	14
17	**(*R*)-II.3-Bu^t**	H	Bu^t	16	15	-9
18	**(*R*)-II.1-Bu^t**	H	Bu^t	16	20	10
19	**(*R*)-II.4-Bu^t**	H	Bu^t	16	13	0
20	**(*R*)-II.2-Bu^t**	H	Bu^t	16	25	11

[a]Reaction conditions: catalyst ($6.4\cdot10^{-3}$ mmol), NaOMe ($3.2\cdot10^{-2}$ mmol), substrate (3.2 mmol), T = 25 °C and P_{H2} = 30 bar, solvent = Pr^{i}OH (2 mL). The conversion and *ee* were determined by GC. [b]The *ee* is reported with respect to the *R*- configuration.

Dialkyl ketones are another challenging substrates for asymmetric hydrogenation. The activity of the rhodium complex with (P,SBu^t) ligand in the hydrogenation of cyclohexyl methyl ketone (**II.12**) was studied (Scheme II.4, Table II.9). Interestingly, even with 0.2% of catalyst the activity of rhodium complexes was higher than that of the iridium complex **(*R*)-I.124-Bu^t** and full conversion was obtained within 16 h for all Rh-catalysts. The activity trend for the rhodium precatalysts is the same as that in acetophenone hydrogenation (Fig. II.11). Unfortunately, the enantioselectivity of this catalyzed transformation under these (non-optimized) conditions was very low (*ee* < 10%).

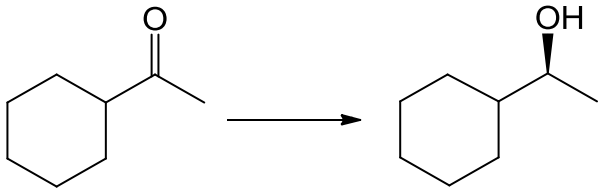

II.12 **II.13**

Scheme II.4 Reagents: [M(P,SR)(diene)X], H_2, Pr^{i}OH, MeONa.

Table II.9. The results of asymmetric hydrogenation of cyclohexyl methyl ketone **II.12** depending on the reaction time.[a]

Entry	Catalyst	*t*, h	Conversion, %	*ee*, %[b]
1	**(*R*)-I.124-Bu^t**	2	52	-7
2	**(*R*)-II.3-Bu^t**	2	49	3
3	**(*R*)-II.1-Bu^t**	2	25	6
4	**(*R*)-II.4-Bu^t**	2	45	3
5	**(*R*)-II.2-Bu^t**	2	45	9
6	**(*R*)-I.124-Bu^t**	5	66	-10
7	**(*R*)-II.3-Bu^t**	5	89	4
8	**(*R*)-II.1-Bu^t**	5	30	7
9	**(*R*)-II.4-Bu^t**	5	86	4
10	**(*R*)-II.2-Bu^t**	5	79	7
11	**(*R*)-I.124-Bu^t**	16	80	-9
12	**(*R*)-II.3-Bu^t**	16	100	4
13	**(*R*)-II.1-Bu^t**	16	99	6
14	**(*R*)-II.4-Bu^t**	16	100	4
15	**(*R*)-II.2-Bu^t**	16	100	6

[a]Reaction conditions: catalyst ($6.4\cdot10^{-3}$ mmol), NaOMe ($3.2\cdot10^{-2}$ mmol), cyclohexyl methyl ketone (3.2 mmol), T = 25 °C and P_{H2} = 30 bar, solvent = Pr^{i}OH (2 mL). The conversion and *ee* were determined by GC. [b]The *ee* is reported with respect to the *R*- configuration.

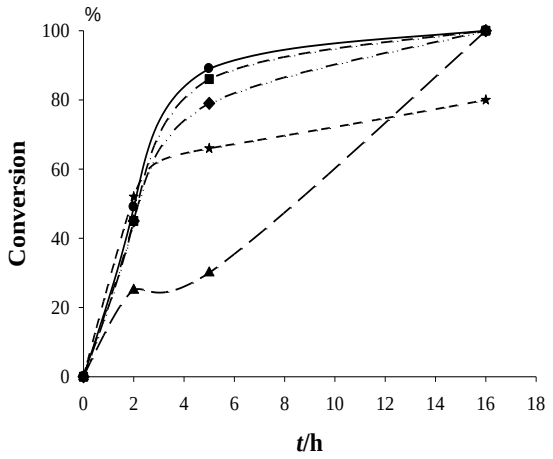

Fig. II.11. Dependence of the cyclohexyl methyl ketone conversion on the time of hydrogenation for several complexes with the (*R*)-(P,SBu^t) ligand: **II.3-Bu^t** (●); **II.1-Bu^t** (▲); **II.4-Bu^t** (■) and **II.2-Bu^t** (♦) and **I.124-Bu^t** (*).

II.2.2 Asymmetric hydrogenation of imine and quinaldine

The rhodium and iridium complexes with the (P,SBu^t)-ligand were also tested as catalysts in the asymmetric hydrogenation of a representative imine (*N*-phenyl-*N*-(1-phenylethylidene)amine, **II.14**) (Scheme II.5, Table II.10) and quinaldine (**II.16**, Scheme II.6, Table II.11). Good conversions

were obtained in both reactions only for iridium complex. A moderate *ee* was obtained only for the imine reduction catalyzed by the iridium complex; the enantioselectivity of this reaction catalyzed by the rhodium complexes and of the quinaldine hydrogenation catalyzed by all complexes was low.

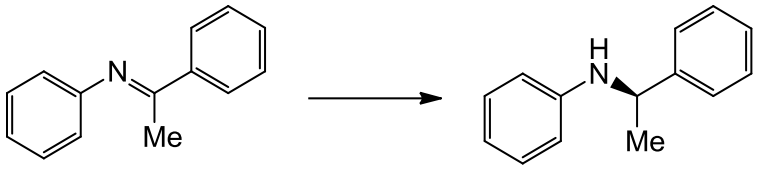

II.14 **II.15**

Scheme II.5 Reagents and conditions: [M(P,SR)(diene)X] (1%), I_2 (3%), H_2, CH_2Cl_2, 16 h.

Table II.10 Asymmetric hydrogenation of *N*-phenyl-*N*-(1-phenylethylidene)amine[a]

Entry	Catalyst	Conversion, %	*ee*, %[b]
1	**(*R*)-I.124-Bu^t**	100	40 (*R*)
2	**(*R*)-II.3-Bu^t**	27	5 (*S*)
3	**(*R*)-II.1-Bu^t**	42	7 (*S*)
4	**(*R*)-II.4-Bu^t**	24	5 (*S*)
5	**(*R*)-II.2-Bu^t**	44	10 (*S*)

[a]Reaction conditions: catalyst ($6.4\cdot10^{-3}$ mmol), I_2 ($1.9\cdot10^{-2}$ mmol), *N*-phenyl-*N*-(1-phenylethylidene)amine (0.6 mmol), T = 25 °C and P_{H2} = 30 bar, solvent = CH_2Cl_2 (2 mL). The conversion and *ee* were determined by GC. [b]The configuration of the resulting imine is indicated in parentheses.

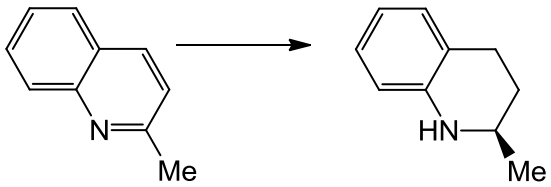

II.16 **II.17**

Scheme II.6 Reagents and conditions: [M(P,SR)(diene)X] (1%), I_2 (3%), H_2, CH_2Cl_2, 16 h.

Table II.11 Asymmetric hydrogenation of quinaldine[a]

Entry	Catalyst	Conversion, %	*ee*, %[b]
1	**(*R*)-I.124-Bu^t**	100	5 (*S*)
2	**(*R*)-II.3-Bu^t**	5	8 (*R*)
3	**(*R*)-II.1-Bu^t**	28	11 (*R*)
4	**(*R*)-II.4-Bu^t**	7	20 (*R*)
5	**(*R*)-II.2-Bu^t**	12	27 (*R*)

[a]Reaction conditions: catalyst ($6.4\cdot10^{-3}$ mmol), I_2 ($1.9\cdot10^{-2}$ mmol), quinaldine (0.6 mmol), T = 25 °C and P_{H2} = 30 bar, solvent = CH_2Cl_2 (2 mL). The conversion and *ee* were determined by GC. [b]The configuration of the resulting quinaldine is indicated in parentheses.

In summary, the rhodium complexes [Rh(P,SR)(diene)X] examined are less effective acetophenone hydrogenation catalysts under the same conditions in which the iridium complex [Ir(P,SBu^t)(COD)Cl] (**I.124-Bu^t**) shows good activity and enantioselectivity, as expected. For the Rh(P,SBu^t)-derivatives the rate of hydrogenation and the reaction enantioselectivity vary in the order COD-Cl > COD-BF_4 > NBD-BF_4 > NBD-Cl, whereas for the series of NBD-Cl complexes (**II.1**) the activity/enantioselectivity vary in the order Bu^t >> Et > Ph > Bz. The data obtained on the influence of various factors on the rate and enantioselectivity of alkylaryl ketones hydrogenation (for example, nonlinear dependence of the acetophenone conversion on the amount of catalyst, the decrease of enantioselectivity during the reaction while maintaining the catalitic activity) suggest a more complicated reaction mechanism than those previously proposed. The investigation of the catalytic hydrogenation of other challenging substrates has shown the prospects of using rhodium complexes in the reduction of dialkyl ketones, while the iridium system is more active in the catalytic hydrogenation of imines.

II.2.3 Hydrogenation of C=C bonds in the presence of C=O bond

It is known that rhodium complexes are good catalysts for the hydrogenation of C=C double bonds. With the aim to investigate the selectivity of rhodium catalyzed hydrogenation of C=O bond in the presence of C=C bond the rhodium complexes were tested in the hydrogenation of 3-methyl-2-cyclohexenone (**II.18**, Scheme II.7). In THF without any additives the reaction with H_2 (30 bar) led to the formation of 3-methylcyclohexanone (**II.19**) as the major product. The reaction, however, was very slow, even though a large catalyst loading of 5% *vs.* substrate was used, and full conversion could not be reached in 16 h (Table II.12). The *cis* configuration of the 3-methylcyclohexanol **II.20** was proven on the basis of the NMR data.

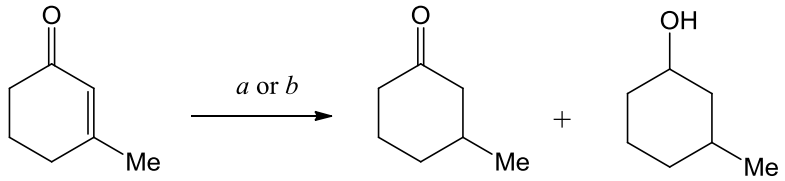

II.18 **II.19** **II.20**

Scheme II.7 Reagents and conditions: [a] [M(P,SR)(diene)X] (5%), H_2, THF, 16 h.
[b] [M(P,SR)(diene)X] (0.2%), H_2, Pr^{i}OH, MeONa, 2 h.

When the reaction was carried out in Pr^{i}OH in the presence of NaOMe, the catalytic activities were much higher and full conversion could be obtained after 2 h with 1% of catalyst (Table II.13, entries *12-14*). When the catalyst/substrate ratio was reduced, the overall conversion decreased (Table II.13, entries *5-11*) after the same reaction time (2h) as expected but the order in catalyst is clearly not

1 (6% conversion with 0.2 mol% **(*R*)-II.1-Bu^t** but 100% with 1 mol%, entries *6/13*) suggesting again the presence of concentration dependent equilibria between different species with different catalytic activity.

Table II.12 Hydrogenation of 3-methyl-2-cyclohexenone **II.18** in THF.[a]

Entry	Catalyst	Conversion, %	Yield of **II.19**, %	Yield of **II.20**, %
1	**(*R*)-II.3-Bu^t**	6	91	9
2	**(*R*)-II.1-Bu^t**	26	89	11
3	**(*R*)-II.4-Bu^t**	10	90	10
4	**(*R*)-II.2-Bu^t**	65	76	24

Reaction conditions: catalyst ($6.4\cdot10^{-3}$ mmol), 3-methyl-2-cyclohexenone (0.13 mmol), T = 25 °C and P_{H2} = 30 bar, solvent = THF (2 mL). Conversion determined by GC.

In all cases, no product of C=O hydrogenation without C=C reduction, namely 3-methyl-2-cyclohexenol, was observed even at very low conversion. This cannot be the result of an immediate reduction of this putative product into **II.20**, because no such product of full reduction was observed in some cases (for instance, entry *6*). Therefore, the product of selective C=O reduction is not observed simply because it does not form. The C=C bond hydrogenation is faster than that of C=O bond but the reactivity difference is not high enough to maintain good selectivities for **II.19** at high conversions. However, **II.20** can be obtained in high yields with perfect chimio diastereoselectivities. More efforts should be now devoted to the determination of the enantioselectivities in these reactions.

Table II.13. Results of the 3-methyl-2-cyclohexenone (**II.18**) hydrogenation in Pr^{i}OH depending on the catalyst/substrate ratio.[a]

Entry	Catalyst	Initial **II.18**, mmol	Rh, % mol	Conversion, %	Yield of **II.19**, %	Yield of **II.20**, %
5	**(*R*)-II.3-Bu^t**	3.2	0.2	33	95	5
6	**(*R*)-II.1-Bu^t**	3.2	0.2	6	100	0
7	**(*R*)-II.4-Bu^t**	3.2	0.2	13	96	4
8	**(*R*)-II.2-Bu^t**	3.2	0.2	3	91	9
9	**(*R*)-II.3-Bu^t**	1.3	0.5	100	20	80
10	**(*R*)-II.1-Bu^t**	1.3	0.5	48	74	26
11	**(*R*)-II.4-Bu^t**	1.3	0.5	22	82	18
12	**(*R*)-II.3-Bu^t**	0.6	1	100	0	100
13	**(*R*)-II.1-Bu^t**	0.6	1	100	0	100
14	**(*R*)-II.4-Bu^t**	0.6	1	100	45	55

[a]Reaction conditions: catalyst ($6.4\cdot10^{-3}$ mmol), NaOMe ($3.2\cdot10^{-2}$ mmol), T = 25 °C and P_{H2} = 30 bar; reaction time 2 h, solvent = Pr^{i}OH (2 mL). The conversion was determined by GC.

II.2.4 Isomerisation of allylic alcohols

According to the literature data rhodium and iridium complexes with diene ligands are efficient catalysts for the isomerisation of allylic alcohols [161]. For example, the isomerisation of different allylic primary alcohols to the corresponding aldehydes in THF at 70°C, catalyzed by a $[Rh(P,P)(COD)]^+$ (P,P = chiral phosphaferrocene) system, was found not only highly effective, but also enantioselective [162]. The ruthenium complex $[RuCl_2(PPh_3)_3]$ proved to be active in the isomerisation of trifluoromethylated allylic alcohols [163]. The iridium complex $[Ir(PCy_3)(Py)(COD)]BAr^F$ catalyzes the isomerisation of allylic alcohols, but only when H_2 was added to reaction mixture for 5 min in the beginning of reaction [164]. To investigate the activity of our rhodium and iridium complexes in allylic isomerisation 1-phenyl-2-propene-1-ol (**II.21**) was chosen as a substrate. The reaction did not proceed when **II.21** was added to the solution of the rhodium precatalyst in THF and stirred at reflux overnight. We therefore decided to use a hydrogen source to reduce the diene ligand in order to open the metal coordination sphere allowing the generation of the catalytically active species from the rhodium diene precatalysts [105]. When the reaction was carried out under a hydrogen pressure (30 bar of H_2) and at room temperature, the conversion was complete for most of the complexes after 1 h yielding 1-phenyl-1-propanol (**II.23**), which is the expected product of hydrogenation of either the the C=C bond of the substrate or the C=O bond of the expected product of isomerization, ethyl phenyl ketone (**II.22**), see Scheme II.8. The results are shown in Table II.14.

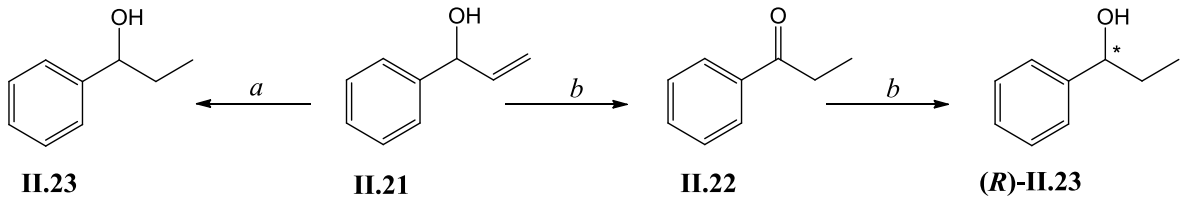

Scheme II.8 Reagents and conditions: [a][M(P,SR)(diene)X] (5%), H_2, THF.
[b][M(P,SR)(diene)X] (1%), Pr^iOH, MeONa.

Table II.14 Hydrogenation of 1-phenyl-2-propene-1-ol (**II.21**) in THF.[a]

Entry	Catalyst	Conversion, %
1	**(*R*)-I.124-Bu^t**	55
2	**(*R*)-II.3-Bu^t**	75
3	**(*R*)-II.1-Bu^t**	100
4	**(*R*)-II.4-Bu^t**	100
5	**(*R*)-II.2-Bu^t**	100

[a]Reaction conditions: catalyst ($6.4 \cdot 10^{-3}$ mmol), 1-phenyl-2-propene-1-ol **II.21** (0.13 mmol), T = 25 °C and P_{H2} = 30 bar, reaction time 1 h, solvent = THF (2 mL). The conversions were determined by GC.

Interestingly, the rhodium catalysts were more efficient than the iridium one in this process. However, there was no enantiomeric enrichment for the 1-phenyl-1-propanol product. This led us to believe that in the presence of H_2 the direct addition of hydrogen to the C=C double bond proceeds faster than the isomerisation of the allylic alcohol. In order to verify whether this reaction may occur via isomerization to the ketone the autoclave was pressurized at 30 bar for only 1 min at room temperature, then the pressure was released and the reaction vessel was stirred for the desired time at reflux either under an argon or a dihydrogen atmosphere at 1 bar. These conditions allowed us to obtain **II.22** as a major product when the process was conducted for 16 h under an argon atmosphere (Table II.15).

Table II.15. Results of the hydrogenation of 1-phenyl-2-propene-1-ol (**II.21**) in THF under various reaction conditions.[a]

Entry	Catalyst	Conversion, %	Time h	Yield of **II.22**, %	Yield of **II.23**, %
6	**(*R*)-I.124-Bu^t**	35[b]	2	6	94
7	**(*R*)-II.3-Bu^t**	92[b]	2	6	94
8	**(*R*)-II.1-Bu^t**	79[b]	2	5	95
9	**(*S*)-I.124-Bz**	9[c]	2	27	73
10	**(*R*)-II.1-Bu^t**	15[c]	2	17	83
11	**(*R*)-II.4-Bu^t**	30[c]	2	27	73
12	**(*S*)-I.124-Bz**	56[c]	16	78	22
13	**(*R*)-II.1-Bu^t**	52[c]	16	83	17
14	**(*R*)-II.4-Bu^t**	100[c]	16	93	7

[a]Reaction conditions: catalyst ($6.4\cdot10^{-3}$ mmol), 1-phenyl-2-propene-1-ol (0.13 mmol), solvent = THF (2 mL). The conversions were determined by GC. [b]P_{H2} = 30 bar, 25 °C, 1 min, then P_{H2} = 1 bar, 70 °C. [c]P_{H2} = 30 bar, 25 °C, 1 min, then Ar, 70 °C.

When the reaction was carried out in Pr^{i}OH in the presence of NaOMe under 30 bar of dihydrogen the racemic 1-phenyl-1-propanol (**II.23**) was obtained in 2 h with only 1% of catalyst (Table II.16).

Table II.16. Results of the hydrogenation of 1-phenyl-2-propene-1-ol (**II.21**) in Pr^{i}OH.[a]

Entry	Catalyst	Conversion, %
1	**(*R*)II.3-Bu^t**	100
2	**(*R*)-II.1-Bu^t**	95
3	**(*R*)-II.4-Bu^t**	100

[a] Reaction conditions: catalyst ($6.4\cdot10^{-3}$ mmol), NaOMe ($3.2\cdot10^{-2}$ mmol), 1-phenyl-2-propene-1-ol (0.6 mmol), T = 25 °C and P_{H2} = 30 bar, reaction time 2 h, solvent = Pr^{i}OH (2 mL). The conversions were determined by GC.

In order to further test whether the reaction proceeds via isomerization to the ketone under transfer hydrogenation conditions (Pr^iOH solvent in the presence of NaOMe), the reaction was carried out under an argon atmosphere at reflux (dihydrogen was not used at all in this catalystic test). After 1 h all substrate was transformed into ethyl phenyl ketone, proving that indeed the Rh complex is a catalyst for allylic isomerization.

Table II.17. Results of the allylic isomerisation of 1-phenyl-2-propene-1-ol (**II.21**)[a]

Entry	Catalyst	*t*, h	Conversion, %	Yield of **II.22**, %	Yield of **II.23**, %	*ee*, %[b]
4	**(*R*)-II.3-Bu^t**	1	56	100	0	-
5	**(*R*)-II.1-Bu^t**	1	100	100	0	-
6	**(*R*)-II.3-Bu^t**	6	100	81	19	14
7	**(*R*)-II.1-Bu^t**	6	100	66	34	17

[a]Reaction condition: catalyst ($6.4\cdot10^{-3}$ mmol), NaOMe ($3.2\cdot10^{-2}$ mmol), 1-phenyl-2-propene-1-ol (0.6 mmol), T = 82 °C. The conversion and *ee* were determined by GC. [b]The *ee* is reported with respect to the *R*- configuration.

The activity of this catalyst is comparable to that of other Ru and Rh complexes reported in the literature [165-167]. For instance, 1-phenyl-2-propene-1-ol (**II.21**) was quantitatively isomerized to the ketone **II.22** in water within 5 min at room temperature when using 5 mol% of the rhodium complex $[Rh(MeCN)_2(COD)]BF_4$ and 10 mol% of PTA (1,3,5-triaza-7-phosphaadamantane) [148] or when using 1 mol % of the ruthenium complex $[Ru(\eta^3{:}\eta^3\text{-}C_{10}H_6)Cl_2(benzimidazol)]$ within 15 min [149]. The isomerisation of **II.21** in the presence of 2 mol % of the ruthenium complex [Ru(η^6-*p*-cymene)Cl_2(1-κP)] (1-κP = 1-(diphenylphosphanyl)-1-[*N*-(hydroxymethylmethyl)carbamoyl]-ferrocene) and 5 mol % $KOBu^t$ in 1,2-dichloroethane at 80 ^oC was less effective: only 79% of the ketone **I.22** was obtained after 20 h under these conditions [167]. The increase of the reaction time led to the slow formation of enantiomerically enriched 1-phenyl-1-propanol (see Table II.17). Thus, it is clear that under H_2 the direct hydrogenation of the C=C bond prevails (since under those conditions the resulting saturated alcohol is racemic).

II.2.5 Conclusive remarks

On the basis of the experimental data that have been obtained and on the existing literature for other systems (Chapter I), the activation of the [Rh(P,SR)(diene)]X precatalysts can be proposed as shown in Scheme II.9. The presence of dihydrogen is necessary for the activation, which involves removal of the chloride ligand and hydrogenation of the diene ligand. The resulting "$Rh(P,SR)^+$" moiety can be stabilized by the alcohol to form the solvated complex, many examples of which have been described in Chapter I. Then, oxidative addition of H_2 may lead to the formation of solvated

Rh(III) dihydride systems. However, all the previous studies highlighted in Chapter I were conducted in the absence of strong base, because this is not necessary for activity in the catalytic hydrogenation of functionalized olefins such as those in Fig. 2. On the other hand, activity in the hydrogenation of ketones can only be observed in the presence of a strong base. Therefore, it is possible that under these conditions the solvated complex is transformed by deprotonation to neutral [(P,SR)Rh^{I}(OPr^{i})($Pr^{i}OH$)] or [(P,SR)Rh^{III}(OPr^{i})($Pr^{i}OH$)H_2] forms, as shown in the last steps on the right hand side of Scheme II.9 (various isomeric possibilities may be envisaged for each system).

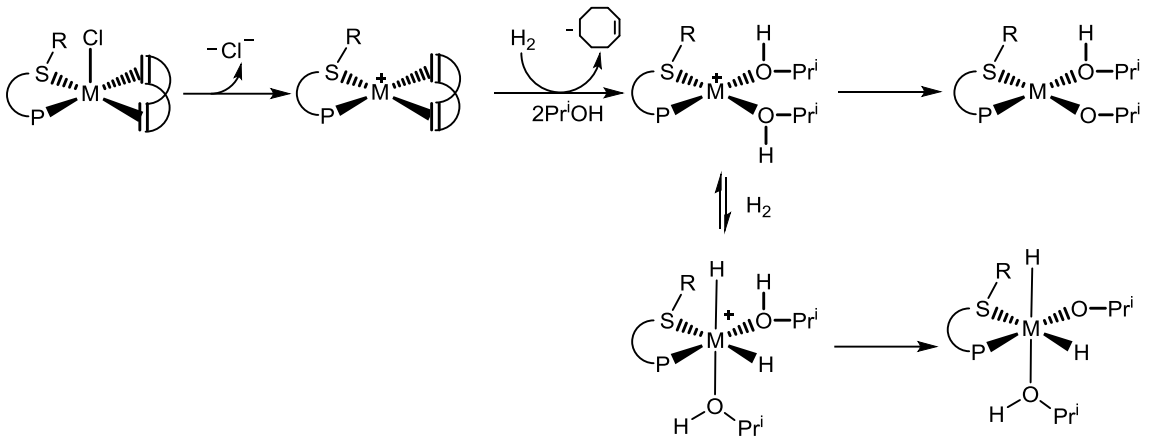

Scheme II.9

II.3 Activation of [Rh(P,SR)(diene)]X complexes for hydrogenation catalysis

After verifying that the [Rh(P,SR)(diene)X] complexes are both structural and functional models of the previously investigated [Rh(P,SR)(COD)Cl] precatalysts, we have proceeded to study the hydrogenation of our complexes by H_2 under stoichiometric conditions using such experimental methods as NMR and UV/Vis spectroscopy, in combination with DFT calculations[1]. The studies were however conducted only in the absence of strong base, in order to verify the formation of the solvated cationic Rh(I) complexes and/or the cationic Rh(III) dihydride complexes, with the perspective of investigating the effect of the strong base in subsequent work.

II.3.1 *Para*hydrogen NMR study

The parahydrogen (p-H_2) induced polarization (PHIP) NMR has been used extensively to probe reaction mechanisms where dihydrogen is involved as a reactant by enabling the detection of species at low concentrations such as intermediates in catalysis [168, 169]. It was first successfully employed by Weitekamp [170], and later Eisenberg and Bargon [171], but is now being employed much more

[1] The DFT calculations were perfomed by Dr. O. Filippov (INEOS).

widely as a consequence of the potential that hyperpolarization methods offer to magnetic resonance imaging and hence health care [172]. When this approach is used in conjunction with DFT calculations the synergy of the two methods becomes readily apparent as species that have previously never been observed are not only predicted but also firmly characterized in solution. Such studies have already been used to rationalize a series of reactions involving ruthenium clusters [173, 174, 175] where they can play a key role by helping with chemical shift and coupling assignments. Furthermore they have established a definitive opportunity to examine the role of electronic states in the oxidative addition of H_2 to a series of 16 electron ruthenium complexes [176, 177] and aided in the understanding of hydrogenation catalysis by a range of palladium complexes, [178, 179] and even to detect unexpected CH bond activation products in conjunction with the well-known complex $W(N_2)_2(DPPE)_2$ [180].

That is why we address the stoichiometric reactivity of two representative compounds containing the same (P,SBu^t) ligand, [Rh(P,SBu^t)(COD)Cl] **II.3-Bu^t** and [Rh(P,SBu^t)(COD)]BF_4 **II.4-Bu^t**, towards H_2 through the eyes of parahydrogen NMR. This part of the thesis was carried out during a 2-month residence at the University of York with the equipment and assistance of the laboratory of Prof. Simon B. Duckett.

II.3.1.1 Reaction with H_2 in CD_3OD in the absence of additives

The addition of *p*-H_2 to d_4-methanol solutions of either [Rh(P,SBu^t)(COD)Cl] (**II.3-Bu^t**) or [Rh(P,SBu^t)(COD)]BF_4 (**II.4-Bu^t**), over the temperature range 233 – 298 K, failed to result in the observation of any detectable hydride containing species. There was, however, evidence for a common slow reaction (ca. 18% conversion in 20 min at 243 K) which transformed the η^2-η^2-COD ligand into a $\kappa^3(\sigma{:}\pi)$-cyclooct-4-enyl ligand and generated the new complex **II.24** (Scheme II.10) in very small amounts by the loss of the proton. The κ^3-ligand in this complex is characterized by signals at δ 4.62, 2.15 and 1.54, see Fig. II.12. This suggests that while slow H_2 addition to the Rh center occurs, rapid reaction transforms the resulting dihydride into **II.24**. This process is followed by reprotonation to give the corresponding alkene after hydride migration as shown in Scheme II.10. The liberation of either HCl or HBF_4 is proposed to give **II.24**. A related H_2 addition to the complex $[Ir(NCCH_3)(PMe_3)(COD)]BF_4$ has been reported [181], where the initial dihydride product $[Ir(H)_2(MeCN)(PMe_3)(COD)]BF_4$ (in CH_2Cl_2) reacts with MeCN to form the monohydride product $[IrH(NCCH_3)_2(PMe_3)(1\text{-}\kappa\text{-}4,5\text{-}\eta\text{-}C_8H_{13})]BF_4$. These species have been isolated and fully characterized. We note that **II.24** is related to this Ir system by the formal loss of a proton. Given that Rh^{III} hydride complexes are known to be less stable than their Ir^{III} analogues this transformation is not unexpected.

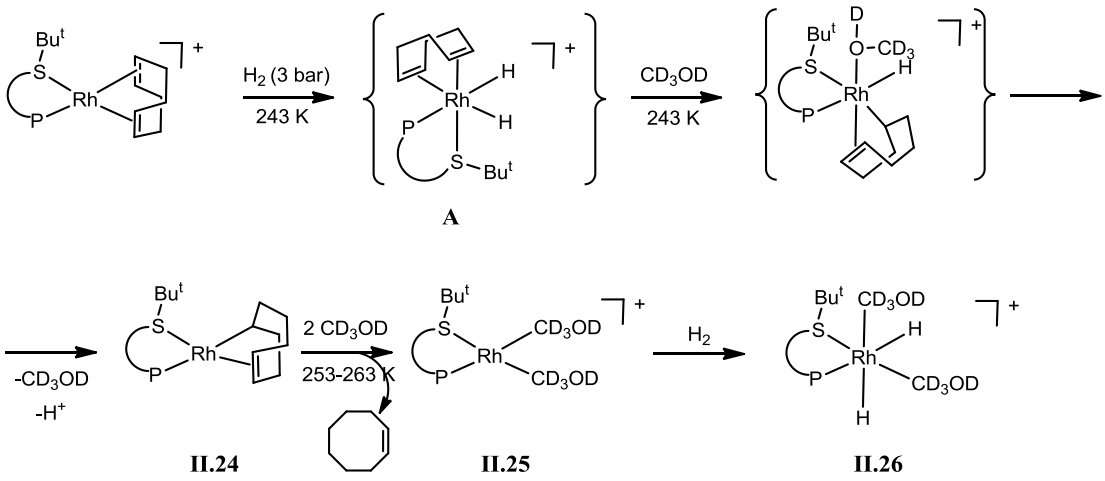

Scheme II.10

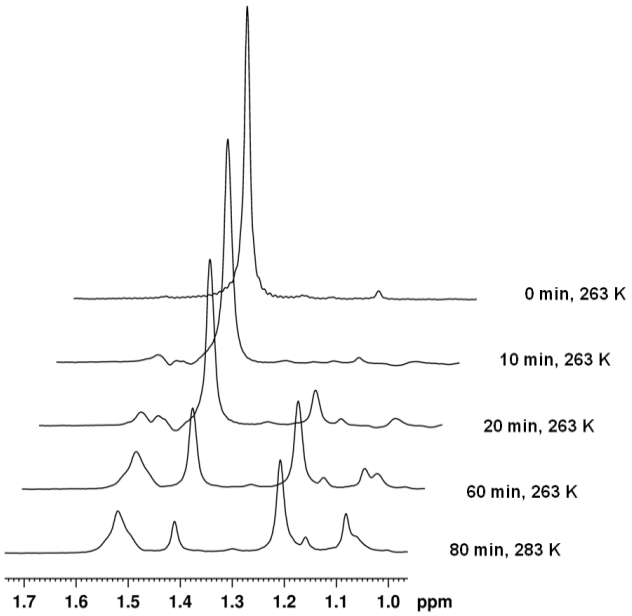

Fig. II.12 Spectrum showing the resonance at δ 1.54 assigned to the κ^3-ligand in complex **II.24**, [Rh(P,SBu^t)(1-κ-4,5-η-C_8H_{13})], and also those of the products of hydrogenation of COD. 1.42 ppm – Bu^t group in the starting material.

At 253 K the generation of cyclooctene was revealed by its characteristic ^{1}H NMR resonance at δ 1.21, which rapidly increases in intensity over the time scale of 20 minutes (Fig. II.13). This demonstrates that the initial H_2 addition to **II.3-Bu^t** or **II.4-Bu^t** proceeds at 253 K. When the temperature was raised to 263 K the formation of cyclooctane was also observed through its characteristic singlet at δ 1.54. Hydride resonances were not observed at any time during this reaction. However, the residual OH signal of methanol (δ 4.86) and the H_2 signal (δ 4.56) show dramatic temperature dependence, coalescing at 263 K thereby suggesting the rapid interchange of these sites,

presumably through the formation of the transient, non-observable hydride species **II.26** from the proposed solvated product **II.25** which is presumably the major complex formed in the reaction (Scheme II.10).

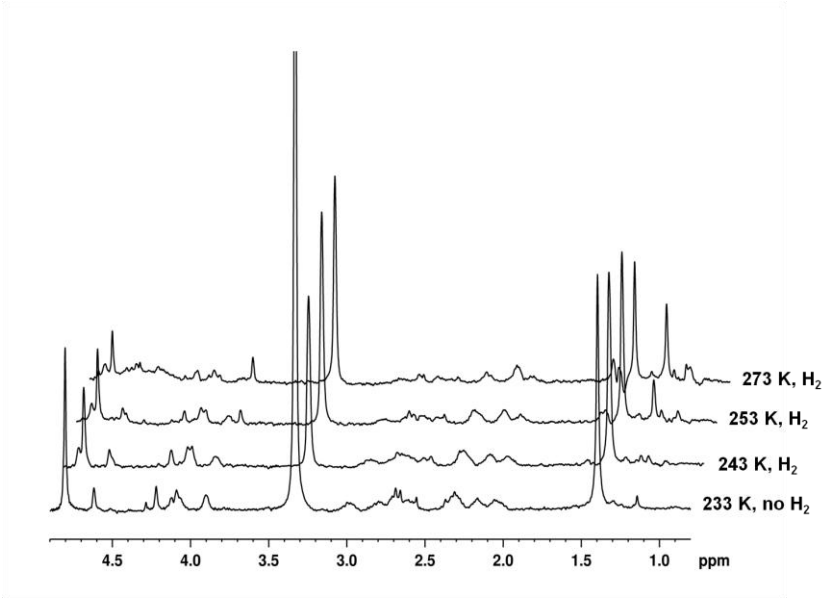

Fig. II.13 ^{1}H NMR spectra of **II.4-Bu^{t}** before and after reaction with H_2, recorded at different temperatures, showing the decrease in the intensity of the–C*H*= proton signal in η^2-η^2-COD at 4.8 ppm and the formation of new products with ^{1}H signals appearing around 4.85, 3.8, 1.54 and 1.2 ppm.

At 273 K the deuteration of H_2, producing HD becomes evident (Fig. II.14). In addition, the phosphine phenyl proton signals evolve to a more complicated shape. This reaction monitoring demonstrates the instability of **II.24** and further suggests that the ultimate formation of a bis(solvent) adduct, $[Rh(P,SBu^{t})(MeOH)_2]^{+}$, **II.25**, takes place even though direct evidence for that could not be obtained. Further H_2 oxidative addition to yield a putative dihydride species **II.26** appears excluded by the absence of observable hydride signals under this conditions (however, see additional discussion below). ^{31}P NMR monitoring of the reaction carried out with regular H_2 at 5 bar pressure and room temperature, still in d_4-methanol solution, with a higher sample concentration (approximately 39 mM instead of 4.6 mM previously used for the ^{1}H NMR monitoring) did not show the appearance of any new resonance. Only the signal for unreacted starting material could be seen at δ 23.8 (J_{PRh} = 143 Hz; **II.4-Bu^{t}**) / δ 21.0 (J_{PRh} = 148 Hz; **II.3-Bu^{t}**) even after 7 h. After 3 days the starting material was completely consumed and the new ^{31}P NMR spectrum showed very few small resonances, the major one being a doublet at δ 43.9 (J_{PRh} = 134.1 Hz). These data suggest that **II.25** is not stable at room temperature.

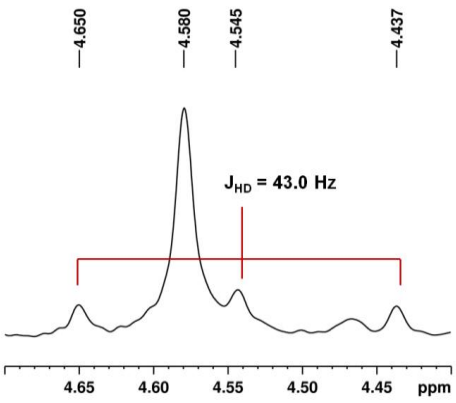

Fig. II.14 ^{1}H NMR spectrum of H_2 (at δ 4.580) and HD (δ 4.545; J_{HD} = 43.0 Hz).

When CD_2Cl_2 was used as solvent the reaction of **II.4-Bu^t** with *p*-H_2 was evident at temperatures down to 233 K. Under these conditions weak signals for a new hydride containing species were detected at δ -9.7 and -23.0. The high field signal yielded a ^{31}P coupling of 188 Hz. These two resonances were broad and neither the J_{HH} nor the J_{RhH} couplings could be quantified. In the corresponding ^{31}P decoupled spectra the δ -23.0 signal yields a J_{HH} splitting of -9 Hz and a J_{RhH} splitting of 20 Hz. The signals for this species were too weak to enable complete characterisation but the large observed J_{HP} for the high field signal is indicative of a *trans* arrangement and a species such as **A** in Scheme II.10 is possible. The addition of 1 ml of MeOH to this solution suppressed the observation of these signals.

The two key observations outlined above (the coalescence of the MeOH and H_2 signals, and the H/D exchange between these two molecules) lead us to speculate on the mechanism associated with these phenomena, which are obviously related to the same process, occurring rapidly on the NMR timescale. Two possible pathways are indicated in Scheme II.11. In pathway *a*, H_2 oxidative addition to **II.25** yields the presumed Rh^{III} dihydride species **II.26** that would be sufficiently acidic to release a proton to the solvent and yield a Rh^{I} monohydride intermediate **II.27**. Reversal of all steps with implication of deuteron incorporation through **II.26'** and leading to **II.25'** completes this exchange pathway. In the alternative pathway *b*, H_2 replaces a methanol ligand to yield an η^2-H_2 complex (non-classical dihydride) **II.28**, which is then deprotonated by the solvent to yield the same monohydride complex **II.27** as detailed above. Addition of deuteron then occurs to the hydride ligand leading to **II.28'**. Both of these pathways can be imagined to occur via initial reaction which places the hydride *trans* to S (as shown in Scheme II.11) or in the alternative position *trans* to P which is not illustrated. Incidentally, the lack of observation of a hydride resonance under these conditions does not exclude the fact that the most stable species (at least at low temperatures) is indeed a mono- or dihydride

complex, since such a species would exist primarily in the form of a deuteride and would therefore be unobservable in the hydride region of the ^{1}H NMR spectrum.

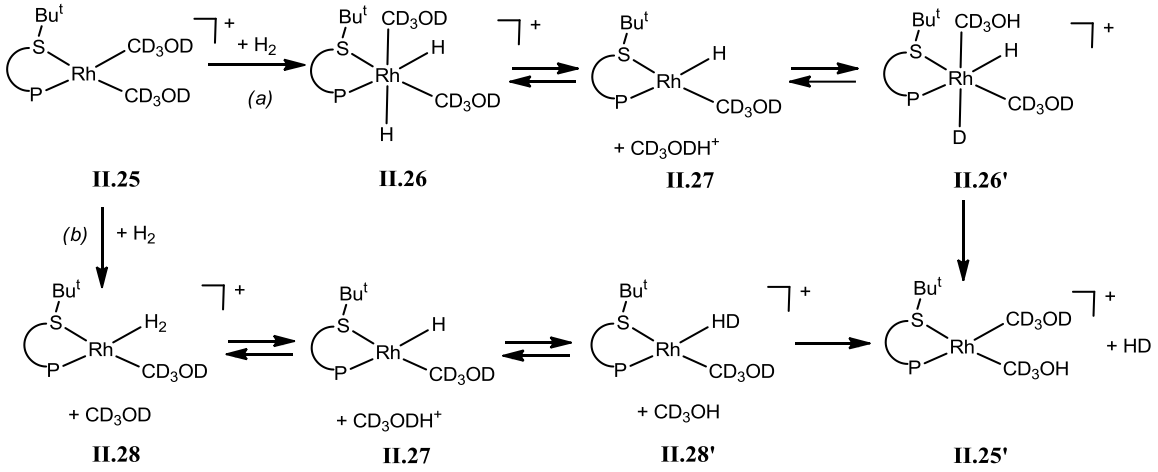

Scheme II.11

2.3.1.2 In CD_3OD in the presence of pyridine

When the analogous reactions of either **II.3-Bu^t** or **II.4-Bu^t** with H_2 were carried out in d_4-methanol solution in the presence of pyridine at low temperature (233 - 283 K), on the other hand, two common and dominant hydride containing products were produced. For example, when a d_4-methanol solution of **II.3-Bu^t** was prepared which contained a 75-fold excess of pyridine and the resulting reaction with *p*-H_2 monitored by ^{1}H NMR spectroscopy at 233 K, four PHIP enhanced hydride signals were observed at δ -13.1, δ -14.3, δ -17.2 and δ -17.6. These hydride ligand signals all contained anti-phase features due to their formation from *p*-H_2 that are associated with their common J_{HH} coupling in addition to in-phase splittings due to further couplings to a single rhodium and single phosphorus centre. A more complete NMR monitoring of this reaction was undertaken after warming the sample to 263 K, during which process the NMR spectral features did not change. The hydride region of the resulting ^{1}H NMR spectrum is shown in Fig. II.15a. The J_{PH} coupling values are all consistent with *cis* hydride phosphorus ligand arrangements. In addition, in the corresponding ^{1}H–^{31}P HMQC NMR spectrum (Fig. II.15b), the δ -13.1 (J_{HH} = -13 Hz, J_{RhH} = 24 Hz) and δ -17.6 (J_{HH} = -13 Hz, J_{RhH} = 19 Hz) signals proved to couple to a single ^{31}P center that was located at δ 47.9 and appeared with a J_{RhP} of 140.0 Hz. These resonances therefore arise from groups within the same complex (**II.29**). In a similar manner the δ -14.3 (J_{HH} = -10 Hz, J_{RhH} = 24 Hz) and δ -17.2 (J_{HH} = -10 Hz, J_{RhH} = 20 Hz) signals arise from a second species (**II.30**) where now the connected ^{31}P resonance appears at δ 45.0 with a J_{RhP} of 141.6 Hz. On the basis of the relative hydride resonance peak areas it can be suggested that **II.29** and **II.30** are formed in a step which shows a kinetic selectivity of approximately 1 : 4 at 233

K, if it is assumed that these resonances result from PHIP derived magnetic states that are created with identical efficiency. When the temperature is raised to 273 K the ratio increases to 1:13.

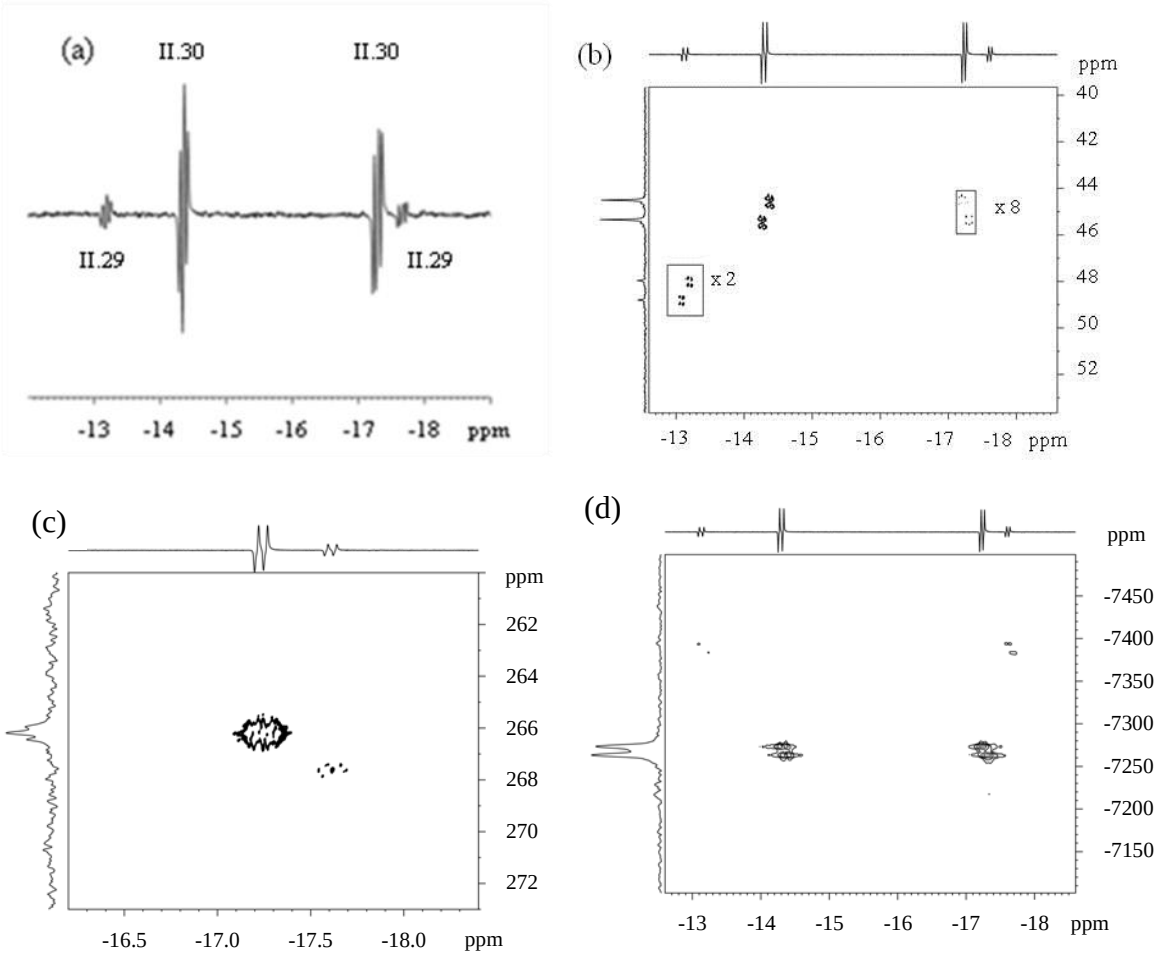

Fig. II.15. NMR spectra showing characteristic resonances of **II.29** and **II.30** observed during reaction of **II.4-Bu^t** in d_4-methanol with *p*-H_2 and 75 equiv of pyridine at 263 K: (a) *p*-H_2 enhanced ^{1}H NMR spectrum showing the hydride region; (b) ^{1}H-^{31}P HMQC NMR spectrum collected using ^{15}N labeled pyridine; (c) ^{15}N labeled, ^{1}H-^{15}N HMQC NMR spectrum; (d) ^{1}H-^{103}Rh HMQC NMR spectrum (in (b) the inset boxes reflect vertical expansions of x 2 and x 8 relative to the baseline).

Upon increasing the solution temperature to 283 K, no change in the relative intensity of the PHIP-enhanced signals was observed. However, upon warming to 298 K and beyond, the hydride signals for **II.29** and **II.30** could no longer be observed. When this experiment was repeated at 263 K with normal dihydrogen, the ratio of the hydride signals of **II.29** and **II.30** was 1:7. When, on the other hand, the reaction was conducted at room temperature (ca. 15 min between bubbling and recording the NMR spectrum), only the presence of compound **II.30** could be detected, reflecting the greater thermodynamic preference for this isomer.

In order to probe the ligand arrangement in compounds **II.29** and **II.30** further, a ^{15}N labelled pyridine sample was examined. Now, the two phosphorus signals associated with these two complexes exhibit additional and identical extra splittings of 50 Hz due to the presence of a resolved *trans* ^{31}P-^{15}N coupling. In the corresponding ^{1}H-^{15}N HMQC NMR spectrum (Fig. II.15c), the hydride signals at δ -17.2 and -17.6 showed strong correlation peaks to ^{15}N resonances at δ 266.2 and δ 267.6 respectively. In addition, a hydride-^{15}N splitting of 20 Hz was exhibited by the two low field hydride resonances of **II.29** and **II.30**. Rhodium signals have also been detected at δ -7268 for **II.29** and δ -7389 for **II.30** through the recording of a ^{1}H-^{103}Rh HMQC spectrum as shown in Fig. 15d.

This information therefore confirms that there are two pyridine ligands attached to the metal center in **II.29** and **II.30**, which are located *trans* to one hydride and to the phosphine ligands. Given the bidentate nature of the P,S ligand it can be further concluded that the second hydride ligand in both **II.29** and **II.30** is *trans* to sulfur. All the NMR data associated with **II.29** and **II.30** resulting from this study are summarized in Table II.18. The similarity of these NMR data suggests that these two products are simply diastereoisomers of one another, differentiated by the ferrocene ligand orientation as shown in Scheme II.12. This product geometry indicates that the initial H_2 oxidative addition takes place over the S-Rh-C axis.

Table II.18 NMR data for complexes **II.29** and **II.30** in MeOD at 283 K

Compound	δ ^{1}H	δ ^{31}P	δ ^{15}N	δ ^{103}Rh
II.29	-13.1, dd, J_{HH} = -13 Hz; J_{RhH} = 24 Hz, J_{RhP} = 140.0 Hz -17.6, dd, J_{HH} = -13 Hz; J_{RhH} = 19 Hz, J_{RhP} = 140.0 Hz	47.9, d	267.6, t, J_{PN} = 50 Hz; J_{NH} = 20 Hz	-7390, d J_{RhP}=131 Hz
II.30	-14.3, dd, J_{HH} = -10 Hz; J_{RhH} = 24 Hz, J_{RhP} = 141.6 Hz -17.2, dd, J_{HH} = -10 Hz; J_{RhH} = 20 Hz, J_{RhP} = 141.6 Hz	45.0, d	266.2, t, J_{PN} = 50 Hz; J_{NH} = 20 Hz	-7268, d J_{RhP}=131 Hz

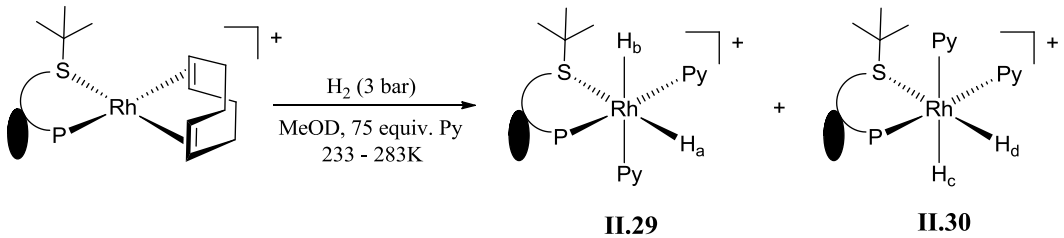

II.29 **II.30**

Scheme II.12

When an nOe experiment was recorded to probe the hydride site interchange process undergone by these complexes at 273 K with the 75 fold excess of pyridine, several exchange processes were observed (as revealed in Fig. II.16). These include a mutual hydride site interchange

within **II.30** which proceeds with an exchange rate constant of 0.785(6) s^{-1} and the interconversion of **II.30** into **II.29** on a slower timescale that places the moving hydride into either site of **II.29** with rates of 0.167(2) s^{-1} where H_c becomes H_a and H_d becomes H_b and 0.160(3) s^{-1} where H_c becomes H_b and H_d becomes H_a. Hence there is a limited selectivity in this process. Isomer **II.29** converts into **II.30** on a faster timescale where the observed rate constant is 1.10(1) s^{-1} for the $H_{a\rightarrow d}$ and $H_{b\rightarrow c}$ transformations and 1.19(1) s^{-1} for the $H_{a\rightarrow c}$ and $H_{b\rightarrow d}$ transformations. The experimental rate constant for hydride site interchange in **II.29** is zero. The derivation of the rate constants for each specific site exchange was carried out by a simultaneous fitting of all the data by Prof. S. B. Duckett at the University of York.

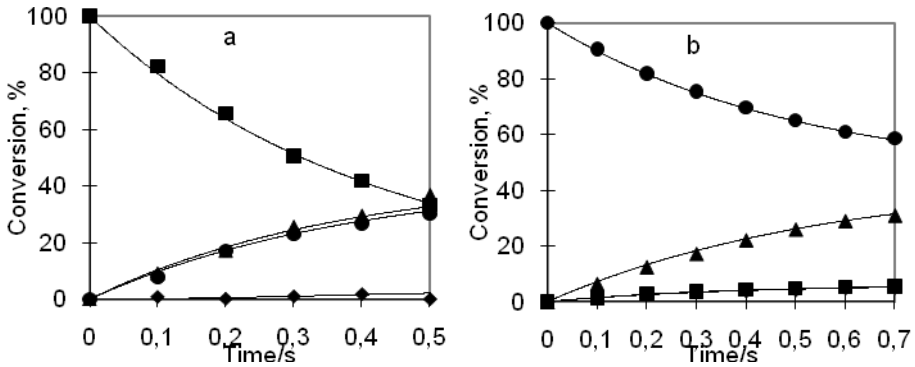

Fig. II.16 Hydride ligand exchange data for the interconversion of **II.29** and **II.30** in the presence of 75-fold excess of py, as probed through the selective excitation of (a) H_a of **II.29** and (b) H_c of **II.30**, over the defined observation period; the observation points are listed as H_a (■), H_b (♦), H_c (●) and H_d (▲) as defined in Scheme II.12. The solid lines correspond to simulated changes that yield the rate constants in the text.

When the process was repeated with a different excess amount of pyridine (8-fold or 173-fold), the values obtained for the site exchange rate constants were different, The overall scheme of hydride site exchange and the rates obtained are summarized in Scheme II.13. Table II.19 shows the list of constraints that were used for the calculation of the exchange rate constants. There was no evidence for hydride exchange into free H_2 or MeOH from **II.29** or **II.30** in these experiments which are limited by the timescale of NMR relaxation. Moreover, contrary to the experiment run in pure CD_3OD there was no coalescence between the solvent and H_2 resonances. We note, however, that the hydride sites of **II.29** and **II.30** are partially deuterated in these experiments. This readily shows up in a ^{31}P-decoupled HMQC measurement as isotopically perturbed signals at δ -13.1, -14.3, -17.2 and -17.6 in the corresponding ^{1}H NMR spectrum for the Rh(H)(D) partners and at δ -14.3 and δ -17.2 for the corresponding ^{31}P signals. Hence, the electronic effect of pyridine coordination stabilizes the dihydride species against deprotonation but does not prevent this phenomenon completely. It still occurs at much slower rates (cf. Scheme II.11).

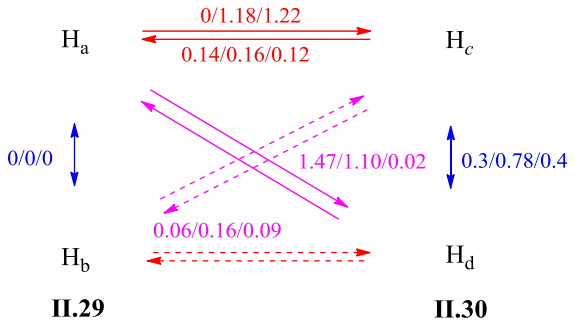

II.29 **II.30**

Scheme II.13 Hydride exchange pathways for products found in the chemistry of compound **II.4-Bu^t**. The three numbers on each arrow are the exchange rates in s^{-1} relative to the solution with an 8-fold, 75-fold and 173-fold excess of pyridine.

Table II.19 List of constraints that were used for the calculation of the exchange rate constants.

$H_a \rightarrow H_b = 0$	$H_b \rightarrow H_e = H_a \rightarrow H_f$
$H_a \rightarrow H_c = 0$	$H_d \rightarrow H_a = H_c \rightarrow H_b$
$H_a \rightarrow H_e = 0$	$H_d \rightarrow H_b = H_c \rightarrow H_a$
$H_b \rightarrow H_c = 0$	$H_d \rightarrow H_e = H_c \rightarrow H_f$
$H_b \rightarrow H_d = 0$	$H_d \rightarrow H_f = H_c \rightarrow H_e$
$H_b \rightarrow H_f = 0$	$H_f \rightarrow H_a = H_e \rightarrow H_b$
$H_e \rightarrow H_a = 0$	$H_f \rightarrow H_b = H_e \rightarrow H_a$
$H_e \rightarrow H_b = 0$	$H_f \rightarrow H_c = H_e \rightarrow H_d$
$H_e \rightarrow H_f = 0$	$H_f \rightarrow H_d = H_e \rightarrow H_c$
	$H_f \rightarrow H_e = H_e \rightarrow H_f$

Since the deuterium label incorporation into the hydride sites was relatively slow, the measurement of precise exchange rate data as would be required for the assembly of an Eyring plot was precluded. Nonetheless, the interconversion between these species has been defined as occurring without H_2 loss. This is reflected in the fact that strong PHIP is only seen when **II.3-Bu^t** or **II.4-Bu^t** are being converted into **II.29** and **II.30**. When we monitor these processes with differing amounts of pyridine, changing the Rh/pyridine ratio from 1:8, to 1:75, and 1:173 we see no change in the relative hydride signal intensities of **II.29** and **II.30**. There is, however, a significant effect on the hydride site interchange rate constants (Scheme II.13). The rate constant for the mutual hydride site exchange in **II.30** falls to 0.3 s^{-1} with an 8-fold excess of pyridine while it is 0.4 s^{-1} with a 173-fold excess. The kinetic effect of pyridine on this rate constant is complex, first promoting the process and then inhibiting it. A similar trend is observed for the $H_{d\rightarrow a}$ (and $H_{c\rightarrow b}$) rate from 0.06 s^{-1} through 0.16 s^{-1} to 0.09 s^{-1} and for the $H_{c\rightarrow a}$ (and $H_{d\rightarrow b}$) rate from 0.14 s^{-1} through 0.16 s^{-1} to 0.12 s^{-1}, though the effect here is less dramatic. In contrast, the $H_{a\rightarrow c}$ ($H_{b\rightarrow d}$) process shows a rate increasing with [py] from 0 s^{-1} through 1.18 s^{-1} to 1.22 s^{-1} while the rate of the $H_{a\rightarrow d}$ ($H_{b\rightarrow d}$) process shows the opposite trend from 1.47 through 1.10 to 0.02 s^{-1}. We can conclude therefore that pyridine plays a role in these processes.

The hydride signal at δ -17.2 in **II.30** shows nOe connections to peaks at δ 8.71, 8.23, 4.67, 3.84 and 1.21, which are due to the *ortho* proton of a pyridine ligand, the *ortho* proton of the phosphine, the ferrocenyl group and the Bu^t group. The second hydride signal in **II.30** which resonates at δ -14.3 shows through space interactions with protons that give rise to resonances at δ 8.71, 8.31, 8.23 and 6.68. The extra signal at δ 8.31 is therefore the *ortho* proton of a second pyridine ligand. In the corresponding ^1H-^{31}P HMQC, the ^{31}P center which resonates at δ 45.0 connects to two aromatic signals at δ 8.23 and 6.78. In contrast, the ^{31}P signal of the minor isomer **II.29** proved to connect with ^1H signals at 8.03 and 7.5 in an HMQC measurement. Furthermore, nOe data confirmed that the signal at δ -13.1 in **II.29** connects with ^1H signals at δ 8.42 and 8.03. The δ 8.42 resonance therefore corresponds to an *ortho*-pyridine signal. This information has therefore confirmed the assignment shown in Scheme II.12. The structure corresponding to **II.30** has therefore the hydride ligand *trans* to pyridine located on the same side as the ferrocenyl group. When a long range ^1H-^{31}P experiment was recorded, further proton signals were located at δ 7.6, 4.8 and 4.2 in **II.30**.

The hydrogenation of the cyclooctadiene ligand is readily evident in these *p*-H_2 enhanced ^1H NMR spectra at 253 K and above. Two sets of polarised signals appear at δ 1.53 and 1.50 due to the CH_2 protons of the hydrogenated components of COE. A further resonance is evidenced at δ 1.41 for the backbone signals as described above. In these ^1H NMR spectra the corresponding cyclooctane signal appears at δ 1.2 and forms very slowly at 273 K.

When the reaction of the chloride derived precursor **II.3-Bu^t** with normal dihydrogen was monitored in an analogous experiment in d_4-methanol solution with only a 15 fold excess of pyridine (instead of 75 in the experiment described above) two new transient hydride resonances initially appeared at 273 K, but could be seen only within the first few minutes and then disappeared. The problem with this measurement is, however, that it relies on detecting a weak signal from magnetisation that is at thermal equilibrium. When this reaction was repeated with *p*-H_2 the same transient resonances were seen only within the first few minutes and then disappeared in favor of another four species, namely **II.29** and **II.30** and two new species **II.31** and **II.32** (Fig. II.17). The initial transient species is tentatively assigned to the bis(MeOH) adduct, **II.26**.

The hydride signals of **II.31** appear at δ -12.3 and -18.7 with Rh-H couplings of 25.1 Hz and 26.8 Hz, respectively, and a common J_{HH} coupling of -5.9 Hz. The hydride ligand signals from species **II.32** are, however, much weaker than those of **II.31** and appear at δ -15.0 (J_{RhH} = 20 Hz, J_{HH} = -9 Hz) and δ -17.8 (J_{RhH} = 15, J_{HH} = -9 Hz). The relative ratio of the hydride signals for **II.31**, **II.29**, **II.30**, and **II.32** is 0.9:7.0:39.6:1 at 273 K. In a series of 2D measurements the δ -12.3 hydride signal proved to connect with a δ 34.3 ^{31}P resonance where J_{RhP} = 140 Hz, while the δ -15.0 hydride signal connects with a ^{31}P resonance at δ 51.4 that exhibits a J_{RhH} coupling of 148 Hz. The relative intensity of the signals for **II.31** and **II.32** proved to fall as the excess of pyridine is increased. When labelled pyridine

is employed both of the sets of hydride signals show limited broadening but no *trans*-^{15}N coupling is evident. We therefore assign **II.31** and **II.32** to chloride containing [Rh(H)$_2$(P,SR)(pyridine)Cl] as shown in Scheme II.14. This deduction is further supported by the fact that while the relative intensities of the signals for **II.29** and **II.30** seem to remain constant regardless of the pyridine concentration, those for **II.31** and **II.32** drop as the pyridine concentration increases.

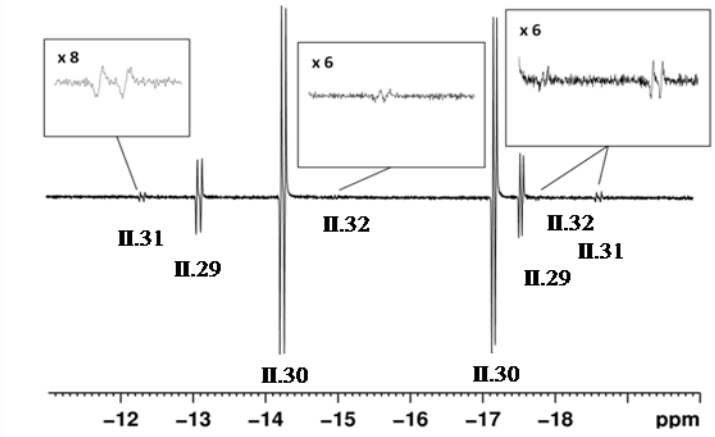

Fig. II.17 NMR spectra showing characteristic hydride resonances of **II.29**, **II.30**, **II.31** and **II.32** (as indicated) observed during reaction of **II.3-Bu^t** in d$_4$-methanol with *p*-H$_2$ and 45-fold excess of pyridine at 273 K.

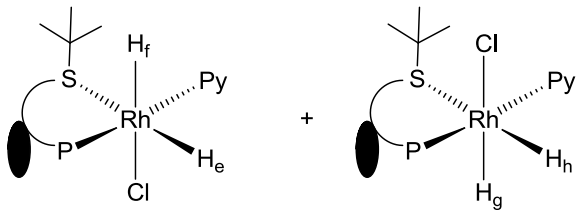

II.31 **II.32**

Scheme II.14

When a series of EXSY measurements were undertaken to examine the dynamic behaviour of this complex reaction system, interconversion between **II.31**, **II.29** and **II.30** was evident, with the signals for **II.32** being too weak to monitor.

When the pyridine excess was 75 fold, several exchange processes were observed (as revealed in Scheme II.15). The experimental rate constant for the $H_{e\rightarrow c}$ and $H_{e\rightarrow d}$ processes (**II.31→II.30**) were indistinguishable at 31 s^{-1}. In contrast the corresponding rate constant for $H_{e\rightarrow a}$ and $H_{e\rightarrow b}$ (**II.31→II.29**) was zero, as was mutual H_e-H_f interchange (**II.31**). These values reduce from 31 s^{-1} to 20 s^{-1} to 3 s^{-1} as the pyridine excess falls from 75 fold through 45 fold to 15 fold. Hence this process is pyridine dependent.

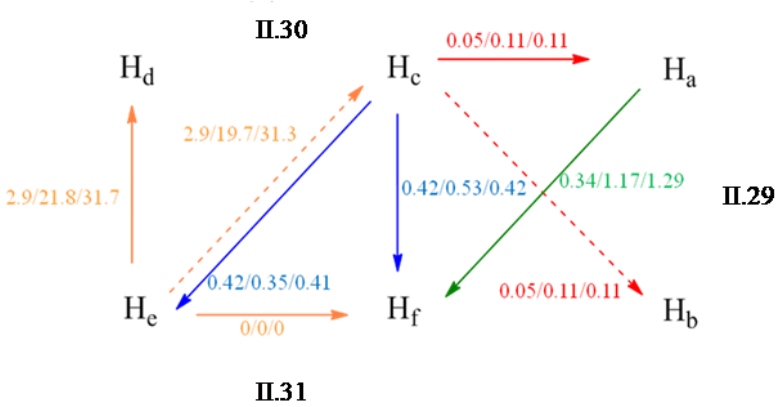

Scheme II.15. Hydride exchange pathways for the products found in the chemistry of compound **II.3-Bu^t**. The three numbers on each arrow are the exchange rates in s^{-1} relative to the solution with an 15-fold, 45-fold and 75-fold excess of pyridine.

Concerning the **II.30→II.31** process, the $H_{c\rightarrow e}$ rate constant is 0.41 s^{-1}, and the $H_{c\rightarrow f}$ rate has a similar value. The corresponding rates for the **II.30→II.29** process are slightly smaller than those found when tetrafluroborate derivative **II.4-Bu^t** is employed ($H_{c\rightarrow a}$ and $H_{c\rightarrow b}$ are again similar at 0.1 s^{-1} *vs*. 0.16 s^{-1} for **II.4-Bu^t**). The new rate constants for **II.29→II.30** with hydride position retention are zero when **II.3-Bu^t** is the precursor and 1.1 s^{-1} when **II.4-Bu^t** is employed. **II.29** does, however, form **II.31** with rate constants 1.3 s^{-1} for $H_{a\rightarrow f}$ and zero for $H_{a\rightarrow e}$. The observed hydride site exchange rate constants at 273 K measured on sample **II.3-Bu^t** for different pyridine concentrations are reported in Scheme II.15.

Thus, the reaction of [Rh(P,StBu)(COD)Cl] (**II.3-Bu^t**) or [Rh(P,SBu^t)(COD)]BF_4 (**II.4-Bu^t**) with H_2 in MeOH gives rise to COD hydrogenation and formation of a solvent stabilized product. The formation of hydride species cannot be observed in view of a very rapid H/D exchange between H_2 and the solvent. Addition of pyridine slows down this exchange process and allows observation of diastereometric dihydride complexes, $[Rh(P,SBu^t)(H)_2(L)_2]^+$, the stereochemistry of which was fully elucidated. The hydride site exchange rates have been derived from EXSY NMR experiments. In combination with DFT calculations (see below), these rates and their dependence on [py] will be used to elucidate the isomerization and site exchange mechanisms.

II.3.1.3 In CD_3OD in the presence of acetonitrile

In a further study, a d_4-methanol sample of **II.3-Bu^t** containing 110 equiv of acetonitrile was prepared. No reaction of **II.3-Bu^t** with H_2 was evident until 273 K. At this point, the corresponding ^1H NMR spectrum contained two PHIP polarized hydride peaks at δ -14.5 and -17.6. These hydride signals again appear as simple anti-phase doublets with additional phosphorus and rhodium couplings

(Fig. II.18). The signal at δ -14.5 exhibits a J_{HH} coupling of 11 Hz, a J_{HP} coupling of 20 Hz and a J_{RhH} coupling of 21 Hz while the corresponding splittings of the δ -17.6 signal are 12, 17 Hz and 20 Hz respectively. In the corresponding $^{1}H–^{31}P$ HMQC NMR spectrum, the δ -14.5 signal and the δ -17.2 signal proved to couple to a single ^{31}P centre located at δ 47.6 which exhibited a J_{RhP} splitting of 148 Hz. These results suggest that hydrogenation of **II.3-Bu^{t}** in the presence of acetonitrile selectively forms the MeCN analogue (**II.33**) of **II.29** (Scheme II.16).

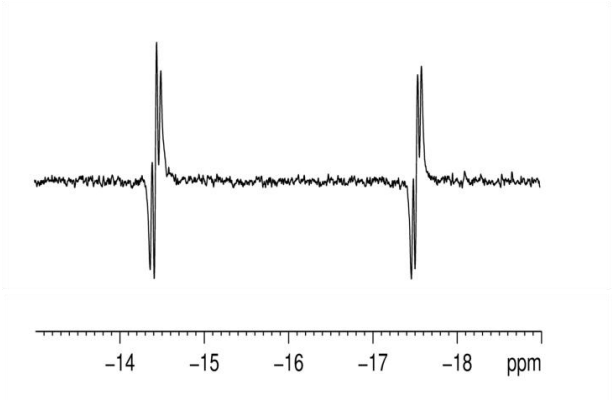

Fig. II.18 *p*-H_2 enhanced ^{1}H NMR spectrum showing the hydride region of **II.33** observed during reaction of **II.3-Bu^{t}** in d_4-methanol with *p*-H_2 and acetonitrile at 273 K.

There are a number of similarities between these data and those of **II.29**. For example, all the couplings suggest a *cis* P-H ligand arrangement and the chemical shifts are reflective of hydride ligands *trans* to sulfur and nitrogen. The coordination of MeCN has therefore the same effect as that of pyridine in reducing the hydride acidity and reducing the speed of the H/D exchange between H_2 and the solvent.

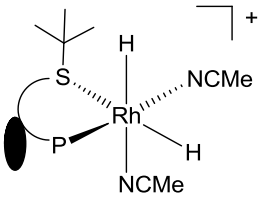

II.33

Scheme II.16

II.3.1.4 Hydrogenation studies

We have also explored the activity of these systems as hydrogenation catalysts. When a d_4-methanol sample of **II.3-Bu^{t}** containing 20 µl (75 equiv) of pyridine and diphenylacetylene was examined at 258 K, limited hydrogenation was evident and strongly enhanced signals for **II.29**, **II.30**,

II.31 and **II.32** were visible which exceed those in the analogous experiment without the alkyne. Under these conditions at 258 K the ratio of the *p*-H_2 enhanced hydride signals of **II.29** and **II.30** was 1:3.8. In contrast, when a similar sample was examined without pyridine, more rapid, but still slow, hydrogenation of diphenylacetylene occured; signals for both *cis* and *trans* stilbene were evident. These signals appear in an OPSY (Only Para-hydrogen SpectroscopY) measurement which was used to detect only protons that were previously located in a single molecule of *p*-H_2. No hydride signals were observed during these measurements.

When hydrogenation of the more reactive substrate phenylacetylene by **II.3-Bu^t** was examined in d_4-methanol using *p*-H_2, PHIP polarized signals could be readily seen for the styrene product at 263 K when no pyridine was present. However no hydride signals were still visible in this experiment. In contrast, when a 10-fold excess of phenylacetylene and acetonitrile was added there was evidence for both the formation of **II.33** and the hydrogenation of phenylacetylene. Formation of the dihydride species together with phenylacetylene hydrogenation was also reported for complexes [Rh(η^2-O_2Z)(PR_3)$_2$] (Z = CCH_3, CCF_3, CBu^t, S(O)-*p*-C_6H_4-CH_3; PR_3 = PPr^i_3, $PPhPr^i_2$, PPh_2Pr^i) [182].

Thus, the experimental results presented evidence that H_2 is able to hydrogenate the COD ligand in compounds **II.3-Bu^t** and **II.4-Bu^t** in MeOH, presumably yielding a [Rh(P,SBu^t)(MeOH)$_2$]$^+$ product (**II.25**). However, any further oxidative addition of H_2 to yield a putative dihydride product [Rh(H)$_2$(P,SBu^t)(MeOH)$_2$]$^+$ (**II.26**) would not be evidenced by ^{1}H NMR if there was rapid H/D exchange as suggested. On the other hand, further H_2 oxidative addition takes place in the presence of pyridine or MeCN to produce observable dihydridorhodium(III) species, at least in equilibrium amounts at the low temperatures used in these NMR experiments and these species are observable thanks to a reduced deprotonation rate in the presence of the more donating MeCN or pyridine ligands.

II.3.2 DFT study of H_2 addition to Rh(P,SR) complexes

To get deeper understanding of the experimental results, the relative stability of the [Rh(P,SBu^t)L$_2$]$^+$ (L = MeOH, py, MeCN) complexes and their ability to oxidatively add H_2 was further explored by means of DFT calculations, as well as the relative stability of all possible product isomers (Scheme II.17). The associated calculations were carried out using either the B3LYP functional or the M06 functional.[2]

The hypothetical replacement of the COD ligand in [Rh(P,SBu^t)(COD)]$^+$ (**II.4-Bu^t**) with two L donors to yield **I^L** (without COD hydrogenation) was found at the B3LYP level as endoergic when L = MeOH (ΔE = 15.4 kcal/mol, ΔG = 24.7 kcal/mol) and exoergic for the other two ligands (ΔE/ΔG are -6.4/+4.4 kcal/mol for L = py and -1.5/+6.0 for L = MeCN). However, in consideration of the energy gain of the COD hydrogenation process (ΔE = -34.4 or ΔG = -18.5 kcal/mol for the hydrogenation to

[2] Calculations were performed by Dr. Oleg Filippov, INEOS.

cyclooctene; ΔE = -64.3 or ΔG = -33.1 kcal/mol for the hydrogenation to cyclooctane), all the underlying reactions become favourable.

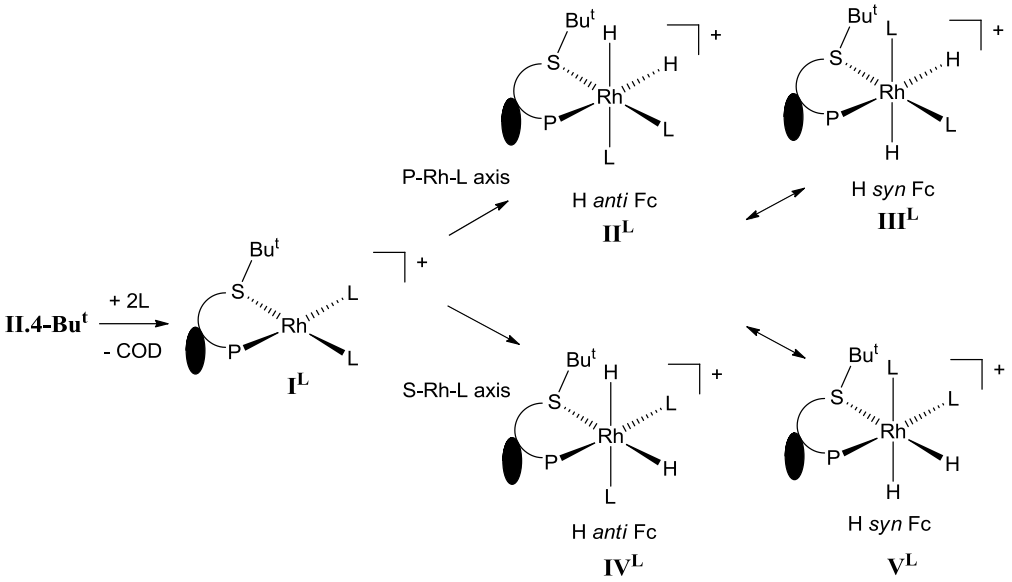

Scheme II.17

The oxidative addition of H_2 to $\mathbf{I^L}$ was also found to be energetically favourable for all three ligand systems, as shown by the data collected in Table II.20. It should be noted that while the gas phase free energies are positive, the computed values do not take into account stabilisation from solvation and the partial quenching of translational and rotational modes in the condensed phase.

Table II.20 Relative gase phase energies (ΔE) and Gibbs free energies (ΔG, in parentheses) in kcal mol^{-1} for the products of H_2 oxidative addition to $\mathbf{I^L}$

L	Functional	$\mathbf{II^L}$	$\mathbf{III^L}$	$\mathbf{IV^L}$	$\mathbf{V^L}$
MeOH	B3LYP	-8.5(+2.6)	-10.5(+1.3)	-14.1(-2.5)	-17.6(-6.5)
py	B3LYP	-4.5(+7.4)	-4.9(+7.9)	-10.1(+1.5)	-10.0(+2.1)
py	M06	+4.5(+15.2)	+2.2(+14.7)	-2.5(+7.8)	-3.5(+6.0)
MeCN	B3LYP	-4.2(+5.6)	-4.9(+6.0)	-8.5(+1.7)	-10.9(-0.1)

Furthermore, the hydride complexes were observed at low temperatures, where the detrimental effect of the positive TΔS contribution is smaller (for instance, the calculated ΔG for the oxidative addition to $\mathbf{I^{py}}$ to yield $\mathbf{V^{py}}$ at the M06 level decreased from +6.0 to +4.9 kcal/mol when applying the thermochemical corrections at 253 K instead of 298 K) and indeed the hydride resonances were lost upon warming the NMR tubes to higher temperatures (*vide supra*). For the pyridine system, the calculations have also been carried out at the M06 level, showing a slightly less favourable process. We note that the oxidative addition process for L = MeOH is predicted by these calculations to be

more favourable than for the other two ligands. Therefore, failure to observe the corresponding hydride resonances by ^{1}H NMR during the experiments appears indeed attributable to the accumulation of deuteride species by rapid H/D exchange. The dihydride complex is, though, at least sufficiently accessible to allow the H/D process to take place as suggested in Scheme II.11.

The computational results also suggest that the two isomers resulting from the H-H addition across the S-Rh-L axis are energetically preferred independent on L, in agreement with the assignment of the NMR spectra. The stereochemistry of structure **IV** corresponds to that of **II.29** and **II.33** and **V** corresponds to **II.30**. Structure $\mathbf{V}^{py}$ is slightly less stable than $\mathbf{IV}^{py}$ at the B3LYP level, but more stable at the M06 level in agreement with the NMR evidence. For L = MeCN and MeOH, the calculations also indicate greater stability for isomer $\mathbf{V}^{L}$, even at the B3LYP level, whereas the NMR assignment indicates that the observed compound **II.33** has the same configuration as **IV**.

A second question addressed by the DFT study is the mechanism for the H-site exchange in the two observed isomers for the pyridine systems (**II.29** and **II.30**, or $\mathbf{IV}^{py}$ and $\mathbf{V}^{py}$), in an attempt to rationalize the curious pyridine concentration effect on the various site exchange rates. The simplest way to imagine the isomerisation process, given the known strong *trans* labilizing effect of the hydride ligands, involves dissociation of a neutral donor placed *trans* to a hydride ligand (either the sulphur donor of the bidentate P,S ligand or a pyridine molecule) and rearrangement of the coordination sphere, as shown in Scheme II.18 for the specific case of thioether dissociation. The putative 5-coordinate intermediate **A** would then rearrange to its diastereoisomer **B** (same chirality at ferrocene and inverted chirality at rhodium) by either concerted hydride migration and rotation of the P,S ligand or via tautomerization to the dihydrogen complex **C** followed by P,S rotation to yield the rotamer **D**. Hydride site exchange can be envisaged by rotation of the dihydrogen ligand in the intermediates **C** and **D**. The observation of such a ligand exchange process by NMR is not inconsistent provided the lifetime of the rapidly relaxing dihydrogen form is short [135, 136].

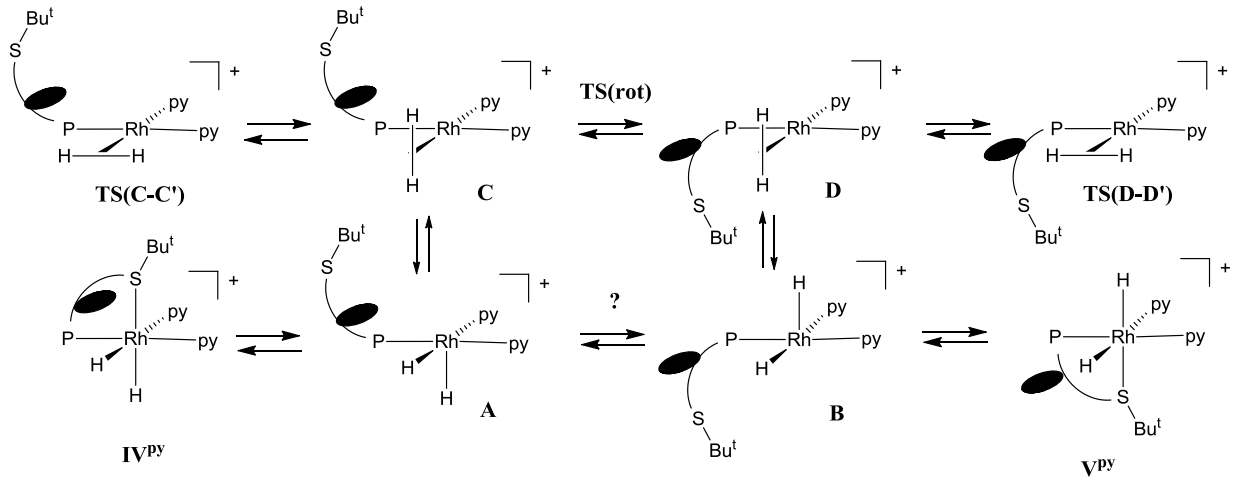

Scheme II.18

All calculations of this pathway were carried out with the M06 functional, since this is expected to better handle the long range dispersion interactions involved in the ligand dissociation processes. They show that pyridine dissociation is less favourable than the P,S ligand thioether arm dissociation. The most favourable dihydride complex resulting from pyridine dissociation, $[Rh(H)_2(P,SBu^t)(py)]^+$, is located at 29.7 kcal/mol from $\mathbf{V^{py}}$, while the isomeric non-classical complex $[Rh(H_2)(P,SBu^t)(py)]^+$ is more stable at only 18.3 kcal/mol from $\mathbf{V^{py}}$. However, the most stable dihydride complex resulting from dissociation of the thioether arm (**B** in Scheme II.18) is only 12.4 kcal/mol from $\mathbf{V^{py}}$, with **A** being only slightly higher at +14.7 kcal/mol and the nonclassical isomers **C** and **D** are even more stabilized at +11.8 and +8.3 kcal/mol, respectively. Therefore, the isomerization pathway shown in Scheme II.18 can be summarized as in Fig. II.19.

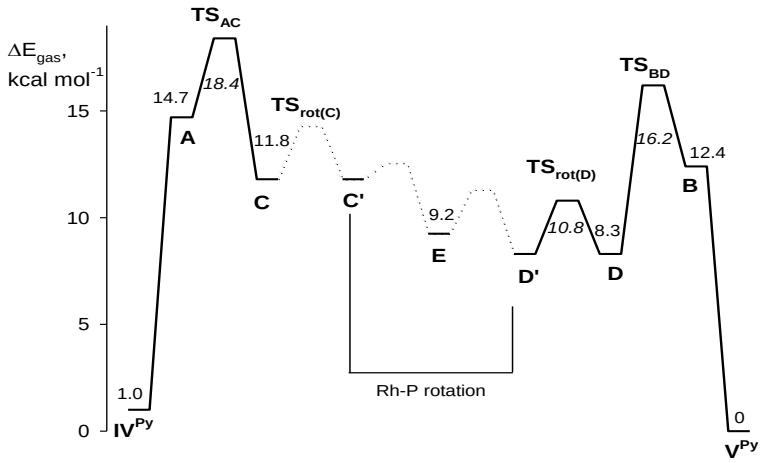

Fig. II.19 Energy profile (gas phase energies in kcal/mol) of the isomerization pathway of Scheme II.18.

Rearrangement of the classical to the nonclassical dihydrides occurs via localized transition states $\mathbf{TS_{AC}}$ and $\mathbf{TS_{BD}}$ at +18.4 and +16.2 kcal/mol. A more direct pathway from $\mathbf{IV^{py}}$ to **C** and from $\mathbf{V^{py}}$ to **D** could not be found. The P,S ligand rotation pathway involved in the interconversion of **C** and **D** was not straightforward to investigate for the location of a stationary point, but a manual scan of the dihedral N-Rh-P-C angle (see Fig. II.20) led to the identification a new local minimum corresponding to a new rotational intermediate **E** and two maxima, the highest point being 4.3 kcal/mol higher than **D** (+12.6 kcal/mol from $\mathbf{V^{py}}$). The search for a more direct pathway from **A** to **B** was unsuccessful. The barrier for site exchange was calculated for **D** and turned out rather low (2.5 kcal/mol, or + 10.8 kcal/mol from $\mathbf{V^{py}}$), lower than the barriers required to go back to the stable classical dihydride isomers.

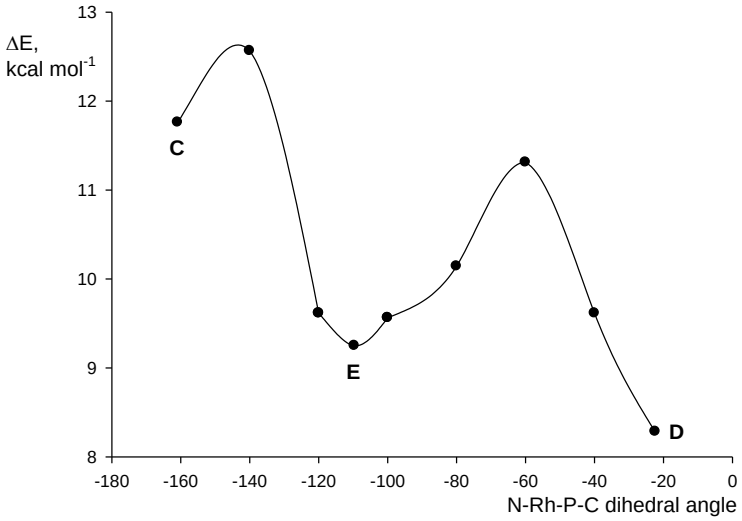

Fig. II.20. Relaxed potential energy surface scan (dihedral N-Rh-P-C taken as reaction coordinate). Energies are relative to $\mathbf{V^{Py}}$ adduct.

The results in Fig. II.19 are in agreement with certain experimental observations. Isomerization from $\mathbf{V^{py}}$ (**II.30**) to $\mathbf{IV^{py}}$ (**II.29**) requires transiting over the $\mathbf{TS_{AC}}$ barrier, whereas the site exchange in **II.30** may occur by simple access of the nonclassical intermediate and facile H_2 rotation, followed by the reverse pathway to $\mathbf{V^{py}}$ through the lower $\mathbf{TS_{BD}}$ barrier. This agrees with the faster site exchange relative to the **II.30** → **II.29** process. During the reverse isomerization of $\mathbf{IV^{py}}$ (**II.29**) to $\mathbf{V^{py}}$ (**II.30**), on the other hand, once the highest $\mathbf{TS_{AC}}$ barrier is passed and the intermediate **C** is generated, the isomerization process through P,S ligand rotation and the lower energy $\mathbf{TS_{BD}}$ occurs faster than the reverse generation of $\mathbf{IV^{py}}$, consistent with the fact that site exchange for **II.29** is not observed.

A most interesting experimental result is that the transformation of the minor isomer (**II.29**) into the major one (**II.30**) occurs preferentially as $H_{a\rightarrow c}$ and $H_{b\rightarrow d}$ at low [py] but preferentially as $H_{a\rightarrow d}$ and $H_{b\rightarrow c}$ at high [py] (see Scheme II.13). The former situation, according to Scheme II.18, would be compatible with a concerted pathway directly converting **A** to **B** without transiting through the nonclassical intermediate (arrows with question mark in Scheme II.18) through a transition state at lower energy than $\mathbf{TS_{AC}}$ and $\mathbf{TS_{BD}}$. As stated above, such a pathway could not be located but we cannot exclude that it exists. At greater pyridine concentrations, this pathway may be blocked by reversible coordination of pyridine to **A** and **B**.

Reversal of the relative rates of site exchange requires a new isomerisation pathway, resulting in selective migration of the axial H ligand in the square pyramidal geometry of **A** and **B** without moving the second H ligand in the equatorial plane. One attractive possibility for this transformation is a selective deprotonation of the axial site in **A** by excess pyridine, which is the strongest base present in solution, to yield a square planar monohydride intermediate $[RhH(\kappa^1\text{-}P,S)(py)_2]$, followed by

reprotonation at the opposite face of the square plane to afford **B**. This pathway is closely related to one of the proposed pathways for the H/D exchange between H_2 and solvent in pure CD_3OH (through intermediates **II.26** and **II.27** of Sceme II.11). No calculations were carried out, however, to confirm the feasibility of this pathway. The fact that this strong pyridine concentration effect is observed for the exchange rates associated to the transformation of the major isomer into the minor one (**II.30** → **II.29**) but not for those associated to the transformation of the minor isomer into the major one (**II.29** → **II.30**) is consistent with the need to overcome the smaller $\mathbf{TS_{BD}}$ barrier in the first step to achieve the rapid site scrambling. Hence, if the transition state of the putative site-conserving concerted pathway is lower than $\mathbf{TS_{AC}}$ but higher or comparable to $\mathbf{TS_{BD}}$, then the site exchange would remain operative even at low pyridine concentration. For the same reason, a very large concentration of pyridine does not afford a selective site inversion because collapse to the nonclassical intermediate promotes non selective deprotonation.

The presented results have explored the precatalyst activation phase for hydrogenation processes carried out in alcohol solvents with $[Rh(L,L')(diene)]^+$ systems, using $[Rh(P,SBu^t)(COD)]^+$ as a model compound. The COD ligand is removed by hydrogenation to yield a putative $[Rh(P,SBu^t)(CH_3OH)_2]^+$ complex which promotes a very rapid H/D exchange between H_2 and the solvent, possibly via a dihydride species $[Rh(H)_2(P,SBu^t)(CH_3OH)_2]^+$ that is accessible according to the DFT calculations. Addition of L (pyridine or MeCN) slows down this exchange, allowing the observation of diasteromeric dihydride species at low temperature. Evidence has also been obtained for equilibrium deprotonation of these cationic dihydride complexes in the presence of strong bases (e.g. excess pyridine). This phenomenon is presumably linked to the need of a strong base promoter for the catalytic action of these compounds and of the iridium analogues in the ionic hydrogenation of polar unsaturated substrates [32].

II.3.3 Study of solvated complex formation from the norbordadiene precursor II.2-Bu^t

According to the literature (see Chapter I), the activation of NBD-containing complexes by hydrogenation is a much faster process than the activation of the corresponding COD complexes. Therefore, additional studies of the activation process for the (P,SR)Rh system used in this thesis were carried out on the example of complex **II.2-Bu^t** as precursor using regular H_2 as reagent.

Bubbling H_2 for 2 min into an acetonitrile solution of **II.2-Bu^t** ($1.1 \cdot 10^{-2}$ mol/L) at ambient temperature led to the formation of the acetonitrile solvated complex $[Rh(P,SBu^t)(CD_3CN)_2]^+$, which was stable enough to allow the characterization by ^1H, ^{13}C, ^{31}P and two dimentional (COSY, HMQC, HMBC) NMR spectrometry (the data are in the Experimental part), but unfortunately the compound could not be isolated as a solid. There was evidence of hydrogenation of NBD ligand to norbornane (δ 2.18, 1.22, 1.04). An identical ^{31}P signal at δ 34.3 (d, J_{P-Rh} = 170 Hz) was also obtained upon

hydrogenation of the COD analogue **II.4-Bu^t** under these conditions. However, substantial amounts (ca. 30%) of the starting material remained after 15 min of H_2 bubbling in agreement with the expected slower reaction. Under these conditions, there was no evidence for the formation of the dihydride complex **II.33** (Scheme II.16). Specifically, the ^{31}P resonance of this compound is quite different from that observed for the dihydride complex, which was generated at low temperature after the addition of *p*-H_2 to the solution of **II.3-Bu^t** in CD_3OD in the presence of MeCN (see section II.3.1.3 above).

This observation demonstrates that the dihydrogen oxidative addition to the solvated Rh(I) complex to yield the solvated Rh(III) dihydride complex (Scheme II.10 with MeCN in place of CD_3OD), is an equilibrated process which is displaced mostly to the Rh(I) complex at room temperature. Therefore, the observation of the hydride resonances of the solvated Rh(III) dihydride complex when the reaction was carried out with *p*-H_2 in CD_3OD in the presence of L (pyridine, MeCN) is mostly attributable to the lower temperatures used in this experiment, which favor the oxidative addition process, and to the hydride peak enhancement resulting from the hyperpolarization of the *p*-H_2 reagent. In this respect, it has to be remarked that all the other resonances attributed to the solvated Rh(III) dihydride complexes (^{31}P, ^{15}N, ^{103}Rh) and reported in section **II.3.1** came from HMQC experiments where polarization was transferred to these nuclei from the hyperpolarized Rh(III) hydride resonances. Therefore, any other ^{31}P, ^{15}N, and ^{103}Rh resonance of other species in solution, even though they may be dominant in concentration, would remain undetected in those experiments.

Upon addition of dihydrogen to the solution of **II.2-Bu^t** in d_4-methanol under the same conditions, the ^{31}P NMR spectra showed the disappearance of the peak of the starting material and the appearance of a new peak at δ 40.5 ppm (J_{PRh} = 202 Hz) which is attributed to the methanol complex $[Rh(P,SBu^t)(CD_3OD)_2]^+$, **II.24**. This species slowly (within a day) decomposes in solution, whereas $[Rh(P,SBu^t)(CD_3CN)_2]^+$ derivative is more stable (up to 5 days).

When d_6-acetone was used as the reaction solvent the formation of $[Rh(P,SBu^t)(d_6\text{-acetone})_2]^+$ was also observed after 2 min (δ 39.9 ppm, J_{PRh} = 197 Hz), but further addition of dihydrogen to this solution led to the observation of additional doublets in the ^{31}P NMR spectrum at δ 45.7 (J_{PRh} = 228 Hz) and 35.9 ppm (J_{PRh} = 197 Hz), possibly related to complexes with L = iso-propanol (product of acetone hydrogenation) (see Fig. 21). Once again, no hydride resonances could be obserbed in the corresponding ^{1}H NMR spectrum under these conditions.

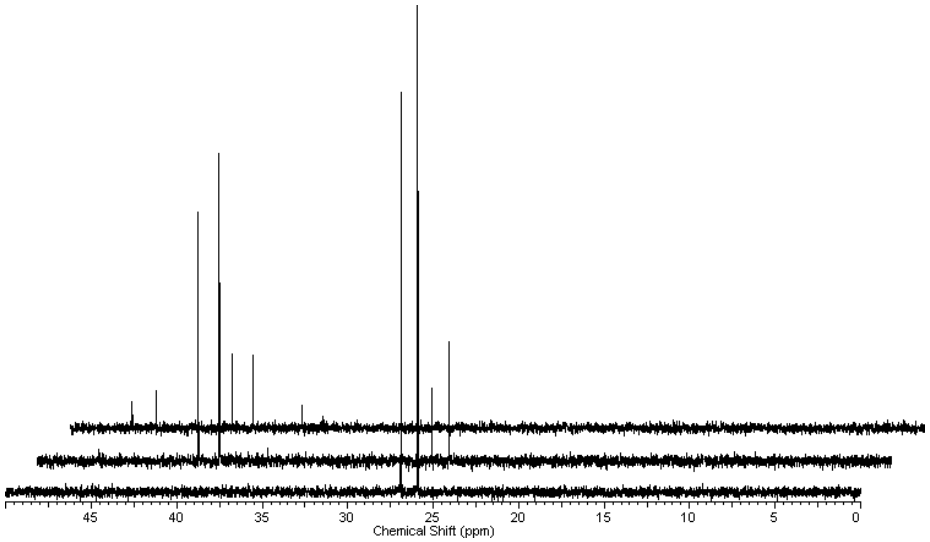

Fig. II.21. ^{31}P NMR spectra of **II.2-Bu^t** in d_6-acetone ($3.3 \cdot 10^{-2}$ mol/L) recorded before and after 4 and 8 min of reaction with H_2, respectively, showing the decrease in the intensity of the signal of **II.2-Bu^t** (doublet at δ 26.4, J_{PRh} = 158.9 Hz) and the formation of new products with ^{31}P signals appearing around δ 35.9 (J_{PRh} = 197 Hz), 39.9 (J_{PRh} = 197 Hz) and 45.7 (J_{PRh} = 228 Hz).

In conclusion, use of the more reactive NBD precursor **II.2-Bu^t** for the diene hydrogenation study allowed a faster and selective generation of the solvated Rh(I) complex $[(P,SR)Rh(L)_2]^+$ system with L = CD_3OD, MeCN or CD_3COCD_3. Resonances for the solvated Rh(III) dihydride complexes were not observed in these cases, proving that the H_2 oxidative addition equilibrium is mostly shifted toward the solvated Rh(I) complex at room temperature.

II.3.4 Study of precatalyst activation by UV/Vis spectroscopy

The ligand influence on the Rh precatalyst hydrogenation was further investigated with continuous dihydrogen bubbling (1 atm of incoming pressure) through the solution of **II.1-R**-**II.4-R** and with monitoring by UV-visible spectroscopy using an in-situ probe with a 5 mm path length. The decrease of a metal-ligand charge transfer (MLCT) band with λ_{max} at 420 nm for the COD complexes (445 nm for the NBD ones) and the increase of the absorption at lower and higher wavelengths (λ = 350, 485 nm and 400, 520 nm were chosen as reference wavelengths for COD and NBD derivatives, respectively) was followed in time (Fig. II.22). This experimental set-up required lower concentrations of the Rh complexes (ca. 10^{-3} M) relative to those used in the NMR experiments (ca. 10^{-2} M). Consequently, the observed reaction rates, dA/dt, were much lower.

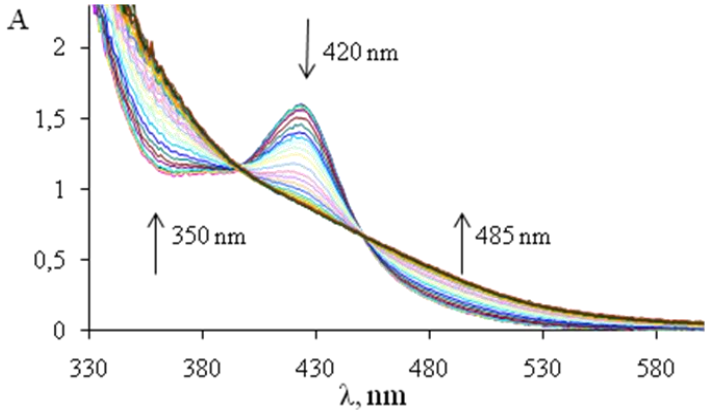

Fig. II.22. Evolution of the UV-visible spectrum during the stoichiometric hydrogenation of **II.4-Bu^t** ($5\cdot10^{-3}$ mmol) in 5 mL Pr^{i}OH at 25.0°C and 1.0 bar overall pressure with a cycle time of 5 min; total reaction time 130 min.

In neat alcohol (MeOH or Pr^{i}OH were used) the changes in the three bands occurred simultaneously as shown by the presence of two isobestic points (Fig. II.22). Such spectral pattern resembles that described in the literature [105, 107] for the stoichiometric hydrogenation of [Rh(P,P)(diene)]$^+$, but in contrast to those data the hydrogenation of [Rh(P,SR)(diene)]$^+$ complexes appeared to have an induction period. This is clearly shown in Fig. II.23 by the recorded trace of the absorption at 420 nm (COD complexes) or 445 nm (NBD complexes) as a function of the reaction time. The length of the induction period (Table II.21) depended on the nature of the ligand. For complexes containing the same sulfur substituent (Bu^t), this induction period was shorter for the NBD complexes (**II.1-Bu^t** and **II.2-Bu^t**) than for the COD complexes (**II.3-Bu^t** and **II.4-Bu^t**), whereas for complexes with different sulfur substituents (**II.1-R**) it was shorter for the Bu^t complex (120 s) than for the Bz (600 s) and Ph (840 s) substituent.

Table II.21 Length of the induction period (τ) and observed rate constants (k_{obs}) for the stoichiometric hydrogenation of different rhodium complexes in Pr^{i}OH.

Entry	Complex		τ, s	k_{obs}, s^{-1}
1	**II.1-Bu^t**	NBD Cl	120	$9\cdot10^{-4}$
2	**II.1-Bz**	NBD Cl	600	$2.7\cdot10^{-3}$
3	**II.1-Ph**	NBD Cl	840	$5\cdot10^{-4}$
4	**II.2-Bu^t**	NBD BF_4	240	$2.7\cdot10^{-3}$
5	**II.3-Bu^t**	COD Cl	360	$6\cdot10^{-4}$
6	**II.4-Bu^t**	COD BF_4	900	$2\cdot10^{-4}$

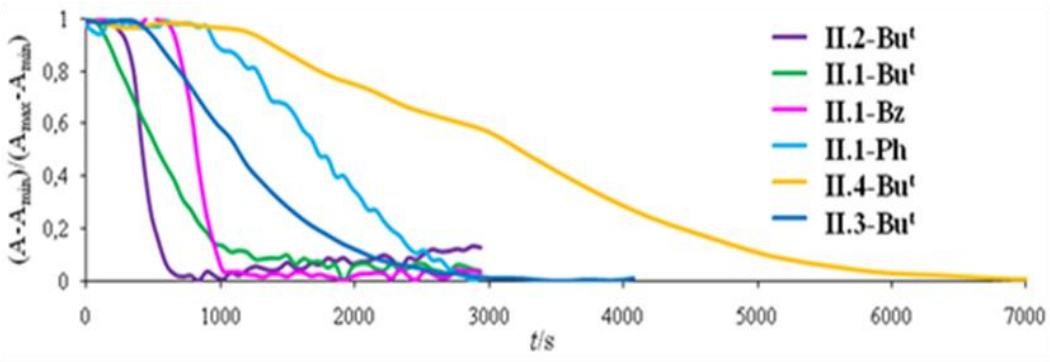

Fig. II.23. Normalized absorption for the 420 nm band (COD complexes) or 445 nm band (NBD complexes) as a function of the reaction time (conditions: $5 \cdot 10^{-3}$ mmol of complex in 5 mL iPrOH at 25.0 °C and 1.0 bar of overall pressure).

The addition of pyridine to the methanol solution of **II.3-Bu^t** or **II.4-Bu^t** changes the kinetic behavior of the reaction (Fig. II.24). The isosbestic points were not observed in this case, meaning that there is accumulation of a colored intermediate in this case. However, the final UV-visible spectrum is identical to that obtained in the absence of pyridine (Fig. II.22), indicating the formation of the same species, presumably the solvated complex $[Rh(P,SBu^t)(MeOH)_2]^+$ as suggested by the NMR investigation. It should also be remarked that the presence of an induction time is much less obvious in this case.

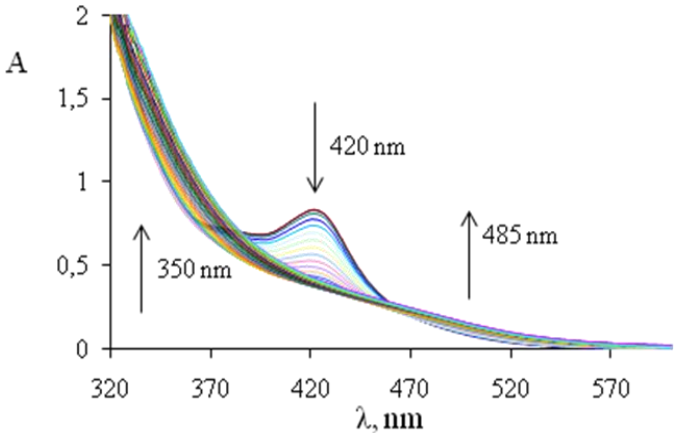

Fig. II.24. Evolution of the UV-visible spectrum during the stoichiometric hydrogenation of **II.3-Bu^t** ($5 \cdot 10^{-3}$ mmol) in the presence of pyridine (0.375 mmol) in 5 mL MeOH at 25.0 °C and 1.0 bar overall pressure with a cycle time of 5 min.

Indeed, the decrease of the band at λ_{max} = 420 nm is accompanied by the simultaneous absorption increase at 485 nm, whereas absorption at lower wavelengths (the reference wavenumber 350 nm) starts to increase only after 2400 s (Fig. II.25). An accurate kinetic analysis of this process

and the identification of the presumed intermediate require deeper studies that are planned for the continuation of this research project.

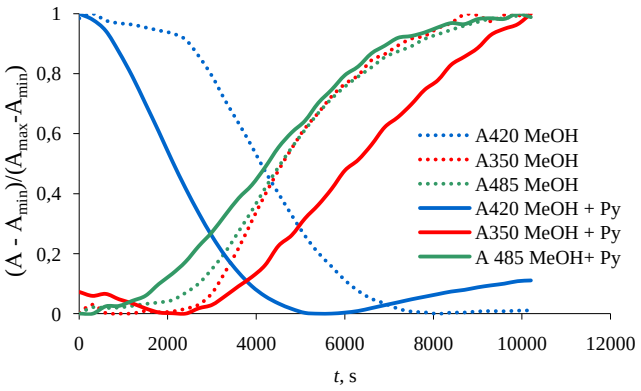

Fig. II.25. Normalized absorption of different bands as a function of the reaction time for the stoichiometric hydrogenation of **II.3-Bu^t** ($5 \cdot 10^{-3}$ mmol) in 5 mL MeOH in the absence and in the presence of pyridine (0.375 mmol) at 25.0 °C and 1.0 bar overall pressure.

Thus, these results suggest that the activation step leading to the formation of the solvated complex $[Rh(P,SBu^t)(MeOH)_2]^+$ occurs in at least two steps, at least for the reaction carried out in the presence of pyridine. As indicated in the literature review part, the stoichiometric hydrogenation of $[Rh(diene)(PP)]^+$ has also been rationalized by Heller *et al.* [105] as involving two steps, which have been assigned to the hydrogenation of the two C=C bonds in a stepwise manner through two processes that are pseudo-first order under constant hydrogen pressure:

$$[Rh(P,P)(diene)]^+ \xrightarrow{k'_1 = k_1 \cdot [H_2]} [Rh(P,P)(alkene)]^+ \xrightarrow{k'_2 = k_2 \cdot [H_2]} [Rh(P,P)(solv)_2]^+ + \text{alkane}$$

where the concentration of the $[Rh(P,P)(alkene)]^+$ intermediate was very low because $k'_2 >> k'_1$ and because the following ligand exchange equilibrium is shifted to the right hand side:

$$[Rh(P,P)(alkene)]^+ + \text{Solvent} \leftrightarrow [Rh(P,P)(Solv)_2]^+ + \text{alkene}.$$

We have not, however, detected an intermediate that can be interpreted as $[Rh(P,P)(alkene)]^+$ in the low-temperature NMR study. On the other hand, we found evidence for another complex having the stoichiometry $[Rh(P,SBu^t)(1\text{-}\kappa\text{-}4,5\text{-}\eta\text{-}C_8H_{13})]$ when using the COD precursor. This is obtained by H_2 oxidative addition and insertion of one of the COD double bonds, followed by deprotonation (see Scheme II.10). Therefore, we may propose an alternative kinetic interpretation of a two-step activation

process as shown in Scheme II.19. The proposed mechanism does not depend on the presence of pyridine. However, the relative rates of the two steps would be affected by the pyridine presence.

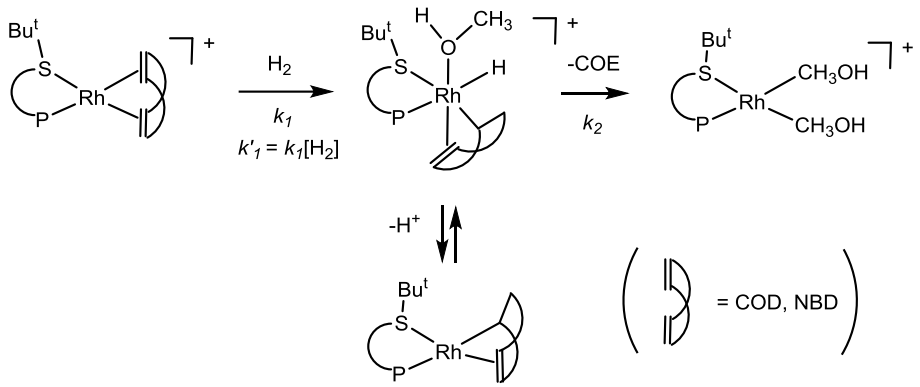

Scheme II.19

According to this kinetic scheme, the observation of isosbestic points as in the experiment carried out in pure alcohol indicates that there is no observable accumulation of a colored intermediate. In the presence of pyridine, on the other hand, the two rates would be comparable allowing the accumulation of the intermediate. The reason for this phenomenon may be associated to the deprotonation equilibrium of the cationic intermediate $[Rh(P,SBu^t)(1\text{-}\kappa\text{-}4,5\text{-}\eta\text{-}C_8H_{13})H]^+$ that is formed first by the H_2 oxidative addition and insertion. This intermediate is also necessary for the reductive elimination and expulsion of the hydrogenated diene. In the presence of pyridine (a strong Brønsted base), the deprotonated product would be favoured, slowing down the second step and allowing accumulation of the intermediate. In the absence of pyridine, on the other hand, the intermediate would remain more on the protonated side, allowing the second step to proceed much faster.

For the experiment carried out in the absence of pyridine, the observed rate constant corresponds to the rate of the first step ($k_{obs} = k'_1[H_2]$). The slope of the middle part of kinetic curves in Fig. II.23 is reported in Table II.21 as observed rate constant k_{obs}. This preliminary treatment shows numerically that the rate of the reaction is dependent on the ligand. The hydrogenation proceeds faster in case of the NBD complexes than in case of COD complexes. A comparison of entries 1-3 in Table II.21 also shows a marked effect of the sulfur substituent on the rate of the hydrogenation process, the rate increasing in the order Ph < Bu^t < Bz. Finally, the rate also depends on the anion used in the precatalyst, the chlorides being slower than the BF_4 salts (*cf.* entries 1/4 and 5/6). These rates, however, vary only by a factor of 3 and, curiously, while the reaction is faster for the BF_4 salt in the case of the NBD systems, it is faster for the Cl complex in the case of the COD systems.

One point that remains obscure at the moment is the origin of the induction time, which was particularly evident when the hydrogenation was carried out in pure alcohol. This induction time also

has a sharp dependence on the nature of the R substituent, diene and X nature. The clarification of this point will require futher investigations.

II.3.5 Conclusive remarks

It has been established in this spectroscopic section, in line with the literature knowledge, that the [Rh(diene)(P,SBu^t)X] compounds react with H_2 to induce diene hydrogenation and expulsion from the coordination sphere to initially produce solvated [Rh(P,SBu^t)(Solv)$_2$]$^+$ complexes that are rather unstable under room temperature conditions (stability increasing in the order MeOH, MeCOMe < MeCN). The NBD derivative reacts more rapidly and allows better identification of the solvated complexes by NMR spectroscopy. The H_2 oxidative addition to these complexes to produce solvated cationic Rh^{III} dihydride complexes does not significantly occur at room temperature, but can be highlighted at low temperature by the use of both regular H_2 and especially *para*hydrogen. The rapid H/D exchange between *para*-H_2 and CD_3OD that is observed in the absence of additional donors (py, MeCN) is additional evidence for the equilibrium formation of the Rh^{III} species. The chirality of the (P,SR) ligand gives rise as expected to a mixture of two diastereoisomers for [Rh(P,SR)H$_2$(Solv)$_2$]$^+$ and an NMR investigation for the mixture obtained with Solv = py has highlighted a [py]-dependent intramolecular and intermolecular hydride site exchange, which has been mechanistically rationalized on the basis of DFT calculations.

Preliminary kinetics investigations by UV-visible monitoring have shown evidence for a multistep process in MeOH solution, where at least two steps proceed at comparable rates when pyridine is present, thus leading to the accumulation of one (or more) intermediate(s) and to the absence of isosbestic points, whereas the first step is slower than the following ones in the absence of pyridine (isosbestic points were observed). The nature of the intermediate(s) remains to be clarified, although an interesting possibility seems complex [Rh(P,SBu^t)(1-κ-4,5-η-C$_8$H$_{13}$)], which was also identified at low-temperature in the *para*hydrogen NMR experiment. The origin of the induction times that are observed especially in the absence of pyridine, however, remains obscure.

III Experimental part

III. 1 General

All reactions were carried out under an argon atmosphere using standard Schlenk techniques. Solvents were carefully dried by conventional methods and distilled under argon before use. The (*R*/*S*)-2-diphenylphosphanyl-(R-thiomethyl)ferrocene ligands (R = Et, Bu^t, Ph, Bz) were prepared according to a published procedure from racemic 2-(diphenylthiophosphanylferrocenyl)-methanol [29]. Compounds $[Rh(COD)Cl]_2$, $[Rh(NBD)Cl]_2$ and $[Rh(COD)_2]BF_4$ were purchased from Strem Chemicals and used as received. ^1H, $^{13}C\{^1H\}$ and $^{31}P\{^1H\}$ NMR spectra of [Rh(P,SR)(diene)]X rhodium complexes were recorded with a Bruker Avance 500 FT-NMR spectrometer. The resonances were calibrated relative to the residual solvent peaks and are reported with positive values downfield from TMS. For all characterized compounds, the peak assignments in the ^1H and ^{13}C NMR spectra were based on COSY, HSQC and HMBC 2D experiments. HRMS were obtained from dichloromethane solutions with a Xevo G2 Q TOF spectrometer by the electrospray method. IR spectra of these complexes were recorded at room temperature with a Nicolet 6700 spectrometer in the solid state (as nujol mulls) using polyethylene cells for the low frequency region. All ketones were used as received without any purification. The purity of the substrates was checked by GC before use. Quinaldine and 1-phenyl-2-propene-1-ol were purified by distillation before use. *N*-Phenyl-*N*-(1-phenylethylidene)amine was synthesized from aniline and acetophenone according to standard methods using a Dean-Stark apparatus [183]. The optical purities and the conversions for the hydrogenation experiments were determined by chiral GC on Supelco BETADEX™ 225 (for ketones and 1-phenyl-2-propene-1-ol) and Varian Chirasil-DEX C (for the imines and 3-methyl-2-cyclohexenone) instruments.

III.2 Synthesis

III.2.1 General procedure for the synthesis of [Rh(P,SR)(NBD)Cl], II.1-R.

In a Schlenk tube, under nitrogen, ligand (P,SR) (0.793 mmol) was dissolved in dichloromethane (5 mL) and $[Rh(NBD)Cl]_2$ (183 mg, 0.396 mmol) was added. The solution was stirred for 4 h at room temperature and 15 mL of pentane was then added to yield a yellow precipitate. The precipitate was filtered under argon and washed with pentane to give [Rh(P,SR)(NBD)Cl].

[Rh(P,SBu^t)(NBD)Cl] (**II.1-Bu^t**, yield: 97%). ^1H NMR (500 MHz, $CDCl_3$): δ 8.48 (m, 2H, Ph); 7.53 (m, 3H, Ph); 7.3–7.2 (m, 3H, Ph); 6.93 (br dd, 2H, Ph, J_{HH} = 7.2 Hz, J_{HP} = 9.7 Hz); 5.06 (d (AB), 1H, CH_2Fc, J_{HH} = 13.8 Hz); 4.56 (s, 1H, subst. Cp); 4.30 (s, 1H, subst. Cp); 4.14 (s, 1H, subst. Cp); 3.90 (s, 5H, Cp); 3.84 (d (AB), 1H, CH_2Fc, J_{HH} = 13.8 Hz); 3.78 (s, 2H, CH NBD); 3.61 (s, 2H, CH

NBD); 3.57 (s, 2H, CH NBD); 1.51 (s, 9H, Bu^t) 1.23 (s, 2H, CH_2 NBD). $^{13}C\{^1H\}$ NMR (125 MHz, $CDCl_3$): δ 136.3 (d, Ph, J_{CP} = 12.8 Hz); 135.3 (d, quat Ph, J_{CP} = 45.6 Hz); 133.8 (d, quat Ph, J_{CP} = 45.6 Hz); 132.3 (d, Ph, J_{CP} = 9.2 Hz); 130.4 (d, Ph, J_{CP} = 2.2 Hz); 128.7 (d, Ph, J_{CP} = 1.8 Hz); 127.7 (d, Ph, J_{CP} = 10.4 Hz); 127.2 (d, Ph, J_{CP} = 9.2 Hz); 91.3 (d, quat Cp, J_{CP} = 18.6 Hz); 73.3 (s, subst. Cp); 71.9 (d, subst. Cp, J_{CP} = 7.6 Hz); 71.5 (d, quat Cp, J_{CP} = 7.6 Hz); 71.0 (s, Cp); 69.0 (d, subst. Cp, J_{CP} = 5.2 Hz); 61.4 (s, CH_2 NBD); 60.2 (br s, CH NBD); 55.9 (br s, CH NBD); 48.5 (s, CH NBD); 46.0 (s, S-C(CH_3)); 31.3 (s, S-C(CH_3)); 28.8 (CH_2Fc). $^{31}P\{^1H\}$ NMR (202 MHz, $CDCl_3$): δ 23.6 (d, $J_{P–Rh}$ = 159 Hz). MS (ESI) m/z: 667.081 ($M - Cl^-$, 100%).

[Rh(P,SPh)(NBD)Cl] (**II.1-Ph**, yield: 98%). ^1H NMR (500 MHz, $CDCl_3$): δ 8.52 (m, 2H, Ph); 7.73 (br d, J_{HH} = 7.5 Hz, 2H, Ph); 7.58 (m, 3H, Ph); 7.4–7.1 (m, 6H, Ph); 6.62 (m, 2H, Ph); 5.37 (br d (AB), 1H, CH_2Fc, J_{HH} = 13 Hz); 4.45 (br s, 1H, subst. Cp); 4.28 (br d (AB), 1H, CH_2Fc, J_{HH} = 13 Hz); 4.24 (br s, 1H, subst. Cp); 4.03 (br s, 1H, subst. Cp); 3.88 (s, 5H, Cp); 3.54 (s, 4H, CH NBD); 3.40 (s, 2H, CH NBD); 1.17 (s, 2H, CH_2 NBD). $^{13}C\{^1H\}$ NMR (125 MHz, $CDCl_3$): δ 136.2 (d, Ph, J_{CP} = 13.0 Hz); 135.3 (d, quat Ph, J_{CP} = 46.8 Hz); 135.1 (quat Ph); 133.3 (d, quat Ph, J_{CP} = 46.0 Hz); 131.6 (d, Ph, J_{CP} = 9.3 Hz); 130.6 (d, Ph, J_{CP} = 2.2 Hz); 130.3 (Ph); 129.0 (Ph); 128.6 (d, Ph, J_{CP} = 1.8 Hz); 127.9 (d, Ph, J_{CP} = 10.5 Hz); 127.5 (Ph); 127.2 (d, Ph, J_{CP} = 9.4 Hz); 89.0 (d, quat Cp, J_{CP} = 18.6 Hz); 72.6 (s, subst. Cp); 72.4 (d, subst. Cp, J_{CP} = 7.7 Hz); 71.0 (s, Cp); 70.8 (d, quat Cp, J_{CP} = 40 Hz); 69.1 (d, subst. Cp, J_{CP} = 5.0 Hz); 60.8 (d, J_{CRh} = 5.3 Hz, CH_2 NBD); 59.1(d, J_{CRh} = 7.6 Hz, CH NBD); 54.2 (br s, CH NBD); 48.2 (s, CH NBD); 34.1 (CH_2Fc). $^{31}P\{^1H\}$ NMR (202 MHz, $CDCl_3$): δ 23.8 (d, $J_{P–Rh}$ = 154 Hz). MS (ESI) m/z: 687.049 ($M - Cl^-$, 100%).

[Rh(P,SBz)(NBD)Cl] (**II.1-Bz**, yield: 99%). ^1H NMR (500 MHz, $CDCl_3$): δ 8.46 (m, 2H, Ph); 7.59 (m, 3H, Ph); 7.45–7.25 (m, 8H, Ph); 6.88 (m, 2H, Ph); 4.32 (br s, 1H, subst. Cp); 4.25 (br s, 1H, subst. Cp); 4.13 (br d (AB), 1H, CH_2Fc, J_{HH} = 12 Hz); 4.08 (s, 1H, subst. Cp); 4.00 (m, 1H CH_2Fc + 1H CH_2Ph); 3.73 (s, 5H, Cp); 3.70 (d (AB), 1H, CH_2Ph); 3.52 (br s, 4H, NBD); 3.42 (br s, 2H, NBD); 1.19 (s, 2H, CH_2 NBD). $^{13}C\{^1H\}$ NMR (125 MHz, $CDCl_3$): δ 143.4 (quat Ph); 136.0 (d, Ph, J_{CP} = 13.3 Hz); 135.5 (d, quat Ph, J_{CP} = 43.8 Hz); 134.6 (d, quat Ph, J_{CP} = 44.8 Hz); 131.4 (d, Ph, J_{CP} = 9.4 Hz); 130.5 (d, Ph, J_{CP} = 2.0 Hz); 129.5 (Ph); 128.71 (Ph); 128.66 (d, Ph, J_{CP} = 1.8 Hz); 127.9 (d, Ph, J_{CP} = 10.4 Hz); 127.7 (Ph); 127.4 (d, Ph, J_{CP} = 9.1 Hz); 88.6 (d, quat Cp, J_{CP} = 19.7 Hz); 72.6 (s, subst. Cp); 72.5 (d, subst. Cp, J_{CP} = 7.6 Hz); 70.7 (s, Cp); 70.4 (d, quat Cp, J_{CP} = 38.9 Hz); 69.1 (d, subst. Cp, J_{CP} = 4.7 Hz); 60.4 (s, CH_2 NBD); 53.8 (br s, CH NBD); 49.9 (br s, CH NBD); 48.1 (s, CH NBD); 40.6 (CH_2Ph); 31.3 (CH_2Fc). $^{31}P\{^1H\}$ NMR (202 MHz, $CDCl_3$): δ 20.3 (d, $J_{P–Rh}$ = 147 Hz). MS (ESI) m/z: 701.067 ($M - Cl^-$, 100%).

[Rh(P,SEt)(NBD)Cl] (**II.1-Et**, yield: 99%). ^1H NMR (500 MHz, $CDCl_3$): δ 8.44 (m, 2H, Ph); 7.59 (m, 3H, Ph); 7.27 (m, 3H, Ph); 6.87 (m, 2H, Ph); 4.52 (s, 1H, subst. Cp); 4.37 (br d (AB), 1H, CH_2Fc, J_{HH} = 12 Hz); 4.29 (s, 1H, subst. Cp); 4.14 (s, 1H, subst. Cp); 4.06 (br d (AB), 1H, CH_2Fc, J_{HH}

= 12 Hz); 3.83 (s, 5H, Cp); 3.60 (br m, 4H, CH NBD); 3.42 (br s, 2H, CH NBD); 2.81 (m, 1H, CH_2CH_3); 2.57 (m, 1H, CH_2CH_3); 1.38 (t, 3H, CH_3, J_{HH} = 6.7 Hz); 1.22 (s, 2H, CH_2 NBD). $^{13}C\{^1H\}$ NMR (125 MHz, $CDCl_3$): δ 135.9 (d, Ph, J_{CP} = 13.2 Hz); 135.5 (d, quat Ph, J_{CP} = 44.3 Hz); 134.2 (d, quat Ph, J_{CP} = 44.8 Hz); 131.4 (d, Ph, J_{CP} = 9.5 Hz); 130.5 (d, Ph, J_{CP} = 2.2 Hz); 128.7 (d, Ph, J_{CP} = 1.8 Hz); 127.9 (d, Ph, J_{CP} = 10.4 Hz); 127.5 (d, Ph, J_{CP} = 9.2 Hz); 88.8 (d, quat Cp, J_{CP} = 19.4 Hz); 72.7 (s, subst. Cp); 72.5 (d, subst. Cp, J_{CP} = 7.7 Hz); 70.8 (s, Cp); 70.2 (d, quat Cp, J_{CP} = 38 Hz); 69.0 (d, subst. Cp, J_{CP} = 4.8 Hz); 60.7 (s, CH_2 NBD); 55.3 (br s, CH NBD); 51.2 (br s, CH NBD); 48.2 (s, CH NBD); 30.8 (CH_2Fc); 29.7 (d, J_{CRh} = 3.4 Hz, CH_2CH_3); 13.4 (CH_3). $^{31}P\{^1H\}$ NMR (202 MHz, $CDCl_3$): δ 21.3 (d, $J_{P–Rh}$ = 148 Hz). MS (ESI) m/z: 639.049 ($M - Cl^-$, 100%).

III.2.2 Synthesis of [Rh(P,SBu^t)(NBD)]BF_4, II.2-Bu^t.

In a Schlenk tube, under nitrogen, complex [Rh(P,SBu^t)(NBD)Cl] (0.148 mmol) was dissolved in dichloromethane (5 mL) and 5 ml of a water solution of $NaBF_4$ (20 mg, 0.178 mmol) was added. The organic phase was separated and dried over anhydrous sodium sulfate. After solvent evaporation, [Rh(P,SBu^t)(NBD)]BF_4 was obtained as a yellow solid. ^1H NMR (500 MHz, $CDCl_3$): δ 7.69 (m, 2H, Ph); 7.55–7.50 (m, 6H, Ph); 7.40 (m, 2H, Ph); 5.85–5.65 (br m, 2H, CH NBD); 4.77 (s, 1H, subst. Cp); 4.64 (s, 5H, Cp); 4.49 (m, 1H, subst. Cp); 4.35–4.30 (br s, 3H, CH NBD); 4.12 (m, 1H, subst. Cp); 3.96 (d (AB), 1H, CH_2Fc, J_{HH} = 12.2 Hz); 3.90–3.70 (br s, 1H, CH NBD); 2.81 (d (AB), 1H, CH_2Fc, J_{HH} = 12.2 Hz); 1.69 (br s, 2H, CH_2 NBD); 1.37 (s, 9H, Bu^t). ^{13}C $\{^1H\}$ NMR (125 MHz, $CDCl_3$): δ 134.0 (d, Ph, J_{CP} = 13.2 Hz); 132.1 (d, Ph, J_{CP} = 2.2 Hz); 131.7 (d, Ph, J_{CP} = 9.9 Hz); 131.3 (d, Ph, J_{CP} = 2.4 Hz); 129.6 (d, quat Ph, J_{CP} = 45.8 Hz); 129.5 (d, Ph, J_{CP} = 10.6 Hz); 129.0 (d, Ph, J_{CP} = 10.8 Hz); 126.0 (d, quat Ph, J_{CP} = 52.3 Hz); 85.9 (d, quat Cp, J_{CP} = 18.5 Hz); 83.8 (br s, CH NBD); 75.8 (d, subst. Cp, J_{CP} = 6.8 Hz); 72.2 (s, subst. Cp); 72.0 (s, CH NBD); 71.0 (s, Cp); 70.0 (br s, CH NBD); 68.9 (d, subst. Cp, J_{CP} = 5.7 Hz); 67.8 (d, CH_2 NBD, $J_{C\text{-}Rh}$ = 4.4 Hz); 64.7 (d, quat Cp, J_{CP} = 55.2 Hz); 54.8 (s, S-C(CH_3)); 31.0 (s, S-C(CH_3)); 29.1 (d, CH_2Fc, J_{CP} = 5.3 Hz. ^{31}P NMR (202 MHz, $CDCl_3$): δ 26.1 (d, $J_{P–Rh}$ = 158 Hz). MS (ESI) m/z: 667.081 ($M - BF_4^-$, 100%).

III.2.3 General procedure for the synthesis of [Rh(P,SR)(COD)Cl], II.3-R.

In a Schlenk tube, under nitrogen, ligand (P,SBu^t) (0.797 mmol) was dissolved in dichloromethane (5 mL) and $[Rh(COD)Cl]_2$ (196 mg, 0.397 mmol) was added. The solution was stirred for 4 h at room temperature and 15 mL of pentane was then added to form a yellow precipitate. The precipitate was filtered under nitrogen and washed with pentane, to give [Rh(P,SR)(COD)Cl]. Only in the case of R = Bu^t, the product could be isolated in a pure state. Yield: 64%. R = Bu^t. ^1H NMR (500 MHz, CDCl3): δ 8.06 (m, 2H, Ph); 7.55–7.25 (m, 8H, Ph); 4.64 (br s, 1H, subst. Cp); 4.36 (br s, 1H, subst. Cp); 4.35–4.20 (m, 2H, 1 subst. Cp + 1 CH_2Fc); 4.09 (s, 5H, Cp); 3.91 (br d (AB), 1H,

CH_2Fc, J_{HH} = 12.9 Hz); 2.48 (m, 2H, CH_2 COD); 2.32 (m, 2H, CH_2 COD); 1.99 (m, 2H, CH_2 COD); 1.87 (m, 2H, CH_2 COD); 1.41 (s, 9H, Bu^t). ^{13}C HNMR (125 MHz, $CDCl_3$): δ 135.1 (d, Ph, J_{CP} = 11.9 Hz); 134.4 (d, quat Ph, J_{CP} = 43.6 Hz); 133.9 (d, Ph, J_{CP} = 10.5 Hz); 133.2 (d, quat Ph, J_{CP} = 43.4 Hz); 130.1 (d, Ph, J_{CP} = 1.7 Hz); 129.5 (Ph); 127.7 (d, Ph, J_{CP} = 10.0 Hz); 127.5 (d, Ph, J_{CP} = 9.6 Hz); 90.6 (d, quat Cp, J_{CP} = 14.1 Hz); 74.6 (d, subst. Cp, J_{CP} = 7.6 Hz); 74.3 (d, quat Cp, J_{CP} = 42.2 Hz); 71.3 (d, subst. Cp, J_{CP} = 6.9 Hz); 71.1 (s, Cp); 69.8 (d, subst. Cp, J_{CP} = 7.2 Hz); 43.0 (s, S-C(CH_3)); 31.9 (v. br s, CH_2 COD); 31.1 (s, S-C(CH_3)); 30.3 (v. br s, CH_2 COD), 28.6 (br s, CH_2Fc). ^{31}P NMR (202 MHz, $CDCl_3$): δ 21.0 (d, $J_{P–Rh}$ = 148 Hz). MS (ESI) m/z: 683.112 ($M - Cl^-$, 100%).

Essential spectroscopic parameters for the other compounds: R = Ph: δ 28.0 (d, $J_{P–Rh}$ = 166 Hz). R = Bz: δ 31.1 (d, $J_{P–Rh}$ = 170 Hz). R = Et: δ 22.8 (d, $J_{P–Rh}$ = 144 Hz).

III.2.4 General procedure for the synthesis of [Rh(P,SR)(COD)]BF_4, II.4-R.

In a Schlenk tube, under nitrogen, ligand (P,SR) (0.305 mmol) was dissolved in dichloromethane (5 mL) and [Rh(COD)$_2$]BF_4 (124 mg, 0.305 mmol) was added. The solution was stirred for 30 min at room temperature and 15 mL of pentane was then added to yield a yellow precipitate. The precipitate was filtered under argon and washed with pentane to give [Rh(P,SR)(COD)]BF_4.

[Rh(P,SBu^t)(COD)]BF_4 (**II.4-Bu^t**, yield 99%). ^1H NMR (500 MHz, $CDCl_3$): δ 7.60–7.35 (m, 10H, Ph); 5.78 (br s, 2H, CH COD); 4.78 (br s, 1H, subst. Cp); 4.64 (s, 5H, Cp); 4.48 (br s, 1H, subst. Cp); 4.12 (br s, 1H, subst. Cp); 4.00–3.95 (m, 2H, 1H CH COD + 1H CH_2Fc); 3.85 (br s, 1H, CH COD); 2.87 (m, 1H, CH_2 COD); 2.71 (m, 1H, CH_2 COD); 2.69 (d (AB), 1H, CH_2Fc, J_{HH} = 12.2 Hz); 2.59 (m, 1H, CH_2 COD); 2.49 (m, 1H, CH_2 COD); 2.39 (m, 1H, CH_2 COD); 2.30 (m, 1H, CH_2 COD); 2.07 (m, 1H, CH_2 COD); 1.96 (m, 1H, CH_2 COD); 1.37 (s, 9H, Bu^t). $^{13}C\{^1H\}$ NMR (125 MHz, $CDCl_3$): δ 133.9 (d, Ph, J_{CP} = 12.7 Hz); 132.3 (d, Ph, J_{CP} = 2.0 Hz); 132.1 (d, Ph, J_{CP} = 9.0 Hz); 131.6 (d, Ph, J_{CP} = 2.2 Hz); 130.0 (d, ipso Ph, J_{CP} = 44.4 Hz); 129.5 (d, Ph, J_{CP} = 10.4 Hz); 128.8 (d, Ph, J_{CP} = 10.0 Hz); 125.9 (d, ipso Ph, J_{CP} = 50.6 Hz); 104.4 (dd, CH COD, J_{CP} = 9.7 Hz, J_{CRh} = 7.1 Hz); 102.1 (dd, CH COD, J_{CP} = 9.4 Hz, J_{CRh} = 6.1 Hz); 85.5 (d, ipso Cp, J_{CP} = 17.7 Hz); 82.1 (d, CH COD, J_{CRh} = 11.3 Hz); 81.3 (d, CH COD, J_{CRh} = 12.6 Hz); 76.1 (d, subst. Cp, J_{CP} = 6.7 Hz); 73.1 (s, subst. Cp); 71.0 (s, Cp); 69.2 (s, subst. Cp, J_{CP} = 5.7 Hz); 63.2 (d, ipso Cp, J_{CP} = 56.1 Hz); 55.7 (s, S-C(CH_3)); 35.7 (s, CH_2 COD); 31.5 (CH_3); 31.0 (s, CH_2 COD); 29.2 (s, CH_2Fc); 28.7 (s, CH_2 COD); 27.0 (s, CH_2 COD). $^{31}P\{^1H\}$ NMR (202 MHz, $CDCl_3$): δ 23.8 (d, $J_{P–Rh}$ = 143 Hz). MS (ESI) m/z: 683.112 ($M - BF_4^-$, 100%).

[Rh(P,SPh)(COD)]BF_4 (**II.4-Ph**, yield: 80%). ^1H NMR (500 MHz, $CDCl_3$): δ 7.80–7.35 (m, 15H, Ph); 5.17 (m, 1H, CH COD); 4.72 (br s, 1H, subst. Cp); 4.70 (s, 5H, Cp), 4.49 (br s, 1H, subst. Cp); 4.29 (m, 1H, CH COD); 4.17 (d (AB), 1H, CH_2Fc, J_{HH} = 12.3 Hz); 4.12 (m, 1H, CH COD); 4.09

(br s, 1H, subst. Cp); 4.01 (m, 1H, CH COD); 3.04 (d (AB), 1H, CH_2Fc, J_{HH} = 12.3 Hz); 2.80 (m, 1H, CH_2 COD); 2.68 (m, 1H, CH_2 COD), 2.46 (m, 2H, CH_2 COD); 2.36 (m, 1H, CH_2 COD); 2.14 (m, 1H, CH_2 COD) 2.04 (m, 1H, CH_2 COD) 1.96 (m, 1H, CH_2 COD). $^{13}C\{^1H\}$ NMR (125 MHz, $CDCl_3$): δ 134.1 (d, Ph, J_{CP} = 12.7 Hz); 132.7 (Ph); 131.9 (d, Ph, J_{CP} = 9.4 Hz); 131.7 (Ph); 131.3 (Ph); 130.4 (Ph); 130.4 (d, ipso Ph, J_{CP} = 45.1 Hz); 129.9 (d, Ph, J_{CP} = 10.1 Hz); 125.9 (d, ipso Ph, J_{CP} = 49.5 Hz); 107.0 (br s, CH COD); 103.3 (dd, CH COD, J_{CP} = 9.0 Hz, J_{CRh} = 6.0 Hz); 86.2 (d, CH COD, J_{CRh} = 11.8 Hz); 84.8 (d, ipso Cp, J_{CRh} = 16.9 Hz); 84.1 (d, CH COD, J_{CRh} = 10.8 Hz); 75.9 (d, subst. Cp, J_{CP} = 6.2 Hz); 72.9 (br s, subst. Cp); 71.3 (br s, Cp); 69.1 (d, subst. Cp, J_{CP} = 5.8 Hz); 64.6 (d, ipso Cp, J_{CP} = 55.9 Hz); 37.9 (d, CH_2Fc, J_{CP} = 4.6 Hz); 34.4 (s, CH_2 COD); 30.3 (s, CH_2 COD); 30.0 (s, CH_2 COD); 27.1 (s, CH_2 COD). $^{31}P\{^1H\}$ NMR (202 MHz, $CDCl_3$): δ 22.1 (d, $J_{P–Rh}$ = 144 Hz). MS (ESI) m/z: 703.081 ($M - BF_4^-$, 100%).

[Rh(P,SBz)(COD)]BF_4 (**II.4-Bz**, yield 42%). ^1H NMR (500 MHz, CDCl3): δ 7.70 (m, 2H, Ph); 7.60–7.50 (m, 8H, Ph); 7.34 (m, 5H, Ph); 5.57 (m, 2H, CH COD); 4.54 (br s, 6H, Cp + 1H, subst. Cp); 4.42 (br s, 1H, subst. Cp); 4.19 (d (AB), 1H, CH_2Ph, J_{HH} = 13.8 Hz); 4.13 (br s, 1H, subst. Cp); 4.03 (d (AB), 1H, CH_2Ph, J_{HH} = 13.8 Hz); 3.97 (m, 2H, CH COD); 3.50 (d (AB), 1H, CH_2Fc, J_{HH} = 12.5 Hz); 2.92 (m, 1H, CH_2 COD), 2.76 (m, 1H, CH_2 COD); 2.67 (d (AB), 1H, CH_2Fc, J_{HH} = 12.5 Hz); 2.60 (m, 2H, CH_2 COD); 2.48 (m, 1H, CH_2 COD) 2.36 (m, 1H, CH_2 COD) 2.13 (m, 2H, CH_2 COD). $^{13}C\{^1H\}$ NMR (125 MHz, $CDCl_3$): δ 134.2 (d, Ph, J_{CP} = 12.9 Hz); 133.7 (quat Ph); 132.3 (d, Ph, J_{CP} = 9.8 Hz); 132.1 (d, Ph, J_{CP} = 2.3 Hz); 131.4 (d, Ph, J_{CP} = 2.3 Hz); 130.2 (d, quat Ph, J_{CP} = 46.2 Hz); 129.8 (d, Ph, J_{CP} = 10.5 Hz); 129.5 (Ph); 129.1 (Ph); 128.8 (d, Ph, J_{CP} = 10.11 Hz); 127.9 (d, Ph, J_{CP} = 10.4 Hz); 128.4 (Ph); 127.2 (d, quat Ph, J_{CP} = 49.6 Hz); 105.8 (dd, CH COD, J_{CP} = 9.6 Hz, J_{CRh} = 7.1 Hz); 102.7 (dd, CH COD, J_{CP} = 9.9 Hz, J_{CRh} = 6.5 Hz); 85.3 (d, CH COD, J_{CRh} = 10.9 Hz); 85.1 (d, CH COD, J_{CRh} = 11.6 Hz); 75.4 (br s, subst. Cp); 72.6 (br s, subst. Cp); 71.4 (br s, Cp); 69.2 (br s, subst. Cp); 42.6 (CH_2Ph); 34.2 (d, CH_2 COD, J_{CP} = 3.5 Hz); 31.5 (d, CH_2Fc, J_{CP} = 4.6 Hz); 31.0 (d, CH_2 COD, J_{CP} = 3.5 Hz); 29.7 (d, CH_2 COD, J_{CP} = 3.5 Hz); 27.6 (d, CH_2 COD, J_{CP} = 3.5 Hz). $^{31}P\{^1H\}$ NMR (202 MHz, $CDCl_3$): δ 21.8 (d, $J_{P–Rh}$ = 144 Hz).

[Rh(P,SEt)(COD)]BF_4 (**II.4-Et**, yield: 76%). ^1H NMR (500 MHz, $CDCl_3$): δ 7.77–7.62 (m, 2H, Ph); 7.61–7.35 (m, 8H, Ph); 5.43 (m, 1H, CH COD); 5.33 (m, 1H, CH COD); 4.74 (br s, 1H, subst. Cp); 4.65 (s, 5H, Cp); 4.48 (m, 1H, subst. Cp); 4.12 (br s, 1H, subst. Cp); 4.06–3.82 (m, 3H, 2H CH COD + 1H CH_2Fc); 2.99 (m, 1H, CH_2CH_3); 2.92–2.80 (m, 1H, CH_2 COD); 2.80–2.25 (m, 6H, 5H CH_2 COD + 1H CH_2CH_3); 2.70 (d (AB), 1H, CH_2Fc, J_{HH} = 12.6 Hz); 2.20–2.00 (m, 2H, CH_2 COD); 1.32 (t, 3H, CH_3, J_{HH} = 7.2 Hz). $^{13}C\{^1H\}$ NMR (125 MHz, $CDCl_3$): δ 134.2 (d, Ph, J_{CP} = 13.0 Hz); 132.3 (d, Ph, J_{CP} = 2.2 Hz); 132.0 (d, Ph, J_{CP} = 9.5 Hz); 131.5 (d, Ph, J_{CP} = 2.4 Hz); 130.2 (d, quat Ph, J_{CP} = 45.4 Hz); 129.6 (d, Ph, J_{CP} = 10.5 Hz); 128.8 (d, Ph, J_{CP} = 10.0 Hz); 129.1 (Ph); 126.5 (d, quat Ph, J_{CP} = 49.3 Hz); 104.7 (dd, CH COD, J_{CP} = 9.6 Hz, J_{CRh} = 7.3 Hz); 103.3 (dd, CH COD, J_{CP} = 10.0 Hz, J_{CRh} =

6.2 Hz); 85.8 (d, quat Cp, J_{CP} = 16.1 Hz); 84.9 (d, CH COD, J_{CRh} = 11.7 Hz); 83.9 (d, CH COD, J_{CRh} = 10.9 Hz); 75.7 (d, subst. Cp, J_{CP} = 5.9 Hz); 72.6 (s, subst. Cp); 71.2 (s, Cp); 69.0 (s, subst. Cp, J_{CP} = 5.4 Hz); 64.9 (d, quat Cp, J_{CP} = 55.6 Hz); 34.6 (d, CH_2 COD, J_{CP} = 3.5 Hz); 32.8 (CH_2CH_3); 30.9 (s, CH_2 COD); 30.3 (d, CH_2Fc, J_{CP} = 5.1 Hz); 29.5 (s, CH_2 COD); 27.3 (s, CH_2 COD); 15.0 (CH_3). $^{31}P\{^1H\}$ NMR (202 MHz, $CDCl_3$): δ 22.9 (d, $J_{P–Rh}$ = 144 Hz). MS (ESI) m/z: 655.081 ($M - BF_4^-$, 100%).

III.2.5 General procedure for the synthesis of $[Rh(P,Bu^t)(Solv)_2]^+$ (Solv = CD_3OD, CD_3CN, $CD_3C(O)CD_3$).

In NMR tube, under argon, complex **II.2-Bu^t** ($1.3 \cdot 10^{-2}$ mmol) was dissolved in required solvent (1.2 mL). The hydrogen was bubled to the solution of complex **II.2-Bu^t** for 2 min at ambient temperature under normal pressure. The hydrogen was replaced by argon and the NMR spectra of obtained solvate complex was recorded.

$[Rh(P,Bu^t)(CD_3CN)_2]^+$. ^1H NMR (500 MHz, CD_3CN): δ 7.70–7.66 (m, 2H, Ph); 7.54–7.48 (m, 4H, Ph); 7.41–7.45 (m, 4H, Ph); 4.62 (s, 5H, Cp + br s, 1H, subst. Cp); 4.38 (t, 1H, subst. Cp, J_{HH} = 5.0 Hz); 3.80 (dd (AB), 1H, CH_2Fc, J_{HH} = 10.0 Hz); 3.72 (m, 1H, subst. Cp); 2.94 (d (AB), 1H, CH_2Fc, J_{HH} = 10.0 Hz); 1.31 (s, 9H, Bu^t). $^{13}C\{^1H\}$ NMR (125 MHz, CD_3CN): δ 133.3 (d, quat Ph, J_{CP} = 62.9 Hz); 133.2 (d, Ph, J_{CP} = 11.3 Hz); 132.9 (d, Ph, J_{CP} = 12.6 Hz); 132.2 (d, Ph quat, J_{CP} = 56.6 Hz); 130.3 (d, Ph, J_{CP} = 2.5 Hz); 130.2 (d, Ph, J_{CP} = 2.5 Hz); 128.5 (d, Ph, J_{CP} = 10.1 Hz); 128.0 (d, Ph, J_{CP} = 10.1 Hz); 86.5 (quat Cp) 73.7 (d, subst. Cp, J_{CP} = 6.3 Hz); 72.3 (d, subst. Cp); 71.0 (s, Cp); 68.1 (d, subst. Cp, J_{CP} = 6.3 Hz); 69.5 (quat Cp); 69.0 (s, subst. Cp, J_{CP} = 5.4 Hz); 51.2 (s, $\underline{C}(CH_3)$); 29.6 (s, $C(\underline{CH_3})$); 27.9 (d, CH_2Fc, J_{CP} = 5.0 Hz); $^{31}P\{^1H\}$ NMR (202 MHz, CD_3CN): δ 34.3 (d, $J_{P–Rh}$ = 170 Hz).

Essential spectroscopic parameters for the other compounds: S = CD_3OD: δ 40.5 (d, $J_{P–Rh}$ = 202 Hz). S = $CD_3C(O)CD_3$: δ 39.9 (d, $J_{P–Rh}$ = 197 Hz).

III.3 Catalytic experiments

III.3.1 General procedure for the ketone asymmetric hydrogenation

A solution containing $6.4 \cdot 10^{-3}$ mmol of precatalyst, $3.2 \cdot 10^{-2}$ mmol of CH_3ONa (5 equiv.) and 3.2 mmol of substrate (500 equiv.) in 2 ml of isopropanol was transferred into a 5 ml glass vial which was then placed under argon into a stainless steel autoclave equipped with a magnetic stirring bar. The reaction vessel was pressurized with H_2 to 30 bars and stirred for the desired time at controlled temperature. The reaction was stopped by venting the H_2 atmosphere. The pure products were obtained by chromatography of the reaction mixture on silica gel using dichloromethane as eluent and analyzed by chiral GC for the determination of the conversion and enantiomeric excess. In a synthetic version

of this procedure, using [Ir(P,SBu^t)(COD)Cl] as precatalyst, the enantiomerically enriched product 1-phenylethanol was isolated in 96% yield (*ee* 61%).

III.3.2 Enantiomeric stability of 1-phenylethanol

A solution containing $6.4 \cdot 10^{-3}$ mmol of [Rh(P,SBu^t)(COD)Cl], $3.2 \cdot 10^{-2}$ mmol of CH_3ONa (5 equiv.) and 3.2 mmol of enantiomerically enriched 1-phenylethanol (500 equiv., *ee* 61%) in 2 ml of isopropanol was transferred into a 5 ml glass vial which was then placed under argon into a stainless steel autoclave equipped with a magnetic stirring bar. The reaction vessel was pressurized with H_2 to 30 bars and stirred for 2 h at room temperature. The reaction was stopped by venting the H_2 atmosphere. The pure product was obtained by chromatography of the reaction mixture on silica gel using dichloromethane as eluent and then analyzed by chiral GC. Yield 100%, *ee* 59%.

III.3.3 General Procedure for the imine asymmetric hydrogenation

A solution containing $6.4 \cdot 10^{-3}$ mmol of precatalyst, $1.9 \cdot 10^{-2}$ mmol of I_2 (3 equiv.) and 0.64 mmol of substrate (100 equiv.) in 2 ml of dichloromethane was transferred into a 5 ml glass vial which was then placed under argon into a stainless steel autoclave equipped with a magnetic stirring bar. The reaction vessel was pressurized with H_2 to 30 bars and stirred for the desired time at room temperature. The reaction was stopped by release of pressure. The pure products were obtained by chromatography of the reaction mixture on silica gel using dichloromethane as eluent and then analyzed by chiral GC.

III.3.4 General Procedure for the 3-methyl-2-cyclohexenone hydrogenation in THF

A solution containing $6.4 \cdot 10^{-3}$ mmol of precatalyst and 0.13 mmol of substrate (20 equiv.) in 2 ml of THF was transferred into a 5 ml glass vial which was then placed under argon into a stainless steel autoclave equipped with a magnetic stirring bar. The reaction vessel was pressurized with H_2 to 30 bars and stirred for the desired time at room temperature. The reaction was stopped by venting the H_2 atmosphere. The pure products were obtained by chromatography of the reaction mixture on silica gel using dichloromethane as eluent and analyzed by NMR and chiral GC for the determination of the conversion and enantiomeric excess.

III.3.5 General Procedure for the 1-phenyl-2-propene-1-ol hydrogenation in THF

A solution containing $6.4 \cdot 10^{-3}$ mmol of precatalyst and 0.13 mmol of substrate (20 equiv.) in 2 ml of THF was transferred into a 5 ml glass vial which was then placed under argon into a stainless steel autoclave equipped with a magnetic stirring bar. The reaction vessel was pressurized with H_2 to 30 bars and stirred for the desired time at room temperature. Then pressure was released and reaction vessel was stirred for the desired time at controlled temperature in argon or hydrogen atmosphere at 1

bar. The pure products were obtained by chromatography of the reaction mixture on silica gel using dichloromethane as eluent and then analyzed by NMR and chiral GC for the determination of the conversion and enantiomeric excess.

III.3.6 General Procedure for the 1-phenyl-2-propene-1-ol hydrogenation in Pr^{i}OH

A solution containing $6.4 \cdot 10^{-3}$ mmol of precatalyst, $3.2 \cdot 10^{-2}$ mmol of CH_3ONa (5 equiv.) and 0.64 mmol of substrate (100 equiv.) in 2 ml of isopropanol was transferred into a 5 ml glass vial which was then placed under argon into a stainless steel autoclave equipped with a magnetic stirring bar. The reaction vessel was pressurized with H_2 to 30 bars and stirred for the desired time at controlled temperature. The reaction was stopped by venting the H_2 atmosphere. The pure products were obtained by chromatography of the reaction mixture on silica gel using dichloromethane as eluent and analyzed by NMR and chiral GC for the determination of the conversion and enantiomeric excess.

III.3.7 General Procedure for the 1-phenyl-2-propene-1-ol allylic isomerisation in Pr^{i}OH

In a Schlenk tube under argon atmosphere solution containing $6.4 \cdot 10^{-3}$ mmol of precatalyst, $3.2 \cdot 10^{-2}$ mmol of CH_3ONa (5 equiv.) and 0.64 mmol of substrate (100 equiv.) in 2 ml of isopropanol was stirred for the desired time at reflux. The pure products were obtained by chromatography of the reaction mixture on silica gel using dichloromethane as eluent and analyzed by NMR and chiral GC for the determination of the conversion and enantiomeric excess.

III.4 NMR experiments with *para*hydrogen

III.4.1 General

NMR measurements were made using NMR tubes that were fitted with J. Young's valves and solutions were degassed on a high vacuum line prior to H_2 addition. The samples were prepared in a glovebox by addition of the specified deuterated solvents to the solid complex in the NMR tube. For the *p*-H_2 induced polarization (PHIP) experiments, hydrogen enriched in the para spin state was prepared by cooling H_2 to 36 K over the paramagnetic catalyst Fe_2O_3 which was doped on silica [168, 169, 184]. All the resulting NMR studies were then carried out with sample concentrations of approximately 4.6 mM and all spectra were recorded on a Bruker Avance III 400 NMR spectrometer. ^{1}H NMR chemical shifts are reported in ppm relative to the residual ^{1}H signal of the solvent which for CHD_2OD is δ3.31 and for $CDHCl_2$ is δ5.37.

III.4.2 Sample preparation

2.5 mg of either [Rh(P,SBu^t)(COD)Cl] (**II.3-Bu^t**) or [Rh (P,SBu^t)(COD)]$^+$BF$_4^-$ (**II.4-Bu^t**) were dissolved in 0.5 mL of d_4-methanol and 20 μL pyridine (75 fold) was added into the solution. The combine solution was taken up by syringe and transferred to a Young`s tap NMR tube. The sample in NMR tube was degassed on a high-vacuum line via three `cool`-pump-thaw cycles (the sample was cooled to -78°C rather than frozen in liquid N_2 to avoide cracking of the NMR tube upon thawing). *Para*hydrogen, at pressure of 3 atmospheres was then admitted to the NMR tube.

The sample was shaken (to replenish p-H_2 in solution) for approximately 10 seconds in the magnetic field about 65 G, and rapidly (within 5 seconds) inserted into the NMR spectrometer, after which spectra were immediately acquired.

III.4.3 Kinetics of hydride exchange

The ligand exchange studies were completed using the EXSY protocol [185]. A selected resonance was probed and the magnetisation flow was followed as a function of the reaction time between zero and 1 second, in steps typically of 0.1 seconds. The intensity data was then simulated using a differential model, based on least-mean squares fit to experiment, in order to extract the associated experimental site-exchange rate constants. In order to improve the data specificity and accuracy, the exchange process was followed in separate experiments from each site (where possible). Under these conditions the total error was minimized in the rate constant fitting process using the solver routine in excel. The jack-knife method [186] was then used to estimate the individual rate constant errors which are included as (1) where this signals +/- for the 95 % confidence limit.

III.5 General procedure of UV/Vis spectroscopic experiments

Hydrogen gas (99,9999% pure, water impurity <5 ppm) was produced by water electrolysis using H_2 generator (“NPP Chimelectronics”, Moscow). Outcoming pressure was kept at 1 atm. UV-visible spectra were recorded on Varian Cary 50 spectrometer equipped with stainless steel dip probe coupler (5 mm path length).

In four-necked round bottom flask, under argon, complex **II.4-Bu^t** ($5 \cdot 10^{-3}$ mmol) was dissolved in required solvent (5 mL). Then the dip probe coupler was placed into the flask. The hydrogen was bubbled using a glass capillary through the solution of complex **II.4-Bu^t** for the desired time at ambient temperature under normal pressure. The spectra were recorded every 1-5 min until the band of the starting material has not disappeared.

III.6 X-ray crystallography

A single crystal of each compound was mounted under inert perfluoropolyether on the tip of a cryoloop and cooled in the cryostream of either an Oxford-Diffraction XCALIBUR SAPPHIRE-I CCD diffractometer or an Agilent Technologies GEMINI EOS CCD diffractometer. Data were collected using the monochromatic Mo Kα radiation (λ = 0.71073). The structures were solved by direct methods (SIR97) [187] and refined by least-squares procedures on F^2 using SHELXL-97 [188]. All H atoms attached to carbon were introduced in idealised positions and treated as riding on their parent atoms in the calculations. The drawing of the molecules was realized with the help of ORTEP3 [189]. Crystallographic data (excluding structure factors) have been deposited with the Cambridge Crystallographic Data Centre - CCDC 872062 for **II.2-Bu^t**, CCDC 872063 for **II.4-Bz**, CCDC 872064 for **II.4-Ph**.

III.7 Computational details

III.7.1 Geometry optimisation for II.1-R, II.2-R, II.3-R and II.4-R complexes

Calculations were performed with the Gaussian 09 package [190] using the B3LYP hybrid functional [191] under the DFT approach, since it performs better in frequency calculations. All carbon and hydrogen atoms were described with the 6-31G(d,p) basis set, whereas the 6-31++G(d,p) basis set was applied to the P, S, B, F and Cl atoms. Effective core potentials (ECP) and its associated SDD basis set [192-195] supplemented with f-polarization functions (SDD(f)) [196] were applied for the Rh, Ir and Fe atoms. Geometry optimizations were performed for the neutral NBD and COD complexes **II.1-R** and **II.3-R** with R = Ph and Bu^t without any ligand simplification. Calculations were also carried out on the isolated cation of **II.3-Ph** and on the iridium analogue [Ir(P,SBu^t)(COD)Cl]. No scaling factors were applied to the calculated low-frequency vibrations. Since the inclusion of anharmonicity effects in the case of **II.3-Bu^t** did not lead to any significant change in the Rh–Cl frequency values (Table III.2), this method was not applied to the other calculations.

III.7.2 DFT study of [Rh(P,SBu^t)(COD)]X complexes activation

Calculations were performed with the Gaussian09 package [190] using the B3LYP [191] and M06 [198] functionals under the DFT approach. All carbon and hydrogen atoms were described with the 6-31G(d,p) basis set, whereas the 6-31++G(d,p) basis set was applied to the atoms of ligands involved in the bonding with Rh (P, S atoms, hydride ligands, OH group of methanol and N atoms of pyridine and acetonitrile). Effective core potentials (ECP) and its associated SDD basis set [192-195] supplemented with f-polarization functions (SDD(f)) [197] were applied for the Rh and Fe atoms.

Geometry optimizations were performed without any ligand simplification for the cationic $[Rh(P,SBu^t)L_2]^+$ and $[Rh(H)_2(P,SBu^t)L_2]^+$ complexes (L = pyridine, CH_3OH, CH_3CN).

Frequency calculations were performed for all optimized complexes in the gas phase and reported without use of scaling factors. The nature of all the stationary points on the potential energy surfaces was confirmed by a vibrational analysis [198]. Transition state (TS) structures showed only one negative eigenvalue in their diagonalized force constant matrices, and their associated eigenvectors were confirmed to correspond to the motion along the reaction coordinate under consideration using the Intrinsic Reaction Coordinate (IRC) method [199].

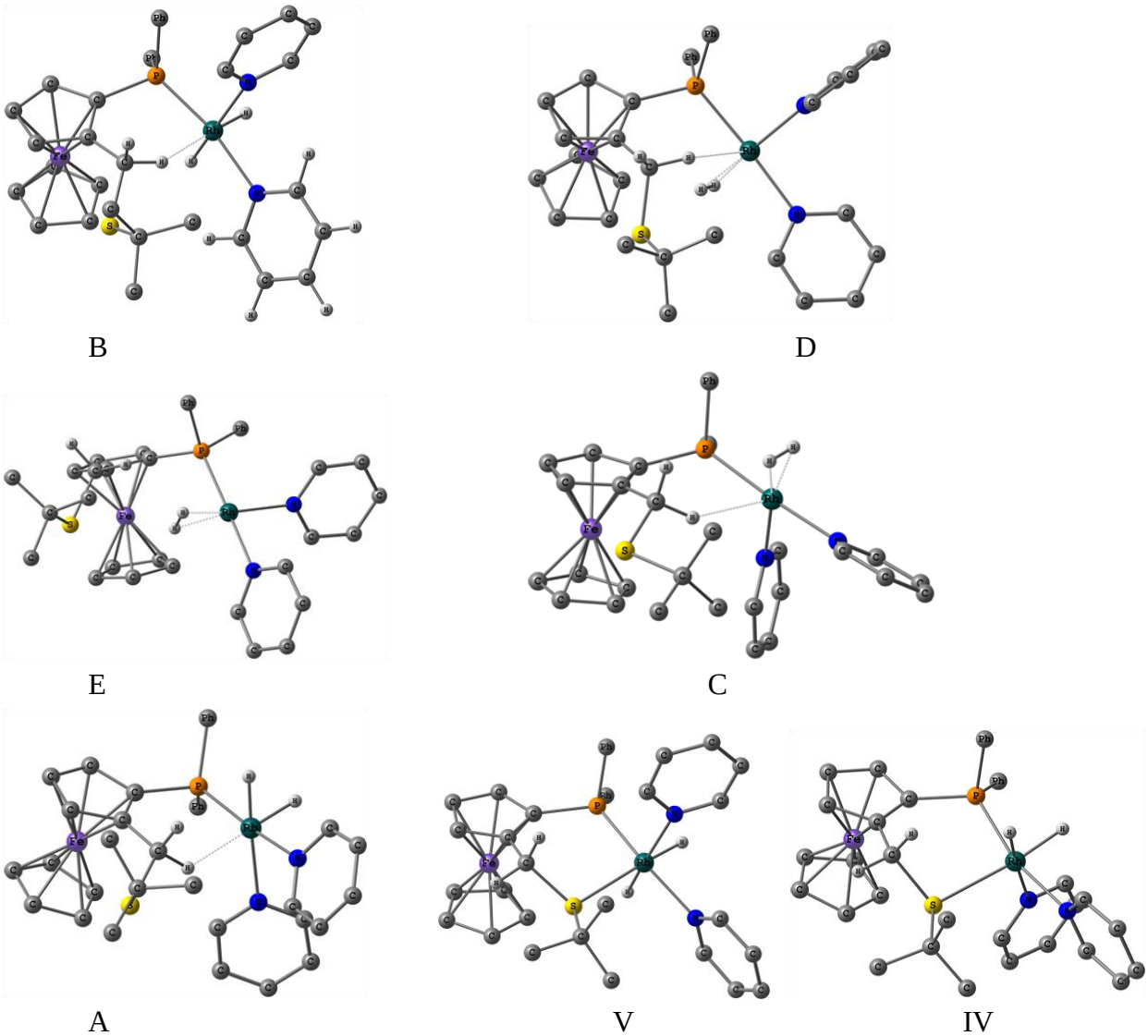

Fig. III.1 M06 optimized geometries of selected complexes. Ph ligands, hydrogen atoms of aromatics and Bu^t group are omitted for clarity.

Table III.1 Crystal data and structure refinement parameters for **II.2-Bu^t**, **II.4-Bz** and **II.4-Ph**.

	II.2-Bu^t	**II.4-Ph**	**II.4-Bz**
Empirical formula	$C_{34}H_{37}FePRhS, BF_4$	$C_{37}H_{37}FePRhS, BF_4, CH_2Cl_2$	$C_{38}H_{39}FePRhS, BF_4, CH_2Cl_2$
Formula weight	754.24	875.19	889.22
Temperature, K	180(2)	180(2)	180(2)
Wavelength, Å	0.71073	0.71073	0.71073
Crystal system	Orthorhombic	Orthorhombic	Triclinic
Space group	$P2_12_12_1$	$Pca2_1$	Pī
a, Å	10.663	26.321(5)	11.5390(8)
b, Å	16.983	9.652(5)	12.8367(8)
c, Å	17.435	14.209(5)	13.5655(8)
α, °	90	90	108.445(6)
β, °	90	90	101.880(5)
γ, °	90	90	98.703(5)
Volume, Å^3	3157.3	3610(2)	1813.9(2)
Z	4	4	2
Density (calc), Mg m^{-3}	1.587	1.610	1.628
Abs. coefficient, mm^{-1}	1.146	1.158	1.154
F(000)	1536	1776	904
Crystal size, mm^3	0.54 × 0.47 × 0.18	0.56 × 0.22 × 0.07	0.43 × 0.22 × 0.16
Theta range, °	3.02 to 27.10	2.98 to 26.36	3.12 to 26.37
Reflections collected	12 237	19 753	14 216
Indpt reflections (R_{int})	6118 (0.0344)	7239 (0.0342)	7393 (0.0506)
Completeness, %	98.5	99.8	99.8
Absorption correction	Multi-scan	Multi-scan	Multi-scan
Max. and min. transm.	1.0 and 0.619	1.0 and 0.7726	1.0 and 0.77764
Refinement method	F^2	F^2	F^2
Data/restr./param.	6118/24/388	7250/1/442	7408/24/478
Goodness-of-fit on F^2	1.094	1.037	1.039
R_1, wR_2 [I > 2σ(*I*)]	0.0381, 0.0926	0.0340, 0.0833	0.0453, 0.1227
R_1, wR_2 (all data)	0.0461, 0.0954	0.0399, 0.0857	0.0555, 0.1297
Flack's parameter	0.08(3)	−0.005(18)	
Residual density, e Å^{-3}	0.959 and −1.030	0.752 and −0.587	0.868 and −1.678

Table III.2 Anharmonicity correction on selected low frequency modes for compound **II.3-Bu^t**.

Mode #	ν(harm)	ν(anharm)	Intencity	Δν(harm-anharm)	
38	296	275	5	21	
37	288	241	0	47	
36	**275**	**273**	**18**	**1**	**(Rh-Cl stretching mode)**
35	270	204	0	66	
34	257	243	5	14	
33	257	245	2	11	
32	253	239	4	13	
31	248	236	3	12	
30	239	223	2	16	

[a]Anharmonicity was taken into account only for a few low frequency modes between 300 and 230 cm^{-1}. For the most intense mode, #36, which corresponds to the Rh-Cl stretch, there is a negligible difference. All other low intensive modes possess a significant contribution of bending modes of the C-H bonds of the Bu^t and COD groups. The CH vibrations are usually very sensitive to anharmonic corrections.

IV Conclusions and perspectives

The present thesis was motivated by the remarkable efficiency of the [Ir(P,SR)(COD)Cl] precatalysts, containing the ferrocene phosphine thioether ligands of type CpFe[η^5-1,2-$C_5H_3(CH_2SR)(PPh_2)$] developed in our laboratory, for the enantioselective ketone hydrogenation at relatively low temperature and H_2 pressure and in the presence of strong bases. Based on previous literature knowledge, it was presumed that the active form of the catalyst would consist of some type of solvated species, but all reported literature studies have addressed this type of catalytic system (mostly for Rh and very little for Ir) under the conditions in which they catalyze the hydrogenation of functionalized alkenes, which do not require the use of a strong base. From the few available literature reports, solvated Ir species appear less stable and therefore less amenable to spectroscopic and mechanistic investigations than those of Rh. Therefore, the objective of this thesis was to (1) prepare analogous Rh complexes with the (P,SR) ligands available in the laboratory; (2) evaluate their catalytic performance in the ketone hydrogenation and in other reactions; and (3) investigate the pre-catalyst activation process.

The first two objectives have been completely achieved. Complexes [Rh(P,SR)(diene)X] have been prepared for R = Et, Bu^t, Ph and Bz not only for diene = COD and X = Cl but also for all combinations of diene = COD, NBD and X = Cl, BF_4. The structure of these complexes has been investigated in the solid state and in solution on the basis of single crystal diffraction, IR and NMR spectroscopies, and the experimental results have been completed by DFT calculations, to establish that the complexes have similarities and a few minor differences relative to the [Ir(P,SR)(COD)Cl] complexes, allowing them to be considered structural models of the Ir pre-catalysts.

The application of these precatalysts to the hydrogenation of acetophenone under the same conditions previously optimized for the Ir systems have revealed that they are also functional models of the Ir catalysts, although they produce the 1-phenylethanol hydrogenation product with lower activities and lower enantioselectivities. The new Rh complexes have also been tested as catalysts for the hydrogenation of other ketones (methyl *p*-fluorophenyl ketone, *tert*-butyl phenyl ketone, methyl cyclohexyl ketone), an imine (*N*-phenyl-*N*-(1-phenylethylidene)amine), quinaldine, and an α,β-unsaturated ketone (3-methyl-2-cyclohexenone), and for the isomerization of a representative allylic alcohols (1-phenyl-2-propene-1-ol). The performance found for all the hydrogenation processes was not outstanding. However, one interesting result was the observation of a selective hydrogenation of 3-methyl-2-cyclohexenone at the C=C bond (at low catalyst loadings) whereas the product of total hydrogenation is obtained at higher catalyst loadings. The isomerization of 1-phenyl-2-propene-1-ol was haunted by the need to use H_2 to activate the precatalyst, therefore contaminating the process by the follow-up hydrogenation of the isomerized product ethyl phenyl ketone to 1-phenyl-1-propanol.

However, excellent selectivities in the desired isomerization product could be obtained by activating the precatalyst for a short time with H_2 and then conducting the catalytic process under Ar, and even better in the absence of any pre-activation by H_2, even though this reaction required higher temperatures. Interstingly, the Rh systems are more active catalysts than the Ir analogs for this reaction.

The spectroscopic investigations have only been carried out so far in the absence of base, therefore they only probe the initial stage of the precatalyst activation. The results that have been obtained on the (P,SBu^t) complexes demonstrate that these are activated in the same way as the previously investigated diphosphine analogues, leading to solvated complexes of type $[Rh(P,SBu^t)(Solv)_2]^+$ in MeOH, acetone or MeCN. The subsequent H_2 oxidative addition to generate solvated Rh^{III} dihydride species is thermodynamically unfavourable at room temperature but can be observed at lower temperatures. The formation of the solvated Rh^I complexes appears to proceed via one (or more) intermediate(s) which may correspond to complex $[Rh(P,SBu^t)(1\text{-}\kappa\text{-}4,5\text{-}\eta\text{-}C_8H_{13})]$ (from the COD precursor) as suggested by the low-temperature NMR study.

The kinetic experiments carried out so far and presented in this manuscript are only preliminary and require further work in order to better elucidate this mechanism. For instance, a global spectra analysis will be required to verify the presence of two (or more) steps and the experiment should be repeated at different pyridine concentration, in the presence of other bases, and the rate constants derived for the two (or more) steps should be compared with those obtained in pure MeOH. In addition, further experiments are required to discover the origin of the puzzling induction time observed (reproducibly) for the hydrogenation in pure MeOH. Future efforts need to be dedicated especially to the spectroscopic investigation of the catalyst activation process in the presence of a strong base, in order to identify spectroscopically and hopefully even isolate in the solid state the product(s) that is(are) formed. It would also be interested to repeat these investigations for the Ir precatalysts, even though the activated Ir species may be even more elusive and difficult to identify than the Rh species studied in the present thesis. The key point that merits attention is the full understing of the role of the strong base in this catalytic mechanism. Indeed, while the strong base is not at all necessary for the catalyzed hydrogenation of olefins, it is absolutely essential for the catalyzed hydrogenation of polar substrates. Therefore, the nature of the catalytically active species and the mechanism of the ketone hydrogenation process is probably quite different than that proposed and widely accepted for the hydrogenation of the olefins. Naturally, these additional experimental mechanistic investigations should be accompanied by a thorough computational study of the catalytic cycle, which is indeed already ongoing in collaboration with Prof. Agustí Lledós of the Universitat Autónoma Barcelona.

References

1. Osborn, J. A. The preparation and properties of tris(triphenylphosphine)halogeno rhodium(I) and some reactions thereof including catalytic homogeneous hydrogenation of olefins and acetylenes and their derivatives / J. A. Osborn, F. H. Jardine, J. F. Young, G. Wilkinson // J. Chem. Soc. A. – 1966. – P. 1711-1732.

2. Crabtree, R. H. Cationic iridium diolefin complexes as alkene hydrogenation catalysts and the isolation of some related hydrido complexes / R. H. Crabtree, H. Felkin, G. E. Morris // J. Organomet. Chem. – 1977. – V. 141. – P. 205-215.

3. Lu, S.-M. Asymmetric Hydrogenation of Quinolines Catalyzed by Iridium with Chiral Ferrocenyloxazoline Derived N,P Ligands / S.-M. Lu, X.-W. Han, Y.-G. Zhou // Adv. Synth. & Catal. – 2004. – V. 346. – P. 909-912.

4. Zhu, S.-F. Well-Defined Chiral Spiro Iridium/Phosphine−Oxazoline Cationic Complexes for Highly Enantioselective Hydrogenation of Imines at Ambient Pressure / S.-F. Zhu, J.-B. Xie, Y.-Z. Zhang, S. Li, Q.-L. Zhou // J. Am. Chem. Soc. – 2006. – V. 128. – P. 12886-12891.

5. Imamoto, T. Enantioselective Hydrogenation of Acyclic Aromatic N-Aryl Imines Catalyzed by an Iridium Complex of (S,S)-1,2-Bis(tert-butylmethylphosphino)ethane / T. Imamoto, N. Iwadate, K. Yoshida // Org. Lett. – 2006. – V. 8. – P. 2289-2292.

6. Hou, G. Enantioselective Hydrogenation of N−H Imines / G. Hou, F. Gosselin, W. Li, C. McWilliams, Y. Sun, M. Weisel, P. D. O'Shea, C.-y. Chen, I. W. Davies, X. Zhang // J. Am. Chem. Soc. – 2009. – V. 131. – P. 9882-9883.

7. Tang, W. J. Highly Enantioselective Hydrogenation of Quinoline and Pyridine Derivatives with Iridium-(P-Phos) Catalyst / W. J. Tang, J. Tan, L. J. Xu, K. H. Lam, Q. H. Fan, A. S. C. Chan // Adv. Synth. Catal. – 2010. – V. 352. – P. 1055-1062.

8. Tang, W. Highly efficient and enantioselective hydrogenation of quinolines and pyridines with Ir-Difluorphos catalyst / W. Tang, Y. Sun, L. Xu, T. Wang, Q. Fan, K.-H. Lam, A. S. C. Chan // Organic & Biomolecular Chemistry. – 2010. – V. 8. – P. 3464-3471.

9. Cartigny, D. Iridium-Difluorphos-Catalyzed Asymmetric Hydrogenation of 2-Alkyl- and 2-Aryl-Substituted Quinoxalines: A General and Efficient Route into Tetrahydroquinoxalines / D. Cartigny, T. Nagano, T. Ayad, J.-P. Genet, T. Ohshima, K. Mashima, V. Ratovelomanana-Vidal // Adv. Synth. Catal. – 2010. – V. 352. – P. 1886-1891.

10. Dota, R. Chiral Xyliphos Complexes for the Catalytic Imine Hydrogenation Leading to the Metolachlor Herbicide: Isolation of Catalyst–Substrate Adducts / R. Dorta, D. Broggini, R. Stoop, H. Ruegger, F. Spindler, A. Togni // Chem. Eur. J. – 2004. – V. 10. – P. 267-278.

11. Blaser, H.-U. The Chiral Switch of (S)-Metolachlor: A Personal Account of an Industrial Odyssey in Asymmetric Catalysis / H.-U. Blaser // Adv. Synth. Catal. – 2002. – V. 344. – P. 17-31.

12. Sawamura, M. Gold(I)-Catalyzed Asymmetric Aldol Reaction of N-Methoxy-N-methyl-.alpha.-isocyanoacetamide (.alpha.-Isocyano Weinreb Amide). An Efficient Synthesis of Optically Active .beta.-Hydroxy .alpha.-Amino Aldehydes and Ketones / M. Sawamura, Y. Nakayama, T. Kato, Y. Ito // J. Org. Chem. – 1995. – V. 60. – P. 1727-1732.

13. Sawamura, M. An Enantioselective Two-Component Catalyst System: Rh−Pd-Catalyzed Allylic Alkylation of Activated Nitriles / M. Sawamura, M. Sudoh, Y. Ito // J. Am. Chem. Soc. – 1996. – V. 118. – P. 3309-3310.

14. Kuwano, R. Asymmetric aldol reaction of 2-cyanopropionates catalysed by *trans*-chelating chiral diphosphine ligand TRAP–rhodium(I) complex / R. Kuwano, H. Miyazaki, Y. Ito // Chem. Commun. – 1998. – P. 71-72.

15. Kuwano, R. Synthesis of a trans-chelating chiral diphosphine ligand with only planar chirality and its application to asymmetric hydrosilylation of ketones / R. Kuwano, T. Uemura, M. Saitoh, Y. Ito // Tetrahedron Lett. – 1999. – V. 40. – P. 1327-1330.

16. Kuwano, R. Catalytic Asymmetric Hydrogenation of Heteroaromatic Compounds, Indoles / R. Kuwano, K. Sato, T. Kurokawa, D. Karube, Y. Ito // J. Am. Chem. Soc. – 2000. – V. 122. – P. 7614-7615.

17. Ireland, T. Ferrocenyl ligands with two phosphanyl substituents in the alpha,epsilon positions for the transition metal catalyzed asymmetric hydrogenation of functionalized double bonds / T. Ireland, G. Grossheimann, C. Wieser-Jeunesse, P. Knochel // Angew. Chem. Int. Ed. – 1999. – V. 38. – P. 3212-3215.

18. Lotz, M. New ferrocenyl Ligands with broad applications in asymmetric catalysis / M. Lotz, K. Polborn, P. Knochel // Angew. Chem., Int. Ed. Engl. – 2002. – V. 41. – P. 4708-4711.

19. Spindler, F. Modular chiral ligands: the profiling of the Mandyphos and Taniaphos ligand families / F. Spindler, C. Malan, M. Lotz, M. Kesselgruber, U. Pittelkow, A. Rivas-Nass, O. Briel, H. U. Blaser // Tetrahedron: Asymmetry. – 2004. – V. 15. – P. 2299-2306.

20. Sturm, T. A novel class of ferrocenyl-aryl-based diphosphine ligands for Rh- and Ru-catalysed enantioselective hydrogenation // T. Sturm, W. Weissensteiner, F. Spindler // Adv. Synth. Catal. – 2003. – V. 345. – P. 160-164.

21. Richards, C. J. Synthesis of phosphinoferrocenyloxazolines. New ligands for asymmetric catalysis / C. J. Richards, A. W. Mulvaney // Tetrahedron: Asymmetry. – 1996. – V. 7. – P. 1419-1430.

22. Nishibashi, Y. Synthesis and structure of novel chiral oxazolinylferrocenes and oxazolinylferrocenylphosphines, and their rhodium(I)-complexes / Y. Nishibashi, K. Segawa, Y. Arikawa, K. ohe, M. Hidai, S. Uemura // J. Organomet. Chem. – 1997. – V. 546. – P. 381-398.

23. Geisler, F. M. Chiral Phosphinooxazolines with a Pentamethylferrocene Backbone: Synthesis and Use as Ligands in Asymmetric Catalysis / F. M. Geisler, G. Helmchen // J. Org. Chem. – 2006. – V. 71. – P. 2486-2492.

24. Sutcliffe, O. B. Planar chiral 2-ferrocenyloxazolines and 1,1′-bis(oxazolinyl)ferrocenes - syntheses and applications in asymmetric catalysis / O. B. Sutcliffe, M. R. Bryce // Tetrahedron: Asymmetry. – 2003. – V. 14. – P. 2297-2325.

25. Malacea, R. Coordination Chemistry and Diphenylacetylene Hydrogenation Catalysis of Planar Chiral Ferrocenylphosphane-Thiether Ligands with Cyclooctadieneiridium(I) / R. Malacea, E. Manoury, L. Routaboul, J.-C. Daran, R. Poli, J. P. Dunne, A. C. Withwood, C. Godard, S. B. Duckett // Eur. J. Inorg. Chem. – 2006. – P. 1803–1816.

26. Malacea, R. Parahydrogen studies of H_2 addition to Ir(I) complexes, containing chiral phosphine-thioether ligands: implication for catalysis / R. Malacea, J.-C. Daran, S. B. Duckett, J. P. Dunne, C. Godard, E. Manoury, R. Poli, A. C. Whitwood // Dalton Trans. – 2006. – P. 3350-3359.

27. Malacea, R. Palladium and platinum complexes with planar chiral 1,2-disubstituted ferrocenes containing phosphine and thioether donor groups / R. Malacea, L. Routaboul, E. Manoury, J.-C. Daran, R. Poli // J. Organomet. Chem. – 2008. – V. 693. – P. 1469-1477.

28. Malacea, R. Synthesis, characterization and crystal structures of two new platinum complexes with planar chiral 1, 2-disubstituted ferrocenes containing phosphine and thioether donor groups / R. Malacea, L. Routaboul, E. Manoury, J.-C. Daran, R. Poli // J. Mol. Struct. – 2008. – V. 890. – P 249-254.

29. Routaboul, L. New ferrocenyl P,S and S,S ligands for asymmetric catalysis / L. Routaboul, S. Vincendeau, J.-C. Daran, E. Manoury // Tetrahedron: Asymmetry. – 2005. – V. 16. – P. 2685-2690.

30. Routaboul, L. New Phosphorus Dendrimers with Chiral Ferrocenyl Phosphine-Thioether Ligands on the Periphery for Asymmetric Catalysis / L. Routaboul, S. Vincendeau, C.-O. Turrin, A.-M. Caminade, J.-P. Majoral, J.-C. Daran, E. Manoury // J. Organomet. Chem. – 2007. – V. 692. – P. 1064-1073.

31. Diab, L. Higly regioselective Palladium-catalyzed methoxycarbonylation of styrene using chiral ferrocene- and biphosphole-based ligands / L. Diab, M. Gouygou, E. Manoury, P. Kalck, M. Urrutigoïty // Tetrahedron Lett. – 2008. – V. 49. – P. 5186-5189.

32. Le Roux, E. Highly Efficient Asymmetric Hydrogenation of Alkyl Aryl Ketones Catalyzed by Iridium Complexes with Chiral Planar Ferrocenyl Phosphino-Thioether Ligands / E. Le Roux, R.

Malacea, E. Manoury, R. Poli, L. Gonsalvi, M. Peruzzini // Adv. Synth. & Catal. – 2007. – V. 349. – P. 309-313.

33. Poyatos, M. Complexes with Poly(N-heterocyclic carbene) Ligands: Structural Features and Catalytic Applications / M. Poyatos, J. A. Mata, E. Peris // Chem. Rev. – 2009. – V. 8. – P. 3677-3707.

34. Diez-Gonzalez, S. N-Heterocyclic Carbenes in Late Transition Metal Catalysis / S. Diez-Gonzalez, N. Marion, S. P. Nolan // Chem. Rev. – 2009. – V. 8. – P. 3612-3676.

35. Mata, J. A. Reactivity Differences in the Syntheses of Chelating N-Heterocyclic Carbene Complexes of Rhodium Are Ascribed to Ligand Anisotropy / J. A. Mata, A. R. Chianese, J. R. Miecznikowski, M. Poyatos, E. Peris, J. W. Faller, R. H. Crabtree // Organometallics. – 2004. – V. 23. – P. 1253-1263.

36. Riederer, S. K. U. Impact of Ligand Modification on Structures and Catalytic Activities of Chelating Bis-Carbene Rhodium(I) Complexes / S. K. U. Riederer, P. Gigler, M. P. Hogerl, E. Herdtweck, B. Bechlars, W. A. Herrmann, F. E. Kuhn // Organometallics. – 2010. – V. 29. – P. 5681-5692.

37. Neveling, A. Thione complexes of Rh(I): a first comparison with the bonding and catalytic activity of related carbene and imine compounds / A. Neveling, G. R. Julius, S. Cronje, C. Esterhuysen, H. G. Raubenheimer // Dalton Trans. – 2005. – P. 181-192.

38. Viciano, M. An N-Heterocyclic Carbene/Iridium Hydride Complex from the Oxidative Addition of a Ferrocenyl–Bisimidazolium Salt: Implications for Synthesis / M. Viciano, E. Mas-Marza, M. Poyatos, M. Sanau, R. H. Crabtree, E. Peris // Angew. Chem. Int. Ed. – 2005. – V. 44. – P. 444-447.

39. Gonell, S. Y-Shaped Tris-N-Heterocyclic-Carbene Ligand for the Preparation of Multifunctional Catalysts of Iridium, Rhodium, and Palladium / S. Gonell, M. Poyatos, J. A. Mata, E. Peris // Organometallics. – 2012. – V. 31. – P. 5606-5614.

40. Peng, H. M. Quinoline-Tethered N-Heterocyclic Carbene Complexes of Rhodium and Iridium: Synthesis, Catalysis, and Electrochemical Properties / H. M. Peng, R. D. Webster, X. Li // Organometallics. – 2008. – V. 27. – P. 4484-4493.

41. Sinha, A. M ultifaceted Coordination of Naphthyridine-Functionalized N-Heterocyclic Carbene: A Novel "Ir^{III}(C^N)(C^C)" Compound and Its Evaluation as Transfer Hydrogenation Catalyst / A. Sinha, S. M. Rahaman, M. Sarkar, B. Saha, P. Daw, J. K. Bera // Inorg. Chem. – 2009. – V. 48. – P. 11114-11122.

42. Gierz, V. 1,10-Phenanthroline Analogue Pyridazine-Based N-Heterocyclic Carbene Ligands / V. Gierz, C. Maichle-Mossmer, D. Kunz // Organometallics. – 2012. – V. 31. – P. 739-747.

43. Gierz, V. Rhodium Complexes Bearing 1,10-Phenanthroline Analogue Bis-NHC Ligands Are Active Catalysts for Transfer Hydrogenation of Ketones / V. Gierz, A. Urbanaite, A. Seyboldt, D. Kunz // Organometallics. – 2012. – V. 31. – P. 7532-7538.

44. Dyson, G. Synthesis and Structural Variation of Iron, Rhodium, Palladium, and Silver Complexes of Chiral N-Heterocyclic Carbene-Phenoxyimine Hybrid Ligand / Dyson, J.-C. Frison, S. Simonovic, A. C. Whitwood, R. E. Douthwaite // Organometallics. – 2008. – V. 27. – P. 281-288.

45. Baker, M. V. Synthesis and structure of N-heterocyclic carbene complexes of rhodium and iridium derived from an imidazolium-linked cyclophane / M. V. Baker, S. K. Brayshaw, B. W. Skelton, A. H. White, C. C. Williams // J. Organomet. Chem. – 2005. – V. 690. – P. 2312-2322.

46. Jeletic, M. S. Mono- and Bimetallic Rhodium(I) Complexes Supported by New C_2-Symmetric Bis-N-heterocyclic Carbene Ligands: Metalation via C=C Bond Cleavage under Mild Conditions / M. S. Jeletic, I. Ghiviriga, K. A. Abboud, A. S. Veige // Organometallics. – 2007. – V. 26. – P. 5267-5270.

47. Lowry, R. J. New Constrained-Geometry C_2-Symmetric Di-N-heterocyclic Carbene Ligands and Their Mono- and Dinuclear Rhodium(I) Complexes: Design, Synthesis, and Structural Analysis / R. J. Lowry, M. K. Veige, O. Clement, K. A. Abboud, I. Ghiviriga, A. S. Veige // Organometallics. – 2008. – V. 27. – P. 5184-5195.

48. Jeletic, M. S. New iridium and rhodium chiral di-N-heterocyclic carbene (NHC) complexes and their application in enantioselective catalysis / M. S. Jeletic, M. T. Jan, I. Ghiviriga, K. A. Abboud, A. S. Veige // Dalton Trans. – 2009. – P. 2764-2776.

49. Lowry, R. J. The next generation of C_2-symmetric ligands: A di-N-heterocyclic carbene (NHC) ligand and the synthesis and X-ray characterization of mono- and dinuclear rhodium(I) and iridium(I) complexes / R. J. Lowry, M. T. Jan, K. A. Abboud, I. Ghiviriga, A. S. Veige // Polyhedron. – 2010. – V. 29. – P. 553-563.

50. Jeletic, M. S. Synthesis and characterization of κ-2-*bis*-*N*-heterocyclic carbene rhodium(I) catalysts: Application in enantioselective arylboronic acid addition to cyclohex-2-enones / M. S. Jeletic, R. J. Lowry, J. M. Swails, I. Ghiviriga, A. S. Veige // J. Organomet. Chem. – 2011. – V. 696. – P. 3127-3134.

51. Jeletic, M. S. Chemical Exchange Saturation Transfer (CEST) as a Tool to Measure Ligand Flexibility of Chelating Chiral Di-*N*-heterocyclic Carbene Complexes / M. S. Jeletic, C. E. Lower, I. Ghiviriga, A. S. Veige // Organometallics. – 2011. – V. 30. – P. 6034-6043.

52. Wang, C.-Y. Rhodium(I) complexes containing a bulky pyridinyl N-heterocyclic carbene ligand: Preparation and reactivity / C.-Y. Wang, Y.-H. Liu, S.-M. Peng, S.-T. Liu // J. Organomet. Chem. – 2006. – V. 691. – P. 4012-4020.

53. Wang, C.-Y. Synthesis of Iridium Pyridinyl N-Heterocyclic Carbene Complexes and Their Catalytic Activities on Reduction of Nitroarenes / C.-Y. Wang, C.-F. Fu, Y.-H. Liu, S.-M. Peng, S.-T. Liu // Inorg. Chem. – 2007. – V. 14. – P. 5779-5786.

54. Kallstrom, K. Asymmetric hydrogenation of tri-substituted alkenes with Ir-NHC-thiazole complexes / K. Kallstrom, P. G. Andersson // Tetrahedron Lett. – 2006. – V. 47. – P. 7477-7480.

55. Nanchen, S. Synthesis and Application of Chiral N-Heterocyclic Carbene–Oxazoline Ligands: Iridium-Catalyzed Enantioselective Hydrogenation / S. Nanchen, A. Pfaltz // Chem. Eur. J. – 2006. – V. 12. – P. 4550-4558.

56. Chen, D. New Optically Active N-Heterocyclic Carbene Complexes for Hydrogenation: A Tale with an Atropisomeric Twist / D. Chen, V. Banphavichit (Bee), J. Reibenspies, K. Burgess // Organometallics. – 2007. – V. 26. – P. 855-859.

57. Nanchen, S. Chiral Phosphino- and (Phosphinooxy)-Substituted N-Heterocyclic Carbene Ligands and Their Application in Iridium-Catalyzed Asymmetric Hydrogenation/ S. Nanchen, A. Pfaltz // Helv. Chim. Acta. – 2006. – V. 89. – P. 1559-1573.

58. Bolm, C. Synthesis of iridium complexes with novel planar chiral chelating imidazolylidene ligands / C. Bolm, T. Focken, G. Raabe // Tetrahedron: Asymmetry. – 2003. – V. 14. – P. 1733-1746.

59. Focken, T. Synthesis of iridium complexes with new planar chiral chelating phosphinyl-imidazolylidene ligands and their application in asymmetric hydrogenation / T. Focken, G. Raabe, C. Bolm // Tetrahedron: Asymmetry. – 2004. – V. 15. – P. 1693-1706.

60. O, W. W. N. Primary Amine Functionalized N-Heterocyclic Carbene Complexes of Iridium: Synthesis, Structure, and Catalysis / W. W. N. O, A. J. Lough, R. H. Morris // Organometallics. – 2013. – V. 32. – P. 3808-3818.

61. Jimenez, M. V. Iridium(I) Complexes with Hemilabile N-Heterocyclic Carbenes: Efficient and Versatile Transfer Hydrogenation Catalysts / M. V. Jimenez, J. Fernandez-Tornos, J. J. Perez-Torrente, F. J. Modrego, S. Winterle, C. Cunchillos, F. J. Lahoz, L. A. Oro // Organometallics. – 2011. – V. 30. – P. 5493-5508.

62. Slivarichova, M. Synthesis and Structural Characterization of Rhodium Complexes featuring Ditopic N-Heterocyclic Carbene/Thione Donors / M. Slivarichova, M. F. Haddow, H. Othman, G. R. Owen // Eur. J. Inorg. Chem. – 2013. – P. 2782-2788.

63. Gade, L. H. A Modular Assembly of Chiral Oxazolinylcarbene-Rhodium Complexes: Efficient Phosphane-Free Catalysts for the Asymmetric Hydrosilylation of Dialkyl Ketones / L. H. Gade, V. Cesar, S. Bellemin-Laponnaz // Angew. Chem. Int. Ed. – 2004. – V. 43. – P. 1014-1017.

64. Cesar, V. Cationic and Neutral Rhodium(I) Oxazolinylcarbene Complexes / V. Cesar, S. Bellemin-Laponnaz, L. H. Gade // Eur. J. Inorg. Chem. – 2004. – P. 3436-3444.

65. Cesar, V. Designing the “Search Pathway” in the Development of a New Class of Highly Efficient Stereoselective Hidrosilylation Catalysts / V. Cesar, S. Bellemin-Laponnaz, H. Wadepohl, L. H. Gade // Chem. Eur. J. – 2005. – V. 11. – P. 2862-2873.

66. Canac, Y. NHC-Derived Bis(amidiniophosphine) Ligands of Rh(I) Complexes: Versatile cis-trans Chelation Driven by an Interplay of Electrostatic and Orbital Effects / Y. Canac, N. Debono, L. Vendier, R. Chauvin // Inorg. Chem. – 2009. – V. 48. – P. 5562-5568.

67. Barthes, C. P(CH)P Pincer Rhodium(I) Complexes: The Key Role of Electron-Poor Imidazoliophosphine Extremities / C. Barthes, C. Lepetit, Y. Canac, C. Duhayon, D. Zargarian, R. Chauvin // Inorg. Chem. – 2013. – V. 52. – P. 48-58.

68. Kitamura, K. Homogeneous asymmetric hydrogenation of functionalized ketones / K. Kitamura, T. Ohkuma, S. Inoue, N. Sayo, H. Kumobayashi, S. Akutagawa, T. Ohta, H. Takaya, R. Noyori // J. Am. Chem. Soc. – 1988. – V. 110. – P. 629-631.

69. Ohkuma, T. Practical Enantioselective Hydrogenation of Aromatic Ketones / T. Ohkuma, H. Ooka, S. Hashiguchi, T. Ikariya, R. Noyori // J. Am. Chem. Soc. – 1995. – V. 117. – P. 2675-2676.

70. Zhang, Z. Three-Hindered Quadrant Phosphine Ligands with Aromatic Ring Backbone for the Rhodium-Catalyzed Asynnetric Hydrogenation of Functionalized Alkenes / Z. Zhang, K. Tamura, D. Mayama, M. Sugiya, T. Imamoto // J. Org. Chem. – 2012. – V. 77. – P. 4184-4188.

71. Norman, D. W. Bidentates versus Monodentates in Asymmetric Hydrogenation Catajysis: Synergic Effects on Rate and Allosteric Effects on Enantioselectivity / D. W. Norman, C. A. Carraz, D. J. Hyett, P. G. Pringle, J. B. Sweeney, A. G. Orpen, H. Phetmung, R. L. Wingad // J. Am. Chem. Soc. – 2008. – V. 130. – P. 6842-6847.

72. Bravo, M. J. New Enantiopure P,P-Bidentate Bis(diamidophosphite) Ligands. Application in Asymmetric Rhodium-Catalyzed Hydrogenation / M. J. Bravo, R. M. Ceder, G. Muller, M. Rocamora // Organometallics. – 2013. – V. 32. – P. 2632-2642.

73. Dahlenburg, L. P-Modular bis(phosphines) based on the 1,2-trans-disubstituted cyclopentane framework in synthesis, coordination chemistry, and catalysis / L. Dahlenburg // Coord. Chem. Rev. – 2005. – V. 249. – P. 2962-2992.

74. Khiri, N. Enantioselective Hydrogenation Catalysis Aided by a σ-Bonded Calix[4]arene to a *P*-Chirogenic Aminophosphane Phosphinite Rhodium Complex / N. Khiri, E. Bertrand, M.-J. Ondel-Eymin, Y. Rousselin, J. Bayardon, P. D. Harvey, S. Juge // Organometallics. – 2010. – V. 29. – P. 3622-3631.

75. Stradiotto, M. A Catalitically Active, Charge-Neutral Rh(I) Zwitterion Featuring a P,N-Substituted “Naked” Indenide Ligand / M. Stradiotto, J. Cipot, R. McDonald // J. Am. Chem. Soc. – 2003. – V. 125. – P. 5618-5619.

76. Phillips, A. D. A New Class of Rhodium(I) k^1-*P* and k^2-*P,N* Complexes with Rigid RTN(R) Ligands (RTN = 7-Phospha-3-methyl-1,3,5-triazabicyclo[3.3.1]nonane) / A. D. Phillips, S. Bolano, S. S. Bosquain, J.-C. Daran, R. Malacea, M. Peruzzini, R. Poli, L. Gonvalvi // Organometallics. – 2006. – V. 25. – P. 2189-2200.

77. Bruck, A. Investigation of the Dynamic Solution Behavior of Chloro(diene)rhodium(I) Phosphine Complexes with a Pendant Unsaturated Heterocycle at Phosphorus (2-pyridyl, 2-imidazyl; diene = COD, NBD) / A. Bruck, K. Ruhland // Organometallics. – 2009. – V. 28. – P. 6383-6401.

78. Maurer, F. Development of Catalysts for the Stereoselective Hydrogenation of *α,β*-Unsaturated Ketones / F. Maurer, V. Huch, A. Ullrich, U. Kazmaier // J. Org. Chem. – 2012. – V. 77. – P. 5139-5143.

79. Hounjet, L. J. Comparison of Structure and Reactivity of Phosphine-Amido and Hemilabile Phosphine-Amine Chelates of Rhodium / L. J. Hounjet, R. McDonald, M. J. Ferguson, M. Cowie // Inorg. Chem. – 2011. – V. 50. – P. 5361-5378.

80. Wurstenberg, B. Homogeneous Hydrogenation of Tri- and Tetrasubstituted Olefins: Comparison of Iridium-Phospinooxazoline [Ir-PHOX] Complexes and Crabtree Catalysts with Hexafluorophosphate (PF_6) and Tetrakis [3,5-bis(trifluoromethyl)phenyl] borate (BArF) as Counterions / B. Wustenberg, A. Pfaltz //Adv. Synth. Catal. – 2008. – V. 350. – P. 174-178.

81. Cheemala, M. N. New P,N-Ferrocenyl Ligands for the Asymmetric Ir-Catalyzed Hydrogenation of Imines / M. N. Cheemala, P. Knochel // Org. Lett. – 2007. – V. 9. – P. 3089-3092.

82. Park, K. Synthesis of New Late Transition Metal P,P-, P,N-, and P,O- Complexes Using Phosphonium Dimers as Convenient Ligand Precursors / K. Park, P. O. Lagaditis, A. J. Lough, R. H. Morris // Inorg. Chem. – 2013. – V. 52. – P. 5448-5456.

83. Ahlmann, M. Synthesis and coordination behaviour of 2-(*ortho*-phosphinophenyl)-functionalised 1,3-dioxolanes and 1,3-dioxanes towards a [(COD)Rh]-complex fragment – models for immobilised complexes / M. Ahlmann, O. Walter // J. Organomet. Chem. – 2004. – V. 689. – P. 3117-3131.

84. Barquin, M. Iridium and Rhodium Complexes with Hemilable Ligand [2-(1,3-dioxolane-2-yl)phenyl]diphenylphosphane – Bevaviour in Solution and Structural Characterization / M. Barquin, R. Ciganda, M. A. Garralda, L. Ibarlucea, C. Mendicute-Fierro, A. Rodriguez-Dieguez, J. M. Seco // Eur. J. Inorg. Chem. – 2013. – P. 1225-1235.

85. Leon, T. P-Stereogenic Secondary Iminophosphorane Ligands and Their Rhodium(I) Complexes: Taking Adventage of NH/Ph Tautomerism / T. Leon, M. Parera, A. Roglans, A. Riera, X. Vedraguer // Angew. Chem. – 2012. – V. 124. – P. 7057-7061.

86. Jimenez, M. V. Cationic Rhodium Complexes with Hemilabile Phosphine Ligands as Polimerization Catalyst for High Molecular Weight Stereoregular Poly(phenylacetylene) / M. V.

Jimenez, J. J. Perez-Torrente, M. I. Bartolome, E. Vispe, F. J. Lahoz, L. A. Oro // Macromolecules. – 2009. – V. 42. – P. 8146-8156.

87. Jimenez, M. V. Rational design of efficient rhodium catalysts for the anti-markovnikov oxidative amination of styrene / M. V. Jimenez, J. J. Perez-Torrente, M. I. Bartolome, F. J. Lahoz, L. A. Oro // Chem. Commun. – 2010. – V. 46. – P. 5322–5324.

88. Jimenez, M. V. Rhodium(I) Complexes with Hemilable Phosphines: Rational Design for Efficient Oxidative Amination Catalysis / M. V. Jimenez, M. I. Bartolome, J. J. Perez-Torrente, F. J. Lahoz, L. A. Oro // ChemCatChem. – 2012. – V. 4. – P. 1298-1310

89. Hua, C. New Rhodium(I) and Iridium(I) Complexes Containing Mixed Pyrazolyl-1,2,3-Triazolyl Ligands As Catalysts for Hydroamination / C. Hua, K. Q. Vuong, M. Bhadbhade, B. A. Masserle // Organometallics. – 2012. – V. 31. – P. 1790-1800.

90. Kina, A. Enantiomerically Pure Rhodium Complexes Bearing 1,5-Diphenyl-1,5-cyclooctadiene as a Chiral Diene Ligand. Their Use as Catalysts for Asymmetric 1,4-Addition of Phenylzinc Chloride / A. Kina, K. Ueyama, T. Hayashi // Org. Lett. – 2005. – V. 7. – P. 5889-5892.

91. Dahlenburg, L. Rhodium(I) Complexes Containing β-Animo Alcohol and 1,2-Diamine Ligands: Synthesis, Structures, and Catalytic Applications / L. Dahlenburg, H. Treffer, C. Farr, F. W. Heinemann, A. Zahl // Eur. J. Inorg. Chem. – 2007. – P. 1738-1751.

92. Noyori, R. Asymmetric Catalysis by Architectural and Functional Molecular Engineering: Practical Chemo- and Stereoselective Hydrogenation of Ketones / R. Noyori, T. Ohkuma // Angew. Chem. Int. Ed. – 2001. – V. 40. – P. 40-73.

93. Blaser, H. U. Selective Hydrogenation for Fine Chemicals: Recent Trends and New Developments / H. U. Blaser, C. Malan, B. Pugin, F. Spindler, H. Steiner, M. Studer // Adv. Synth. Catal. – 2003. – V. 345. – P. 103-151.

94. Malacea, R. Asymmetric hydrosilylation, transfer hydrogenation and hydrogenation of ketones catalyzed by iridium complexes / R. Malacea, R. Poli, E. Manoury // Coord. Chem. Rev. – 2010. – V. 254. – P. 729-752.

95. Tang, W. New Chiral Phosphorus Ligands for Enantioselective Hydrogenation / W. Tang, X. Zhang // Chem. Rev. – 2003. – V. 103. – P. 3029-3069.

96. Nugent, T. C. Chiral Amine Synthesis – Recent Developments and Trends for Enamide Reduction, Reductive Amination, and Imine Reduction / T. C. Nugent, M. El-Shazly // Adv. Synth. Catal. – 2010. – V. 352. – P. 753-819.

97. Fleury-Bregeot, N. Highlights of Transition Metal-Catalyzed Asymmetric Hydrogenation of Imines / N. Fleury-Bregeot, V. de la Fuente, S. Castillon, C. Claver // ChemCatChem. – 2010. – V. 2. – P. 1346-1371.

98. Xie, J. H. Transition Metal-Catalyzed Enantioselective Hydrogenation of Enamines and Imines / J. H. Xie, S. F. Zhu, Q. L. Zhou // Chem. Rev. – 2011. – V. 111. – P. 1713-1760.

99. Wang, D.-S. Asymmetric Hydrogenation of Heteroarenes and Arenes / D.-S. Wang, Q.-A. Chen, S.-M. Lu, Y.-G. Zhou // Chem. Rev. – 2012. – V. 112. – P. 2557-2590.

100. Young, J. F. Hydride Intermediates in Homogeneous Hydrogenation Reactions of Olefins and Acetylenes using Rhodium Catalysts / J. F. Young, J. A. Osborn, F. H. Jardine, G. Wilkinson // Chem. Commun. – 1965. – P. 131-132.

101. Shapley, J. R. Preparation and Catalytic Properties of Some Cationic Iridium(III) and Rhodium(III) Dihydrido Complexes / J. R. Shapley, R. R. Schrock, J. A. Osborn // J. Am. Chem. Soc. – 1969. – V. 91. – P. 2816-2817.

102. Schrock, R. R. Preparation and Properties of Some Cationic Complexes of Rhodium (I) and Rhodium (III) / R. R. Schrock, J. A. Osborn // J. Am. Chem. Soc. – 1971. – V. 93. – P. 2397-2407.

103. Schrock, R. R. Catalytic Hydrogenation Using Cationic Rhodium Complexes. I. Evolution of the Catalytic System and the Hydrogenation of Olefins / R. Schrock, J. A. Osborn // J. Am. Chem. Soc. – 1976. – V. 98. – P. 2135-2143.

104. Halpern, J. Novel coordination chemistry and catalytic properties of cationic 1,2-bis(diphenylphosphino)ethanerhodium(I) complexes / J. Halpern, D. P. Riley, A. S. C. Chan, J. J. Pluth // J. Am. Chem. Soc. – 1977. – V. 99. – P. 8055-8057.

105. Preetz, A. Rhodium-Complex-Catalyzed Asymmetric Hydrogenation: Transformation of Precatalysts into Active Species / A. Preetz, H.-J. Drexler, C. Fisher, Z. Dai, A. Borner, W. Baumann, A. Spannenberg, R. Thede, D. Heller // Chem. Eur.J. – 2008. – V. 14. – P. 1445-1451.

106. Preetz, A. BINAP: rhodium–diolefin complexes in asymmetric hydrogenation / A. Preetz, H.-J. Drexler, S. Schulz, D. Heller // Tetrahedron: Asymmetry. – 2010. – V. 21. – P. 1226-1231.

107. Preetz, A. Cationic Rhodium-BINAP Complexes: Full Characterization of Solvate- and Arene-Bridged Dimeric Species / A. Preetz, C. Fisher, C. Kohrt, H.-J. Drexler, W. Baumann, D. Heller // Organometallics. – 2011. – V. 30. – P. 5155-5159.

108. Moxham, G. L. A Second-Generation Catalyst for Intermolecular Hydroacylation of Alkenes and Alkynes Using β-S-Substituted Aldehydes: The Role of a Hemilabile P-O-P Ligand / G. L. Moxham, H. E. Randell-Sly, S. K. Brayshaw, R. L. Woodward, A. S. Weller, M. C. Willis // Angew. Chem. Int. Ed. – 2006. – V. 45 – P. 7618-7622.

109. Drexler, H.-J. Part III. COD versus NBD precatalysts. Dramatic difference in the asymmetric hydrogenation of prochiral olefins with five-membered diphosphine Rh-hydrogenation catalysts / H.-J. Drexler, W. Baumann, A. Spannenberg, C. Fisher, D. Heller // J. Organomet. Chem. – 2001. – V. 621. – P. 89-102.

110. Preetz, A. Asymmetric Hydrogenation. Dimerization of Solvate Complexes: Synthesis and Characterization of Dimeric $[Rh(DIPAMP)]_2^{2+}$, a Valuable Catalyst Precursor / A. Preetz, W. Baumann, C. Fisher, H.-J. Drexler, T. Schmidt, R. Thede, D. Heller // Organometallics. – 2009. – V. 28. – P. 3673-3677.

111. Fisher, C. Trinuclear rhodium hydride complexes / C. Fisher, C. Kohrt, H.-J. Drexler, W. Baumann, D. Heller // Dalton Trans. – 2011. – V. 40. – P. 4162-4166.

112. Fisher, C. The Influence of Substituents in Diphosphine Ligands on the Hydrogenation Activity and Selectivity of the Corresponding Rhodium Complexes as Exemplified by ButiPhane / C. Fisher, S. Schulz, H.-J. Drexler,C. Selle, M. Lotz, M. Sawall, K. Neymeyr, D. Heller // ChemCatChem. – 2012. – V. 4. – P. 81-88.

113. Preetz, A. Asymmetric Ring Opening of Benzo-7-oxabicyclo-[2.2.1]heptadienes with Cationic Rhodium Complexes / A. Preetz, C. Kohrt, H.-J. Drexler, A. Torres, H. Buschmann, M. G. Lopez, D. Heller // Adv. Synth. Catal. – 2010. – V. 352. – P. 2073-2080.

114. Imamoto, T. Rigid P-Chiral Phosphine Ligands with *tret*-Butylmethylphosphino Groups for Rhodium-Catalyzed Asymmetric Hydrogenation of Functioalized Alkenes / T. Imamoto, K. Tamura, Z. Zhang, Y. Horiuchi, M. Sugiya, K. Yoshida, A. Yanagisawa, I. D. Gridnev // J. Am. Chem. Soc. – 2012. – V. 134. – P. 1754-1769.

115. Gridnev, I. D. Asymmetric Hydrogenation Catalyzed by a Rhodium Complex of (*R*)-(*tret*-Butylmethylphosphino)(di-*tret*-butylphosphino)-methane: Scope of Enantioselectivity and Mechanistic Study // I. D. Gridnev, T. Imamoto, G. Hoge, M. Kouchi, H. Takanashi // J. Am. Chem. Soc. – 2008. – V. 130. – P. 2560-2572.

116. Kohrt, C. Formation of Trinuclear Rhodium-Hydride Complexes $[\{Rh(PP^*)H\}_3(\mu_2\text{-}H)_3(\mu_3\text{-}H)][anion]_2$—During Asymmetric Hydrogenation? / C. Kohrt, W. Baumann, A. Spanneberg, H.-J. Drexler, I. D. Gridnev, D. Heller // Chem. Eur. J. – 2013. – V. 19. – P. 7443-7451.

117. Gridnev, I. D. Mechanism of Asymmetric Hydrogenation Catalyzed by a Rhodium Complex of (*S*,*S*)-1,2-Bis(tret-butylmethylphosphino)ethane. Dihydride Mechanism of Asymmetric Hydrogenation / I. D. Gridnev, N. Higashi, K. Asakura, T. Imamoto // J. Am. Chem. Soc. – 2000. – V. 122. – P. 7183-7194.

118. Gridnev, I. D. Asymmetric Hydrogenation Catalyzed by (*S*,*S*)-R-BisP*-Rh and (*R*,*R*)-R-MiniPHOS Complexes: Scope, Limitations, and Mechanism / I. D. Gridnev, Y. Yoshinori, N. Higashi, H. Tsuruta, M. Yasutake, T. Imamoto // Adv. Synth. Catal. – 2001. – V. 343. – P. 118-136.

119. Gridnev, I. D. Formation of a Stable Rhodium(I) Dihydride Complex and Its Reactions with Prochiral Substrates of Asymmetric Hydrogenation / I. D. Gridnev, N. Higashi, T. Imamoto // Organometallics. – 2001. – V. 20. – P. 4542-4553.

120. Kohrt, C. Molecular Vibration Spectroscopy Studies on Novel Trinuclear Rhodium-7-Hydride Complexes of the General Type {[Rh(PP*)X]$_3$(μ_2-X)$_3$(μ_3-X)}(BF$_4$)$_2$ (X = H, D) / C. Kohrt, S. Hansen, H.-J. Drexler, U. Rosenthal, A. Schulz, D. Heller // Inorg. Chem. – 2012. – V. 51. – P. 7377-7383.

121. Preetz, A. Halide bridged trinuclear rhodium complexes and their inhibiting influence on catalysis / A. Preetz, C. Kohrt, A. Meissner, S. Wei, H.-J. Drexler, H. Buschmann, D. Heller // Catal. Sci. Technol. – 2013. – V. 3. – P. 462-468.

122. Preetz, A. Trinuclear Rhodium Complexes and Their Relevance for Asymmetric Hydrogenation / A. Preetz, W. Baumann, H.-J. Drexler, C. Fisher, J. Sun, A. Spannenberg, O. Zimmer, W. Hell, D. Heller // Chem. Asian. J. – 2008. – V. 3. – P. 1979-1982.

123. Mikami, K. Racemic but *Tropos* (Chirally Flexible) BIPHEP Ligands for Rh(I)-Complexes: Highly Enantioselective Ene-Type Cyclization of 1,6-Enynes / K. Mikami, S. Kataoka, Y. Yusa, K. Aikava // Org. Lett. – 2004. – V. 6. – P. 3699-3701.

124. Gridnev, I. D. Captured at last: a catalyst–substrate adduct and a Rh-dihydride solvate in the asymmetric hydrogenation by a Rh-monophosphine catalyst / I. D. Gridnev, E. Alberico, S. Gladiali // Chem. Commun. – 2012. – V. 48. – P. 2186-2188.

125. Alberico, E. Unravelling the Reaction Path of Rhodium–MonoPhos-Catalysed Olefin Hydrogenation / E. Alberico, W. Baumann, J. G. de Vries, H.-J. Drexler, S. Gladiali, D. Heller, H. J. W. Henderickx, L. Lefort // Chem. Eur. J. – 2011. – V. 17. – P. 12683-12695.

126. Burk, M. J. Rh-DuPHOS-Catalyzed Enantioselective Hydrogenation of Enol Esters. Application to the Synthesis of Highly Enantioenriched α-Hydroxy Esters and 1,2-Diols // M. J. Burk, C. S. Kalberg, A. Pizzano // J. Am. Chem. Soc. – 1998. – V. 120. – P. 4345-4353.

127. Heller, D. The Inhibiting Influence of Aromatic Solvents on the Activity of Asymmetric Hydrogenations / D. Heller, H.-J. Drexler, A. Spannenberg, B. Heller, J. You, W. Baumann // Angew. Chem. Int. Ed. – 2002. – V. 41. – P. 777-780

128. Fisher, C. Investigations into the Formation and Stability of Cationic Rhodium Diphosphane η^6-Arene Complexes / C. Fisher, R. Thede, H.-J. Drexler, A. Konig, W. Baumman, D. Heller // Chem. Eur. J. – 2012. – V. 18. – P. 11920-11928.

129. Fisher, C. Cationic η^6-Coordinated BINAP Rhodium Complexes with Benzene and Toluene / C. Fisher, C. Selle, H.-J. Drexler, D. Heller // Z. Anorg. Allg. Chem. – 2012. – V. 638. – P. 907-908.

130. Fisher, C. Formation of Stable Rhodium η^6-Arene Complexes with Aniline Derivatives / C. Fisher, A. Konig, H.-J. Drexler, D. Heller // Z. Anorg. Allg. Chem. – 2012. – V. 638. – P. 905-906.

131. Schmidt, T. Novel Contributions to the Mechanism of the Enantioselective Hydrogenation of Dimethyl Itaconate with Rhodium Complexes / T. Schmidt, Z. Dai, H.-J. Drexler, W. Baumann, C. Jager, D. Pfeifer, D. Heller // Chem. Eur. J. – 2008. – V. 14. – P. 4469-4471.

132. Drexler, H.-J. Are β-Acylaminoacrylates Hydrogenated in the Same Way as α-Acylaminoacrylates? / H.-J. Drexler, W. Baumann, T. Schmidt, S. Zhang, A. Sun, A. Spannenberg, C. Fisher, H. Buschmann, D. Heller // Angew. Chem. Int. Ed. – 2005. – V. 44. – P. 1184-1188.

133. Drexler, H.-J. Cationic Rh-bisphosphine-diolefin complexes as precatalysts for enantioselective catalysis—what information do single crystal structures contain regarding product chirality? / H.-J. Drexler, S. Zhang, A. Sun, A. Spannenberg, A. Arrieta, A. Preetz, D. Heller // Tetrahedron: Asymmetry. – 2004. – V. 15. – P. 2139-2150.

134. Schmidt, T. About the Crystal Structure of [Rh((*S*,*S*)-DIPAMP)- ((*Z*)-2-benzoylamino-3-(3,4-dimethoxyphenyl)-methyl Acrylate)]BF_4: Major or Minor Catalyst − Substrate Complex? / T. Schmidt, W. Baumann, H.-J. Drexler, A. Arrieta, D. Heller // Organometallics. – 2005. – V. 24. – P. 3842-3848.

135. Schmidt, T. Unusual Deactivation in the Asymmetric Hydrogenation of Itaconic Acid / T. Schmidt, H.-J. Drexler, J. Sun, Z. Dai, W. Baumann, A. Preetz, D. Heller // Adv. Synth. Catal. – 2009. – V. 351. – P. 750-754.

136. Evans, D. A. Application of Chiral Mixed Phosphorus/Sulfur Ligands to Enantioselective Rhodium-Catalyzed Dehydroamino Acid Hydrogenation and Ketone Hydrosilylation Processes // D. A. Evans, F. E. Michael, J. S. Tedrow, K. R. Campos // J. Am. Chem. Soc. – 2003. – V. 125. – P. 3534-3543.

137. Gridnev, I. D. Asymmetric Hydrogenation of Enamides with Rh-BisP* and Rh-MiniPHOS Catalysts. Scope, Limitations, and Mechanism / I. D. Gridnev, M. Yasutake, N. Higashi, T. Imamoto // J. Am. Chem. Soc. – 2001. – V. 123. – P. 5268-5276.

138. Yasutake, M. Highly Enantioselective Hydrogenation of (*E*)-*β*-(Acylamino)acrylates Catalyzed by Rh(I)-Complexes of Electron-Rich P-Chirogenic Diphosphines / M. Yasutake, I. D. Gridnev, N. Higashi, T. Imamoto // Org. Lett. – 2001. – V. 3. – P. 1701-1704.

139. Gridnev, I. D. Interconversion of Monohydride Intermediates in Rh(I)-Catalyzed Asymmetric Hydrogenation of Dimethyl 1-Benzoyloxyethenephosphonate / I. D. Gridnev, N. Higashi, T. Imamoto // J. Am. Chem. Soc. – 2001. – V. 123. – P. 4631-4632.

140. Giernoth, R. PHIP Detection of a Transient Rhodium Dihydride Intermediate in the Homogeneous Hydrogenation of Dehydroamino Acids / R. Giernoth, H. Heinrich, N. J. Adams, R. J. Deeth, J. Bargon, J. M. Brown // J. Am. Chem. Soc. – 2000. – V. 122. – P. 12381-12382.

141. Heinrich, H. Observation of a stable *cis*-diphosphine solvate rhodium dihydride derived from PHANEPHOS / H. Heinrich, R. Giernoth, J. Bargon, J. M. Brown // Chem. Commun. – 2001. – P. 1296-1297.

142. Gridnev, I. D. Mechanism of enantioselection in Rh-catalyzed asymmetric hydrogenation. The origin of utmost catalytic performance / I. G. Gridnev, T. Imamoto // Chem. Commun. – 2009. – P. 7447-7464.

143. Gridnev, I. D. On the Mechanism of Stereoselection in Rh-Catalyzed Asymmetric Asymmetric Hydrogenation: A General Approach for Predicting the Sense of Enantioselectivity / I. D. Gridnev, T. Imamoto // Acc. Chem. Res. – 2004. – V. 37. – P. 633-644.

144. O'Connor, A. R. Synthesis, Characterisation, and Reactivity of Arene-Stabillized Rhodium Complexes / A. R. O'Connor, W. Kaminsky, D. M. Heinekey, K. I. Goldberg // Organometallics. – 2011. – V. 30. – P. 2105-2116.

145. O'Connor, A. R. Synthesis and Characterisation of Iridium(I) and Iridium(III) Complexes Containing Dialkylbiphenylphosphines / A. R. O'Connor, W. Kaminsky, B. C. Chan, D. M. Heinekey, K. I. Goldberg // Organometallics. – 2013. – V. 32. – P. 4016-4019.

146. Mazet, C. A Combined Experimental and Computational Study of Dihydrido(Phosphinooxazoline)iridium Complexes / C. Mazet, S. P. Smidt, M. Meuwly, A. Pfaltz // J. Am. Chem. Soc. – 2004. – V. 126. – 14176-14181.

147. Roseblade, S. J. Iridium-Catalyzed Asymmetric Hydrogenation of Olefins / S. J. Roseblade, A. Pfaltz // Acc. Chem. Res. – 2007. – V. 40. – P. 1402-1411.

148. Dahlenburg, L. Iridium Complexes with Chiral and Achiral β-Aminophosphane Ligands: Catalysts for >C=O Hydrogenation and H/D Exchange Involving both Homo- and Heterolytic H_2 Activation / L. Dahlenburg, R. Gotz // Eur. J. Inorg. Chem. – 2004. – P. 888-905.

149. Flores-Santos, L. Cationic Iridium Complexes with Chiral Dithioether Ligands: Synthesis, Characterisation and Reactivity under Hydrogenation Conditions / L. Flores-Santos, E. Martin, A. Aghmiz, M. Dieguez, C. Claver, A. M. Masdeu-Bulto, M. A. Munoz-Hernandez // Eur. J. Inorg. Chem. – 2004. – P. 2315-2323.

150. Dobereiner, G. E. Iridium-Catalyzed Hydrogenation of N-Heterocyclic Compounds under Mild Conditions by an Outer-Sphere Pathway / G. E. Dobereiner, A. Nova, N. D. Schley, N. Hazari, S. J. Miller, O. Eisenstein, R. H. Crabtree // J. Am. Chem. Soc. – 2011. – V. 133. – 7547-7562.

151. Hauptman, E. Synthesis of Novel (P,S) Ligands Based on Chiral Nonracemic Episulfides. Use in Asymmetric Hydrogenation / E. Hauptman, P. J. Fagan, W. Marshall // Organometallics. – 1999. – V. 18. – P. 2061-2073.

152. Gladiali, S. Chiral Complexes of Rh^I Containing Binaphthalene-Core P,S-Heterobidentate Ligands − Synthesis, Characterization, and Catalytic Activity in Asymmetric Hydrogenation of α,β-

Unsaturated Acids and Esters / S. Gladiali, F. Grepioni, S. Medici, A. Zucca, Z. Berente, L. Kollar // Eur. J. Inorg. Chem. – 2003. – P. 556-561.

153. Teixidor, F. The "$Rh(PPh_3)_2$" and "Rh(cod)" Fragments as Probes To Compare the Coordinating and Electronic Characteristics of C−SR and C−PPh_2 in Heterodisubstituted Carborane Ligands / F. Teixidor, R. Benakki, C. Vinas, R. Kivekas, R. Sillanpaa // Organometallics. – 1998. – V. 17. – P. 4630-4633.

154. Evans, D. A. Application of Chiral Mixed Phosphorus/Sulfur Ligands to Enantioselective Rhodium-Catalyzed Dehydroamino Acid Hydrogenation and Ketone Hydrosilylation Processes / D. A. Evans, F. E. Michael, J. S. Tedrow, K. R. Campos // J. Am. Chem. Soc. – 2003. – V. 125. – P. 3534-3543.

155. Khiar, N. Asymmetric Enamide Hydrogenation Using Phosphinite Thioglycosides: Synthesis of d- and l-Aminoesters Using d-Sugars as Catalyst Precursors / N. Khiar, R. Navas, B. Suarez, E. Alvarez, I. Fernandez // Org. Lett. – 2008. – V. 10. – P. 3697-3700.

156. Browning, J. Coordination chemistry of $[CH_2(PPh_2)(P(Y)R_2)]$ and $[CH(PPh_2)(P(Y)R_2)]^-$, Y = S or Se, R = Ph or ^{t}Bu: rhodium, iridium and ruthenium complexes; ^{13}C ^{31}P, and ^{77}Se NMR studies; and the crystal and molecular structures of $[Ir(cod)CH_2(PPh_2)(P(S)^tBu_2)$-*P,S*$]BF_4 \cdot CHCl_3$, $[Rh(cod)CH_2(PPh_2)(P(S)^tBu_2)$-*P,S*$ClO_4 \cdot CH_2Cl_2$ [Rh(cod)CH(PPh_2) ($P(S)Ph_2$)-*P,S*] and $[RuCl_2$(*p*-cymene)$CH_2(PPh_2)(P(S)Ph_2)$-*P*$] \cdot CH_2Cl_2$ / J. Browning, G. W. Bushnell, K. R. Dixon, R. W. Hilts // J. Organomet. Chem. – 1993. – V. 452. – P. 205-218.

157. Faller, J. W. Hemilability and nonrigidity in metal complexes of bidentate P,P=S donor ligands / J. W. Faller, S. C. Milheiro, J. Parr // J. Organomet. Chem. – 2008. – V. 693. – P. 1478-1493.

158. Browning, J. Coordination chemistry of $[C(PPh_2)(P(S)Ph_2)_2]^-$: ^{31}P NMR of rhodium, iridium and platinum complexes, and the crystal and molecular structures of $[Rh(cod)\{C(PPh_2)(P(S)Ph_2)_2$-*P,S*$\}] \cdot CH_2Cl_2$ and $[RhI_2(^tBuNC)_2\{C(PPh_2)(P(S)Ph_2)_2$-*P,S*$\}]$ / J. Browning, K. R. Dixon, N. J. Meanwell, F. Wang // J. Organomet. Chem. – 1993. – V. 460. – P. 117-126.

159. Lee, H. S. Rhodium and Iridium Phosphinothiolato Complexes. Synthesis and Crystal Structures of Mononuclear $[M(cod)($*S,P*-$SC_2B_{10}H_{10}PPh_2)]$ and Dinuclear $[M_2(CO)_2($*S,P*-μ-$SC_2B_{10}H_{10}PPh_2)]$ (M = Rh, Ir) and Their Performance in Catalytic Carbonylation / H. S. Lee, J. Y. Bae, D. H. Kim, H. S. Kim, S. J. Kim, S. Cho, J. Ko, S. O. Kang // Organometallics. – 2002. – V. 21. – P. 210-219.

160. Ito, J. Enhancement of enantioselectivity by alcohol additives in asymmetric hydrogenation with bis(oxazolinyl)phenyl ruthenium catalysts / J. Ito, T. Teshima, H. Nishiyama // Chem. Commun. – 2012. – V. 48 – P. 1105-1107.

161. Ahlsten, N. Allylic alcohols as synthetic enolate equivalents: Isomerisation and tandem reactions catalysed by transition metal complexes / N. Ahlsten, A. Bartoszewicza, B. Martin-Matute // Dalton Trans. – 2012. – V. 41. – P. 1660-1670.

162. Bizet, V. Ruthenium-Catalyzed Redox Isomerization of Trifluoromethylated Allylic Alcohols: Mechanistic Evidence for an Enantiospecific Pathway / V. Bizet, X. Pannecoucke, J.-L. Renaud, D. Cahard // Angew. Chem. Int. Ed. – 2012. – V. 51. – P. 6467 –6470.

163. Tanaka, K. Catalyzed by a Rhodium/Phosphaferrocene Complex / K. Tanaka, S. Qiao, M. Tobisu, M. M.-C. Lo, G. C. Fu // J. Am. Chem. Soc. – 2000. – V. 122. – P. 9870-9871.

164. Mantilli, L. / Structure–Activity Relationship in the Iridium-Catalyzed Isomerization of Primary Allylic Alcohols / L. Mantilli, D. Gerard, C. Besnard, C. Mazet // Eur. J. Inorg. Chem. – 2012. – P. 3320–3330.

165. Ahlsten, N. Rhodium-catalysed isomerisation of allylic alcohols in water at ambient temperature / N. Ahlsten, H. Lundberg, B. Martin-Matute // Green Chem. – 2010. – V. 12. – P. 1628–1633.

166. Diez, J. Imidazole Based Ruthenium(IV) Complexes as Highly Efficient Bifunctional Catalysts for the Redox Isomerization of Allylic Alcohols in Aqueous Medium: Water as Cooperating Ligand / J. Diez, J. Gimeno, A. Lledos, F. J. Suarez, C. Vicent // ACS Catal. – 2012. – V. 2. – P. 2087−2099.

167. Schulz, J. Arene–Ruthenium Complexes with Phosphanylferrocenecarboxamides Bearing Polar Hydroxyalkyl Groups – Synthesis, Molecular Structure, and Catalytic Use in Redox Isomerizations of Allylic Alcohols to Carbonyl Compounds / J. Schulz, I. Cisarova, P. Stepnicka // Eur. J. Inorg. Chem. – 2012. – P. 5000–5010.

168. Duckett, S. B. Application of *Para*hydrogen Induced Polarization Techniques in NMR Spectroscopy and Imaging / S. B. Duckett, R. E. Mewis // Acc. Chem. Res. – 2012. – V. 45. – P. 1247-1257.

169. Green, R. A. The theory and practice of hyperpolarization in magnetic resonance using *para*hydrogen / R. A. Green, R. W. Adams, S. B. Duckett, R. E. Mewis, D. C. Williamson, G. G. R. Green // Prog. Nucl. Magn. Reson. Spectrosc. – 2012. – V. 67. – P. 1-48.

170. Bowers, C. R. Parahydrogen and synthesis allow dramatically enhanced nuclear alignment / C. R. Bowers, D. P. Weitekamp // J. Am. Chem. Soc. – 1987. – V. 109. – P. 5541-5542.

171. Eisenschmid, T. C. Para hydrogen induced polarization in hydrogenation reactions / T. C. Eisenschmid, R. U. Kirss, P. P. Deutsch, S. I. Hommeltoft, R. Eisenberg, J. Bargon, R. G. Lawer, A. L. Balch // J. Am. Chem. Soc. – 1987. – V. 109. – P. 8089-8091.

172. Goldman, K. Metabolic Imaging and Other Applications of Hyperpolarized $^{13}C^{1}$ / K. Golman, J. S. Petersson // Acad. Radiol. – 2006. – V. 13. – P. 932-942.

173. Blazina, D. NMR Studies of $Ru_3(CO)_{10}(PMe_2Ph)_2$ and $Ru_3(CO)_{10}(PPh_3)_2$ and Their H_2 Addition Products: Detection of New Isomers with Complex Dynamic Behavior / D. Blazina, S. B. Duckett, P. J. Dyson, B. F. G. Johnson, J. A. B. Lohman, C. J. Sleigh // J. Am. Chem. Soc. – 2001. – V. 123. – P. 9760-9768.

174. Blazina, D. Catalytic Hydrogenation by Triruthenium Clusters: A Mechanistic Study with Parahydrogen-Induced Polarization / D. Blazina, S. Duckett, P. Dyson, J. Lohman // Chem.-Eur. J. – 2003. – V. 9. – P. 1045-1061.

175. Al-Ibadi, M. A. M. Characterisation of tri-ruthenium dihydride complexes through the computation of NMR parameters / M. A. M. Al-Ibadi, S. B. Duckett, J. E. McGray // Dalton Trans. – 2012. – V. 41. – P. 4618-4625.

176. Schott, D. Ruthenium Dihydride Complexes: NMR Studies of Intramolecular Isomerization and Fluxionality Including the Detection of Minor Isomers by Parahydrogen-Induced Polarization / D. Schott, C. J. Sleigh, J. P. Lowe, S. B. Duckett, R. J. Mawby, M. G. Partridge // Inorg. Chem. – 2002. – V. 41. – P. 2960-2970.

177. Schott, D. The reaction of $M(CO)_3(Ph_2PCH_2CH_2PPh_2)$ (M = Fe, Ru) with *para*hydrogen: probing the electronic structure of reaction intermediates and the internal rearrangement mechanism for the dihydride products / D. Schott, P. Gallaghan, J. Dunne, S. B. Duckett, C. Godard, J. M. Goicoechea, J. N. Harvey, J. P. Lowe, R. J. Mawby, G. Muller, R. N. Perutz, R. Poli, M. K. Whittlesey // Dalton Trans. – 2004. – P. 3218-3224.

178. Lopez-Serrano, J. A *para*-Hydrogen Investigation of Palladium-Catalyzed Alkyne Hydrogenation / J. Lopez-Serrano, S. B. Duckett, S. Aiken, K. Q. Almeida Lenero, E. Drent, J. P. Dunne, D. Konya, A. C. Whitwood // J. Am. Chem. Soc. – 2007. – V. 129. – P. 6513-6527.

179. Lopez-Serrano, J. Palladium-Catalyzed Hydrogenation: Detection of Palladium Hydrides. A Joint Study Using Para-Hydrogen-Enhanced NMR Spectroscopy and Density Functional Theory / J. Lopez-Serrano, S. B. Duckett, A. Lledos // J. Am. Chem. Soc. – 2006. – V. 128. – P. 9596-9597.

180. Eguillor, B. Detection of Unusual Reaction Intermediates during the Conversion of $W(N_2)_2(dppe)_2$ to $W(H)_4(dppe)_2$ and of H_2O into H_2 / B. Eguillor, P. J. Caldwell, M. C. R. Cockett, S. B. Duckett, R. O. John, J. M. Lynam, C. J. Sleigh, I. Wilson // J. Am. Chem. Soc. – 2012. – V. 134. – P. 18257-18265.

181. Martin M. Versatility of Cyclooctadiene Ligands in Iridium Chemistry and Catalysis / M. Martin, E. Sola, O. Torres, P. Plou, L. A. Oro // Organimetallics. – 2003. – V. 22. – P. 5406-5417.

182. Mohring, U. Kinetic and mechanistic investigation of the sequential hydrogenation of phenylacetylene catalyzed by rhodium(I) phosphine complexes of the type $[Rh(\eta^2\text{-}O_2Z)(PR_3)_2]$ / U. Mohring, M. Schafer, F. Kukla, M. Schlaf, H. Werner // J. Mol. Catal. A: Chem. – 1995. V. 99. – P. 55-63.

183. March, J. Advanced Organic Chemistry / J. March. - 3rd ed. - New Yok: Wiley-Interscience, 1985. - 796 p.

184. Duckett, S. B. Applications of the parahydrogen phenomenon: A chemical perspective / S. B. Duckett, C. J. Sleigh // Prog. Nucl. Magn. Reson. Specrosc. – 1999. – V. 34. – P. 71-92.

185. Atkinson, K. D. Spontaneous Transfer of *Para*hydrogen Derived Spin Order to Pyridine at Low Magnetic Field / K. D. Atkinson, M. J. Cowley, P. I. P. Elliott, S. B. Duckett, G. G. R. Green, J. Lopez-Serrano, A. C. J. Whitwood // J. Am. Chem. Soc. – 2009. – V. 131. – P. 13362-13368.

186. Harris. D. C. Nonlinear Least-Squares Curve Fitting with Microsoft Excel Solver / D. C. Harris // J. Chem. Educ. – 1998. – V. 75. – P. 119-121.

187. Altomare, A. *SIR*97: a new tool for crystal structure determination and refinement / A. Altomare, M. C. Burla, M. Camalli, G. L. Cascarano, C. Giacovazzo, A. Guagliardi, A. G. G. Moliterni, G. Polidori, R. Spagna // J. Appl. Crystallogr. – 1999. – V. 32. – P. 115-119.

188. Scheldrick, G. M. A short history of *SHELX* / G. M. Sheldrick // Acta Crystallogr., Sect. A: Found. Crystallogr. – 2008. – V. 64. – P.112-122.

189. Farrugia, L. J. *ORTEP*-3 for Windows - a version of *ORTEP*-III with a Graphical User Interface (GUI) / L. J. Farrugia // J. Appl. Crystallogr. – 1997. – V. 30. – P. 565.

190. Frisch, M. J. Gaussian 09 / M. J. Frisch, G. W. Trucks, H. B. Schlegel, G. E. Scuseria, M. A. Robb, J. R. Cheeseman, G. Scalmani, V. Barone, B. Mennucci, G. A. Petersson, H. Nakatsuji, M. Caricato, X. Li, H. P. Hratchian, A. F. Izmaylov, J. Bloino, G. Zheng, J. L. Sonnenberg, M. Hada, M. Ehara, K. Toyota, R. Fukuda, J. Hasegawa, M. Ishida, T. Nakajima, Y. Honda, O. Kitao, H. Nakai, T. Vreven, J. A Montgomery Jr., J. E. Peralta, F. Ogliaro, M. Bearpark, J. J. Heyd, E. Brothers, K. N. Kudin, V. N. Staroverov, R. Kobayashi, J. Normand, K. Raghavachari, A. Rendell, J. C. Burant, S. S. Iyengar, J. Tomasi, M. Cossi, N. Rega, N. J. Millam, M. Klene, J. E. Knox, J. B. Cross, V. Bakken, C. Adamo, J. Jaramillo, R. Gomperts, R. E. Stratmann, O. Yazyev, A. J. Austin, R. Cammi, C. Pomelli, J. W. Ochterski, R. L. Martin, K. Morokuma, V. G. Zakrzewski, G. A. Voth, P. Salvador, J. J. Dannenberg, S. Dapprich, A. D. Daniels, Ö. Farkas, J. B. Foresman, J. V. Ortiz, J. Cioslowski, D. J. Fox. - , Revision A.02. - Wallingford CT: Gaussian, Inc., 2009.

191. Lee, C. T. Development of the Colle-Salvetti correlation-energy formula into a functional of the electron-density / C. T. Lee, W. T. Yang, R. G. Parr // Phys. Rev. – 1993. – V. 98. – P. 785-789.

192. Andrae, D. Energy-adjusted *ab initio* pseudopotentials for the second and third row transition elements / D. Andrae, U. Haussermann, M. Dolg, H. Stoll, H. Preuss // Theor. Chim. Acta. – 1990. – V. 77. – P. 123-141.

193. Haussermann, U. Accuracy of energy-adjusted quasirelativistic *ab initio* pseudopotentials. All-electron and pseudopotential benchmark calculations for Hg, HgH and their cations / U.

Haussermann, M. Dolg, H. Stoll, H. Preuss, P. Schwerdtfeger, R. M. Pitzer // Mol. Phys. – 1993. – V. 78. – P. 1211-1224.

194. Kuchle, W. Energy – adjusted pseudopotentials for the actinides. Parameter sets and test calculations for thorium and thorium monoxide / W. Kuchle, M, Dolg, H. Stoll, H. Preuss // J. Chem. Phys. – 1994. – V. 100. – 7535-7542.

195. Leininger, T. The accuracy of the pseudopotential approximation. II. A comparison of various core sizes for indium pseudopotentials in calculations for spectroscopic constants of InH, InF, and InCl / T. Leininger, A. Nicklass, H. Stoll, M. Dolg, P. Svhwerdtfeger // J. Chem. Phys. – 1996. – V. 105. – 1052-1059.

196. Ehlers, A. W. A set of f-polarization functions for pseudo-potential basis sets of the transition metals Sc-Cu, Y-Ag and La-Au / A.W. Ehlers, M. Böhme, S. Dapprich, A. Gobbi, A. Höllwarth, V. Jonas, K.F. Köhler, R. Stegmann, A. Veldkamp, G. Frenking // Chem. Phys. Lett. – 1993. – V. 208. – P. 111-114.

197. Zhao, Y. The M06 suite of density functionals for main group thermochemistry, thermochemical kinetics, noncovalent interactions, excited states, and transition elements: two new functionals and systematic testing of four M06-class functionals and 12 other functionals / Y. Zhao, D. G. Truhlar // Theor. Chem. Acc. – 2008. – V. 120. – P. 215-241.

198. Fritsch, J. Influence of the polarity of the environment on easily polarizable OH.cntdot..cntdot..cntdot.N .dblharw. O-.cntdot..cntdot..cntdot.H+N hydrogen bonds / J. Fritsch, G. Zundel // J. Phys. Chem. – 1981. – V. 85. – P. 556-561.

199. Kramer, R. Influence of specific interaction effects on the proton-transfer equilibrium in intermolecular hydrogen bonds of carboxylic acids and phenols with amines / R. Kramer, G. Zundel // J. Chem. Soc., Faraday Trans. – 1990. – V. 86. – P. 301-305.